

**ANALYTICAL AND NUMERICAL ANALYSIS OF
CYLINDRICAL AND SPHERICAL PRESSURE VESSELS
WITH SMALL-DIAMETER NOZZLES**

BY

FAISAL MUHAMMAD MUKHTAR

A Dissertation Presented to the
DEANSHIP OF GRADUATE STUDIES

KING FAHD UNIVERSITY OF PETROLEUM & MINERALS

DHAHRAN, SAUDI ARABIA

In Partial Fulfillment of the
Requirements for the Degree of

DOCTOR OF PHILOSOPHY

In

Civil Engineering

May, 2015

KING FAHD UNIVERSITY OF PETROLEUM & MINERALS

DHAHRAN- 31261, SAUDI ARABIA

DEANSHIP OF GRADUATE STUDIES

This dissertation, written by **FAISAL MUHAMMAD MUKHTAR** under the direction of his dissertation advisor and approved by his dissertation committee, has been presented to and accepted by the Dean of Graduate Studies, in partial fulfillment of the requirements for the degree of **DOCTOR OF PHILOSOPHY IN CIVIL ENGINEERING**.



Dr. Omar A. Al-Swailem
Department Chairman (A)



Prof. Salam A. Zummo
Dean of Graduate Studies

Date

24/5/15



Prof. Husain J. Al-Gahtani
(Advisor)



Prof. Al-Farabi M. Sharif
(Member)



Prof. Fiazuddin Zaman
(Member)



Dr. Ali H. Al-Gadhib
(Member)



Dr. Mehmet Sunar
(Member)

© Faisal Muhammad Mukhtar

2015

*This Dissertation is dedicated to
All those who supported me on this journey*

ACKNOWLEDGEMENTS

Firstly, I thank Allah (SWT) for His countless blessings bestowed upon me and for granting me the courage and wisdom to complete this research work.

I gratefully acknowledge King Fahd University of Petroleum & Minerals (KFUPM) for providing me with the opportunity to undergo my graduate program and the excellent facilities made available for me to conduct my research.

Great supportive roles of Department of Civil & Environmental Engineering, KFUPM, the chairman, Dr. Omar A. Al-Swailem and the immediate past chairman, Prof. Nedal T. Al-Ratrout (current Dean of Academic Development, KFUPM) are highly appreciated.

My profound gratitude goes to my PhD Dissertation Adviser, Prof. Husain J. Al-Gahtani for his kind and immeasurable guidance and assistance during the course of my research. I also want to thank my other PhD Dissertation Committee members, namely, Prof. Al-Farabi M. Sharif, Prof. Fiazuddin Zaman, Dr. Ali H. Al-Gadhib and Dr. Mehmet Sunar for their guidance, patience and good humor.

I acknowledge the support of Messrs Anas Al-Mousa and Muhammed Zahid Ayar for their valuable help in facilitating my use of computing resources in the Information & Computer Science Department of KFUPM.

I appreciate the role of my family members and friends for their continuous prayers, support and encouragement.

FMM, May 2015

TABLE OF CONTENTS

ACKNOWLEDGEMENTS	v
TABLE OF CONTENTS	vi
LIST OF TABLES	x
LIST OF FIGURES	xi
NOMENCLATURE	xv
DISSERTATION ABSTRACT	xvii
DISSERTATION ABSTRACT (ARABIC)	xviii
CHAPTER ONE	1
INTRODUCTION	1
1.1 GENERAL	1
1.2 RESEARCH SIGNIFICANCE	2
1.3 RESEARCH AIM AND OBJECTIVES	4
1.4 SCOPE AND LIMITATIONS	5
1.5 RESEARCH METHODOLOGY	5
1.5.1 Literature Review	5
1.5.2 Selection of Geometrical Ratios to be used in the Analyses	6
1.5.3 Selection of Software for Numerical Simulation	6
1.5.4 Computer Implementation of Analytical Solutions	7
1.5.5 Development of Finite Element Models	7
1.5.6 Analytical Simulation of the Selected Pressurized Vessel-Nozzle Configurations	7
1.5.7 Numerical Simulation of the Selected Pressurized Vessel-Nozzle Configurations	7
1.5.8 Development of Design Charts	8
1.5.9 Development of Closed-Form Solution Models for the Stress Concentration Factors ...	8
1.5.10 Models' Validation	9
CHAPTER TWO	11
LITERATURE REVIEW	11
2.1 ANALYSIS OF SPHERICAL VESSEL - CYLINDRICAL NOZZLE JUNCTION	11
2.1.1 Analytical Solution	11
2.1.2 Numerical Solution	12
2.2 ANALYSIS OF CYLINDRICAL VESSEL - CYLINDRICAL NOZZLE JUNCTION ...	19
2.2.1 Analytical Solution	19
2.2.2 Numerical Solution	22
2.3 REINFORCEMENT AROUND PRESSURE VESSEL - NOZZLE JUNCTURE	27

2.4 CLOSED-FORM EXPRESSIONS OF SCF FOR PRESSURE VESSEL - NOZZLE JUNCTURES	35
2.5 PRESSURE VESSELS DESIGN CODES.....	39
CHAPTER THREE	40
GOVERNING EQUATIONS OF AXI-SYMMETRICALLY LOADED SPHERICAL VESSEL-CYLINDRICAL NOZZLE JUNCTURE.....	40
3.1 GENERAL STRESSES ACTING ON SPHERICAL SHELL ELEMENT	40
3.2 EQUILIBRIUM EQUATIONS.....	41
3.3 U AND V FORMULATIONS.....	42
3.4 CYLINDRICAL NOZZLE ATTACHMENT	48
CHAPTER FOUR.....	49
GOVERNING EQUATIONS OF CYLINDRICAL VESSEL - CYLINDRICAL NOZZLE JUNCTURE	49
4.1 CYLINDRICAL VESSEL	49
4.2 CYLINDRICAL NOZZLE ATTACHMENT	51
CHAPTER FIVE	53
ANALYTICAL SOLUTION MODELS	53
5.1 EXACT ANALYTICAL SOLUTION FOR SPHERICAL VESSEL.....	53
5.1.1 Solution Due to the Effect of Discontinuity Forces and Moments	53
5.1.2 Solution Due to the Effect of Internal Pressure	58
5.2 APPROXIMATE ANALYTICAL SOLUTIONS FOR SPHERICAL VESSEL.....	59
5.2.1 Approximation by considering fourth order equation [3]	60
5.2.2 Approximation by Considering Two Second-Order Equations	61
5.3 ANALYTICAL SOLUTION FOR THE CYLINDRICAL NOZZLE ATTACHMENT... 71	
5.3.1 Solution Due to the Effect of Discontinuity Forces and Moments	71
5.3.2 Solution Due to the Effect of Internal Pressure	72
CHAPTER SIX.....	73
FORMULATIONS AND COMPUTER IMPLEMENTATION	73
6.1 NON-DIMENSIONALIZATION OF SOLUTION VARIABLES.....	73
6.1.1 Non-Dimensionalization of Approximate Solution Variables for the Spherical Vessel.....	74
6.1.2 Non-Dimensionalized Solution Variables for the Cylindrical Nozzle.....	76
6.2 DISCONTINUITY ANALYSIS AND DISCONTINUITY EQUATIONS.....	77
6.2.1 Spherical Vessels intersected by Radial Cylindrical Nozzles.....	78
6.2.2 Cylindrical Vessels intersected by Radial Cylindrical Nozzles	81
6.3 COMPUTER IMPLEMENTATION OF ANALYTICAL MODELS	82

6.3.1 Exact Analytical Model for Spherical Vessels with Moderate-To-Large Diameter Nozzles.....	82
6.3.2 Approximate Analytical Model for Spherical Vessels with Moderate-To-Large Diameter Nozzles.....	86
6.4 COMPUTER IMPLEMENTATION OF NUMERICAL MODELS	89
6.4.1 Spherical and Cylindrical Vessels with Moderate-To-Large Diameter Nozzles	89
6.4.2 Spherical and Cylindrical Vessels with Small-Diameter Nozzles	92
CHAPTER SEVEN	97
ANALYSIS AND DEVELOPMENT OF DESIGN CHARTS FOR SPHERICAL PRESSURE VESSELS WITH MODERATE-TO-LARGE DIAMETER CYLINDRICAL NOZZLES	97
7.1 INTRODUCTION.....	97
7.2 FINITE ELEMENT, EXACT VERSUS APPROXIMATE SOLUTIONS.....	99
7.3 ρ -SCF PLOTS VERSUS INDIVIDUAL SCF- rR PLOTS.....	108
7.4 STUDY ON THE TYPE AND LOCATION OF MAXIMUM STRESS AT THE VESSEL-NOZZLE JUNCTURE	115
CHAPTER EIGHT	121
ANALYSIS AND DEVELOPMENT OF DESIGN CHARTS FOR CYLINDRICAL PRESSURE VESSELS WITH MODERATE-TO-LARGE DIAMETER CYLINDRICAL NOZZLES.....	121
8.1 NUMERICAL EXPERIMENTS, RESULTS AND DISCUSSIONS	121
8.2 COMPARISON WITH THE PREDICTION BY OTHER MODELS.....	133
8.3 DESIGN CHARTS FOR CYLINDRICAL VESSELS INTERSECTED BY MODERATE-TO-LARGE-DIAMETER NOZZLES.....	137
CHAPTER NINE.....	141
MODELING AND ANALYSIS OF SCF FOR SPHERICAL PRESSURE VESSELS WITH SMALL DIAMETER NOZZLES.....	141
9.1 USE OF SOLID VERSUS SHELL ELEMENTS	141
9.2 NUMERICAL EXPERIMENTS, RESULTS AND DISCUSSIONS	142
9.3 COMPARISON WITH AREA REPLACEMENT METHOD	148
9.4 OVERALL DESIGN CHARTS: SPHERICAL VESSEL-CYLINDRICAL NOZZLE JUNCTURES	151
CHAPTER TEN	155
MODELING AND ANALYSIS OF SCF FOR CYLINDRICAL PRESSURE VESSELS WITH SMALL DIAMETER NOZZLES	155
10.1 INTRODUCTION.....	155
10.2 NUMERICAL EXPERIMENTS, RESULTS AND DISCUSSIONS	155
10.3 COMPARISON WITH THE PREDICTION BY OTHER MODELS.....	161

10.4 OVERALL DESIGN CHARTS: CYLINDRICAL VESSEL-CYLINDRICAL NOZZLE JUNCTURES.....	165
CHAPTER ELEVEN.....	169
DEVELOPMENT OF SIMPLIFIED EXPRESSIONS OF SCF	169
11.1 SPHERICAL VESSELS	169
11.1.1 Spherical Vessels with Moderate-To-Large-Diameter Nozzles.....	169
11.1.2 Spherical Vessels with Small-Diameter Nozzles	181
11.2 CYLINDRICAL VESSELS	183
11.2.1 Cylindrical Vessels with Moderate-To-Large-Diameter Nozzles.....	183
11.2.2 Cylindrical Vessels with Small-Diameter Nozzles	189
11.3 SUMMARIZED EXPRESSIONS OF SCF FOR SPHERICAL AND CYLINDRICAL VESSELS.....	191
CHAPTER TWELVE.....	192
CONCLUSIONS AND RECOMMENDATIONS	192
12.1 CONCLUSIONS	192
12.2 RECOMMENDATIONS	195
REFERENCES	197
APPENDIX A:.....	206
MATHEMATICA CODES FOR ANALYTICAL SOLUTIONS OF SPHERICAL VESSEL-CYLINDRICAL NOZZLE JUNCTURES	206
APPENDIX B:.....	226
BEHAVIOUR OF THE MEMBRANE STRESSES IN SPHERICAL VESSEL- CYLINDRICAL NOZZLE JUNCTURES	226
APPENDIX C:.....	229
FINITE ELEMENT SOLUTION OF SCF FOR CASES WITH NO HANDY ANALYTICAL SOLUTIONS	229
VITA	274

LIST OF TABLES

Table 2- 1: Pressure Vessel Codes	39
Table 6- 1: Coordinates Transformation in Cylindrical Vessels with Moderate-To-Large-Diameter Nozzles	95
Table 6- 2: Coordinates Transformation in Cylindrical Vessels with Small-Diameter Nozzles	95
Table 6- 3: Coordinates Transformation in Spherical Vessels with Small-Diameter Nozzles	96
Table 7- 1: Expressions of Membrane Stresses for Internally Pressurized Vessels (Thin Shells).....	97
Table 7- 2: Predictions of Vessel's and Nozzle's SCF by the Exact, FEM and Approximate Solutions	102
Table 7- 3: Minimum r/R and ρ Values for the Validity of Thin Shell Assumption	111
Table 7- 4: Type and Location of Maximum Stress at the Vessel-Nozzle Junction	117
Table 8- 1: Predictions of Vessel's and Nozzle's SCF by the Finite Element Analysis.....	125
Table 9- 1: Expressions of Membrane Stresses for Internally Pressurized Vessels.....	142
Table 9- 2: FEM Predictions of SCF for Spherical Vessels with Small-Diameter Nozzles	147
Table 9- 3: Predictions of SCF for Spherical Vessels with Small-Diameter Nozzles: FEM versus Area Replacement Method [92].....	150
Table 10- 1: FEM Predictions of SCF for Cylindrical Vessels with Small-Diameter Nozzles	159
Table 11- 1: 2-Parameter Models for the Discontinuity Forces, Moments and SCF for Spherical Vessel-Cylindrical Nozzle Intersection.....	175
Table 11- 2: Predictions of SCF by the Simplified Models for Spherical Vessels with Moderate-to-Large-Diameter Nozzles Compared against FEM.....	177
Table 11- 3: Predictions of SCF by the Simplified Models for Spherical Vessels with Small-Diameter Nozzles	181
Table 11- 4: Predictions of SCF by the Simplified Models for Cylindrical Vessels with Moderate-to-Large-Diameter Nozzles	184
Table 11- 5: Predictions of SCF by the Simplified Models for Cylindrical Vessels with Small-Diameter Nozzles	189
Table 11- 6: Summary of the Unknown Constants Appearing in the Simplified General Expression of SCF for Spherical and Cylindrical Vessels.....	191

LIST OF FIGURES

Figure 2- 1: Literature Trend in the Use of Finite Elements for Various Topics in Pressure Vessels and Piping for the Period from 1976 to 2004 [17]	14
Figure 2- 2: Hole Configurations on the Spherical Vessel Considered by Fuad et al. [31]	18
Figure 2- 3: Pad Reinforcement for (a) Flush Nozzle (b) Protruding Nozzle	28
Figure 2- 4: Shell Integral Reinforcement for (a) Flush Nozzle (b) Protruding Nozzle	28
Figure 2- 5: Nozzle Integral Reinforcement for (a) Flush Nozzle (b) Protruding Nozzle	28
Figure 2- 6: Conical Pad Reinforcement for Nozzle proposed by Calladine [67]	29
Figure 2- 7: Modified Design of Pad Reinforcement suggested by Kitching And Kannas [68]	30
Figure 2- 8: Idea of Area Replacement Method adopted in Refs. [92] and [93] for (a) Spherical Vessel (b) Cylindrical Vessel	36
Figure 3- 1: Action of (a) Stresses, and (b) Resultant Forces on an Element Cut from a Shell	40
Figure 3- 2: Portion of the Shell above the Parallel Circle	44
Figure 4- 1: Cylindrical Vessel with a Circular Cutout	49
Figure 4- 2: Circular Cutout on Shallow Cylindrical Shell described by Cartesian and Polar Coordinate Systems	49
Figure 5- 1: An Element AB of the Meridian	55
Figure 5- 2: Internal Pressure, Resultant Edge Forces and Moments Acting on the Spherical Vessel and Nozzle	59
Figure 5- 3: Sign Convention and Relationship between ϕ , ϕ_0 and ψ	63
Figure 5- 4: Segment of a Spherical Shell under the Action of Edge Loadings: (a) Moment (b) Shear	64
Figure 6- 1: Edge Forces and Displacements/Rotations at the Spherical Shell-Cylindrical Nozzle Juncture in (a) Dimensional and (b) Non-Dimensionalized Form	78
Figure 6- 2: Edge Displacements at the Cylindrical Shell-Cylindrical Nozzle Juncture	81
Figure 6- 3: Edge Forces at the Cylindrical Shell-Cylindrical Nozzle Juncture	82
Figure 6- 4: Flowchart for the Exact Analytical Solution of Spherical Vessels with Moderate-to-Large-Diameter Nozzles	83
Figure 6- 5: Flowchart for the Approximate Analytical Solution of Spherical Vessels with Moderate-to-Large-Diameter Nozzles	87
Figure 6- 6: Flowchart for FEM Solution of Vessels with Moderate-to-Large-Diameter Nozzles using COMSOL	90
Figure 6- 7: Flowchart for FEM Solution of Vessels with Small-Diameter Nozzles using COMSOL	93
Figure 7- 1: Minimum Requirements for Validity of Shell Theory and Approximate Solution for Spherical Vessel-Cylindrical Nozzle Juncture	98
Figure 7- 2: Quarter Model for the Spherical Vessel-Nozzle Juncture (a) Geometry (b) Mesh	99
Figure 7- 3: Comparison between FEM/Exact (dashed) and Approximate (continuous) Solutions for a Vessel-Nozzle Juncture with $RT = 50$, $tT = 0.25$ and $rR = 0.1$ for (a) Nozzle (b) Spherical Vessel	101
Figure 7- 4: Comparison between FEM/Exact (dashed) and Approximate (continuous) Solutions for a Vessel-Nozzle Juncture with $RT = 50$, $tT = 0.25$ and $rR = 0.2$ for (a) Nozzle (b) Spherical Vessel	101
Figure 7- 5: SCF in Sphere due to Internal Pressure (adopted from Ref. [9])	110

Figure 7- 6: Non-Uniqueness of the ρ -SCF Plots with the Vessel's Geometric Ratios for (a) $tT = 1.0$ (b) $tT = 0.5$ (c) $tT = 0.25$ (d) $tT = 0$	110
Figure 7- 7: FEM/Exact (dashed line) and Approximate (continuous line) Variation of Maximum SCF with Geometric Ratios for $RT = 100$: (a) Vessel (b) Nozzle.....	112
Figure 7- 8: Variation of SCF in the Spherical Vessel (right set of graphs) and Nozzle (left set of graphs) with Geometric Ratios for Constant $RT = 50$	113
Figure 7- 9: Variation of SCF in the Spherical Vessel (right set of graphs) and Nozzle (left set of graphs) with Geometric Ratios for Constant $RT = 75$	113
Figure 7- 10: Variation of SCF in the Spherical Vessel (right set of graphs) and Nozzle (left set of graphs) with Geometric Ratios for Constant $RT = 100$	114
Figure 7- 11: Variation of SCF in the Spherical Vessel (right set of graphs) and Nozzle (left set of graphs) with Geometric Ratios for Constant $RT = 125$	114
Figure 7- 12: Variation of SCF in the Spherical Vessel (right set of graphs) and Nozzle (left set of graphs) with Geometric Ratios for Constant $RT = 150$	115
Figure 7- 13: Vessel-Nozzle Juncture with Difference in the Location of the Maximum Stresses: (a) Vessel-Nozzle Orientation and Position Variables (b) $tT = 0.25$, $RT = 50$ and $rR = 0.1$ (c) $tT = 1.0$, $RT = 75$ and $rR = 0.4$ (d) $tT = 1.5$, $RT = 150$ and $rR = 0.5$	116
Figure 8- 1: Quarter Model for the Cylindrical Vessel-Nozzle Juncture (a) Geometry (b) Mesh	122
Figure 8- 2: Variation of the Four Types of Stresses in the Main Cylindrical Vessel for a Typical Vessel-Nozzle Juncture with $RT = 50$, $tT = 0.5$ and $rR = 0.1$	123
Figure 8- 3: Variation of the Four Types of Stresses in the Cylindrical Nozzle for a Typical Vessel-Nozzle Juncture with $RT = 50$, $tT = 0.5$ and $rR = 0.1$	124
Figure 8- 4: von Mises Stress Plot for the Top Surface of a Typical Vessel-Nozzle Configuration with $RT = 50$, $tT = 0.5$ and $rR = 0.1$	124
Figure 8- 5: Comparison between Predictions of the Present Work with other Established SCF Models for $RT = 50$ and (a) $tT = 0.25$ (b) $tT = 0.5$ (c) $tT = 0.75$ (d) $tT = 1.0$ (e) $tT = 1.25$ (f) $tT = 1.5$	134
Figure 8- 6: Comparison between Predictions of the Present Work with other Established SCF Models for $RT = 100$ and (a) $tT = 0.25$ (b) $tT = 0.5$ (c) $tT = 0.75$ (d) $tT = 1.0$ (e) $tT = 1.25$ (f) $tT = 1.5$	135
Figure 8- 7: Comparison between Predictions of the Present Work with other Established SCF Models for $RT = 150$ and (a) $tT = 0.25$ (b) $tT = 0.5$ (c) $tT = 0.75$ (d) $tT = 1.0$ (e) $tT = 1.25$ (f) $tT = 1.5$	136
Figure 8- 8: Variation of SCF in the Cylindrical Vessel (left set of graphs) and Nozzle (right set of graphs) with Geometric Ratios for Constant $RT = 50$ as predicted by the FEM	138
Figure 8- 9: Variation of SCF in the Cylindrical Vessel (left set of graphs) and Nozzle (right set of graphs) with Geometric Ratios for Constant $RT = 75$ as predicted by the FEM	138
Figure 8- 10: Variation of SCF in the Cylindrical Vessel (left set of graphs) and Nozzle (right set of graphs) with Geometric Ratios for Constant $RT = 100$ as predicted by the FEM	139
Figure 8- 11: Variation of SCF in the Cylindrical Vessel (left set of graphs) and Nozzle (right set of graphs) with Geometric Ratios for Constant $RT = 125$ as predicted by the FEM	139
Figure 8- 12: Variation of SCF in the Cylindrical Vessel (left set of graphs) and Nozzle (right set of graphs) with Geometric Ratios for Constant $RT = 150$ as predicted by the FEM	140
Figure 9- 1: Axi-Symmetric Model for the Spherical Vessel-Nozzle Juncture (a) Geometry (b) Corner Fillet and Lines (shown in dark) for Stress Evaluation	143
Figure 9- 2: Geometry Discretization (a) Overall mesh (b) Refined Mesh at the Junction	144
Figure 9- 3: Variation of the Four Types of Stresses in the Main Spherical Vessel for a Typical Vessel-Nozzle Juncture with $RT = 50$, $tT = 0.5$ and $rR = 0.05$	145

Figure 9- 4: Variation of the Four Types of Stresses in the Cylindrical Nozzle for a Typical Vessel-Nozzle Junctionure with $RT = 50$, $tT = 0.5$ and $rR = 0.05$	145
Figure 9- 5: von Mises Stress Plot for a Typical Vessel-Nozzle Configuration with $RT = 50$, $tT = 0.5$ and $rR = 0.05$	146
Figure 9- 6: Stress Raising Effect of Fillet in Area Replacement Method (adopted from [92]).....	149
Figure 9- 7: Variation of SCF in the Spherical Vessel (left set of graphs) and Nozzle (right set of graphs) with Geometric Ratios for Constant $RT = 50$ as predicted by the FEM.....	152
Figure 9- 8: Variation of SCF in the Spherical Vessel (left set of graphs) and Nozzle (right set of graphs) with Geometric Ratios for Constant $RT = 75$ as predicted by the FEM.....	153
Figure 9- 9: Variation of SCF in the Spherical Vessel (left set of graphs) and Nozzle (right set of graphs) with Geometric Ratios for Constant $RT = 100$ as predicted by the FEM.....	153
Figure 9- 10: Variation of SCF in the Spherical Vessel (left set of graphs) and Nozzle (right set of graphs) with Geometric Ratios for Constant $RT = 125$ as predicted by the FEM.....	154
Figure 9- 11: Variation of SCF in the Spherical Vessel (left set of graphs) and Nozzle (right set of graphs) with Geometric Ratios for Constant $RT = 150$ as predicted by the FEM.....	154
Figure 10- 1: Quarter Model for the Cylindrical Vessel-Nozzle Junctionure (a) Geometry (b) Lines (shown in dark) for Stress Evaluation to avoid Singularity	156
Figure 10- 2: Geometry Discretization (a) Overall Mesh (b) Refined Mesh at the Junction.....	157
Figure 10- 3: Variation of the Four Types of Stresses in the Main Cylindrical Vessel for a Typical Vessel-Nozzle Junctionure with $RT = 50$, $tT = 0.5$ and $rR = 0.05$	158
Figure 10- 4: Variation of the Four Types of Stresses in the Cylindrical Nozzle for a Typical Vessel-Nozzle Junctionure with $RT = 50$, $tT = 0.5$ and $rR = 0.05$	158
Figure 10- 5: von Mises Stress Plot for a Typical Vessel-Nozzle Configuration with $RT = 50$, $tT = 0.5$ and $rR = 0.05$	159
Figure 10- 6: Comparison between Prediction of the Present Work with other Established SCF Models for $RT = 50$ and (a) $tT = 0.25$ (b) $tT = 0.5$ (c) $tT = 0.75$ (d) $tT = 1.0$ (e) $tT = 1.25$ (f) $tT = 1.5$	162
Figure 10- 7: Comparison between Prediction of the Present Work with other Established SCF Models for $RT = 100$ and (a) $tT = 0.25$ (b) $tT = 0.5$ (c) $tT = 0.75$ (d) $tT = 1.0$ (e) $tT = 1.25$ (f) $tT = 1.5$	163
Figure 10- 8: Comparison between Prediction of the Present Work with other Established SCF Models for $RT = 150$ and (a) $tT = 0.25$ (b) $tT = 0.5$ (c) $tT = 0.75$ (d) $tT = 1.0$ (e) $tT = 1.25$ (f) $tT = 1.5$	164
Figure 10- 9: Variation of SCF in the Cylindrical Vessel (left set of graphs) and Nozzle (right set of graphs) with Geometric Ratios for Constant $RT = 50$ as predicted by the FEM	166
Figure 10- 10: Variation of SCF in the Cylindrical Vessel (left set of graphs) and Nozzle (right set of graphs) with Geometric Ratios for Constant $RT = 75$ as predicted by the FEM	166
Figure 10- 11: Variation of SCF in the Cylindrical Vessel (left set of graphs) and Nozzle (right set of graphs) with Geometric Ratios for Constant $RT = 100$ as predicted by the FEM	167
Figure 10- 12: Variation of SCF in the Cylindrical Vessel (left set of graphs) and Nozzle (right set of graphs) with Geometric Ratios for Constant $RT = 125$ as predicted by the FEM	167
Figure 10- 13: Variation of SCF in the Cylindrical Vessel (left set of graphs) and Nozzle (right set of graphs) with Geometric Ratios for Constant $RT = 150$ as predicted by the FEM	168
Figure 11- 1: Typical Variation of SCF with rR and RT for $tT = 1.25$ and the Corresponding 2-D Fit for the (a) Vessel, and (b) Nozzle	173

Figure 11- 2: Typical 1-D Fitting of the SCF in the Nozzle for $rR = 0.5$ and $RT = 150$	174
Figure 11- 3: Comparison between Predictions by the Actual Analytical Solution and the Proposed Models for (a) Q , and (b) M	176
Figure B1: Variation in the Location of the Maximum Stresses for Different Selected Geometric Ratios	176

NOMENCLATURE

The following nomenclature is used in this proposal. Other symbols are explained where they appear in the text.

ν	Poisson's ratio
E	Modulus of elasticity
φ	Colatitude angle
p	Internal pressure
R_n	Nozzle radius
R_v	Vessel radius
T_n	Nozzle thickness
T_v	Vessel thickness
V	Angle of rotation of a tangent to a meridian
Q_φ	Shearing force per unit length
N_φ	Normal stress in the meridional direction per unit length
N_θ	Normal stress in the direction of the parallel circle per unit length
M_φ	Meridional bending moment per unit length
M_θ	Bending moment in the direction of the parallel circle per unit length
δ	Horizontal displacement of a point on the parallel circle
u	Displacement in the direction of the tangent to the parallel circle
v	Displacement in the direction of the tangent to the meridian
w	Radial displacement

SCF Stress concentration factor

σ_a Axial stress

σ_h Circumferential/Hoop stress

$D_v = \frac{ET_v^3}{12(1-\nu^2)}$ Vessel's flexural stiffness

$D_n = \frac{ET_n^3}{12(1-\nu^2)}$ Nozzle's flexural stiffness

F Stress function

β Curvature parameter

$$\rho = \frac{R_n}{\sqrt{R_v T_v}}$$

i Imaginary number

DISSERTATION ABSTRACT

Name: Faisal Muhammad Mukhtar
Title: Analytical and Numerical Analysis of Spherical and Cylindrical Pressure Vessels with Small-Diameter Nozzles
Major Field: Civil Engineering (Structures)
Date of Degree: May, 2015

In most cases, shell theory is used in analyzing pressure vessel-nozzle junctures as regions that constitute potential sources of weakness as a result of the high stress concentrations developed. Exact analytical methods are available for spherical vessel-nozzle intersections. However, they are unfit for practical design purposes unless when approximated. The problem is compounded in the case of cylindrical vessel-nozzle junctures because, coupled with the high level of complexity and non-readiness for handy analysis of practical design problems, the available analytical shell solutions are not exact. Furthermore, for both the spherical and cylindrical vessels, these solutions cease to hold when the nozzle configuration violates the thin shell assumption. This raises a concern when a need arises to analyze spherical and cylindrical vessels intersected by small-diameter nozzles. Again, most of the analyses available in the literature concentrate on evaluating the vessel stresses, paying little or no attention to the nozzle. Many researchers have pointed out the shortcoming of such approach, yet no studies have been dedicated to report, simultaneously, a comprehensive behavior of both the vessel's and nozzle's stresses in their analyses.

This research work develops and studies FEM solution models (valid for any nozzle diameter) of discontinuity stresses in spherical and cylindrical vessels. Two different theories, the shell and the elasticity theories, are used to solve the vessel problem intersected by moderate-to-large-diameter nozzles and small-diameter nozzles, respectively. Adequacy of the approximate analytical solutions for the spherical shells relative to the exact and FEM solutions is also studied in the analysis. Illustrations are made on how the developed models perform better than many existing ones in terms of consideration of the possibility of critical stresses existing in the nozzles rather than only in the main vessel. Design charts are developed for the vessels with moderate-to-large-diameter nozzles and augmented by those with small-diameter nozzles to yield the overall design charts valid for any possible nozzle dimension. Contrary to the common practice in the literature, the developed charts are presented in such a way to depict the location of maximum stresses on the juncture. In addition, they provide an alternative presentation of the SCF values that are believed to be more accurate and all-encompassing than the conventional ρ -SCF plots. Finally, handier analytical and empirical closed-form SCF models for regions around the vessel-nozzle intersections are developed. The results generated in this study form a large database that has been missing in the previous collection of literature. Hence, it becomes handy for possible usage by any other interested researcher for future studies.

DOCTOR OF PHILOSOPHY
KING FAHD UNIVERSITY OF PETROLEUM AND MINERALS
Dhahran, Saudi Arabia.

DISSERTATION ABSTRACT (ARABIC)

ملخص الرسالة

الاسم الكامل: فيصل محمد مختار

عنوان الرسالة: التحليل والتمثيل العددي لضغط الأوعية الكروية والاسطوانية مع فتحات ذات قطر صغير

التخصص : الهندسة المدنية (انشاءات)

تاريخ الدرجة العلمية: مايو 2015م

انه في معظم الحالات، يتم استخدام نظرية القشريات في تحليل الضغط عند مناطق اتصال الفتحات والتي تشكل مصادر محتملة للضعف نتيجة للتركيزات العالية للإجهادات. هناك أساليب تحليلية دقيقة متاحة للفتحات في الأوعية الكروية. ومع ذلك، فهي غير صالحة للأغراض العملية للتصميم إلا عن طريق التقريب. المشكلة تتزايد في حالة الفتحات في الأوعية الاسطوانية لأنها عالية التعقيد وغير قابلة للتحليل بشكل مفيد للتصاميم العملية، كما ان حلول التحليلية للقشريات المتاحة ليست دقيقة. وعلاوة على ذلك، فانه لكلا من الاوعية الكروية والاسطوانية، تعتبر هذه الحلول غير قابلة عندما تكون ترتيب الفتحات لا يتناسب مع فرضيات القشريات الدقيقة. وهذه تنشأ عندما تكون الحاجة إلى تحليل الاوعية الكروية والاسطوانية عند الفتحات ذات القطر الصغير. ومرة أخرى، فان معظم التحليلات المتاحة في الابحاث السابقة كانت مركزة على تقييم الاجهادات للأوعية ، مع اهتمام ضئيل أو معدوم إلى اجهادات الفتحات. وقد أشار العديد من الباحثين الى هذا النقص في النهج، ولكنه لم توجد الى الان دراسات تبحث في وقت واحد سلوك الإجهادات في كلا من الاوعية و عند الفتحات.

هذا العمل البحثي يقوم على التطوير والدراسة لنماذج حل FEM (بحيث تكون صالحة لأي فتحة وباي قطر) ولعدم استمرارية الاجهادات في الأوعية الكروية والاسطوانية. تم استخدام نظريتين مختلفتين، نظرية القشريات والمرونة، لحل مشكلة الاوعية التي تتقاطع معها فتحات ذات قطر بين متوسطة وكبيرة وفتحات ذات قطر الصغير، على التوالي. حيث تم دراسة الدقة للتحليل التقريبي لحلول القشريات الكروية بالعلاقة مع FEM. وتم الايضاح ان النماذج المطورة كان أدائها أفضل بمقارنتها من تلك الموجودة وذلك باعتبار احتمالية الاجهادات الحرجة الموجودة في الفتحات والاقتصار في دراسة اجهادات الاوعية الرئيسية. وتم تطوير مخططات لتصميم الاوعية مع

فتحات بين متوسطة وكبيرة القطر و تم مناقشتها مع تلك ذو الفتحات الصغيرة القطر وذلك لإنتاج مخططات تصميم عامة وصالحة لأي فتحة ولأي قطر ممكن. وخلافا للشائع في الابحاث السابقة تم عرض المخططات البيانية المتقدمة لتمثيل الموقع الأقصى للإجهادات عند نقاط الاتصال. بالإضافة إلى ذلك أنها توفر عرضا بديل لقيم SCF التي يعتقد أنها تكون أكثر دقة وشمولية من رسومات p-SCF الاعتيادية. أخيرا، وضعت تحاليل ونماذج تجريبية ل SCF للمناطق حول نقاط اتصال الاوعية مع الفتحة. النتائج التي تم التوصل لها في هذه الدراسة تشكل قاعدة بيانات كبيرة والتي كانت مفقودة في المجموعة الابحاث السابقة. وبالتالي، تصبح في متناول الايدي لاحتمال استخدامها من قبل أي باحث آخر في الدراسات المستقبلية.

**DOCTOR OF PHILOSOPHY
KING FAHD UNIVERSITY OF PETROLEUM AND MINERALS
Dhahran, Saudi Arabia.**

CHAPTER ONE

INTRODUCTION

1.1 GENERAL

As leak proof containers, pressure vessels are designed to house fluid media under pressures and other operating conditions. They are used in a variety of applications ranging from small scale private to large scale industrial sectors such as in mining or oil refineries and plants, nuclear reactor vessels, distillation towers, storage vessels for liquefied gases, recompression chambers, e.t.c. Commonly used shapes of these vessels are cylindrical, spherical, elliptical, e.t.c.

To satisfy requirements of inlet and outlet purposes, openings in pressure vessels are inevitable. Therefore, use is made of nozzles to serve as the channels through which the discharge and/or intake of the pressurized fluid is achieved. Although other shapes are possible but these nozzles are most commonly cylindrical in shape. The effect of discontinuity in the vessel's geometry due to the presence of nozzles causes stress concentrations around the vessel-nozzle junction. As a result, failure of the overall component starts around that region. This necessitates detailed analysis of such critical regions for safer design.

In most cases, shell theory is used in analyzing the problems. Exact analytical methods are available for spherical vessel-nozzle intersections. However, they are unfit for practical design purposes unless when approximated. The problem is compounded in the case of cylindrical vessel-nozzle junctures because, coupled with the high level of

complexity and non-readiness for handy analysis of practical design problems, the available analytical shell solutions are not exact. Furthermore, for both the spherical and cylindrical vessels, these solutions cease to hold when the nozzle configuration violates the thin shell assumption. This raises a concern when a need arises to analyze spherical and cylindrical vessels intersected by small-diameter nozzles. Again, most of the analyses available in the literature concentrate on evaluating the vessel stresses, paying little or no attention to the nozzle. Many researchers have pointed out the shortcoming of such approach, yet no studies have been dedicated to report, simultaneously, a comprehensive behavior of both the vessel's and nozzle's stresses in their analyses.

Modeling and analyses of spherical and cylindrical vessel intersections with cylindrical nozzles of any size will be tackled in this research. Special treatment to vessels with small diameter nozzles will be well focused. Only internal pressure loading mode will be considered. The motivation behind this is the fact that it is the only loading encountered during the pressure testing (hydrostatic or pneumatic) that is usually conducted on newly fabricated or repaired and altered pressure vessels.

1.2 RESEARCH SIGNIFICANCE

In spite of the growing interest by the relevant industries in the safe and economical design of pressure vessels, there still exist some limitations in the available analysis tools and methods when applied to certain geometries of vessel-nozzle configuration. While the rigorous analytical shell solutions are exact in case of spherical vessels, giving solutions for any geometrical ratios, they don't lend themselves so readily to practical design purposes thereby necessitating the adoption of many approximations. The limitations of the approximate solutions, on the other hand, make it less versatile for

certain cases of vessel-nozzle configuration. On the other hand, analytical methods of solutions for cylindrical vessels are highly mathematically involved and yet non-exact in nature.

In addition, the literature covering the analytical aspect of the problem stays relatively dormant after the late seventies. This difficulty motivates the current practice in utilizing numerical tools for the analyses of pressure vessels. The numerical tools require running the specific problem of interest, each time the need arise, using commercial software that require special trainings in addition to the issue of accessibility in some cases. Even when accessible, validation of the numerical results is needed in most cases which is, in some instances, difficult using the existing analytical tools. A need to develop a handy and versatile analytical solution model to study the behavior of these pressure vessels without going into the complex and unfamiliar mathematics is, therefore, evident. Lack of versatile tools for analysis may result in inadequate design that may lead to catastrophic structural failures causing destructions of lives and properties.

Apart from some other secondary benefits, the approach in this study has two obvious primary merits: Furnishing the design industry with handy formulas without the necessary need for numerical simulations and serving as a means of validating, more readily, the numerical simulations if the need be.

The results generated in this study form a large database that has been missing in the previous collection of literature. Hence, it becomes handy for possible usage by any other interested researcher for future studies. Furthermore, the work has the potential of creating more awareness to the relevant industries about how the developed tools can be

helpful in specifying the required pressure vessel-nozzle intersection configuration, thereby establishing confidence in its use. This will help to establish it as a tool in the optimum design of such components.

1.3 RESEARCH AIM AND OBJECTIVES

The aim of the research is development and validation of the solution model, fit for practical computations and design purposes, of stresses for regions around the intersection of pressurized spherical and cylindrical pressure vessels with nozzle diameters ranging from small to large sizes. This will mitigate the need for rigorous and ‘nasty’ calculations needed as established in the literature. Achievement of the above aim will be realized by accomplishing the following primary objectives.

1. Computer implementation of both exact and approximate analytical solutions for the spherical vessel-cylindrical nozzle intersections.
2. Development of finite element models for the spherical vessel-cylindrical nozzle and cylindrical vessel-cylindrical nozzle intersections.
3. Running a large number of finite element simulations for regions around spherical vessel-cylindrical nozzle and cylindrical vessel-cylindrical nozzle and analytical simulations for spherical vessel-cylindrical nozzle intersections of various geometrical ratios to obtain the generic stresses due to internal pressure.
4. Development of a simplified and non-dimensionalized closed-form model, suitable for design purposes, of the stresses due to internal pressure, around spherical vessel-cylindrical nozzle intersection that is valid for any colatitude angle \emptyset .

5. Development of design charts for spherical and cylindrical vessels intersected by radial cylindrical nozzles.
6. Obtain closed-form solution models, as against the conventional graphical representation, of the stress concentration factors for regions around spherical vessel-cylindrical nozzle and cylindrical vessel-cylindrical nozzle intersections.
7. Validation of the developed models and explanations on the ability of the adopted presentation style for the design charts to perform better than many approaches commonly utilized in the literature.

1.4 SCOPE AND LIMITATIONS

Throughout the analyses, the material of the shell is considered homogeneous, isotropic and linearly elastic. Consequently, it will be described in terms of two parameters ν and E .

1.5 RESEARCH METHODOLOGY

The accomplishment of the aim of this research work requires ten major tasks to be completed as outlined below.

1.5.1 Literature Review

A comprehensive literature review in the areas related to the proposed research, including review of literature focusing on

1. Analytical solution of stresses around a spherical vessel-cylindrical nozzle junction.

2. Numerical analysis of stresses around a spherical vessel-cylindrical nozzle junction.
3. Analytical solution of stresses around a cylindrical vessel-cylindrical nozzle junction.
4. Numerical analysis of stresses around a cylindrical vessel-cylindrical nozzle junction.

1.5.2 Selection of Geometrical Ratios to be used in the Analyses

This task was undertaken with the sole aim to identify those geometrical ratios of the vessel-nozzle components that qualifies the nozzle under consideration as a small diameter type or otherwise. In case of the spherical vessels this implies investigating the adequacy or otherwise of the approximate solution methods. In case of both the spherical vessel-nozzle and cylindrical vessel-nozzle components this task will justify the use of solid element to model the vessels with small diameter nozzles based on which different solution and design charts to supplement those of vessels with moderate-to-large-diameter nozzles are developed.

1.5.3 Selection of Software for Numerical Simulation

The basic software packages used in this research are COMSOL [1] and MATHEMATICA [2] for the finite element and analytical approaches, respectively. The use of MATHEMATICA helps in writing and running the codes for the analytical solutions of spherical vessel-cylindrical nozzle problems as well as post-processing numerical results obtained using the COMSOL software.

1.5.4 Computer Implementation of Analytical Solutions

Analytical solution of the spherical vessel with moderate-to-large diameter nozzles was achieved with the aid of MATHEMATICA software package. Two different codes were written, one each for the exact and approximate analytical solutions.

1.5.5 Development of Finite Element Models

Based on the shell theory, finite element models for the spherical and cylindrical vessels with moderate-to-large diameter cylindrical nozzle intersections were developed. Similar models were developed for the vessels with small diameter nozzles using the solid elements based on the elasticity theory. COMSOL software package was used throughout the finite element models' development.

1.5.6 Analytical Simulation of the Selected Pressurized Vessel-Nozzle Configurations

Analytical solutions for the identified geometrical ratios were obtained using the popular models reported in the literature for the spherical vessels intersected by moderate-to-large diameter cylindrical nozzles. The analyses are based on both the exact and approximate methods for thin shell analysis. Degree of deviations of the approximate from the exact models was studied for the purpose of ascertaining the adequacy of the approximate models.

1.5.7 Numerical Simulation of the Selected Pressurized Vessel-Nozzle Configurations

Using the shell model in the COMSOL finite element package, several numerical simulation runs were carried out on both the spherical vessel-cylindrical nozzle and cylindrical vessel-cylindrical nozzle junctures. Validation was made against the analytical

results in case of the spherical vessels, and against the literature results in case of the cylindrical vessels.

Since the validity of shell assumption fails in most cases of vessels with small diameter nozzles use of solid models were utilized to obtain numerical solutions for the cylindrical and spherical vessels intersected by cylindrical nozzles of small diameters.

1.5.8 Development of Design Charts

Parametric analyses of the solutions obtained in 1.5.6 and 1.5.7 were carried out and used to develop design charts for the spherical vessel-cylindrical nozzle and cylindrical vessel-cylindrical nozzle junctures. The charts are drawn in such a way to reflect the contribution of each of the three geometric parameters rR , RT and tT , in contrast to the widely adopted p-SCF graphical representation whose accuracy is doubted for some combinations of the geometric ratios. Ranges of the design curves developed based on the shell and solid elements, respectively, representing vessels with moderate-to-large diameter and those with small diameter nozzles are identified.

1.5.9 Development of Closed-Form Solution Models for the Stress Concentration Factors

Closed-form expression of SCF in the cylindrical and spherical pressure vessels are proposed in this research and are explained under this task.

1.5.6.1 Models for the Spherical Vessel - Cylindrical Nozzle Junctures

Closed form expressions of SCF are obtained for pressurized spherical vessel-cylindrical nozzle juncture. These expressions, based on the popular Hetenyi's analytical solution,

can be used to substitute the more conventional graphical form of presentation. To simulate the phenomenon in a more general sense, non-dimensionalized forms of the solutions are reported as functions of the vessel-nozzle geometrical ratios. Illustrations are made on the application of the symbolic expressions so derived to study the location of maximum stresses on the juncture as well as provide an alternative presentation of the SCF plots that are believed to be more accurate and all-encompassing than the conventional ρ -SCF plots. Another more simplified set of closed-form SCF solutions is obtained based on statistical approach on the results of a parametric analysis.

1.5.6.2 Models for the Cylindrical Vessel - Cylindrical Nozzle Junctions

The mathematics involved in this situation is far more involved than that of spherical shells, the problem being non-axisymmetric. Popular approximate solutions with unanimous acceptance suitable for design purposes (as is the case with Hetenyi's solution for spherical shells) have not been documented for the cylindrical vessels with circular cut-out (as part of the vessel-nozzle juncture). Hence, the proposed model in this study was obtained by comprehensive analysis achieved by running numerous FEM-based numerical simulations. The analytical solution that requires complex and rigorous mathematics is, therefore, approximated by a functional relation by fitting the data obtained from the numerical experiments.

1.5.10 Models' Validation

First, for vessels with moderate-to-large-diameter nozzles, the exact analytical and finite element solutions for the spherical vessels and the literature results for the cylindrical vessels are used as sources for the models' validation. Secondly, the literature results are

used to achieve the validation of models for both the spherical and cylindrical vessels with small-diameter nozzles.

CHAPTER TWO

LITERATURE REVIEW

Organization of the content in this section starts by giving a survey of the literature related to the analytical solution of stresses around a Spherical Shell-Cylindrical Nozzle Junction followed by the numerical approaches in obtaining solutions to the same problem. Similar presentation is given for the case of cylindrical Shell-Cylindrical Nozzle Junction.

2.1 ANALYSIS OF SPHERICAL VESSEL - CYLINDRICAL NOZZLE JUNCTION

2.1.1 Analytical Solution

In attempt to provide an analytical solution to the governing equation(s) of the spherical shell, hypergeometric series solution has been reported by some authors such as [3]. The work in [3], however, only concentrates on finding the first integral of the equation and, hence, is applicable only to the case where there exists no hole at the top of the sphere. They made mention, without working it out due to its complexity, of the possibility of obtaining the second integral which can be useful in cases where the sphere is weakened by a hole.

Leckie [4] presented a solution of spherical shell equations, under axisymmetric loading, in terms of Bessel functions. This solution, based on the Langer Asymptotic Solution [5], is valid for all values of the colatitude angle θ . This approach is applied to obtain solution

of spherical shell equations under both axisymmetric and lateral loading by Leckie [6], to asymmetric bending of spherical shells by Leckie and Penny [7] and to spherical vessel-cylindrical nozzle junction by Penny and Leckie [8]. For sufficiently large \emptyset , the solution simplifies to a more convenient form, the Simplified Asymptotic Solutions which, for $n = 0$ or 1 , simplifies to the Hetenyi's solution mentioned subsequently herein.

Graphs of stress concentration factors have been obtained for spherical vessel-cylindrical nozzle geometry by Leckie and Penny [9] based on the solution presented in [4]. Four loading cases, viz. internal pressure, thrust on the nozzle, moment on the nozzle, and shear force on the nozzle, were considered in the study. The application of the stress concentration factors in design were explained and a discussion on the pad size given.

When the ratio of the spherical shell segment's height to base diameter is less than $1/8$, the theory of shallow spherical shell can be utilized in the analysis. Analyses using the shallow shell equations have been reported by many researchers such as [10-12]. This approach is, however, applicable to cases of non-shallow shells provided the stresses are restricted to shallow zones [13].

Since the aforementioned exact solutions are not handy for practical computations, some attempts have been made to come up with approximate solutions as explained in subsection 2.2.1.

2.1.2 Numerical Solution

A comprehensive survey of literature, covering the period from 1976 to 2004, on the use of finite element method in the numerical analysis of pressure vessels (cylinder and/or

spherical) and piping was compiled by Mackerle [14-17]. Another compilation of the literature, on the use of finite and boundary element methods in the analyses of shells and shell-like structures, covering the period from 1999-2001 was given by the same author in Ref. [18]. The coverage of Ref. [18] is not, however, restricted to pressure vessels. The research trend reported in [17] is shown in Figure 2-1. The author categorized the different topics covered into the following.

STR: Linear and nonlinear, static and dynamic, stress and deflection analyses

STA: Stability problems

THE: Thermal problems

FRA: Fracture mechanics problems

CON: Contact problems

FLU: Fluid–structure interaction problems

MAN: Manufacturing of pipes and tubes

WEL: Welded pipes and pressure vessel components

ELE: Development of special finite elements for pressure vessels and pipes

SOF: Finite element software

OTH: Other topics

Taking the number of published papers as the measure of research activity, it can be observed that the stress analysis and fracture mechanics aspects of pressure vessels receive a higher priority in the field.

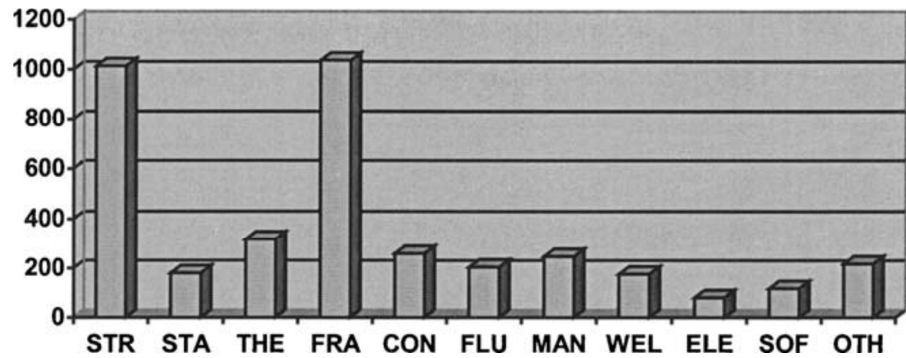


Figure 2- 1: Literature Trend in the Use of Finite Elements for Various Topics in Pressure Vessels and Piping for the Period from 1976 to 2004 [17]

Finite difference method was used by Penny [19] in the analysis of elastic bending of thin shell of revolution subjected to axisymmetric loading and temperature variations. Application of the scheme proved useful when the shell thickness or material properties vary. Five shell element shapes were used to illustrate the capability of the method and validation was made by comparing the results with those of other theories.

A Visual Basic program is developed by Prasad [20] for the analysis of spherical vessel-cylindrical nozzle junction based on the ASME Code formulas. The stresses and displacements of the individual components as well as the whole juncture are determined by discontinuity analysis. Both single and double discontinuity analyses are used to determine the maximum value of the discontinuity forces and moments the component can resist. Validation is achieved using the ANSYS finite element software.

Stress analysis has been carried out by Hardki et al. [21] for nozzle to head junction subjected to applied external load, internal pressure and moments. Use is made of Welding Research Council (WRC) 107 and PV-CodeCalc software (2008) on one hand, and a finite element model using ANSYS in accordance to ASME Section VIII Division 2 on the other.

Al-Gahtani et al. [22] investigated the feasibility of using a local testing as an alternative to the full scale hydrostatic pressure testing of spherical pressure vessels with cylindrical nozzles. Several finite element runs were carried out using different geometric configurations of the vessel, nozzle and cap size in the local testing and comparison made with the full scale loading test. Finally, effect of the cap size was evaluated and conclusion drawn that relatively larger cap diameters must be used before the local testing can simulate the full scale hydrostatic test.

Various analysis methods, based on thin shell theory, were used by Dekker and Brink [23] to obtain the solution of stresses due to pressurized spherical vessel with nozzle attachment. Effect of additional weld material was studied using an axisymmetric 3D finite element model and comparison made using the double discontinuity analysis. Conclusion was reached that any outward weld area offers little reinforcement and that thin shell stress analysis is acceptable.

3D finite element analysis of internally pressurized spherical vessels with cylindrical nozzle attachment is reported by Attwater et al. [24]. Comparison was made between the results achieved and the values found in British Standards for the selected configuration.

Schindler and Zeman [25] examined the stress concentration factors for spherical shell-nozzle connection given in the British Standard Specification for Unfired fusion welded pressure vessels. Comparison was made with the recent finite element simulations. Based on the deviations noticed, possible improvements to the code factors were suggested with the aid of example graphs.

Chaudhari and Jadhav [26] suggested a stress analysis procedure using finite element for pressure vessel-nozzle intersection. Set of recommendations with regards to the element type, size and density of the mesh, transition element size, application of operating loads e.t.c. were given. The procedure reduces modeling and post processing efforts and is applied to a case study of a hydrogen storage tank. Validation of the analysis is achieved by explaining the Welding research council (WRC) methodology.

A finite element analysis for an oblique cylindrical nozzle intersecting a spherical vessel was carried out Naderan-Tahan [27] using ABAQUS software. The emphasis was on stress and strain distributions on both sides of the connection under the action of internal. Although briefly, but the effect of axial load and moment was also studied. The results, in form of stress concentration factors, were presented for various geometric ratios. Variation of the factors was studied for different angles of the nozzle's intersections. Validation of the results was achieved using a literature experimental program and other references. Part of the conclusions drawn is that plotting the SCF is more suitable if made against the parameter R_v / T_v than $\rho = R_n / \sqrt{R_v T_v}$. The former allows the linear interpolation of values thereby reducing the number of models that must be studied.

Luo and Song [28] developed a finite element model to study the effect of round transition on stress distribution of a spherical shell-large diameter nozzle junction. Stress distributions of both flushing and protruding nozzle configurations were analyzed. The results show that, for both the flushing and protruding nozzles, the round transitions have the capability of reducing the stresses compared to those produced in the case of sharp-angled transition. The reduction of up to 8% can be attained.

Optimal shapes of intersecting pressure vessels were sought by Liu et al. [29] using a topology/shape optimization method, the Metamorphic Development, in order to eliminate the stress peaks caused by the opening. Both flush and protruding nozzles were investigated in the study. By growing and degenerating simple initial structures subject to stress constraints, the optimum profiles of minimum mass intersecting structures were obtained. Both rectangular and triangular axisymmetric finite elements were used to arrive at the optimized structures by, metamorphically, developing them in specified infinite design domains for the flush and protruding nozzles, respectively. Detailed elastic finite element analysis was performed to investigate the stress distribution induced due to the applied internal pressure and the effects of profile changes on structural strength. The results prove that the use of protruding nozzle produces better stress distribution than a flush nozzle.

Stress concentration factor of a pressurized sphere-nozzle intersection was determined using a linear elastic finite element analysis by Qadir and Redekop [30]. Both spherical vessels with and without inner-wall thinning damage were modeled using 9-noded 2D axisymmetric elements. The stress concentration factors obtained for the undamaged vessels were verified using the literature experimental and analytical results. Effect of three types of wall-thinning damage, thinning in the nozzle, in the sphere, and in both components, on the stress concentration factor was evaluated. In addition, effect of growth of the local thinned areas on the stress concentration factor was evaluated. Determination of the stress concentration factors for different depths of the local thinned areas was then carried out through a parametric study. Though not directly linked to the topics considered in the present literature review, but part of the study in the above

mentioned reference includes an elastic-plastic fatigue analysis for simulated seismic action for some intersections without and with the local thinned areas.

Finite element analysis was used by Fuad et al. [31] to obtain the stress concentration factors of various adjacent holes configuration in a spherical pressure vessel by adopting the approach of a thin plate, of thickness t , undergoing hydrostatic stresses. The stress concentration factors were based on the Von Mises stress. Six different holes arrangements as shown in Figure 2-2 were adopted. Curves for the stress concentration factors were given with respect to the ratios L/d and d/t . In addition, a formula for employing the results to calculate the allowable stress, for design purpose, was given. Significant effect on the increase in the stress concentration factor with decrease in L/d was reported. While the ratio d/t affects the stress concentration factors for the configurations with two, three and four holes, the effect of this ratio on the same parameter for the last two configurations (with five holes each) is insignificant.

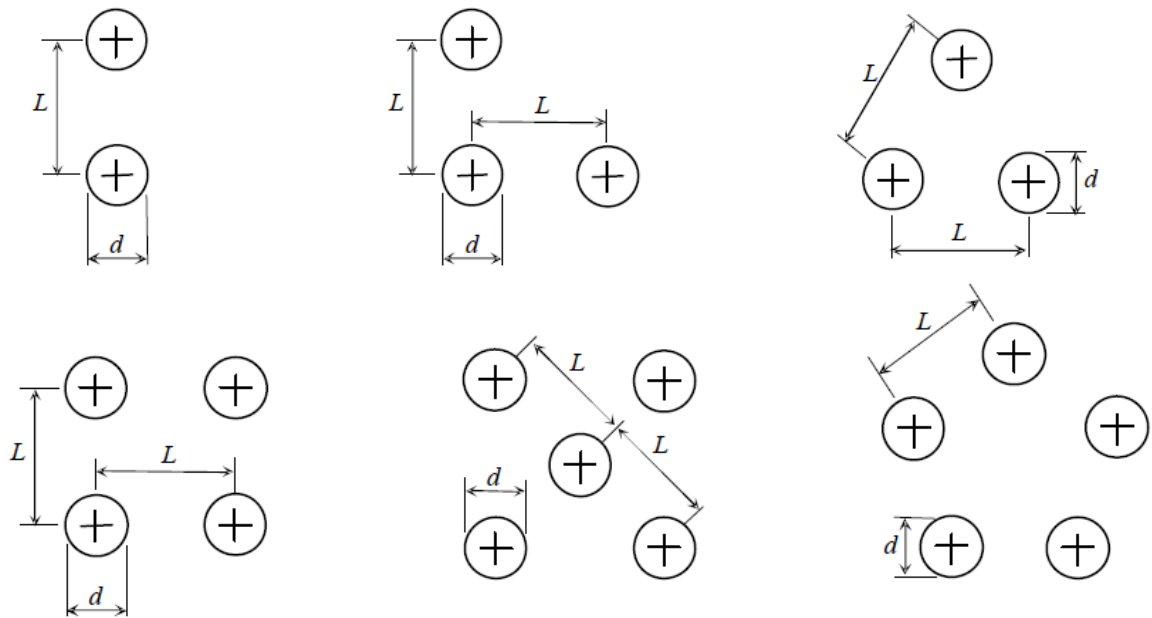


Figure 2- 2: Hole Configurations on the Spherical Vessel Considered by Fuad et al. [31]

2.2 ANALYSIS OF CYLINDRICAL VESSEL - CYLINDRICAL NOZZLE JUNCTION

2.2.1 Analytical Solution

Review of the literature in this section considers both cylindrical shell-cylindrical nozzle intersection and cylindrical shell weakened by a circular hole which is one of the parts of a structure composed of a shell and a branching nozzle.

Naghdi [32] obtained approximate solution, using Donnell's equations of shallow circular cylindrical shell, for stresses in an infinitely long cylindrical shell with weakened by a circular hole subjected to self-equilibrating edge loading. The solutions were first expressed in series containing powers, product of powers, and logarithm of the characteristic parameter βr , where r is the radius of the circular hole. Similar series was used to represent the unknown coefficients of the solution including some constants that depend on the material property and the loading type. These new constants were determined by algebraic manipulations. Examples were given and the accuracy based on some expressions illustrated. In addition, expressions for stress concentration were reported.

Dyke [33] studied the effect of circular hole on cylindrical shell loaded by tension axially, internal pressure and torsion. A single complex differential equation is obtained by manipulating the equations for thin, shallow cylindrical shells. Infinite series of Henkel functions is obtained as the solution based on which the membrane and bending stresses are obtained for intermediate values of the parameter β under the three loading conditions.

Based on his previous formulation in Ref. [34], Lekkerkerker [35] carried out an analytical investigation of stresses around cylinder-to-cylinder intersections. Comprehensive treatment of the problem was given by concentrating more on the cylindrical shell weakened by a circular hole which is one part of a cylindrical shell-cylindrical nozzle component. Expressions of the stress resultants and displacement quantities were given explicitly. Although treatment of boundary conditions is described in general sense, but no mention is made on how the junction analysis with the secondary cylinder (nozzle) can be achieved.

The boundary value problem for the state of stress at the junction of two normally intersecting cylindrical shells under internal pressure has been formulated by Eringen and Suhubi [36], and the resulting equations solved for a small ratio ($<1/3$) of the radii. The edge conditions include those along the intersection curve and at the end of the cylinders. Further analysis of the problem has been given by Maye and Eringen [37].

Using Fourier series and the method of least squares, stress distribution in a circular cylindrical shell was determined by Naghdi and Eringen [38] for self-equilibrating edge load around the lateral surface of the hole. The obtained solution was valid for hole-to-cylinder ratio less than $1/2$. Restriction of this ratio is made to avoid deviation from the true circular arc shape of the intersecting circle. Series form of the solution was obtained and the unknown coefficients of the series determined by expressing the boundary conditions in the form of four infinite series.

A complex variable analytic method was proposed by Diankui and Chao [39] for solving stress concentrations in a cylindrical shell with arbitrary cutout. Graphs of the stress

concentrations obtained by numerical means are given for the shell with circular and elliptic cutout.

Comparison of results from various codes' established calculation methods and finite element method for internal pressure stress intensities at nozzle-cylindrical vessel junctions was carried out by Dekker and Stikvoort [40]. Limitations in some of the calculation methods given in some of these codes were highlighted.

Xue et al. carried out a stress analysis based on the thin shell theory for two normally intersecting cylinders having a large diameter ratio in Ref. [41], for two normally intersecting cylindrical shells having small d/D ratio and subjected to external moments on the ends of main shell in Ref. [42], and for cylindrical shells with normally intersecting nozzles having small d/D ratio and subjected to external branch pipe moments in Refs. [43, 44]. Instead of the Donnell's equations for shallow shells, the modified Morley equation applicable for $R_n / \sqrt{R_v T_v} \ll 1$ is used for the shell with a hole.

Love equation is used to obtain the solution in terms of displacement function for the nozzle with nonplanar end in [41] and Goldenveizer equation for the nozzle with nonplanar end in [42-44]. Expressions of the boundary forces and displacements on the intersecting curve are given as periodic functions of θ and expanded in Fourier series. Numerical quadrature is used to obtain every harmonics of Fourier coefficients of boundary forces and displacements. Other similar works carried out by Xue, Hwang and co-workers are reported in [45-50].

An improved version of the analytical solutions mentioned in the preceding paragraph for two normally intersecting cylindrical shells has been presented in Ref. [51] and their

range of applicability extended from $d/D \leq 0.8$ and $d/\sqrt{DT_v} \leq 8$ to $d/D \leq 0.9$ and $d/\sqrt{DT_v} \leq 12$. A pair of fourth-order complex-valued partial differential equations (exact Morley equations) was solved to obtain the thin shell theoretical solution. Some additional terms (in terms of complex-valued displacement-stress function) to the resultant forces and moments expressions were used to improve the accuracy of the results. The results for seven load cases (i.e. internal pressure and six external branch pipe load components) were verified using a 3D finite element analysis. Ref. [52] presented a design method based on the analytical approach explained above.

2.2.2 Numerical Solution

For larger values of the parameter β , Dyke [33] used a numerical approach, the collocation procedure, to solve the governing shallow cylindrical shells equation (loaded by axial tension and internal pressure) by terminating the series solution at a finite number of terms to satisfy the boundary conditions. Verification of the results is made using other available theoretical works and the available experimental data.

Finite difference, based on the forward difference formula, was adopted by Pattabiraman and Ramamurti [53] in obtaining solution to the problem of stress concentration around a circular cutout in a cylindrical shell. The approach involved, first, obtaining a solution to the cylindrical shell problem without cutout subjected to an asymmetric loading. Negatives of the stress resultants and stress couples at a given radius from the first solution are combined with a transverse shear force to form the edge conditions of the shell with a cutout of radius a . The overall solution is arrived at, by superposing these

two solutions. Results obtained based on this procedure compare well with those of the closed-form solution.

Dekker and Bos [54] carried out several finite element runs for cylindrical shell with nozzle intersection, under external loads and internal pressure, paying attention to both the shell and nozzle wall stresses. Realizing that local load stresses were sometimes found to be much higher in the nozzle than in the shell, the authors formulated a method called ‘modified improved shrink ring method’ and came up with multiplication charts for deriving local load nozzle stresses from local load shell stresses. Also, stresses due to the internal pressure were investigated and presented in graphical form as functions of a non-dimensional parameter relating the nozzle to shell geometry.

Campen and Spaas [55] developed a finite element model for stress and strain analyses of nozzle-to-cylinder intersections for small diameter ratios ($\leq 1/4$). This is an extension of the method for biaxially loaded nozzle-to-flat plate connection presented in Refs. [56] and [57], which is based upon the finite element method of solids of revolution under non-axisymmetric loadings. The method proved to be useful in predicting the peak strains and strain distribution in reinforced nozzle-cylinder intersection. Comparison between the nozzle-to-flat plate and nozzle-to-cylindrical vessel methods is made and their reliability evaluated by comparison with experimental result.

A comprehensive study of local pressure stresses at the pipe-nozzle juncture was presented by Ha et al. [58] using finite element technique. As with many other several researches based on linear elastic analysis, an assumption was made that the influence of weight and temperature are neglected, all the pipe and nozzle ends are assumed to be

fixed and that they are of sufficient lengths to eliminate the possibility of influence from the end boundary conditions. Several plots of local stress factors are given as function of some pipe-nozzle geometrical parameters, namely, nozzle mean radius/pipe mean radius and pipe mean radius/pipe thickness ratios.

The effect of analysis model on the calculation of stress intensity due to internal pressure for the nozzle attached to cylindrical pressure vessel has been addressed by Lu et al. [59]. The practice of analyzing the cylindrical vessel-cylindrical nozzle intersection by simplifying it to a 2D axisymmetric model is examined. To attain stress response having similar effects, the vessel's radius is in some cases taken larger than the actual value. To study such effect Lu et al. used three different simple 2D axisymmetric models with 1, 1.5 and 2 as the ratios of the vessel radius used to the actual radius. This simplified model was used to compute the pressure and bending stresses for some selected sections, and comparison was made with the results evaluated using the 3D finite element model. The conclusion was that the simplified 2D model with vessel radius equal to the actual radius could represent the behavior of the cylindrical vessel-cylindrical nozzle intersection well.

Liang et al. [60] applied the finite element method to examine the curvature and thickness effects on stress concentrations around a circular hole in an opened shallow cylindrical shell under external pressure. The results indicated that resistance to the external pressure is provided more by the shell with a larger curved angle. Similarly, increase in the shell's thickness yields a gradual decrease in the developed stresses. Design data sheets of the stress distributions around the circular hole are provided at the end as a reference for the designer.

Stress and strength analysis of five fiber reinforced plastic (FRP) pipe tees, subjected to internal pressure, was carried out using 3-D finite element method by Xue et al. [61]. Use was made of Wilson's incompatible element and 16-noded element to deal with the problem of the two intersecting FRP pipes. The results show that there is higher stress concentration in tees made from the anisotropic material than those in isotropic material under the same conditions. Also, failure of the anisotropic tees occurs faster than the isotropic ones in the region where the maximum shear stress occurs due to their lesser shear strength.

Skopinsky [62] presented a numerical procedure for the 3-D finite element analysis of shell intersections. Description of the modified mixed variational formulation, a model of an eight-node 3-D finite element and a computer program (SAIS-3D) for stress analysis of the intersecting shells was given. Comparative study of the 3-D and 2-D finite element analyses for stress distribution in the intersection region and the maximum effective stress was conducted for normally intersecting cylindrical shells under internal pressure. The results have shown the practical applicability of a shell-based 2-D finite element solution for the stress analysis of intersecting shells over a wide range of geometric parameters.

Use of finite element analysis software ALGOR was made by Xu et al. [63] to study the behavior of internal pressure stresses at the pipe to nozzle junction with variation of the intersection angle. Four symmetric points around the juncture were selected along which the stress factors in both the circumferential and longitudinal directions are plotted. A pipe-nozzle with geometric parameters, β (ratio of nozzle to pipe mean radii) of 0.5,

and γ (ratio of nozzle to pipe mean thicknesses) of 50.0 was used. The study shows that relatively less severe local stresses are exhibited by juncture with 90° intersection (a standard nozzle). The stresses increase with decrease in the intersection angle and are more severe when the angle of intersection is further decreased from 45° . Good agreement was achieved between the finite element results of the stress factor in the circumferential direction of the pipe and the equation from the ASME boiler and pressure vessel code.

Stress analysis of a cylindrical pressure vessel loaded by axial and transverse forces on the nozzle's free end was carried out by Petrovic [64] using finite elements method. Envelopes of maximum stress values, maximum values on the envelopes and distances between maximum values on envelopes and the nozzle's outer edge were determined from the obtained stress values around the nozzle's region. Algebraic expressions for these stress values were determined and the values obtained from the expressions were within -12.5 and +12.8% of those from the finite elements. Similarly, the maximum difference between experimental and calculated stress values was found to be 12%.

Pressurized cylindrical vessel-nozzle intersection with wall thinning damage, has been analyzed using a 3D finite element technique by Qadir and Redekop [65]. The effect of variation of the extent of wall thinning damage on the stress concentration factor was studied. Parametric study was conducted by computing the stress concentration factor for various tee joint configurations ranging from undamaged to the wall thinning damaged ones. For the undamaged vessel-nozzle juncture and for a fixed vessel diameter-thickness ratio, D/T_v , the results indicate a rise in the stress concentration factor with an increase in the diameter ratio d/D . Similarly, for a fixed d/D ratio, the stress concentration factor

increases with increase in the ratio D/T_v . Effect of the wall thinning was observed to result in increase in the value of stress concentration factor for the junction with $d/D > 0.2$ and a decrease or negligible increase otherwise.

Numerically determined stress concentration factors for nozzle-cylindrical pressure vessel attachment were presented by Kacmarcik et al. [66] and comparison made with experimental results. The investigation was carried out on two different nozzle geometries for the experimental set-up using strain gauges for the strain measurements for subsequent conversion, using the theory of elasticity, to the stresses. For the numerical simulation, use was made of the ABAQUS finite element analysis software considering quarter of the problem due to symmetry. Lengths of the nozzles and their distances from each other, as well as to other discontinuities on the vessel, were selected large enough to not influence the stress distributions and concentrations. Stress concentration factors defined by maximum principal and maximum von Mises equivalent stresses calculated using the two approaches agree very well.

2.3 REINFORCEMENT AROUND PRESSURE VESSEL - NOZZLE JUNCTURE

In cases where the vessel-nozzle stresses are so high, adoption of reinforcement structures is often made. The structure in form of a pad or integral reinforcement, thicker than the parent vessel (either the main vessel or the nozzle), is used for that purpose. Figures 2-3 to 2-5 indicate the three commonly reinforcement configurations used at the vessel-nozzle juncture.

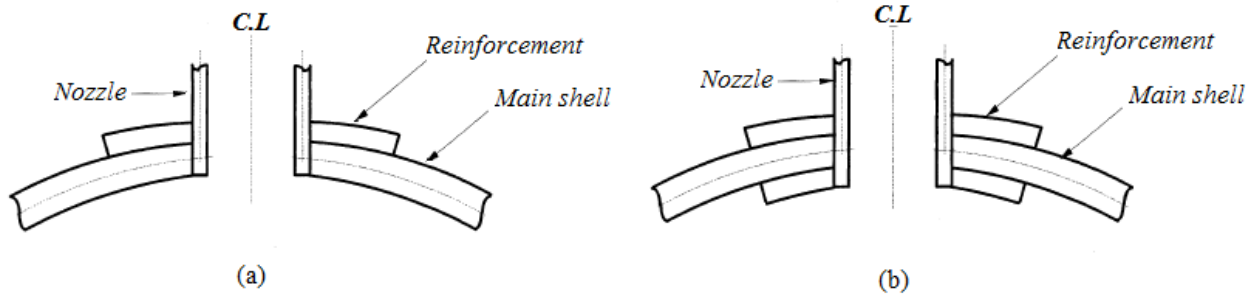


Figure 2- 3: Pad Reinforcement for (a) Flush Nozzle (b) Protruding Nozzle

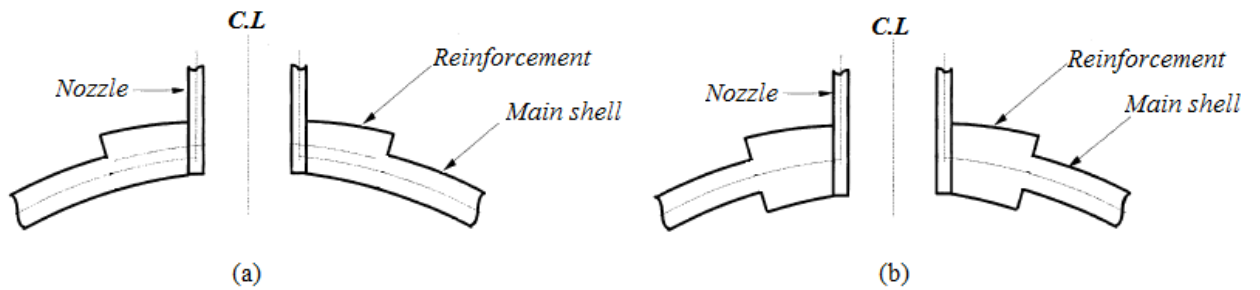


Figure 2- 4: Shell Integral Reinforcement for (a) Flush Nozzle (b) Protruding Nozzle

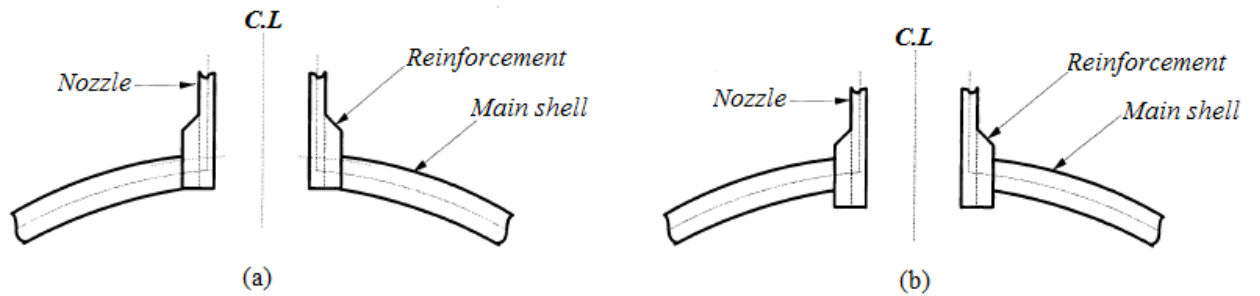


Figure 2- 5: Nozzle Integral Reinforcement for (a) Flush Nozzle (b) Protruding Nozzle

A number of researches have been conducted on the use and analysis/design of nozzle reinforcements for both spherical and cylindrical pressure vessels.

A shallow conical reinforcing pad of constant thickness, as shown in Figure 2-6, was proposed by Calladine [67]. This emerges as a result of a simplified approach based on

plastic design applied to the design problem of reinforcement for openings in thin spherical pressure vessels. The approach was aimed at adjusting the thickness and shape of the vessel around the opening to enable the full limit pressure of the vessel to be carried with relatively little bending action. The proposed reinforcing pad satisfies these requirements. The design has some advantages over the conventional designs in both the plastic and elastic ranges. Unlike the case of unreinforced nozzles, the deformation as a result of steadily increasing the internal pressure does not alter the conical-spherical profile of the vessel and the action is predominantly membrane throughout the elastic, elastic-plastic and plastic ranges.

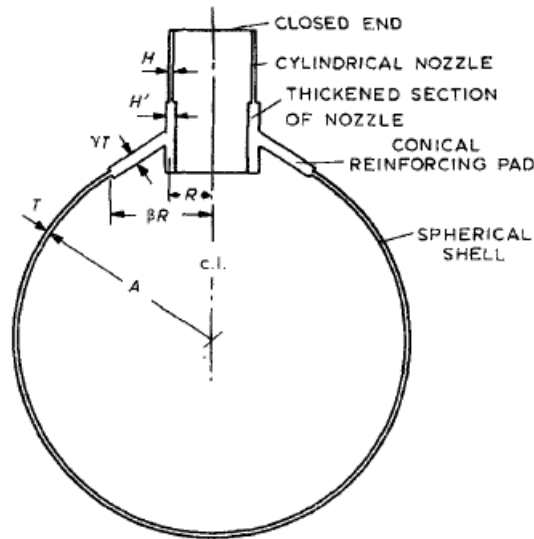


Figure 2- 6: Conical Pad Reinforcement for Nozzle proposed by Calladine [67]

Kitching and Kannas [68] presented a theoretical study showing that a reduction in stress concentration factor can be attained by welding the reinforcement pad to the nozzle alone and neglecting the outer peripheral weld to the main spherical vessel as shown in Figure 2-7. The obvious advantage of their suggested procedure, compared to the common practice of welding the pad to the main vessel at the outer periphery in addition to

welding it to the nozzle at the inner periphery, is attainment of more economical sizes for the reinforcing pad.

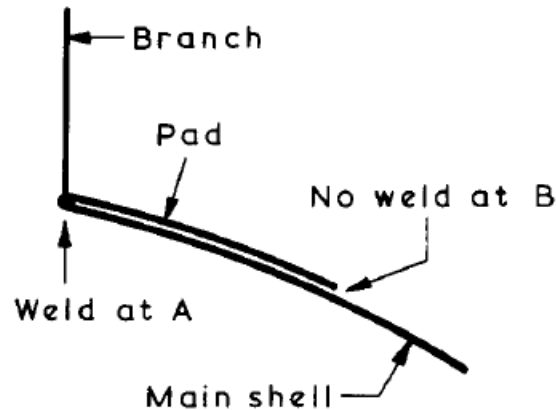


Figure 2- 7: Modified Design of Pad Reinforcement suggested by Kitching And Kannas [68]

Minimum weight approach was used by Yeo and Robinson [69] to analyze a reinforced spherical vessel-cylindrical nozzle intersection. An offset was allowed between the centre-line of the reinforcement and that of the main sphere and the vessel was pressurized with a pressure equal to the limit pressure. The work suggested that, in most circumstances, economical reinforcement may be obtained by making it thicker but less extensive.

Based on literature theoretical and experimental work, charts for the design of pad reinforced nozzles in spherical pressure vessels have been produced by Kannas et al. [70]. They are limited to maximum SCF of 2.25. The maximum principal stress and maximum shear stress yield criteria were both used as bases for the preparation of the charts. Although possible to simplify them for practical design purposes, but these charts are more complex than corresponding charts for integral reinforcement.

Soliman and Gill [71] carried out a theoretical elastic analysis of the stresses caused by a 49.78 kN/m moment applied to a pad reinforced nozzle in a spherical pressure vessel. A 9.5 mm thick pad with 216 mm radius was used to reinforce a 12.7 mm thick spherical vessel with radius of 1830 mm with a nozzle attachment of thickness 12.7 mm and outside diameter 410 mm . Reliability of the analysis was confirmed by experimental results for the stresses except at regions around the weld where the effects of the weld is significant. The same authors presented charts giving the elastic SCF in spherical vessels with pad and integral reinforcements for radial nozzles subjected to radial load and moment in Ref. [72]. Effect of all the geometric parameters are discussed including the limitations of thin shell theory on the validity of the results.

Hsu et al. [73] used a theoretical elastic approach to analyze a radial nozzle in a pad reinforced spherical vessel subjected to a shear force applied at the nozzle/sphere intersection. Based on the maximum principal stress and the maximum shear stress, SCF curves are given for various geometrical parameters. Finally, discussion on the limitations of the thin shell theory based analysis was given.

Use of the approach presented in Ref. [4] for analysis of spherical vessels becomes invalid if the shells (main vessel and the pad) do not join at the intersections of the median lines of their thicknesses or if the pad thickness is so large that the theory of thin shells ceases to apply. For that purpose, Lee and Sohn [74] proposed an approach in which the moment equilibrium equation at the main vessel-reinforcement pad junction is modified by multiplying the vessel edge moment with a correction factor (a cubic function of ratio of the thicknesses of the adjoining parts). Assumptions made are, that middle planes of the reinforcement and the main shell coincide and that the reinforcement

is a thin shell. As a result, use of the formulas given in [75] was adopted and the aforementioned modification made. Three other different approaches, the moment modified, rotation modified and displacement modified methods, were used to solve the same problem and, finally, discussion of the validity of each approach given.

Miranda and Werneck [76] carried out a finite element analysis using ANSYS Workbench to evaluate the stress fields on the vessel-nozzle intersection of cylindrical pressure vessels. Employing the use of 20-node high order solid elements, three 3D models were developed viz: (i) unreinforced vessel-nozzle juncture, (ii) bonded pad reinforced vessel-nozzle juncture (with the pad integrally welded on the vessel-nozzle juncture), and (iii) partially welded pad reinforced vessel-nozzle juncture (with the external periphery of the pad considered bonded, simulating welding lines and friction contact assumed in the pad/vessel contact surface). The third category, more closely, simulates the actual scenario in practice as against the more common modeling approach mentioned in the second category and, hence, is relatively more realistic. Design of the pad was carried out using the Area Replacement Method according to ASME Code. Similar approaches taking into consideration the contact between the reinforcement pad and the main vessel were, earlier, adopted to conduct a finite element analysis of the stresses. See, for example, Refs. [77-79].

Results of a detailed study on the effect of a geometric gap between cylindrical shell and reinforcement pad on the stresses within the region of the junction under a thrust force on the nozzle was presented by Sang et al. [80]. Test nozzles with different gaps were analyzed by both experiment and finite element method. As it is obvious, introduction of the reinforcement pad reduced the stress concentration at the edge of the opening.

However, transference in stress distribution from the edge of the opening to the outside of the pad-cylinder fillet occurs: a high discontinuity stress is induced in the outside region of the pad-cylinder fillet weld. This was attributed to the discontinuity of the geometry and the stiffening effect of the fillet welds. Effect of the gap on the cylinder stresses was reported to be negligible. This was, however, not the case with the nozzle stresses that are somewhat reduced when the gaps increase. A closely related work, but with a moment loading instead, was carried out in Ref. [81].

Using shell theory and finite element method Skopinsky [82] analyzed some models of reinforced and unreinforced nozzle connections under the action of internal pressure and external loads. Comparative study of the reinforcement effects on the maximum stress of radially attached nozzle to main cylindrical vessel intersection was carried out. Some non-dimensional geometric parameters for reinforcements were used in order to see the effect of the choice of a different reinforcement configuration. Results obtained indicate the comparative efficiency of the various typical reinforcements and give useful information for selection of the rational parameters of reinforcement designs. Similar approach was used by Skopinsky and Smetankin [83] to study the effects of reinforcement by carry out stress analysis of reinforced nozzle connections in ellipsoidal heads of pressure. Reinforcement configurations such as the integral, torus transition and protruding nozzle types were considered.

Finlay et al. [84] investigated the effectiveness of finite element data for 92 reinforced butt-welded branch outlet junctions in the light of data for unreinforced fabricated tee junctions. The data suggest that, for thin-walled assemblies, the reinforcement provided

under the ASME B31.3 design is effective for internal pressure load case and all external bending moment loads with the exception of branch out-of-plane bending.

Nash and hitchen [85] carried out a parametric study to determine the optimum diameter of reinforcing pad for nozzles in the knuckle region of an ellipsoidal pressure vessel head. Use of a linear elastic finite element model, available in the ANSYS software, was made. Parameters varied in the study are the nozzle diameter, offset, and wall thickness. Optimum pad sizes achieved were those for the nozzle loads of thrust, in-plane moment and out-of-plane moment. Possibility of calculating the maximum permitted applied stress was made based on the design curves for any nozzle size under the action of one of the aforementioned loading combinations. Some recommendations for allowable offset and treatment of loading combinations were given.

The literature presented above focuses on linear elastic analysis of the reinforced nozzle-vessel attachment. Elastoplastic analysis has also been used to study the problem. For example, Liang et al. [86] used finite element method to carry out stress analysis for opening-reinforcement structures of a cylindrical shell by elastic and elastoplastic constitutive relations. Two sub-models were considered for the pad: integral and contact models. The analysis was carried out for different nozzle sizes and different oblique angles. Similar behavior in the stress distribution of cylindrical shell intersections was achieved between the integral and contact models. However, prediction by the two sub-models shows some differences at the contact surfaces of the shell and the pad. The oblique angle has effect on the stress distribution as well as the maximum stress. But little difference appears in the maximum stress intensity due to varying nozzle diameters. Several other works such as those reported in Refs. [87-91] studied the influence of

vessel-nozzle reinforcement beyond the elastic range assumption. But, since the scope of the present research is limited to linear elastic analysis, no further discussion will be given on the literature covering the non-elastic approach.

2.4 CLOSED-FORM EXPRESSIONS OF SCF FOR PRESSURE VESSEL - NOZZLE JUNCTURES

Lind [92] used a semi-empirical approach, the Area Method, for the analysis of spherical pressure vessel-nozzle intersection. The method reports the stress concentration factor for the average hoop stress, as given in Equation (2.1), as a function of some plane areas around the junction, the thickness and the inside radius of the spherical vessel. Its validity is shown by examples and comparison with the results from photo-elastic tests is made. Similar expression for the stress concentration factor, Equation (2.2), of cylindrical vessel-nozzle junction is given in Ref. [93].

$$K_s = \frac{2GT}{r_i F} \quad \text{for spherical vessel-nozzle connection} \quad (2.1)$$

$$K_s = p \frac{G}{G'} / p \frac{R}{T} = \max\{K_1, K_2\} \quad \text{for cylindrical vessel-nozzle connection} \quad (2.2)$$

where,

$$K_1 = \frac{[1 + 1.77(d/D)\sqrt{D/T} + (d/D)^2\sqrt{s/S}][1 + (T/D)/\sqrt{s/S}]}{1 + (d/D)^2/(s/S)\sqrt{s/S}}$$

$$K_2 = \frac{[1.67\sqrt{s/S}\sqrt{D/T} + 0.565(d/D)][1 + (T/D)/\sqrt{s/S}]}{0.67\sqrt{s/S}\sqrt{D/T} + 0.565(d/D)/(s/S)}$$

$$s = d / (2t), \quad S = D / (2T)$$

The shaded areas G , G' and F and the geometric dimensions are as indicated in the relevant figure.

In both the two cases above, the effect of fillet (bending correction) is accounted for by multiplying the above expression for K_s with a factor K_b , which depends on the geometry of the intersection, to give the total stress concentration factor as follows.

$$K = K_s \times K_b \quad (2.3)$$

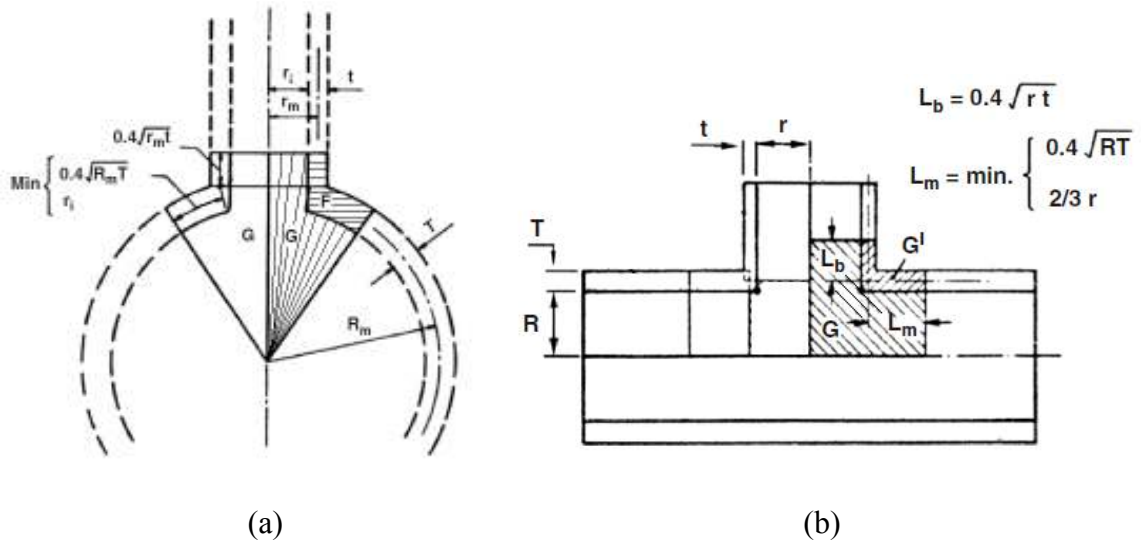


Figure 2- 8: Idea of Area Replacement Method adopted in Refs. [92] and [93] for (a) Spherical Vessel (b) Cylindrical Vessel

Leckie et al. [94] expressed the stress concentration factor of spherical shell with elliptical opening in terms of that of flat plate and a single geometrical variable as follows.

$$K_{shell} = K_{flat\ plate} \times (1 + 1.53\rho) \quad (2.4)$$

where, $\rho = \frac{a}{R} \sqrt{\frac{R}{T}}$ and a is the dimension of the minor axis of the elliptical hole.

The above relation implies that, for a given value of R/T , the maximum stresses are linearly related to the aspect ratio of the elliptical opening a/b and also its size in relation to the shell a/R .

Based on statistical analysis on many pressurized cylindrical vessel-nozzle junctions Money [95] proposed Equation (2.5).

$$K = 2.5 \left[\left(\frac{r}{t} \right)^2 \frac{T}{R} \right]^n \quad (2.5)$$

where,

$$n = \begin{cases} 0.2042, & r/R < 0.7 \\ 0.24145, & r/R > 0.7 \end{cases}$$

Based on the consideration that forces acting on a longitudinal plane of symmetry must be balanced by the hoop stresses in shell and nozzle within restricted surface limits, Decock [96] proposed his expression of the SCF thus.

$$K = \frac{2 + 2 \frac{d}{D} \sqrt{\frac{d}{D} \frac{t}{T}} + 1.25 \frac{d}{D} \sqrt{\frac{D}{T}}}{1 + \frac{t}{T} \sqrt{\frac{d}{D} \frac{t}{T}}} \quad (2.6)$$

Using the least squares method, empirical polynomial equation for the prediction of stress concentration factors for pressurized cylindrical vessel with nozzle has been obtained by Xie and Lu [97]. The stress concentration factors are functions of the ratios nozzle-to-vessel diameter, vessel diameter-to-thickness and nozzle-to-vessel thickness as follows.

$$K = 2.87 + \left[1.38 - 0.72 \left(\frac{t}{T} \right)^{0.5} \right] \left(\frac{D}{T} \right)^{0.43} \left(\frac{d}{D} \right)^{0.9} - \left(\frac{t}{T} \right)^{0.5} \quad (2.7)$$

Fitting the polynomial was achieved by the use of 120 literature experimental data and for the model's verification another 64 experimental data was used. Percentage deviation was observed to be less than those of another three literature empirical equations.

Results of 3D finite element analysis of cylindrical vessel-nozzle juncture was used by Moffat et al. [98] to derive a formula for the effective stress factor, which is equivalent to the SCF, as follows.

$$K_e = \sum_{n=1}^4 a_n (d/D)^{n-1} + \sum_{n=5}^8 a_n (d/D)^{n-5} (t/T) + \sum_{n=9}^{12} a_n (d/D)^{n-9} (D/T)^p + \sum_{n=13}^{16} a_n (d/D)^{n-13} (t/T)(d/T)^p \quad (2.8)$$

where, a_n ($n = 1, 16$) and p are constants.

Gurumurthy [99] developed a simplified formula, Equation (2.9), for SCF by conducting a parametric study on pressurized vessel-nozzle intersection using an axisymmetric finite element analysis.

$$K = 1.75(T/t)^{0.4} (d/D)^{-0.08} (d/\sqrt{DT})^{0.6} \quad (2.9)$$

Although not directly applied to the case of pressure vessel-nozzle component, but several other works reported explicit expressions for stress concentration factors, either for the vessel with a hole, the case of longitudinally welded pipes/vessels, or the spherical head-cylindrical vessel juncture e.t.c. Examples of such are reported in [32] and [100-104].

2.5 PRESSURE VESSELS DESIGN CODES

Several national codes for pressure vessels developed by different countries are available.

These codes specify requirements of design, fabrication, inspection and testing of pressure vessels.

Typical pressure vessel codes, the country and the issuing body are listed in Table 2-1 below. All the codes offer convenient analysis methods based on some assumptions and simplifications that will be fit for design purposes.

Table 2- 1: Pressure Vessel Codes*

Country	Code	Issuing authority
U. S.	ASME Boiler and Pressure Vessel Code (BPVC)	American Society of Mechanical Engineers (ASME)
U. K.	BS 1515 Fusion Welded Pressure Vessels BS 5500 Unfired Fusion Welded Pressure Vessels	British Standard Institute
Germany	AD Merblatter	Arbeitsgemeinschaft Druckbehälter
Italy	ANCC	Associazione Nazionale Per Il Controllo Peula Combustione
Netherlands	Regeis Voor Toestellen	Dienst voor het Stoomvezen
Sweden	Tryckkarls kommissionen	Swedish Pressure Vessel Commission
Australia	AS 1200: SAA Boiler Code AS 1210 Unfired Pressure Vessels	Standards Association of Australia
Belgium	IBN Construction Code for Pressure Vessels	Belgian Standards Institute
Japan	MITI Code	Ministry of International Trade and Industry
France	SNCT Construction Code for Unfired Pressure Vessels	Chaudronnerie et de la Tuyauterie Industrielle

* Source: Chattopadhyay [75]

CHAPTER THREE

GOVERNING EQUATIONS OF AXI-SYMMETRICALLY LOADED SPHERICAL VESSEL - CYLINDRICAL NOZZLE JUNCTURE

This chapter provides an overview of the governing equations of axi-symmetrically loaded spherical vessels under bending. The presentation is based on the work reported in [3], and the sub-sections are organized in such a way as to provide an easy landing at the ultimate set of equations so derived.

3.1 GENERAL STRESSES ACTING ON SPHERICAL SHELL ELEMENT

Consider an element cut from a spherical shell of thickness T_v as shown in Figure 3-1 (a). For equilibrium of the element, symmetry implies that only normal stresses will act on its sides lying in meridian planes. The resultant forces and moments acting on the element as a result of the stresses are as shown in Figure 3-1 (b). Note: From Figure 3-1 (a), $r_0 = R_v \sin \varphi$.

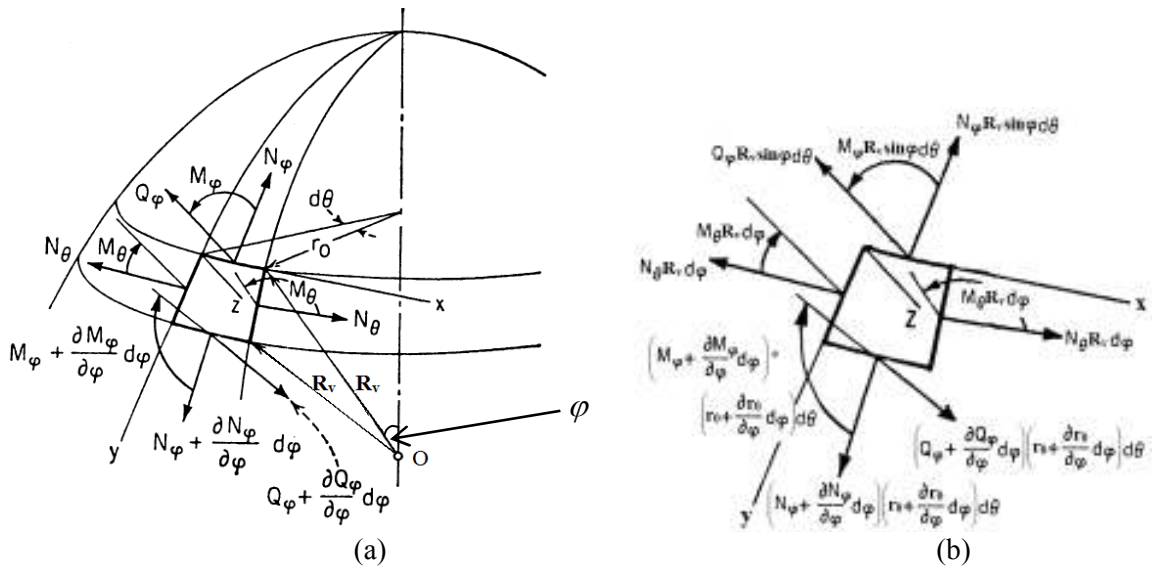


Figure 3- 1: Action of (a) Stresses, and (b) Resultant Forces on an Element Cut from a Shell

The two components of the external load acting upon the element tangent to the meridian and normal to the shell are, respectively,

$$F_y = Y (R_v d\varphi)(r_0 d\theta) = Y R_v^2 \sin \varphi d\varphi d\theta$$

$$F_z = Z (R_v d\varphi)(r_0 d\theta) = Z R_v^2 \sin \varphi d\varphi d\theta$$
(3.1)

3.2 EQUILIBRIUM EQUATIONS

- *Along direction of the tangent to the meridian:*

$$\left(N_\varphi + \frac{dN_\varphi}{d\varphi} d\varphi \right) \left(r_0 + \frac{dr_0}{d\varphi} d\varphi \right) d\theta - N_\varphi R_v \sin \varphi d\theta$$

$$- N_\theta R_v \cos \varphi d\varphi d\theta - r_0 Q_\varphi d\varphi d\theta + Y R_v^2 \sin \varphi d\varphi d\theta = 0$$
(3.2)

Expanding Equation (3.2) and neglecting a small quantity second order, equation of equilibrium in the direction of the tangent becomes

$$r_0 \left(Y R_v - Q_\varphi + \frac{dN_\varphi}{d\varphi} \right) - N_\theta R_v \cos \varphi = 0$$
(3.3)

- *Along direction of the normal to the shell:*

$$N_\varphi R_v \sin \varphi d\theta d\varphi + N_\theta R_v \sin \varphi d\varphi d\theta + \frac{d(Q_\varphi r_0)}{d\varphi} d\varphi d\theta + Z R_v^2 \sin \varphi d\theta d\varphi = 0$$
(3.4)

$$r_0 \left(N_\varphi + Z R_v + \frac{dQ_\varphi}{d\varphi} \right) + N_\theta R_v \sin \varphi = 0$$
(3.5)

- *Moments of all forces with respect to the tangent to the parallel circle*

$$\left(M_\varphi + \frac{dM_\varphi}{d\varphi} d\varphi \right) \left(r_0 + \frac{dr_0}{d\varphi} d\varphi \right) d\theta - M_\varphi R_v \sin \varphi d\theta - M_\varphi R_v \cos \varphi d\varphi d\theta - Q_\varphi R_v \sin \varphi R_v d\varphi d\theta = 0 \quad (3.6)$$

$$r_0 \left(\frac{dM_\varphi}{d\varphi} - Q_\varphi R_v \right) - M_\theta R_v \cos \varphi = 0 \quad (3.7)$$

3.3 U AND V FORMULATIONS

To solve for the five unknowns (N_φ , N_θ , Q_φ , M_φ and M_θ) present in the three equilibrium equations given by (3.3), (3.5) and (3.7), strain-displacement relations (Equation 3.8) and Hooke's law (Equation 3.9) are, first, used to reduce the number of the unknowns to three, as follows.

$$\begin{aligned} \varepsilon_\varphi &= \frac{1}{R_v} \frac{dv}{d\varphi} - \frac{w}{R_v} \\ \varepsilon_\theta &= \frac{v}{R_v} \cot \varphi - \frac{w}{R_v} \end{aligned} \quad (3.8)$$

$$\begin{aligned} N_\varphi &= \frac{Eh}{1-\nu^2} \left[\frac{1}{R_v} \left(\frac{dv}{d\varphi} - w \right) + \frac{\nu}{R_v} (v \cot \varphi - w) \right] \\ N_\theta &= \frac{Eh}{1-\nu^2} \left[\frac{1}{R_v} (v \cot \varphi - w) + \frac{\nu}{R_v} \left(\frac{dv}{d\varphi} - w \right) \right] \end{aligned} \quad (3.9)$$

Similar expressions for the moments are obtained by considering the relative rotations and changes in curvature of the meridian and the plane perpendicular to the meridian. Total rotation of the upper side of the element due to the displacements v and w is the sum of the individual rotations, due to these displacements, with respect to the perpendicular to the meridian plane given as

$$\frac{v}{R_v} + \frac{dw}{R_v d\varphi} \quad (3.10)$$

Similar rotation for the lower side of the element is

$$\frac{v}{R_v} + \frac{dw}{R_v d\varphi} + \frac{d}{d\varphi} \left(\frac{v}{R_v} + \frac{dw}{R_v d\varphi} \right) d\varphi \quad (3.11)$$

Equations (3.10) and (3.11) give the total change in curvature of the meridian as

$$\chi_\varphi = \frac{1}{R_v} \frac{d}{d\varphi} \left(\frac{v}{R_v} + \frac{dw}{R_v d\varphi} \right) \quad (3.12)$$

Change in curvature in the plane perpendicular to the meridian is obtained by considering that each of the lateral sides of the element rotates by an angle given by Equation (3.10). Rotation of the right side in its plane has a component with respect to the y axis given by (3.13). Hence, the change in curvature is as given in Equation (3.14).

$$-\left(\frac{v}{R_v} + \frac{dw}{R_v d\varphi} \right) \cos \varphi d\theta \quad (3.13)$$

$$\chi_\theta = \left(\frac{v}{R_v} + \frac{dw}{R_v d\varphi} \right) \frac{\cos \varphi}{r_0} = \left(\frac{v}{R_v} + \frac{dw}{R_v d\varphi} \right) \frac{\cot \varphi}{R_v} \quad (3.14)$$

Expressions for the moments are obtained by using equations (1.12) and (1.14) and are given by Equation (3.15)

$$\begin{aligned}
M_\varphi &= -D \left[\frac{1}{R_v} \frac{d}{d\varphi} \left(\frac{v}{R_v} + \frac{dw}{R_v d\varphi} \right) + \frac{v}{R_v} \left(\frac{v}{R_v} + \frac{dw}{R_v d\varphi} \right) \cot \varphi \right] = -\frac{D_v}{R_v} \left[\frac{dV}{d\varphi} + vV \cot \varphi \right] \\
M_\theta &= -D \left[\left(\frac{v}{R_v} + \frac{dw}{R_v d\varphi} \right) \frac{\cot \varphi}{R_v} + \frac{v}{R_v} \frac{d}{d\varphi} \left(\frac{v}{R_v} + \frac{dw}{R_v d\varphi} \right) \right] = -\frac{D_v}{R_v} \left[v \frac{dV}{d\varphi} + V \cot \varphi \right]
\end{aligned} \tag{3.15}$$

where, $V = \frac{1}{R_v} \left(v + \frac{dw}{d\varphi} \right)$ is the angle of rotation of a tangent to a meridian.

Three equations in terms of three unknowns (v , w and Q_φ) can be obtained by substituting equations (3.9) and (3.15) into equations (3.3), (3.5) and (3.7). These three equations can be, further, reduced to two equations with two unknowns (v and w) by using the third of these equations to eliminate the shearing force Q_φ . To achieve that, the variables $U = R_v Q_\varphi$ and V (as defined above) are introduced.

The first of the three equations of equilibrium (Equation (3.3)) is rewritten in the form given by Equation (3.16) for the case in which no load is applied to the shell. This form is arrived at, for convenience, by considering the equilibrium of the upper portion of the shell (i.e. the portion above the parallel circle) defined by the angle φ as shown in Figure 3-2.

$$2\pi r_0 N_\varphi \sin \varphi + 2\pi r_0 Q_\varphi \cos \varphi = 0 \tag{3.16}$$

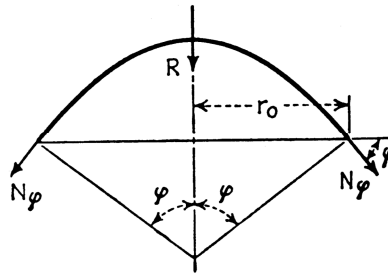


Figure 3- 2: Portion of the Shell above the Parallel Circle

Equation (3.5), for $Z = 0$, gives

$$N_{\theta} R_v \sin \varphi = -N_{\varphi} r_0 - \frac{d(Q_{\varphi} r_0)}{d\varphi} \quad (3.17)$$

The expression

$$N_{\varphi} = -Q_{\varphi} \cot \varphi = -\frac{1}{R_v} U \cot \varphi \quad (3.18)$$

obtained from Equation (3.16) is substituted in Equation (3.17) to give

$$N_{\theta} = -\frac{dQ_{\varphi}}{d\varphi} = -\frac{1}{R_v} \frac{dU}{d\varphi} \quad (3.19)$$

Hence, both N_{φ} and N_{θ} are expressed in terms of U which is, in turn, defined in terms of the shearing force Q_{φ} .

The first equation connecting U and V is obtained thus,

Expressions for N_{φ} and N_{θ} (Equation (3.9)) give

$$\begin{aligned} \frac{dv}{d\varphi} - w &= \frac{R_v}{ET_v} (N_{\varphi} - vN_{\theta}) \\ v \cot \varphi - w &= \frac{R_v}{ET_v} (N_{\theta} - vN_{\varphi}) \end{aligned} \quad (3.20)$$

Differentiating the second of the two equations in (3.20), one gets

$$\frac{dv}{d\varphi} \cot \varphi - \frac{v}{\sin^2 \varphi} - \frac{dw}{d\varphi} = \frac{d}{d\varphi} \left[\frac{R_v}{ET_v} (N_{\theta} - vN_{\varphi}) \right] \quad (3.21)$$

w is eliminated from Equation (3.20) to obtain

$$\frac{dv}{d\varphi} - v \cot \varphi = \frac{1}{ET_v} [R_v(1+v)(N_{\varphi} - N_{\theta})] \quad (3.22)$$

Eliminating $\frac{dv}{d\varphi}$ from equations (3.21) and (3.22) results in

$$\nu + \frac{dw}{d\varphi} = R_\nu V = \frac{\cot \varphi}{ET_\nu} [R_\nu(1+\nu)(N_\varphi - N_\theta)] - \frac{d}{d\varphi} \left[\frac{R_\nu}{ET_\nu} (N_\theta - \nu N_\varphi) \right] \quad (3.23)$$

Substituting the expressions for N_φ and N_θ from equations (3.18) and (3.19), respectively, into Equation (3.23), gives Equation (3.24) relating U and V .

$$\frac{1}{R_\nu} \left(\frac{d^2 U}{d\varphi^2} + \cot \varphi \frac{dU}{d\varphi} - (\cot^2 \varphi - \nu) U \right) = ET_\nu V \quad (3.24)$$

Substituting the expressions for M_φ and M_θ given in Equation (3.15) into the third equation of equilibrium (Equation (3.7)), we obtain the second equation relating U and V as

$$\frac{1}{R_\nu} \left(\frac{d^2 V}{d\varphi^2} + \cot \varphi \frac{dV}{d\varphi} - (\nu + \cot^2 \varphi) V \right) = -\frac{U}{D_\nu} \quad (3.25)$$

Equations (3.24) and (3.25) can be represented in the following simplified form.

$$\begin{aligned} L(U) + \frac{\nu}{R_\nu} U &= ET_\nu V \\ L(V) - \frac{\nu}{R_\nu} V &= -\frac{U}{D_\nu} \end{aligned} \quad (3.26)$$

Where,

$$L(\dots) = \frac{1}{R_\nu} \left(\frac{d^2(\dots)}{d\varphi^2} + \cot \varphi \frac{d(\dots)}{d\varphi} - \cot^2 \varphi (\dots) \right) \quad (3.27)$$

A fourth order equation for each unknown (U and V) can be obtained from the second order simultaneous differential equations (Equation (3.26)) as follows. Starting by performing the operation given by (3.27) on the first of Equation (3.26), gives

$$LL(U) + \nu L\left(\frac{U}{R_v}\right) = ET_v L(V) \quad (3.28)$$

Substituting $L(V) = \frac{\nu}{R_v} V - \frac{U}{D_v} = \frac{\nu}{R_v Eh} \left[L(U) + \frac{\nu}{R_v} U \right] - \frac{U}{D_v}$ from the second of Equation (3.26) into Equation (3.28) gives

$$LL(U) - \frac{\nu^2}{R_v^2} U = -\frac{ET_v}{D_v} U \quad (3.29)$$

Going by similar manner, the second equation is obtained in terms of V as

$$LL(V) - \frac{\nu^2}{R_v^2} V = -\frac{ET_v}{D_v} V \quad (3.30)$$

Letting $\mu^4 = \frac{ET_v}{D_v} - \frac{\nu^2}{R_v^2}$ makes it possible to write both equations (3.29) and (3.30) as

$$LL(U) + \mu^4 U = 0 \quad (3.31)$$

Equation (3.28) can be, further, written as (3.32) or (3.33)

$$L[L(U) + i\mu^2 U] - i\mu^2 [L(U) + i\mu^2 U] = 0 \quad (3.32)$$

$$L[L(U) - i\mu^2 U] + i\mu^2 [L(U) - i\mu^2 U] = 0 \quad (3.33)$$

Hence, solving the second-order equations given in (3.34) implies solving Equation

(3.31)

$$L(U) \pm i\mu^2 U = 0 \quad (3.34)$$

Solution of the above complex differential equations will make it possible to compute the resultant forces and moments acting on the element as a result of the stresses.

3.4 CYLINDRICAL NOZZLE ATTACHMENT

The cylindrical nozzle attached to the spherical shell can be, conveniently, treated as axisymmetric in terms of both geometry and loading and the governing equation is given in Equation (3.35).

$$\frac{d^4 w}{dx^4} + 4k^4 w = \frac{p}{D_n} \quad (3.35)$$

$$\text{where, } k^4 = \frac{3(1-\nu^2)}{R_n^2 T_n^2}$$

CHAPTER FOUR

GOVERNING EQUATIONS OF CYLINDRICAL VESSEL - CYLINDRICAL NOZZLE JUNCTURE

4.1 CYLINDRICAL VESSEL

Configuration of the cylindrical shell with circular cutout, which is one part of the vessel-nozzle component, is shown in Figure 4-1.

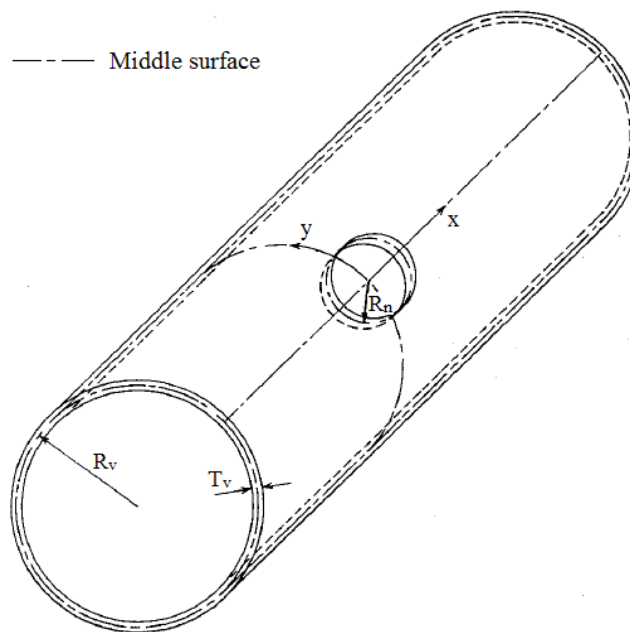


Figure 4- 1: Cylindrical Vessel with a Circular Cutout

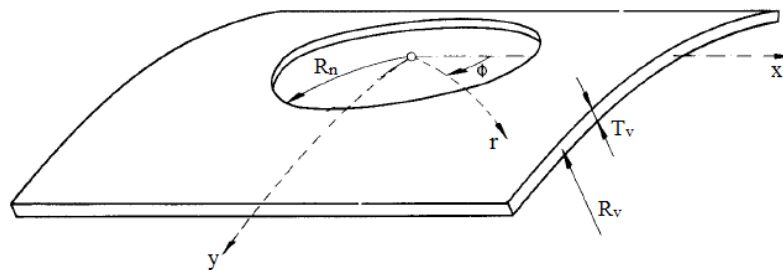


Figure 4- 2: Circular Cutout on Shallow Cylindrical Shell described by Cartesian and Polar Coordinate Systems

Based on the shallow shell theory, the governing differential equations for the cylindrical shell can be written as

$$\begin{aligned} D\nabla^4 w + \frac{1}{R_v} \frac{\partial^2 F}{\partial x^2} &= p \\ \nabla^4 F - \frac{E T_v}{R_v} \frac{\partial^2 w}{\partial x^2} &= 0 \end{aligned} \quad (4.1)$$

where, F is a stress function and $\nabla^2(\dots) = \frac{\partial^2(\dots)}{\partial x^2} + \frac{\partial^2(\dots)}{\partial y^2}$

The two equations in Equation (4.1) can be combined, conveniently, into a single equation as follows

$$\nabla^4 \psi + 8i\beta^2 \frac{\partial^2 \psi}{\partial \bar{x}^2} = 8\beta^2 \quad (4.2)$$

where, $\psi = w - iF$, $\beta^2 = \frac{\sqrt{3(1-\nu^2)}}{4} \rho^2$, $\bar{x} = \frac{x}{R_v}$ and $\bar{y} = \frac{y}{R_v}$

As for any non-homogeneous differential equation, solution to Equation (4.2) is the sum of the particular integral and the homogeneous solution. The membrane solution is the particular integral of Equation (4.3) and only the homogeneous problem given below needs to be considered.

$$\nabla^4 \psi + 8i\beta^2 \frac{\partial^2 \psi}{\partial \bar{x}^2} = 0 \quad (4.3)$$

Equation (4.3) can be written in operationally factored form as

$$L_1 L_2 \psi = 0 \quad (4.4)$$

or

$$\begin{aligned} L_1\psi_1 &= 0 \\ L_2\psi_2 &= 0 \end{aligned} \tag{4.5}$$

where,

$$\begin{aligned} L_1 &= \nabla^2 - 2(1-i)\beta \frac{\partial}{\partial \bar{x}} \\ L_2 &= \nabla^2 + 2(1-i)\beta \frac{\partial}{\partial \bar{x}} \end{aligned} \tag{4.6}$$

Solutions of Equation (4.6) are

$$\begin{aligned} \psi_1 &= e^{(1-i)\beta\bar{x}} \Phi_1(\bar{x}, \bar{y}) \\ \psi_2 &= e^{(1-i)\beta\bar{x}} \Phi_2(\bar{x}, \bar{y}) \end{aligned} \tag{4.7}$$

The complete solution is $\psi = \psi_1 + \psi_2$

The functions ψ_1 and ψ_2 satisfy the differential equation

$$\nabla^2 \Phi + 2i\beta^2 \Phi = 0 \tag{4.8}$$

Solutions to the complex differential equations presented above are mathematically involved and, unlike the case of spherical vessels, popular approximate solutions suitable for design are not available.

4.2 CYLINDRICAL NOZZLE ATTACHMENT

Unlike the case of a cylindrical nozzle attached to a spherical vessel, some difficulties arise when dealing with the nozzle attachment to the cylindrical circular vessel. The problem is not axisymmetric anymore, and extensive computations need to be carried out to arrive at the analytical solution. The classical homogeneous equations derived by

Donnell [105] (Equation (4.9)) and later solved, in explicit form, by Hoff [106] can prove useful in accomplishing that.

$$\begin{aligned}
\nabla^8 w + 4K^4 \frac{\partial^4 w}{\partial x^4} &= 0 \\
\nabla^4 u &= \nu \frac{\partial^3 w}{\partial x^3} - \frac{\partial^3 w}{\partial x \partial \varphi^2} \\
\nabla^4 v &= (2 + \nu) \frac{\partial^3 w}{\partial x^2 \partial \varphi} - \frac{\partial^3 w}{\partial \varphi^3}
\end{aligned} \tag{4.9}$$

where, $K^4 = 3(1 - \nu^2)(R_n / T_n)^2$

CHAPTER FIVE

ANALYTICAL SOLUTION MODELS

Some famous literature analytical models, based on method of asymptotic solution, for the spherical vessel-cylindrical nozzle problems are presented in this chapter. These models are selected to be introduced because they are used subsequently in the analysis presented in Chapter Seven for spherical vessels with moderate-to-large-diameter nozzles. The analytical methods for cylindrical vessel-cylindrical nozzle problems are not presented here due to the fact that the present study aims at providing simple and yet accurate solution models for both the spherical and cylindrical nozzles intersected by cylindrical nozzles. Hence, only the numerical approaches for cylindrical vessel-cylindrical nozzle problems are described (as shown in the next chapter).

5.1 EXACT ANALYTICAL SOLUTION FOR SPHERICAL VESSEL

5.1.1 Solution Due to the Effect of Discontinuity Forces and Moments

Leckie [4] presented a solution of spherical shell equations, under axisymmetric loading, in terms of Bessel functions. This solution, based on the Langer Asymptotic Solution [5], is valid for all values of the colatitude angle φ and is presented in equations (5.1) to (5.14).

$$Q_\varphi = \frac{D_v}{R_v} (A_1 T_1 + A_2 T_2 + A_3 T_3 + A_4 T_4) \quad (5.1)$$

$$N_\varphi = -\frac{D_v}{R_v}(A_1 T_1 + A_2 T_2 + A_3 T_3 + A_4 T_4) \cot \varphi \quad (5.2)$$

$$N_\theta = -\frac{D_v}{R_v}(A_1 \bar{T}_1 + A_2 \bar{T}_2 + A_3 \bar{T}_3 + A_4 \bar{T}_4) \quad (5.3)$$

$$\begin{aligned} M_\varphi = \frac{2\kappa^2 D_v}{R_v^2(1-\nu^2)} & \left[A_1 \left\{ \bar{T}_2 + \nu \cot \varphi T_2 - \frac{\nu}{2\kappa^2} (\bar{T}_1 + \nu \cot \varphi T_1) \right\} \right. \\ & - A_2 \left\{ \bar{T}_1 + \nu \cot \varphi T_1 + \frac{\nu}{2\kappa^2} (\bar{T}_2 + \nu \cot \varphi T_2) \right\} \\ & + B_1 \left\{ \bar{T}_4 + \nu \cot \varphi T_4 - \frac{\nu}{2\kappa^2} (\bar{T}_3 + \nu \cot \varphi T_3) \right\} \\ & \left. - B_2 \left\{ \bar{T}_3 + \nu \cot \varphi T_3 + \frac{\nu}{2\kappa^2} (\bar{T}_4 + \nu \cot \varphi T_4) \right\} \right] \quad (5.4) \end{aligned}$$

$$\begin{aligned} M_\theta = \frac{2\kappa^2 D_v}{R_v^2(1-\nu^2)} & \left[A_1 \left\{ \nu \bar{T}_2 + \cot \varphi T_2 - \frac{\nu}{2\kappa^2} (\nu \bar{T}_1 + \cot \varphi T_1) \right\} \right. \\ & - A_2 \left\{ \nu \bar{T}_1 + \cot \varphi T_1 + \frac{\nu}{2\kappa^2} (\nu \bar{T}_2 + \cot \varphi T_2) \right\} \\ & + B_1 \left\{ \nu \bar{T}_4 + \cot \varphi T_4 - \frac{\nu}{2\kappa^2} (\nu \bar{T}_3 + \cot \varphi T_3) \right\} \\ & \left. - B_2 \left\{ \nu \bar{T}_3 + \cot \varphi T_3 + \frac{\nu}{2\kappa^2} (\nu \bar{T}_4 + \cot \varphi T_4) \right\} \right] \quad (5.5) \end{aligned}$$

$$\begin{aligned} V = \frac{2\kappa^2}{R_v(1-\nu^2)} & \left\{ A_1 \left(T_2 - \frac{\nu}{2\kappa^2} T_1 \right) - A_2 \left(T_1 + \frac{\nu}{2\kappa^2} T_2 \right) \right\} \\ & + B_1 \left(T_4 - \frac{\nu}{2\kappa^2} T_3 \right) - B_2 \left(T_3 + \frac{\nu}{2\kappa^2} T_4 \right) \quad (5.6) \end{aligned}$$

where,

$$T_1 = \sqrt{\frac{\varphi}{\sin \varphi}} \text{ber}' z, \quad T_2 = \sqrt{\frac{\varphi}{\sin \varphi}} \text{bei}' z, \quad T_3 = \sqrt{\frac{\varphi}{\sin \varphi}} \text{ker}' z, \quad T_4 = \sqrt{\frac{\varphi}{\sin \varphi}} \text{kei}' z \quad (5.7)$$

$$\bar{T}_1 = \frac{dT_1}{d\varphi} = -\sqrt{2} \kappa \sqrt{\frac{\varphi}{\sin \varphi}} \left\{ bei z + \frac{1}{2\sqrt{2} \kappa} \left(\frac{1}{\varphi} + \cot \varphi \right) ber' z \right\} \quad (5.8)$$

$$\bar{T}_2 = \frac{dT_2}{d\varphi} = \sqrt{2} \kappa \sqrt{\frac{\varphi}{\sin \varphi}} \left\{ ber z - \frac{1}{2\sqrt{2} \kappa} \left(\frac{1}{\varphi} + \cot \varphi \right) bei' z \right\} \quad (5.9)$$

$$\bar{T}_3 = \frac{dT_3}{d\varphi} = -\sqrt{2} \kappa \sqrt{\frac{\varphi}{\sin \varphi}} \left\{ kei z + \frac{1}{2\sqrt{2} \kappa} \left(\frac{1}{\varphi} + \cot \varphi \right) ker' z \right\} \quad (5.10)$$

$$\bar{T}_4 = \frac{dT_4}{d\varphi} = \sqrt{2} \kappa \sqrt{\frac{\varphi}{\sin \varphi}} \left\{ ker z - \frac{1}{2\sqrt{2} \kappa} \left(\frac{1}{\varphi} + \cot \varphi \right) kei' z \right\} \quad (5.11)$$

$$ber' z = \frac{d}{dz} ber z, \quad bei' z = \frac{d}{dz} bei z, \quad ker' z = \frac{d}{dz} ker z, \quad kei' z = \frac{d}{dz} kei z \quad (5.12)$$

$$4\kappa^4 = \frac{12(1-\nu^2)R_v^2}{T_v^2} - \nu^2 \quad (5.13)$$

$$\text{and } z = \sqrt{2} \kappa \varphi \quad (5.14)$$

The displacement components v and w in the direction of the tangent to the meridian and in the direction of the normal to the shell's middle surface, respectively, can be obtained by considering an element AB of the meridian as shown in Figure 5-1 below.

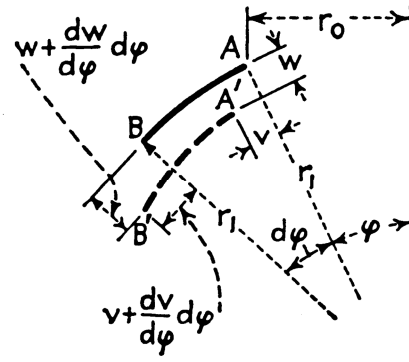


Figure 5- 1: An Element AB of the Meridian

It can be observed, from the figure, that the total change in length of the element AB due to relative deformations of the two ends is

$$\frac{dv}{d\varphi} d\varphi - w d\varphi \quad (5.15)$$

Hence, the strain in the meridional direction is obtained as the ratio of the above change in length to the initial length, $R_v d\varphi$, of the element as follows

$$\varepsilon_\varphi = \frac{1}{R_v} \frac{dv}{d\varphi} - \frac{w}{R_v} \quad (5.16)$$

For an element of a parallel circle of initial radius r_0 , the increase in radius of this circle due to the displacements v and w (Figure 5-1) is

$$v \cos \varphi - w \sin \varphi \quad (5.17)$$

Since the circumference increases in the same proportion as its radius and $r_0 = R_v \sin \varphi$, this implies

$$\varepsilon_\theta = \frac{1}{r_0} (v \cos \varphi - w \sin \varphi) = \frac{1}{R_v} (v \cot \varphi - w) \quad (5.18)$$

w can be eliminated from equations (5.16) and (5.18) to arrive at

$$\frac{dv}{d\varphi} - v \cot \varphi = R_v (\varepsilon_\varphi - \varepsilon_\theta) \quad (5.19)$$

From Hooke's law, we have

$$\begin{aligned}\varepsilon_\varphi &= \frac{1}{ET_v}(N_\varphi - \nu N_\theta) \\ \varepsilon_\theta &= \frac{1}{ET_v}(N_\theta - \nu N_\varphi)\end{aligned}\tag{5.20}$$

Substituting Equation (5.20) in Equation (5.19) and denoting the right hand side by the general function $f(\varphi)$, we have

$$\frac{dv}{d\varphi} - \nu \cot \varphi = \frac{R_v(1+\nu)}{ET_v}(N_\varphi - N_\theta) = f(\varphi)\tag{5.21}$$

The general solution of Equation (5.21) is

$$v = \sin \varphi \left[\int \frac{f(\varphi)}{\sin \varphi} + C \right]\tag{5.22}$$

where, C is a constant of integration that can be determined from the boundary condition.

Having obtained the first displacement component as given by Equation (5.22), the other component w can be obtained from Equation (5.19).

Another important displacement component, denoted as δ , is the displacement in the planes of the parallel circles. This is obtained by projecting the components v and w on that plane to give

$$\delta = v \cos \varphi - w \sin \varphi\tag{5.23}$$

Recognizing that the expression given by Equation (5.23) is the same as the increase in the radius r_0 of the parallel circle, one can write

$$\delta = (R_v \sin \varphi) \varepsilon_\theta = \frac{R_v \sin \varphi}{ET_v} (N_\theta - \nu N_\varphi) = -\frac{\sin \varphi}{ET_v} \left(\frac{dU}{d\varphi} - \nu U \cot \varphi \right) \quad (5.24)$$

Hence, all the quantities defining the bending of a spherical shell by forces and couples uniformly distributed along the edge are as derived above. For sufficiently large φ , the above solution simplifies to a more convenient form, the Simplified Asymptotic Solutions which, for $n = 0$ or 1 (where n is the degree of asymmetry), simplifies to the Hetenyi's solution mentioned subsequently herein.

5.1.2 Solution Due to the Effect of Internal Pressure

As shown in Figure 5-2, the complete solution for the spherical vessel-cylindrical nozzle problem consists of both the bending solution obtained in the previous sub-section and contribution of the effect due to internal pressure. Effect of the internal pressure on the vessel edge displacement and rotation is given in Equation (5.25).

$$\begin{aligned} \delta_{vp} &= \frac{pR_v^2 \sin(\varphi_0)}{2ET_n} (1 - \nu) \\ \theta_{vp} &= 0 \end{aligned} \quad (5.25)$$

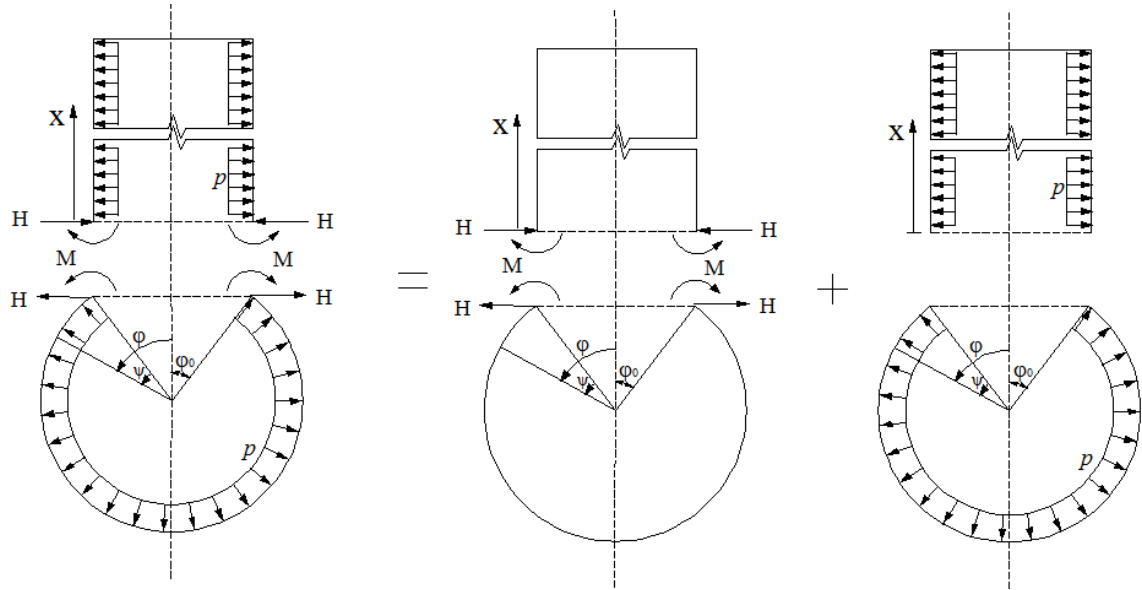


Figure 5- 2: Internal Pressure, Resultant Edge Forces and Moments Acting on the Spherical Vessel and Nozzle

5.2 APPROXIMATE ANALYTICAL SOLUTIONS FOR SPHERICAL VESSEL

Due to the fact that the mathematics involved in section 5.1 for obtaining exact solutions is usually laborious, it becomes unfit for practical design purposes. To circumvent such obstacles some approximate methods have been used to obtain the solutions. Such methods involve neglecting some terms in the differential equation to make it convenient to deal with. Two major approaches/formulations, based on the method of asymptotic integration, towards obtaining approximate solutions will be explained, briefly, as follows. The first refers to the approximation technique by considering a fourth order equation while the second is arrived at by considering two second-order equations. These solutions are accurate for some certain ranges of the shell's geometrical parameter and are presented as follows.

5.2.1 Approximation by considering fourth order equation [3]

Introducing a new $z = Q_\varphi \sqrt{\sin \varphi}$, the fourth order equation (Equation (3.31)) can be written in the following form

$$\frac{d^4 z}{d\varphi^4} + a_2 \frac{d^2 z}{d\varphi^2} + a_1 \frac{dz}{d\varphi} + (\beta^4 + a_0)z = 0 \quad (5.26)$$

Where,

$$\begin{aligned} a_0 &= -\frac{63}{16\sin^4 \varphi} + \frac{9}{8\sin^2 \varphi} + \frac{9}{16}; & a_1 &= \frac{3\cos \varphi}{\sin^3 \varphi}; \\ a_2 &= -\frac{3}{2\sin^2 \varphi} + \frac{5}{2}; & 4\beta^4 &= (1-\nu^2) \left(1 + \frac{12R_v^2}{T_v^2} \right) \end{aligned} \quad (5.27)$$

For thin shells having a very large value of the ratio $\frac{R_v}{T_v}$ and a large value of the angle φ ,

it can be argued that the quantities a_0 , a_1 and a_2 will be much smaller than the quantity $4\beta^4$ and, hence, are neglected. Therefore, Equation (5.26) becomes

$$\frac{d^4 z}{d\varphi^4} + 4\beta^4 z = 0 \quad (5.28)$$

The general solution of Equation (5.28), after making the substitution $z = Q_\varphi \sqrt{\sin \varphi}$, is

$$Q_\varphi = \frac{1}{\sqrt{\sin \varphi}} [e^{\beta\varphi} (C_1 \cos \beta\varphi + C_2 \sin \beta\varphi) + e^{-\beta\varphi} (C_3 \cos \beta\varphi + C_4 \sin \beta\varphi)] \quad (5.29)$$

As the distance from the edge increases, i.e. as φ increases, the first two terms in Equation (5.29) increase while the last two decrease. Since the bending stresses due to

uniformly distributed forces along the edge rapidly die out as the distance from the edge increases, we can take only the last two terms and neglect the first two to obtain Equation (5.30).

$$Q_{\varphi} = \frac{e^{-\beta\varphi}}{\sqrt{\sin \varphi}} (C_3 \cos \beta\varphi + C_4 \sin \beta\varphi) \quad (5.30)$$

From the above expression for Q_{φ} , the already defined expression for U can be used to obtain the forces N_{φ} and N_{θ} from equations (3.18) and (3.19), respectively, and the displacement δ from Equation (5.24). Also, using the earlier defined expression for V the moments M_{φ} and M_{θ} can be obtained from Equation (3.15).

5.2.2 Approximation by Considering Two Second-Order Equations

The approximation in this case is further subdivided into two, as explained in the following sub-sections.

5.2.2.1 Approximation I (Neglecting Two Terms in the Governing Equations) [107]

Unlike the first approximate approach explained above, one may decide not to consider the fourth order equation given in Equation (3.31). Instead, as a basis for an approximate investigation of the bending of a spherical shell, the two second order equations given in Equation (3.26) are considered and re-written as follows.

$$\begin{aligned} \frac{d^2 Q_{\varphi}}{d\varphi^2} + \cot \varphi \frac{dQ_{\varphi}}{d\varphi} - (\cot^2 \varphi - \nu) Q_{\varphi} &= ET_{\nu} V \\ \frac{d^2 V}{d\varphi^2} + \cot \varphi \frac{dV}{d\varphi} - (\cot^2 \varphi + \nu) V &= -\frac{R_{\nu}^2 Q_{\varphi}}{D_{\nu}} \end{aligned} \quad (5.31)$$

For a large value of the angle φ and very small value of T_v (i.e. very thin shell), the quantities Q_φ and V are damped out rapidly as the distance from the edge increases and have the same oscillatory character as has the function given in Equation (5.30). Since β is large for thin shells, this implies

$$\frac{d^2 Q_\varphi}{d\varphi^2} \gg \frac{dQ_\varphi}{d\varphi} \gg Q_\varphi \text{ and } \frac{d^2 V}{d\varphi^2} \gg \frac{dV}{d\varphi} \gg V$$

Thus, one can neglect the terms containing $\frac{dQ_\varphi}{d\varphi}, \frac{dV}{d\varphi}, Q_\varphi$ and V in Equation (5.31) to

obtain

$$\begin{aligned} \frac{d^2 Q_\varphi}{d\varphi^2} &= ET_v V \\ \frac{d^2 V}{d\varphi^2} &= -\frac{R_v^2 Q_\varphi}{D_v} \end{aligned} \tag{5.32}$$

The following fourth order equation is obtained by eliminating V from the two equations above.

$$\frac{d^4 Q_\varphi}{d\varphi^4} + 4\lambda^4 Q_\varphi = 0 \tag{5.33}$$

where,

$$\lambda^4 = 3(1 - \nu^2) \left(\frac{R_v}{T_v} \right)^2 \tag{5.34}$$

The general solution to Equation (5.33) is

$$Q_\varphi = e^{\lambda\varphi} (C_1 \cos \lambda\varphi + C_2 \sin \lambda\varphi) + e^{-\lambda\varphi} (C_3 \cos \lambda\varphi + C_4 \sin \lambda\varphi) \tag{5.35}$$

The first two terms of Equation (5.35) can be neglected because they increase as the angle φ increases. Hence, we have

$$Q_\varphi = e^{-\lambda\varphi} (C_3 \cos \lambda\varphi + C_4 \sin \lambda\varphi) \quad (5.36)$$

The constants C_3 and C_4 can be determined from the boundary conditions.

For convenience, let $\varphi = \varphi_0 + \psi$ as shown in Figure 5-3.

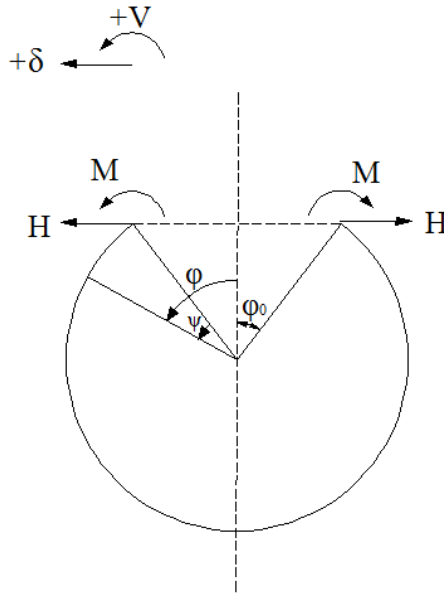


Figure 5- 3: Sign Convention and Relationship between φ , φ_0 and ψ

Substituting $\varphi = \varphi_0 + \psi$ in Equation (5.36), use of the new constants C and γ can be made to obtain

$$Q_\varphi = Ce^{-\lambda\psi} \sin(\lambda\psi + \gamma) \quad (5.37)$$

From equations (3.18) and (3.19), one finds

$$N_\varphi = -Q_\varphi \cot \varphi = -\cot(\varphi_0 + \psi) Ce^{-\lambda\psi} \sin(\lambda\psi + \gamma) \quad (5.38)$$

$$N_\theta = -\frac{dQ_\varphi}{d\varphi} = \lambda\sqrt{2} Ce^{-\lambda\psi} \sin\left(\lambda\psi + \gamma - \frac{\pi}{4}\right) \quad (5.39)$$

The expression for V is obtained from the first of Equation (5.32) as

$$V = \frac{1}{ET_v} \frac{d^2 Q_\phi}{d\phi^2} = -\frac{2\lambda^2}{ET_v} C e^{-\lambda\psi} \cos(\lambda\psi + \gamma) \quad (5.40)$$

Neglecting the terms containing V in Equation (3.15), one finds

$$\begin{aligned} M_\phi &= -\frac{D_v}{R_v} \frac{dV}{d\phi} = -\frac{R_v}{\lambda\sqrt{2}} C e^{-\lambda\psi} \sin\left(\lambda\psi + \gamma + \frac{\pi}{4}\right) \\ M_\theta &= \nu M_\phi = -\frac{R_v \nu}{\lambda\sqrt{2}} C e^{-\lambda\psi} \sin\left(\lambda\psi + \gamma + \frac{\pi}{4}\right) \end{aligned} \quad (5.41)$$

From Equation (5.24), the horizontal component of the displacement is obtained thus,

$$\delta \approx -\frac{\sin\phi}{Eh} \frac{dU}{d\phi} = \frac{a}{Eh} \sin(\alpha + \psi) \lambda \sqrt{2} C e^{-\lambda\psi} \sin\left(\lambda\psi + \gamma - \frac{\pi}{4}\right) \quad (5.42)$$

Equations (5.37) to (5.42) can be used to solve various cases of edge conditions. The edge condition at the junction between the spherical vessel and cylindrical nozzle is the superposition of the two cases shown in Figure 5-4. Hence, the overall solution is a function of the indicated discontinuity force and moment.

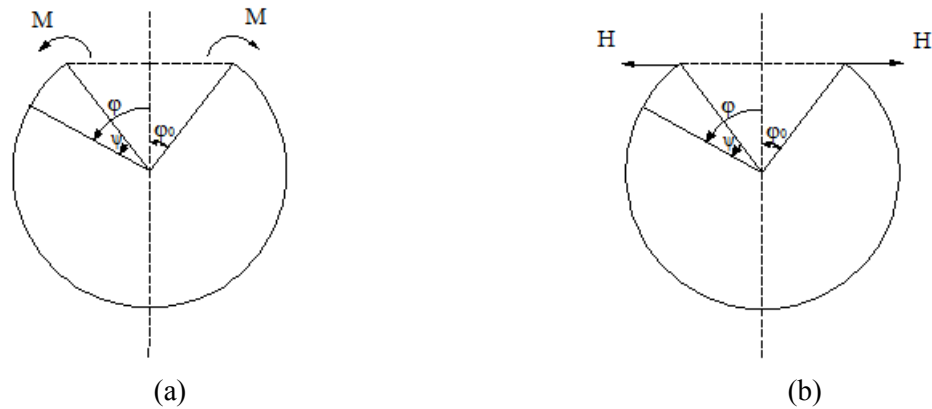


Figure 5- 4: Segment of a Spherical Shell under the Action of Edge Loadings: (a) Moment (b) Shear

Case (a)

Boundary conditions at $\psi = 0$:

$$\begin{aligned} (M_\varphi)_{\varphi=\varphi_0} &= M_{\varphi_0} \\ (N_\varphi)_{\varphi=\varphi_0} &= 0 \end{aligned}$$

From Equation (5.38),

$$(N_\varphi)_{\varphi=\varphi_0} = -\cot(\varphi_0 + 0)C \sin(0 + \gamma) = 0 \quad \Rightarrow \gamma = 0$$

Substituting $\psi = 0$ and $\gamma = 0$ into the first of Equation (5.41), we have

$$(M_\varphi)_{\varphi=\varphi_0} = -\frac{a}{\lambda\sqrt{2}}C \sin\left(0 + 0 + \frac{\pi}{4}\right) = M_{\varphi_0} \quad \Rightarrow C = -\frac{2M_{\varphi_0}\lambda}{R_v}$$

Substituting the above values for C and γ into equations (5.40) and (5.42), results in the following expressions for the rotation and horizontal displacement of the edge.

$$\begin{aligned} (V)_{\psi=0} &= \frac{4\lambda^3 M_{\varphi_0}}{ER_v T_v} \\ (\delta)_{\psi=0} &= \frac{2\lambda^2 \sin \varphi_0}{ET_v} M_{\varphi_0} \end{aligned} \tag{5.43}$$

Case (b)

Boundary conditions at $\psi = 0$:

$$\begin{aligned} (M_\varphi)_{\varphi=\varphi_0} &= 0 \\ (N_\varphi)_{\varphi=\varphi_0} &= -H \cos \varphi_0 \end{aligned}$$

From Equation (5.41),

$$(M_\varphi)_{\varphi=\varphi_0} = -\frac{a}{\lambda\sqrt{2}} C \sin\left(0 + \gamma + \frac{\pi}{4}\right) = 0 \quad \Rightarrow \gamma = -\frac{\pi}{4}$$

From Equation (5.38),

$$N_\varphi = -Q_\varphi \cot \varphi = -\cot(\varphi_0 + \psi) C e^{-\lambda\psi} \sin(\lambda\psi + \gamma)$$

$$(N_\varphi)_{\varphi=\varphi_0} = -\cot(\varphi_0 + 0) C \sin\left(0 - \frac{\pi}{4}\right) = -H \cos \varphi_0 \quad \Rightarrow C = -\sqrt{2} H \sin \varphi_0$$

Substituting the above values for C and γ into equations (5.40) and (5.42) results in

$$\begin{aligned} (V)_{\psi=0} &= \frac{2\lambda^2 \sin \varphi_0}{ET_v} H \\ (\delta)_{\psi=0} &= \frac{2R_v \lambda \sin^2 \varphi_0}{ET_v} H \end{aligned} \quad (5.44)$$

For the combined cases (a and b), we have

$$\begin{aligned} (V)_{\psi=0} &= \frac{4\lambda^3 M_{\varphi_0}}{ER_v T_v} + \frac{2\lambda^2 \sin \varphi_0}{ET_v} H \\ (\delta)_{\psi=0} &= \frac{2\lambda^2 \sin \varphi_0}{ET_v} M_{\varphi_0} + \frac{2R_v \lambda \sin^2 \varphi_0}{ET_v} H \end{aligned} \quad (5.45)$$

5.2.2.2 Approximation II (Neglecting One Term in the Governing Equations) [108]

A better approximation to the solution of Equation (5.31) is obtained by introducing the following variables,

$$\begin{aligned}
Q_1 &= Q_\varphi \sqrt{\sin \varphi} & \Rightarrow Q_\varphi &= \frac{Q_1}{\sqrt{\sin \varphi}} \\
V_1 &= V \sqrt{\sin \varphi} & \Rightarrow V &= \frac{V_1}{\sqrt{\sin \varphi}}
\end{aligned} \tag{5.46}$$

Substituting Equation (5.46) into Equation (3.40) gives

$$\begin{aligned}
\frac{d^2 Q_1}{d\varphi^2} - \frac{1}{8 \sin^2 \varphi} [1 - 4\nu + (5 + 4\nu) \cos 2\varphi] Q_1 &= ET_\nu V_1 \\
4D_\nu \sin^2 \varphi \frac{d^2 V_1}{d\varphi^2} + [3D_\nu \cos^2 \varphi - 2D_\nu \sin^2 \varphi (1 - 2\nu)] V_1 &= -4 \sin^2 \varphi (T_\nu^2 Q_1)
\end{aligned} \tag{5.47}$$

Neglecting the terms containing the quantities Q_1 and V_1 , one arrives at the following.

$$\begin{aligned}
\frac{d^2 Q_1}{d\varphi^2} &= ET_\nu V_1 \\
\frac{d^2 V_1}{d\varphi^2} &= -\frac{R_\nu^2}{D_\nu} Q_1
\end{aligned} \tag{5.48}$$

Solution of Equation (5.48) has the form as that of Equation (5.32) and is given by

$$Q_1 = C e^{-\lambda \psi} \sin(\lambda \psi + \gamma) \tag{5.49}$$

From Equation (5.46)

$$\begin{aligned}
Q_\varphi &= C \frac{e^{-\lambda \psi}}{\sqrt{\sin(\varphi_0 + \psi)}} \sin(\lambda \psi + \gamma) \\
V &= -\frac{2\lambda^2}{Eh} C \frac{e^{-\lambda \psi}}{\sqrt{\sin(\varphi_0 + \psi)}} \cos(\lambda \psi + \gamma)
\end{aligned} \tag{5.50}$$

Following the same approach as that used in obtaining results of equations (5.38), (5.39), (5.41) and (5.42), the following forces, moments and displacement are obtained.

$$\begin{aligned}
N_{\varphi} &= -\cot(\varphi_0 + \psi) C \frac{e^{-\lambda\psi}}{\sqrt{\sin(\varphi_0 + \psi)}} \sin(\lambda\psi + \gamma) \\
N_{\theta} &= -C \frac{\lambda e^{-\lambda\psi}}{2\sqrt{\sin(\varphi_0 + \psi)}} [2\cos(\lambda\psi + \gamma) - (k_1 + k_2)\sin(\lambda\psi + \gamma)]
\end{aligned} \tag{5.51}$$

$$\begin{aligned}
M_{\varphi} &= -\frac{R_v}{2\lambda} C \frac{e^{-\lambda\psi}}{\sqrt{\sin(\varphi_0 + \psi)}} [k_1 \cos(\lambda\psi + \gamma) + \sin(\lambda\psi + \gamma)] \\
M_{\theta} &= -\frac{R_v}{4\nu\lambda} C \frac{e^{-\lambda\psi}}{\sqrt{\sin(\varphi_0 + \psi)}} \{[(1 + \nu^2)(k_1 + k_2) - 2k_2]\cos(\lambda\psi + \gamma) \\
&\quad + 2\nu^2 \sin(\lambda\psi + \gamma)\}
\end{aligned} \tag{5.52}$$

$$\delta = -\frac{R_v \sin(\varphi_0 + \psi)}{ET_v} C \frac{\lambda e^{-\lambda\psi}}{\sqrt{\sin(\varphi_0 + \psi)}} [\cos(\lambda\psi + \gamma) - k_2 \sin(\lambda\psi + \gamma)] \tag{5.53}$$

where,

$$\begin{aligned}
k_1 &= 1 + \frac{1 - 2\nu}{2\lambda} \cot(\varphi_0 + \psi) \\
k_2 &= 1 + \frac{1 + 2\nu}{2\lambda} \cot(\varphi_0 + \psi)
\end{aligned} \tag{5.54}$$

Solving the two cases shown in Figure 5-2 using the formulas given by equations (5.51), (5.52) and (5.53), the following results are obtained for the rotation and horizontal displacement of the edge.

Case (a)

Boundary conditions at $\psi = 0$:

$$\begin{aligned}
(M_{\varphi})_{\varphi=\varphi_0} &= M_{\varphi_0} \\
(N_{\varphi})_{\varphi=\varphi_0} &= 0
\end{aligned}$$

From the first of Equation (5.51),

$$(N_{\varphi})_{\varphi=\varphi_0} = -\cot(\varphi_0 + 0)C \frac{1}{\sqrt{\sin(\varphi_0 + 0)}} \sin(0 + \gamma) = 0 \quad \Rightarrow \gamma = 0$$

Substituting $\psi = 0$ and $\gamma = 0$ into the first of Equation (5.52), we have

$$\begin{aligned} (M_{\varphi})_{\varphi=\varphi_0} &= -\frac{R_v}{2\lambda} C \frac{1}{\sqrt{\sin(\varphi_0 + 0)}} [k_{01} \cos(0 + 0) + \sin(0 + 0)] = M_{\varphi_0} \\ \Rightarrow C &= -\frac{2M_{\varphi_0} \lambda \sqrt{\sin \varphi_0}}{R_v k_{01}} \end{aligned}$$

Substituting the above values for C and γ into the second of Equation (5.50) and Equation (5.53), results in the following expressions for the rotation and horizontal displacement of the edge.

$$\begin{aligned} (V)_{\psi=0} &= \frac{4M_{\varphi_0} \lambda^3}{ER_v T_v k_{01}} \\ (\delta)_{\psi=0} &= \frac{2\lambda^2 \sin \varphi_0}{ET_v k_{01}} M_{\varphi_0} \end{aligned} \quad (5.55)$$

Case (b)

Boundary conditions at $\psi = 0$:

$$\begin{aligned} (M_{\varphi})_{\varphi=\varphi_0} &= 0 \\ (N_{\varphi})_{\varphi=\varphi_0} &= -H \cos \varphi_0 \end{aligned}$$

From the first of Equation (5.51),

$$\begin{aligned} (M_{\varphi})_{\varphi=\varphi_0} &= \frac{R_v}{2\lambda} C \frac{1}{\sqrt{\sin(\varphi_0 + 0)}} [k_{01} \cos(0 + \gamma) + \sin(0 + \gamma)] = 0 \\ \Rightarrow \gamma &= -\cos^{-1} \frac{1}{\sqrt{1 + k_{01}^2}}, \quad \sin \gamma = -\frac{k_{01}}{\sqrt{1 + k_{01}^2}} \end{aligned}$$

From the first of Equation (5.50),

$$\begin{aligned} (N_\varphi)_{\varphi=\varphi_0} &= -\cot(\varphi+0)C \frac{1}{\sqrt{\sin(\varphi+0)}} \sin(0+\gamma) = -\cot(\varphi)C \frac{1}{\sqrt{\sin(\varphi)}} \frac{-k_{01}}{\sqrt{1+k_{01}^2}} = -H \cos \varphi_0 \\ \Rightarrow C &= -\frac{(\sin \varphi_0)^{3/2} \cdot \sqrt{1+k_{01}^2}}{k_{01}} H \end{aligned}$$

Substituting the above values for C , $\sin \gamma$ and $\cos \gamma$ into the second of Equation (5.50) and Equation (5.53) results in

$$\begin{aligned} (V)_{\psi=0} &= \frac{2\lambda^2 \sin \varphi_0}{ET_v k_{01}} H \\ (\delta)_{\psi=0} &= \frac{\lambda R_v \sin^2 \varphi_0}{ET_v} \left(k_{02} + \frac{1}{k_{01}} \right) H \end{aligned} \tag{5.56}$$

For the combined cases (a and b), we have

$$\begin{aligned} (V)_{\psi=0} &= \frac{4\lambda^3}{ER_v T_v k_{01}} M_{\varphi_0} + \frac{2\lambda^2 \sin \varphi_0}{ET_v k_{01}} H \\ (\delta)_{\psi=0} &= \frac{2\lambda^2 \sin \varphi_0}{ET_v k_{01}} M_{\varphi_0} + \frac{\lambda R_v \sin^2 \varphi_0}{ET_v} \left(k_{02} + \frac{1}{k_{01}} \right) H \end{aligned} \tag{5.57}$$

The constants k_{01} and k_{02} in the above expressions are given by

$$\begin{aligned} k_{01} = (k_1)_{\psi=0} &= 1 + \frac{1-2\nu}{2\lambda} \cot \varphi_0 \\ k_{02} = (k_2)_{\psi=0} &= 1 + \frac{1+2\nu}{2\lambda} \cot \varphi_0 \end{aligned} \tag{5.58}$$

In the past, the approach in approximation II was mostly applied for computing edge displacements due to edge loading. It was Hetenyi [108] that, for the first time, presented complete formulas for all the unknown quantities in this approximation. His interesting formulas, till date, prove to be very useful.

Due to the concern that any solution(s) obtained based on the mentioned assumptions would be invalid for the ranges of the vessel geometrical ratios beyond the applicability of the approximate techniques. As reported in the literature [23], this approximate solution ceases to provide reliable results when the parameter $\rho = R_n / \sqrt{R_v T}$ satisfies $\rho < 2.20$ (i.e. small diameter nozzle). As mentioned previously in Chapter One, part of the objectives of the present work involves testing the adequacy and limits of validity of this handy but approximate solution.

5.3 ANALYTICAL SOLUTION FOR THE CYLINDRICAL NOZZLE ATTACHMENT

5.3.1 Solution Due to the Effect of Discontinuity Forces and Moments

Analytical solution presented in Ref. [3] for the cylindrical nozzle attached to the spherical shell is enough to, appropriately, analyze this branch pipe attached to the main vessel. This solution, shown in Equation (5.59), is exact.

$$\delta_{nQM} = -\frac{e^{-\beta x}}{2\beta^3 D_n} [Q \cos \beta x - \beta M (\sin \beta x - \cos \beta x)] \quad (5.59)$$

$$\theta_{nQM} = \frac{e^{-\beta x}}{2\beta^2 D_n} (-Q (\sin \beta x + \cos \beta x) + 2\beta M \cos \beta x)$$

$$M_x = -D_n \frac{d^2(\delta_{nQM})}{dx^2} \quad (5.60)$$

$$M_\theta = \nu M_x$$

$$\begin{aligned}
\delta_{nQM} &= -\frac{e^{-\beta x}}{2\beta^3 D_n} [Q \cos \beta x - \beta M (\sin \beta x - \cos \beta x)] \\
\theta_{nQM} &= \frac{e^{-\beta x}}{2\beta^2 D_n} (-Q (\sin \beta x + \cos \beta x) + 2\beta M \cos \beta x)
\end{aligned}
\tag{5.61}$$

5.3.2 Solution Due to the Effect of Internal Pressure

Displacement and rotation at the edge of the nozzle due to internal pressure are given in Equation (5.62)

$$\begin{aligned}
\delta_{np} &= \frac{pR_n^2}{2ET_n} (2 - \nu) \\
\theta_{np} &= 0
\end{aligned}
\tag{5.62}$$

CHAPTER SIX

FORMULATIONS AND COMPUTER IMPLEMENTATION

The first part of this chapter explains the definitions and notations of the non-dimensionalized variables used for all the problems treated in this research. In addition, non-dimensionalization of the approximate solution variables for the spherical vessel-cylindrical nozzle junctures is carried out. Subsequent sections present computer implementations of both the exact and approximate analytical solutions for the spherical vessel-cylindrical nozzle problem as well as implementation of the finite-element-based numerical model of both the spherical vessel-cylindrical nozzle and cylindrical vessel-cylindrical nozzle problems.

6.1 NON-DIMENSIONALIZATION OF SOLUTION VARIABLES

In order to make the formulation more general, capable of dealing with vessel-nozzle juncture of any arbitrary geometrical ratios, use is made of the following non-dimensional solution variables. This way, the solutions obtained will apply to any specific case by, subsequently, using its actual dimensions and properties.

$$\begin{aligned} \bar{x} &= \frac{x}{R_n}; \quad tT = \frac{T_n}{T_v}; \quad rR = \frac{R_n}{R_v}; \quad rt = \frac{R_n}{T_n} = \frac{rR RT}{tT}; \quad rT = \frac{R_n}{T_v} = rR RT; \\ RT &= \frac{R_v}{T_v}; \quad \varphi_0 = \sin^{-1}(rR); \quad \bar{\delta} = \frac{\delta}{R_n}; \quad \bar{p} = \frac{p}{E}; \quad \bar{\sigma} = \frac{\sigma}{E}; \quad \bar{Q} = \frac{Q}{E R_n}; \quad \bar{M} = \frac{M}{E R_n^2} \end{aligned} \quad (6.1)$$

6.1.1 Non-Dimensionalization of Approximate Solution Variables for the Spherical Vessel

Based on the notations given above, the non-dimensional parameter λ for the spherical vessel can be written in the form given by Equation (6.2).

$$\lambda = \left(3(1 - \nu^2) \left(\frac{R_v}{T_v} \right)^2 \right)^{\frac{1}{4}} = [3(1 - \nu^2)]^{\frac{1}{4}} \sqrt{RT} \quad (6.2)$$

The non-dimensionalized form of Hetenyi's approximate solution is derived and presented in the sub-sequent sub-sections. This method is selected due to its higher accuracy than the remaining approximate methods presented in Chapter Three.

6.1.1.1 Spherical vessel under the action of uniformly distributed edge moment M

Under the action of edge moment M , the two unknowns have been obtained in Chapter Three as

$$\begin{aligned} \gamma &= 0 \\ C &= -\frac{2M\lambda\sqrt{\sin\varphi_0}}{R_vk_{01}} \end{aligned} \quad (6.3)$$

These expressions are substituted into the Hetenyi's formulas [108] to obtain the forces, moments and horizontal displacement at any point on the spherical vessel in non-dimensionalized form as follows.

$$\bar{N}_{\varphi}^{(1)} = \frac{N_{\varphi}^{(1)}}{ER_n} = \cot(\varphi_0 + \psi) \left(\frac{2\lambda\sqrt{\sin(\varphi_0)} \bar{M}.rR}{k_{01}} \right) \frac{e^{-\lambda\psi}}{\sqrt{\sin(\varphi_0 + \psi)}} \sin(\lambda\psi) \quad (6.4)$$

$$\bar{N}_{\theta}^{(1)} = \frac{N_{\theta}^{(1)}}{ER_n} = \left(\frac{2\lambda\sqrt{\sin(\varphi_0)} \bar{M}.rR}{k_{01}} \right) \frac{\lambda e^{-\lambda\psi}}{2\sqrt{\sin(\varphi_0 + \psi)}} [2\cos(\lambda\psi) - (k_1 + k_2)\sin(\lambda\psi)] \quad (6.5)$$

$$\bar{M}_{\varphi}^{(1)} = \frac{M_{\varphi}^{(1)}}{ER_n^2} = \left(\frac{\sqrt{\sin(\varphi_0)} \bar{M}}{k_{01}} \right) \frac{e^{-\lambda\psi}}{\sqrt{\sin(\varphi_0 + \psi)}} [k_1 \cos(\lambda\psi) + \sin(\lambda\psi)] \quad (6.6)$$

$$\bar{M}_{\theta}^{(1)} = \frac{M_{\theta}^{(1)}}{ER_n^2} = \frac{1}{2\nu} \left(\frac{\sqrt{\sin(\varphi_0)} \bar{M}}{k_{01}} \right) \frac{e^{-\lambda\psi}}{\sqrt{\sin(\varphi_0 + \psi)}} \{ [(1 + \nu^2)(k_1 + k_2) - 2k_2] \cos(\lambda\psi) + 2\nu^2 \sin(\lambda\psi) \} \quad (6.7)$$

$$\bar{\delta}^{(1)} = \frac{\delta^{(1)}}{R_n} = RT.rR.\sin(\varphi_0 + \psi) \left(\frac{2\lambda\sqrt{\sin(\varphi_0)} \bar{M}}{k_{01}} \right) \frac{\lambda e^{-\lambda\psi}}{\sqrt{\sin(\varphi_0 + \psi)}} * [\cos(\lambda\psi) - k_2 \sin(\lambda\psi)] \quad (6.8)$$

6.1.1.2 Spherical vessel under the action of uniformly distributed edge force H

The unknowns C and γ corresponding to the case under the action of uniformly distributed edge force H have also been obtained in Chapter Three as

$$\gamma = -\cos^{-1} \left(\frac{1}{\sqrt{1 + k_{01}^2}} \right) \quad (6.9)$$

$$C = -\frac{(\sin \varphi_0)^{3/2} \cdot \sqrt{1 + k_{01}^2}}{k_{01}} H$$

These expressions are treated in a similar manner as is done in the previous sub-section, to obtain the following non-dimensionalized solutions.

$$\bar{N}_{\varphi}^{(2)} = \frac{N_{\varphi}^{(2)}}{ER_n} = \cot(\varphi_0 + \psi) \left(\frac{(\sin \varphi_0)^{3/2} \cdot \sqrt{1 + k_{01}^2}}{k_{01}} \bar{H} \right) \frac{e^{-\lambda\psi}}{\sqrt{\sin(\varphi_0 + \psi)}} \sin(\lambda\psi + \gamma) \quad (6.10)$$

$$\bar{N}_\theta^{(2)} = \frac{N_\theta^{(2)}}{ER_n} = \left(\frac{(\sin \varphi_0)^{3/2} \cdot \sqrt{1+k_{01}^2}}{k_{01}} \bar{H} \right) \frac{\lambda e^{-\lambda \psi}}{2\sqrt{\sin(\varphi_0 + \psi)}} [2 \cos(\lambda \psi + \gamma) - (k_1 + k_2) \sin(\lambda \psi + \gamma)] \quad (6.11)$$

$$\bar{M}_\varphi^{(2)} = \frac{M_\varphi^{(2)}}{ER_n^2} = \frac{\bar{H}}{2\lambda rR} \left(\frac{(\sin \varphi_0)^{3/2} \cdot \sqrt{1+k_{01}^2}}{k_{01}} \right) \frac{e^{-\lambda \psi}}{\sqrt{\sin(\varphi_0 + \psi)}} [k_1 \cos(\lambda \psi + \gamma) + \sin(\lambda \psi + \gamma)] \quad (6.12)$$

$$\bar{M}_\theta^{(2)} = \frac{M_\theta^{(2)}}{ER_n^2} = \frac{\bar{H}}{4\nu\lambda.rR} \left(\frac{(\sin \varphi_0)^{3/2} \cdot \sqrt{1+k_{01}^2}}{k_{01}} \right) \frac{e^{-\lambda \psi}}{\sqrt{\sin(\varphi_0 + \psi)}} * \{[(1+\nu^2)(k_1 + k_2) - 2k_2] \cos(\lambda \psi + \gamma) + 2\nu^2 \sin(\lambda \psi + \gamma)\} \quad (6.13)$$

$$\bar{\delta}^{(2)} = \frac{\delta^{(2)}}{R_n} = RT \cdot \bar{H} \cdot \sin(\varphi_0 + \psi) \left(\frac{(\sin \varphi_0)^{3/2} \cdot \sqrt{1+k_{01}^2}}{k_{01}} \right) \frac{\lambda e^{-\lambda \psi}}{\sqrt{\sin(\varphi_0 + \psi)}} [\cos(\lambda \psi + \gamma) - k_2 \sin(\lambda \psi + \gamma)] \quad (6.14)$$

The total effect is obtained as the superposition of the individual effects from the above two cases as shown in equations (6.15) to (6.17).

$$\bar{N}_\varphi = \bar{N}_\varphi^{(1)} + \bar{N}_\varphi^{(2)} \quad (6.15)$$

$$\bar{N}_\theta = \bar{N}_\theta^{(1)} + \bar{N}_\theta^{(2)}$$

$$\bar{M}_\varphi = \bar{M}_\varphi^{(1)} + \bar{M}_\varphi^{(2)} \quad (6.16)$$

$$\bar{M}_\theta = \bar{M}_\theta^{(1)} + \bar{M}_\theta^{(2)}$$

$$\delta = \delta^{(1)} + \delta^{(2)} \quad (6.17)$$

6.1.2 Non-Dimensionalized Solution Variables for the Cylindrical Nozzle

Solution variables for the cylindrical nozzle attached to spherical vessels are given in Non-dimensionalized forms as follows.

$$\bar{D}_n = \frac{D_n}{E R_n^3} = \frac{1}{12 r t^3 (1 - \nu^2)} \quad (6.18)$$

$$\bar{\beta} = \beta R_n = [3(1 - \nu^2)]^{\frac{1}{4}} \sqrt{r t} \quad (6.19)$$

$$\beta^3 D_n = \frac{\bar{\beta}^3}{r t^3} \left(\frac{E}{12(1 - \nu^2)} \right) \quad (6.20)$$

$$\beta^2 D_n = \frac{\bar{\beta}^2}{r t^2} \left(\frac{E T_n}{12(1 - \nu^2)} \right) \quad (6.21)$$

$$\bar{w}_{nQM} = \frac{w_{nQM}}{R_n} = - \left(\frac{6(1 - \nu^2) r t^3 e^{-\bar{\beta}\bar{x}}}{\bar{\beta}^3} \right) [\bar{Q} \cos \bar{\beta}\bar{x} + \bar{\beta} \bar{M} (\sin \bar{\beta}\bar{x} - \cos \bar{\beta}\bar{x})] \quad (6.22)$$

$$\bar{w}_{np} = \frac{w_{np}}{R_n} = \frac{1}{R_n} \frac{p R_n^2}{2 E T_n} (2 - \nu) = \frac{\bar{p} r t}{2} (2 - \nu) \quad (6.23)$$

The total edge displacement, given in Equation (34), is the sum of the effects due to the action of internal pressure and edge forces and moments.

$$\bar{w}_n = \bar{w}_{np} + \bar{w}_{nQM} \quad (6.24)$$

$$\theta_n = \left(\frac{6(1 - \nu^2) r t^3 e^{-\bar{\beta}\bar{x}}}{\bar{\beta}^2} \right) [-\bar{Q} (\cos \bar{\beta}\bar{x} + \sin \bar{\beta}\bar{x}) + 2 \bar{\beta} \bar{M} \cos \bar{\beta}\bar{x}] \quad (6.25)$$

The non-dimensional moments \bar{M}_x and \bar{M}_θ are given by

$$\bar{M}_x = \frac{M_x}{E R_n^2} = -\bar{D}_n \frac{d^2 \bar{w}_n}{d\bar{x}^2} \quad (6.26)$$

$$\bar{M}_\theta = \nu \bar{M}_x \quad (6.27)$$

6.2 DISCONTINUITY ANALYSIS AND DISCONTINUITY EQUATIONS

Solution of the governing equations presented in Chapter Three and Chapter Four contains many unknown constants that need to be determined by satisfying boundary and

compatibility conditions. These unknowns are in form of edge forces, moments and displacements/rotations due to the pressure and bending effects as shown in figures 6-1 to 6-3 for the spherical shell-cylindrical nozzle and cylindrical shell-cylindrical nozzle junctures. At the discontinuity, the compatibility requirements for displacements and rotations and equilibrium conditions for forces and moments need to be satisfied. The overall solution will be obtained as the sum of the pressure and bending effects solutions.

6.2.1 Spherical Vessels intersected by Radial Cylindrical Nozzles

Original loading, dimensions and unknown discontinuity forces and moments for the spherical vessel-cylindrical nozzle juncture (Figure 6-1(a)) are converted to the equivalent non-dimensionalized form as shown in Figure 6-1(b).

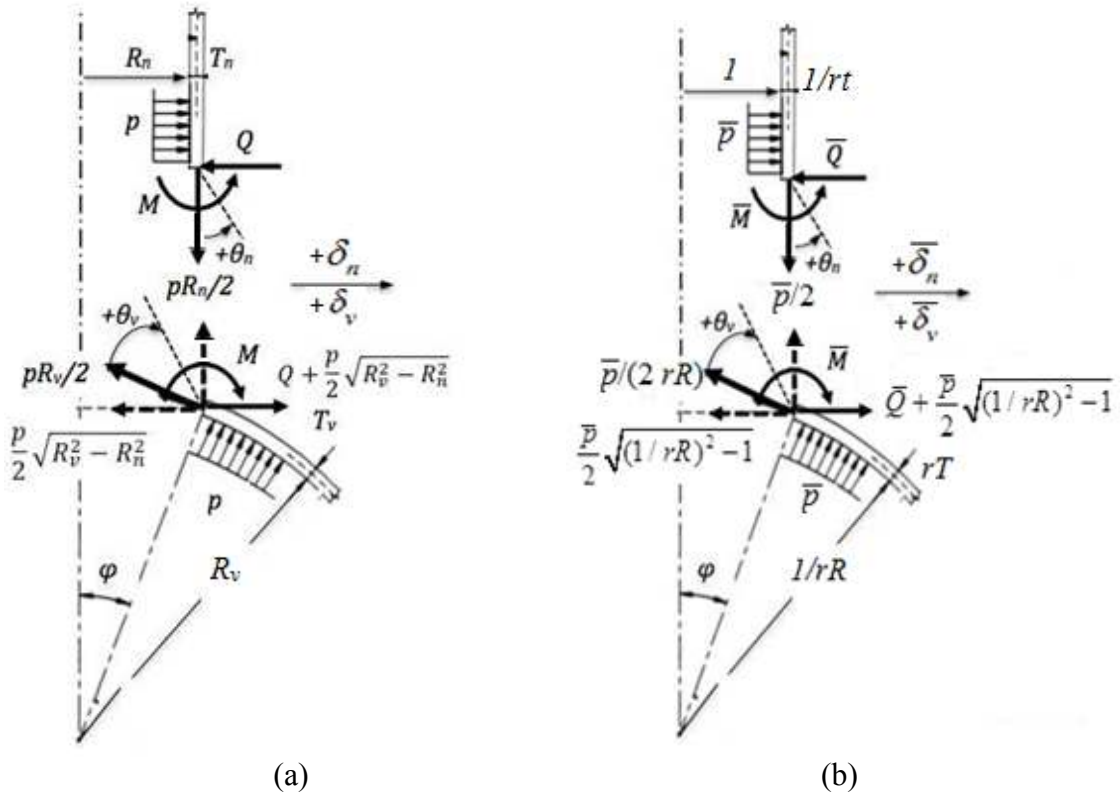


Figure 6- 1: Edge Forces and Displacements/Rotations at the Spherical Shell-Cylindrical Nozzle Juncture in (a) Dimensional and (b) Non-Dimensionalized Form

Horizontal components of the edge force \bar{Q} and that due to internal pressure are summed as given in Equation (6.28).

$$\bar{H} = \frac{H}{ER_n} = \bar{Q} + \frac{\bar{P}}{2} \sqrt{(1/rR)^2 - 1} \quad (6.28)$$

The non-dimensional horizontal displacement of the vessel at the vessel-nozzle juncture ($\psi = 0$) is arrived at by adding the contribution due to the internal pressure and bending effects as follows.

$$\begin{aligned} \bar{w}_v &= \frac{w_v}{R_n} = \frac{\delta_p + \delta(0)}{R_n} \\ &= \left[\frac{(1-\nu)RT \sin \varphi_0}{2rR} \bar{P} + \lambda RT \sin^2 \varphi_0 \left(\frac{1}{k_1} + k_2 \right) \bar{H} + \frac{2\lambda^2 RT . rR \sin \varphi_0}{k_1} \bar{M} \right] \end{aligned} \quad (6.29)$$

In a similar manner, the rotation of a point at the vessel-nozzle juncture ($\psi = 0$) is obtained thus

$$\theta_v = V(0) = \frac{2\lambda^2 RT . rR \sin \varphi_0}{k_1} \bar{H} + \frac{4\lambda^3 RT}{k_1 R r^2} \bar{M} \quad (6.30)$$

Equations (6.31) and (6.32) give the two compatibility conditions at the edge, and are used to arrive at the two unknown edge loads, \bar{Q} and \bar{M} .

$$\bar{w}_n(0) = \bar{w}_v \quad (6.31)$$

$$\theta_n(0) = -\theta_v \quad (6.32)$$

The non-dimensional outer/inner axial and hoop stresses (membrane plus discontinuity effects) in the spherical vessel are obtained thus

$$\begin{aligned}\bar{\sigma}_{\phi(+/-)} &= \frac{\sigma_{\phi(+/-)}}{E} = \frac{1}{E} \left(\frac{pR_v}{2T_v} + \frac{N_{\phi}}{T_v} \mp \frac{6M_{\phi}}{T_v^2} \right) \\ &= \frac{\bar{p}RT}{2} + \bar{N}_{\phi}.rT \mp 6\bar{M}_{\phi}rT^2\end{aligned}\quad (6.33)$$

$$\begin{aligned}\bar{\sigma}_{\theta(+/-)} &= \frac{\sigma_{\theta(+/-)}}{E} = \frac{1}{E} \left(\frac{pR_v}{2T_v} + \frac{N_{\theta}}{T_v} \mp \frac{6M_{\theta}}{T_v^2} \right) \\ &= \frac{\bar{p}RT}{2} + \bar{N}_{\theta}.rT \mp 6\bar{M}_{\theta}rT^2\end{aligned}\quad (6.34)$$

Similarly, the non-dimensional outer/inner stresses (membrane plus discontinuity effects) along the meridional and circumferential/hoop directions in the cylindrical nozzle are obtained as follows.

$$\begin{aligned}\bar{\sigma}_{a(+/-)} &= \frac{\sigma_{a(+/-)}}{E} = \frac{1}{E} \left(\frac{pR_n}{2T_n} \pm \frac{6M_x}{T_n^2} \right) \\ &= \frac{\bar{p}rt}{2} \pm 6\bar{M}_xrt^2\end{aligned}\quad (6.35)$$

$$\begin{aligned}\bar{\sigma}_{h(+/-)} &= \frac{\sigma_{h(+/-)}}{E} = \frac{1}{E} \left(\frac{pR_n}{T_n} + \frac{E}{R_n} w_{nQM} \pm \frac{6M_{\theta}}{T_n^2} \right) \\ &= \bar{p}rt + \bar{w}_{nQM} \pm 6\bar{M}_{\theta}rt^2\end{aligned}\quad (6.36)$$

The SCF values are obtained for the spherical vessel and the nozzle as per equations (6.37) and (6.38), respectively.

$$K_v = \frac{\max(\sigma_{\theta+}, \sigma_{\phi+})}{pR_v / 2T_v} = \frac{2 \max(\bar{\sigma}_{\theta+}, \bar{\sigma}_{\phi+})}{\bar{p}.RT} \quad (6.37)$$

$$K_n = \frac{\max(\sigma_{a+}, \sigma_{h+})}{pR_v / 2T_v} = \frac{2 \max(\bar{\sigma}_{a+}, \bar{\sigma}_{h+})}{\bar{p}.RT} \quad (6.38)$$

The overall SCF is given by Equation (6.39).

$$SCF = \text{Max}(K_v, K_n) \quad (6.39)$$

6.2.2 Cylindrical Vessels intersected by Radial Cylindrical Nozzles

The discontinuity analysis of cylindrical vessel-cylindrical nozzle problem may not be conveniently handled using analytical methods due to a number of reasons. First, while the spherical vessel-cylindrical nozzle is an axisymmetric problem the same approximation cannot be applied to the cylindrical vessel-cylindrical nozzle problem shown in figures 6-2 and 6-3. Another set-back for the cylindrical vessel-cylindrical nozzle problem is the lack of exact closed-form solutions in the literature. Several attempts have been made in the past to achieve that, yet despite their non-exact nature, the approaches are highly mathematically involved. Hence, while the present study uses both analytical and numerical tools in obtaining solutions for spherical vessels intersected by radial cylindrical nozzles, only numerical tools are utilized in obtaining solutions for cylindrical vessels intersected by radial cylindrical nozzles.

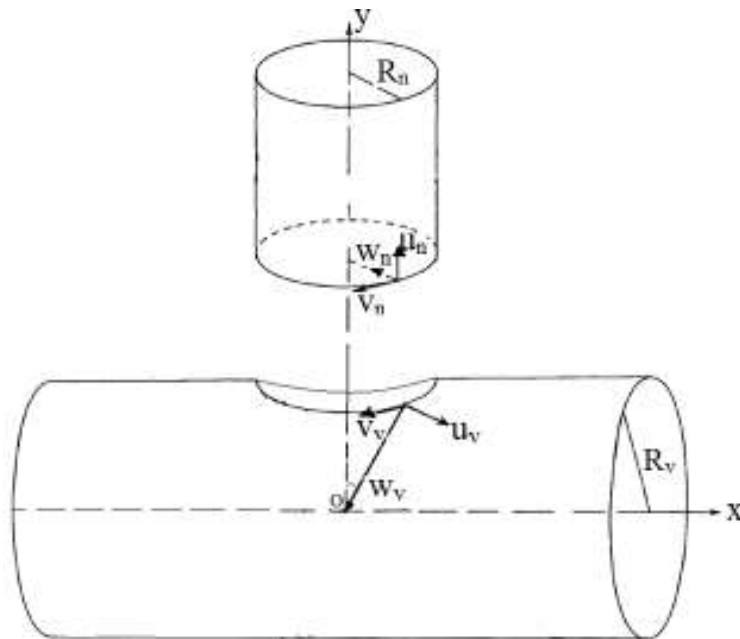


Figure 6- 2: Edge Displacements at the Cylindrical Shell-Cylindrical Nozzle Junction

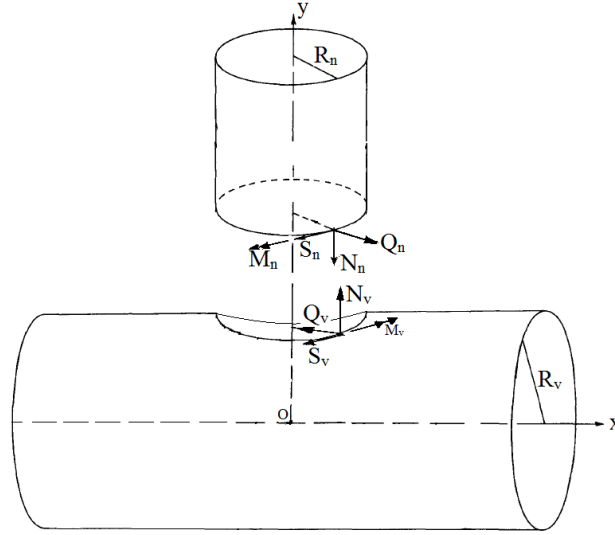


Figure 6- 3: Edge Forces at the Cylindrical Shell-Cylindrical Nozzle Juncture

6.3 COMPUTER IMPLEMENTATION OF ANALYTICAL MODELS

6.3.1 Exact Analytical Model for Spherical Vessels with Moderate-To-Large Diameter Nozzles

Implementation of the exact analytical solution based on Langer Asymptotic Solution presented in Chapter Three is described in the flow chart shown in Figure 6-4. Programming the solution was achieved using MATHEMATICA software package. Because this solution is not in a compact form like the approximate one, the non-dimensionalization of solution variables was achieved in an indirect manner: The vessel's thickness is assumed to be unity throughout the analysis. This way, varying the parameters R_v , T_n and R_n implies, indirectly, varying the geometric ratios RT , tT and rR . In the flowchart, dRT , dtT and drR represent increments in RT , tT and rR , respectively. The subscripts *min* and *max* refers to the desired minimum and maximum values of the parameter in question.

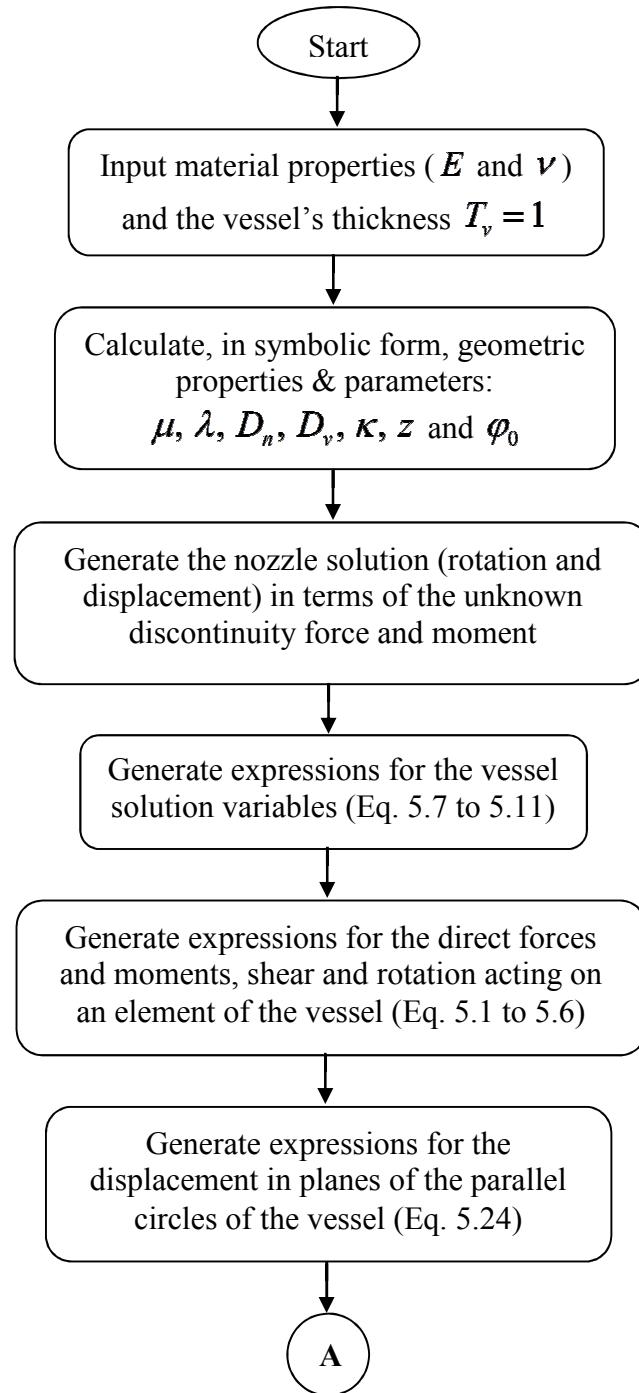


Figure 6- 4: Flowchart for the Exact Analytical Solution of Spherical Vessels with Moderate-to-Large-Diameter Nozzles

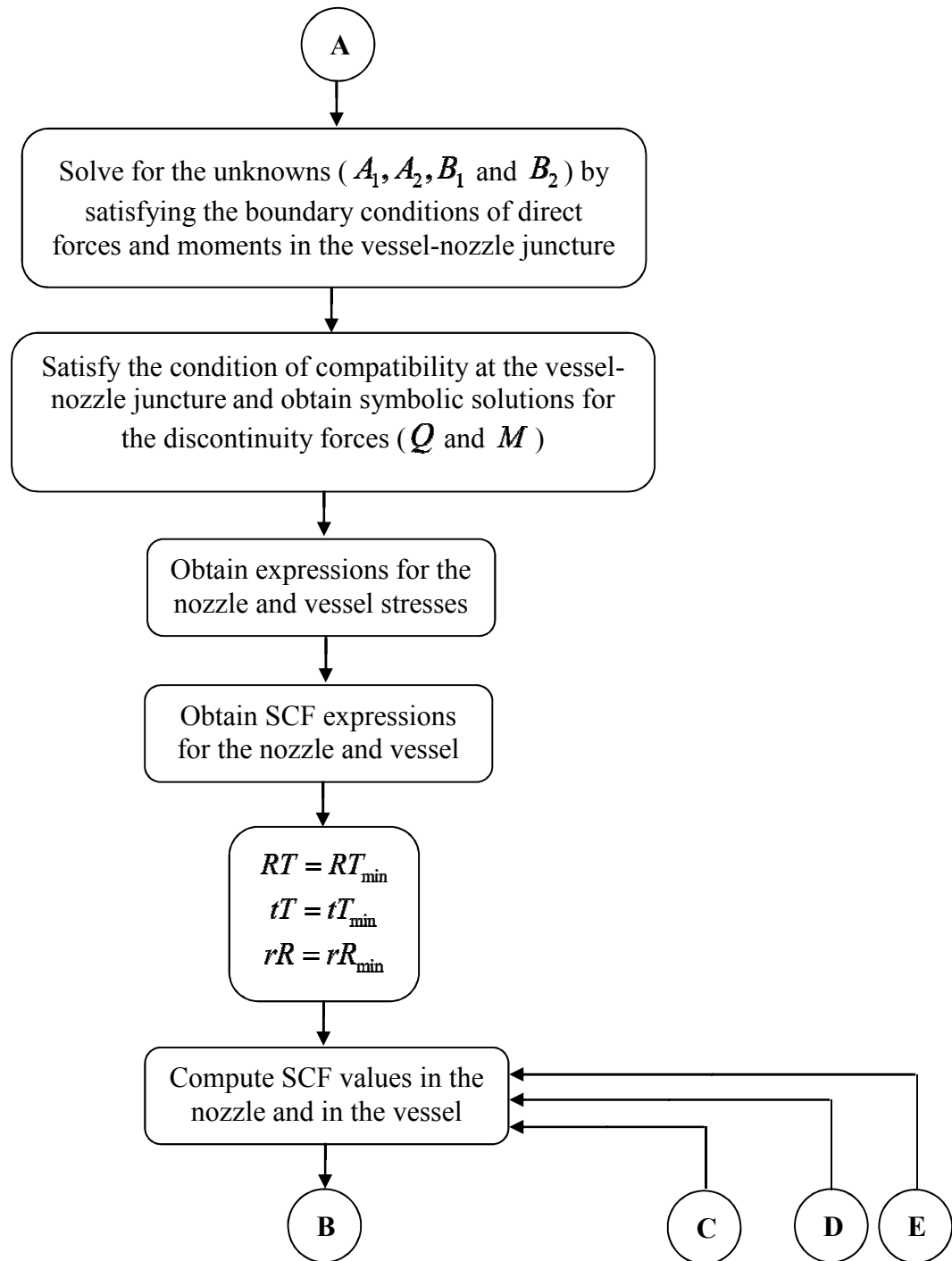


Figure 6- 4 (Cont'd): Flowchart for the Exact Analytical Solution of Spherical Vessels with Moderate-to-Large-Diameter Nozzles

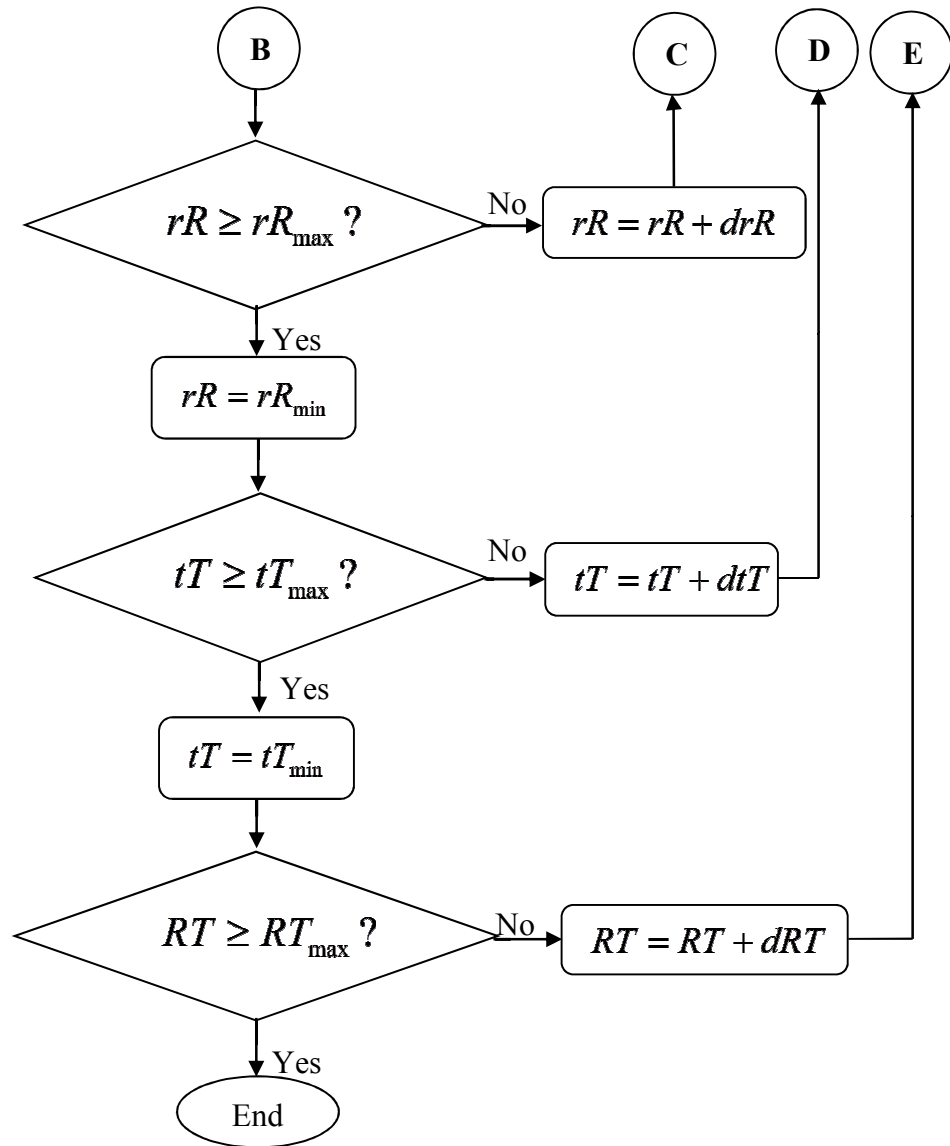


Figure 6- 4 (Cont'd): Flowchart for the Exact Analytical Solution of Spherical Vessels with Moderate-to-Large-Diameter Nozzles

6.3.2 Approximate Analytical Model for Spherical Vessels with Moderate-To-Large Diameter Nozzles

Computer implementation of the approximate analytical solution presented in Chapter Three is described in the flow chart shown in Figure 6-5. MATHEMATICA software package was utilized in programming the solution. Due to its compact/closed-form nature this solution non-dimensionalization of the solution variables was achieved in a direct manner. Similar to the flowchart shown in Figure 6-4, dRT , dtT and drR represent increments in RT , tT and rR , respectively. The subscripts *min* and *max* refers to the desired minimum and maximum values of the parameter in question.

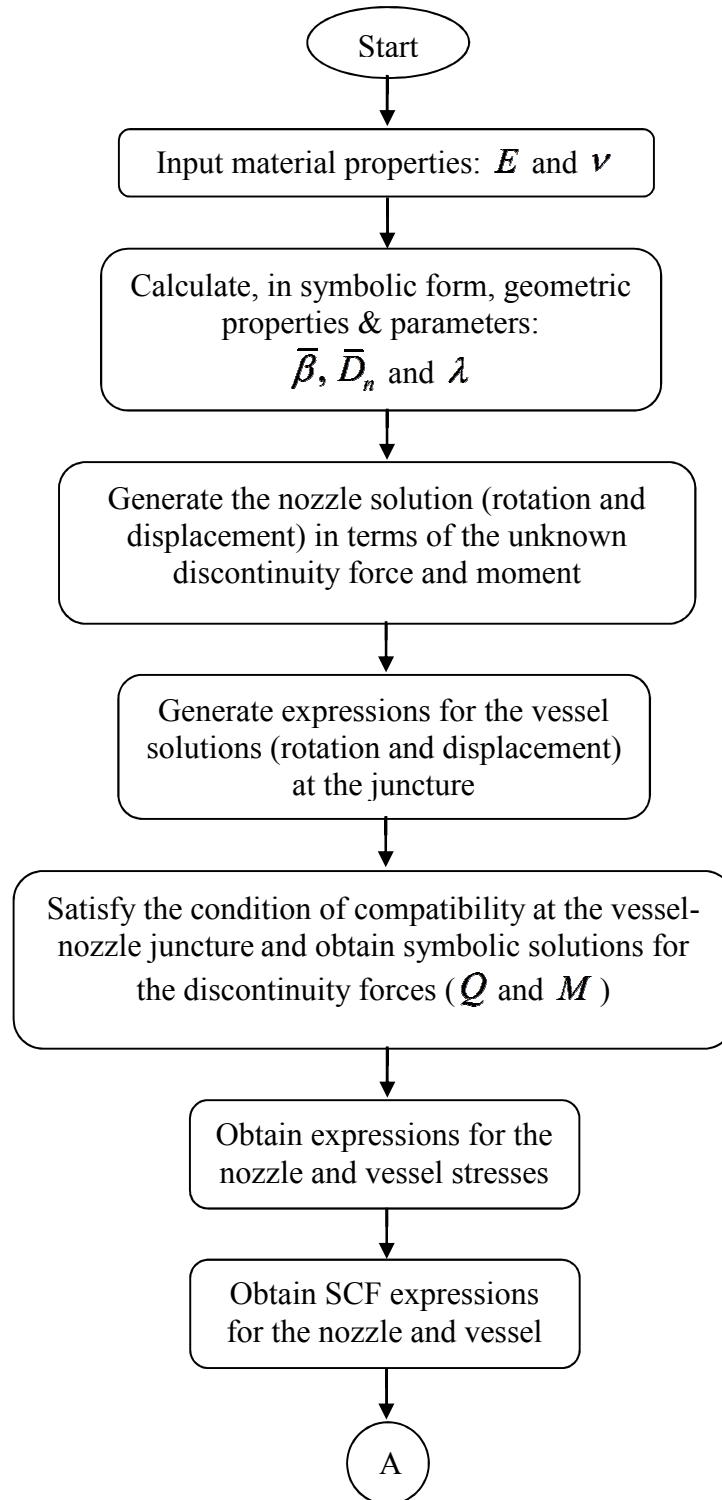


Figure 6- 5: Flowchart for the Approximate Analytical Solution of Spherical Vessels with Moderate-to-Large-Diameter Nozzles

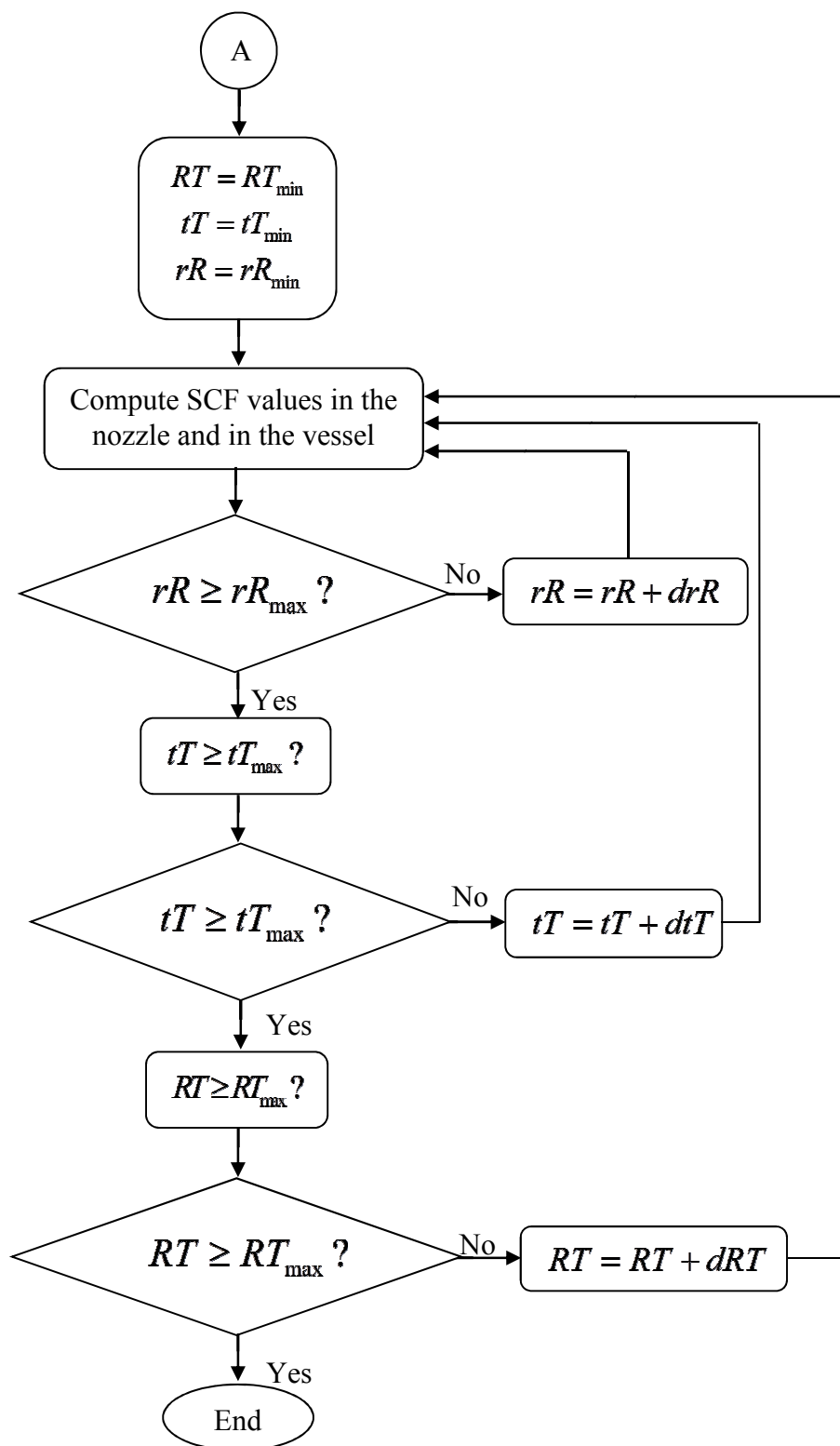


Figure 6- 5 (Cont'd): Flowchart for the Approximate Analytical Solution of Spherical Vessels with Moderate-to-Large-Diameter Nozzles

6.4 COMPUTER IMPLEMENTATION OF NUMERICAL MODELS

6.4.1 Spherical and Cylindrical Vessels with Moderate-To-Large Diameter Nozzles

The finite-element-based numerical model for the spherical vessel intersected by a moderate-to-large-diameter nozzle is implemented as described in the flow chart shown in Figure 6-6. COMSOL multiphysics package was used in achieving that. Carrying out the analysis with non-dimensionalized parameters and solution variables was achieved in a similar manner to that used for the exact analytical method: The vessel's thickness is assumed to be unity throughout the analysis. This way, varying the parameters R_v , T_n and R_n implies, indirectly, varying the geometric ratios RT , tT and rR .

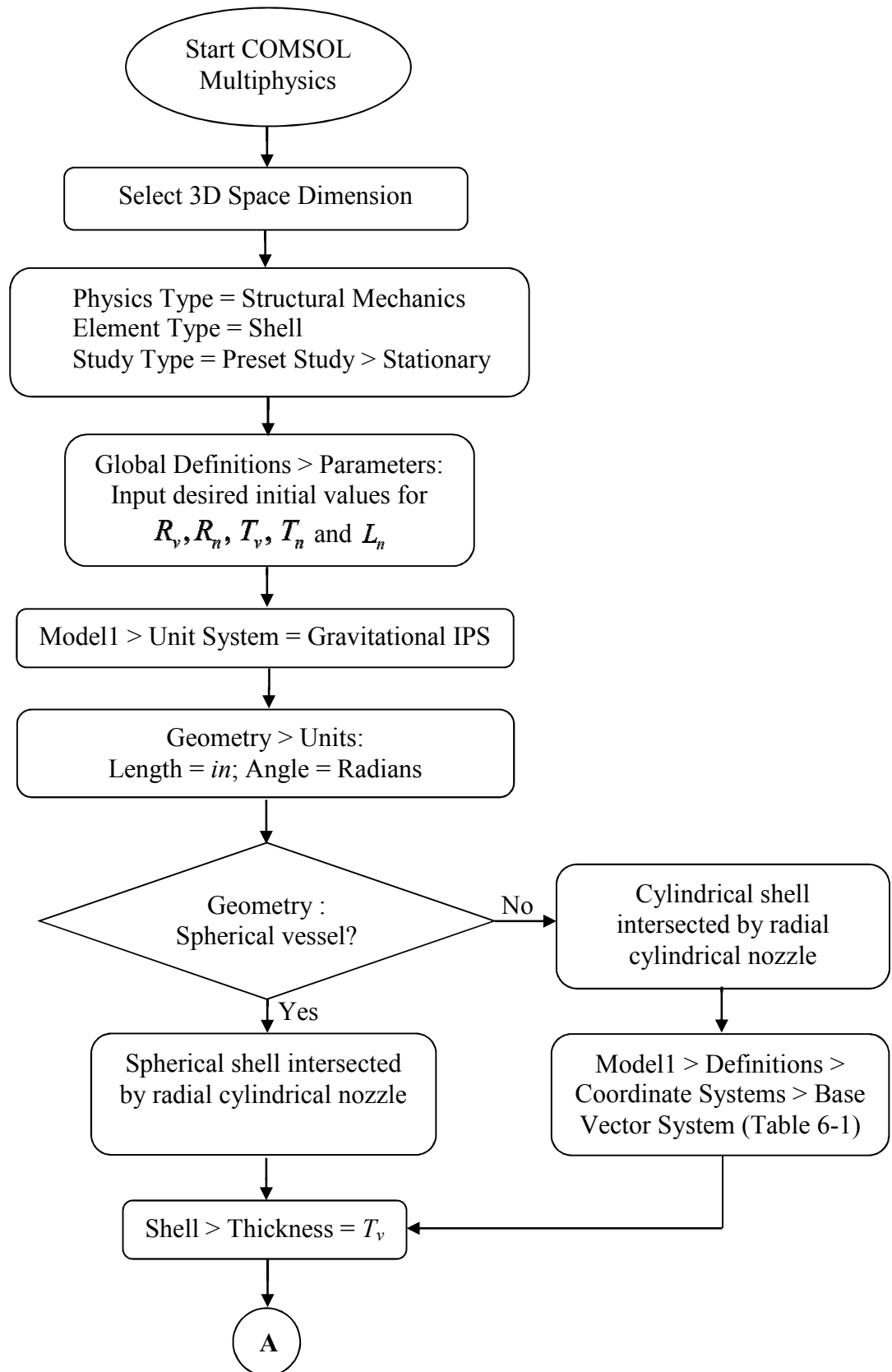


Figure 6- 6: Flowchart for FEM Solution of Vessels with Moderate-to-Large-Diameter Nozzles using COMSOL

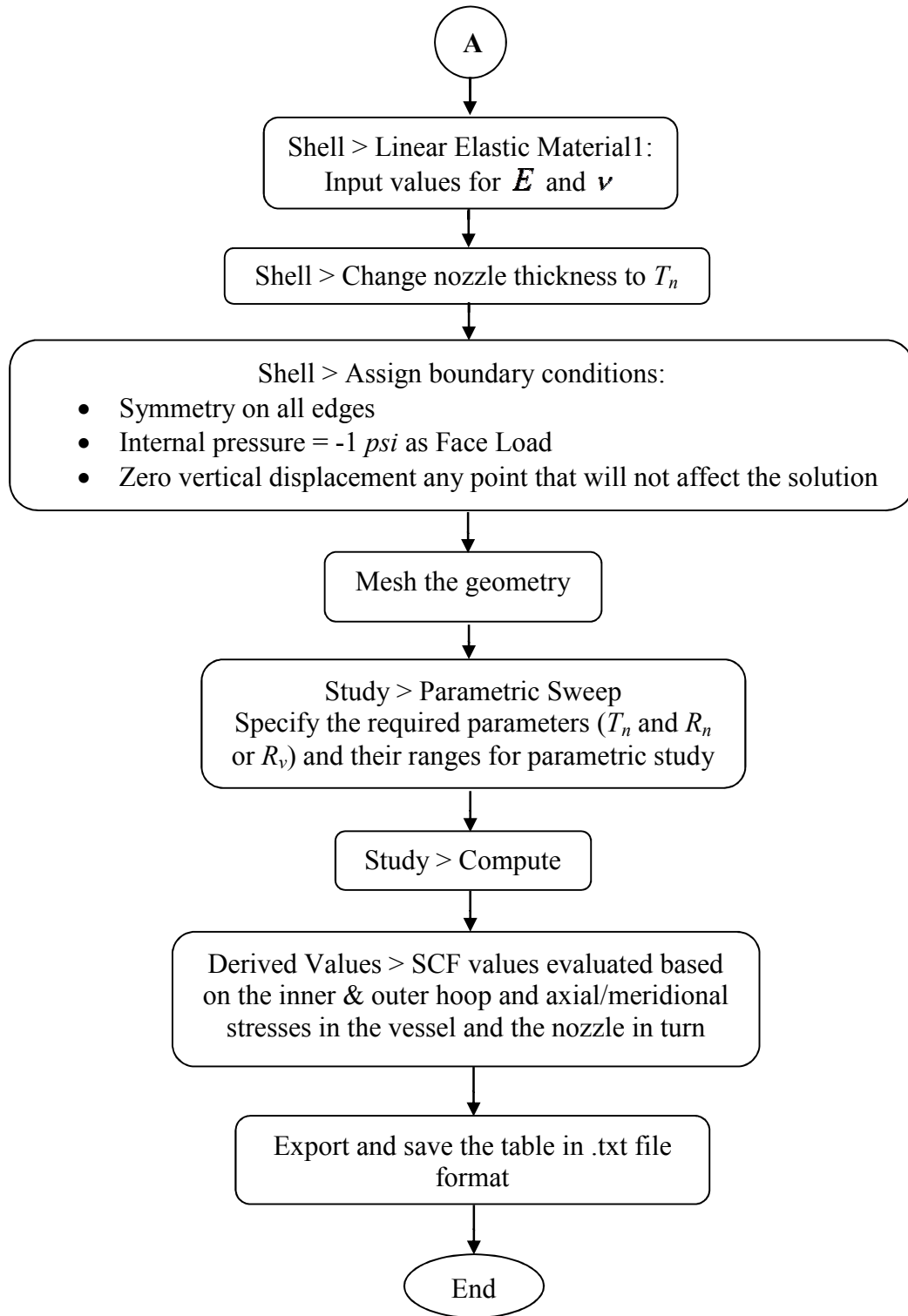


Figure 6- 6 (Cont'd): Flowchart for FEM Solution of Vessels with Moderate-to-Large-Diameter Nozzles using COMSOL

6.4.2 Spherical and Cylindrical Vessels with Small-Diameter Nozzles

Figure 6-7 shows the steps followed in implementing the finite-element-based numerical model for the spherical vessel intersected by a small-diameter nozzle. The vessel's thickness is assumed to be unity throughout the analysis. This way, varying the parameters R_v , T_n and R_n implies, indirectly, varying the geometric ratios RT , tT and rR .

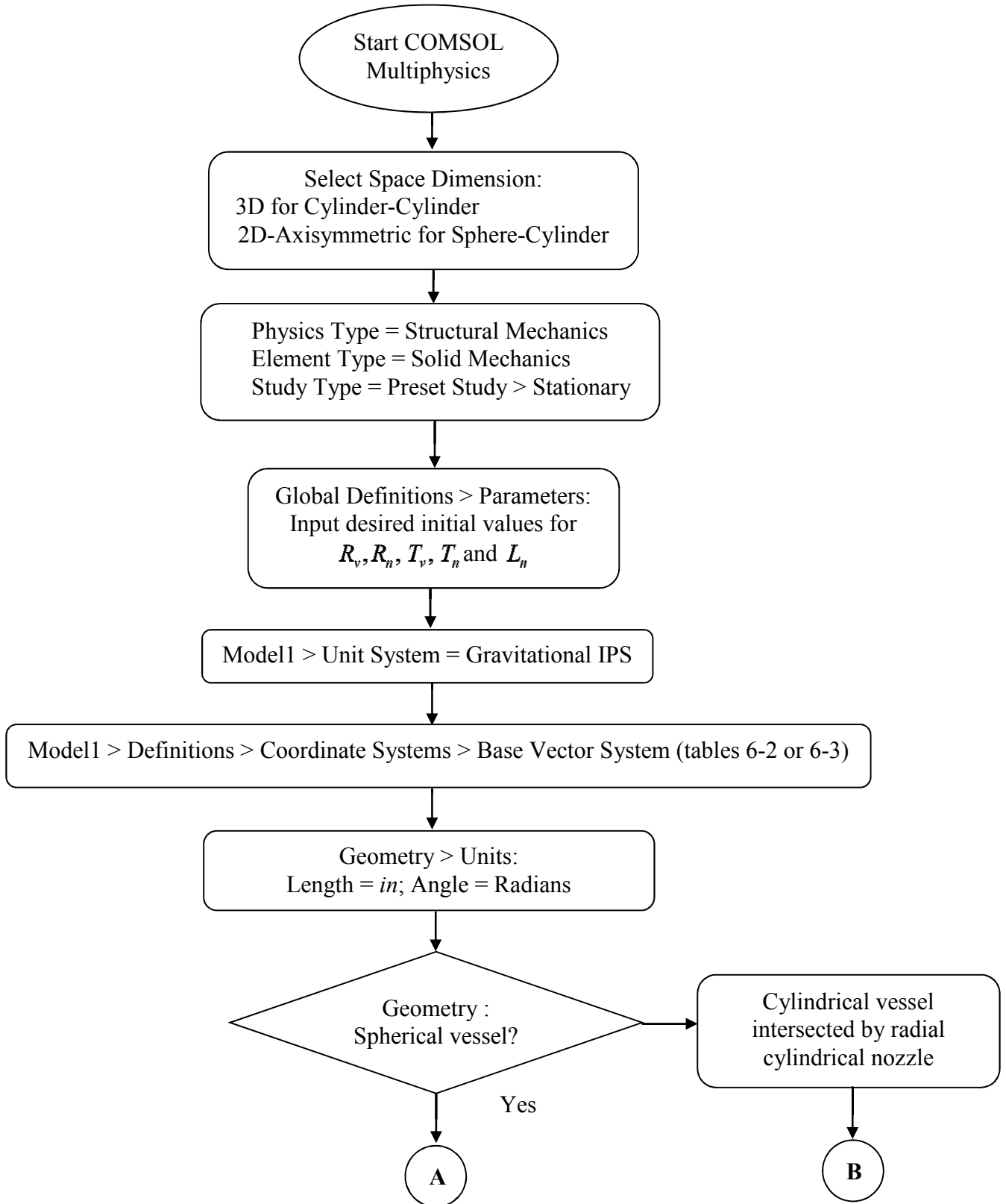


Figure 6- 7: Flowchart for FEM Solution of Vessels with Small-Diameter Nozzles using COMSOL

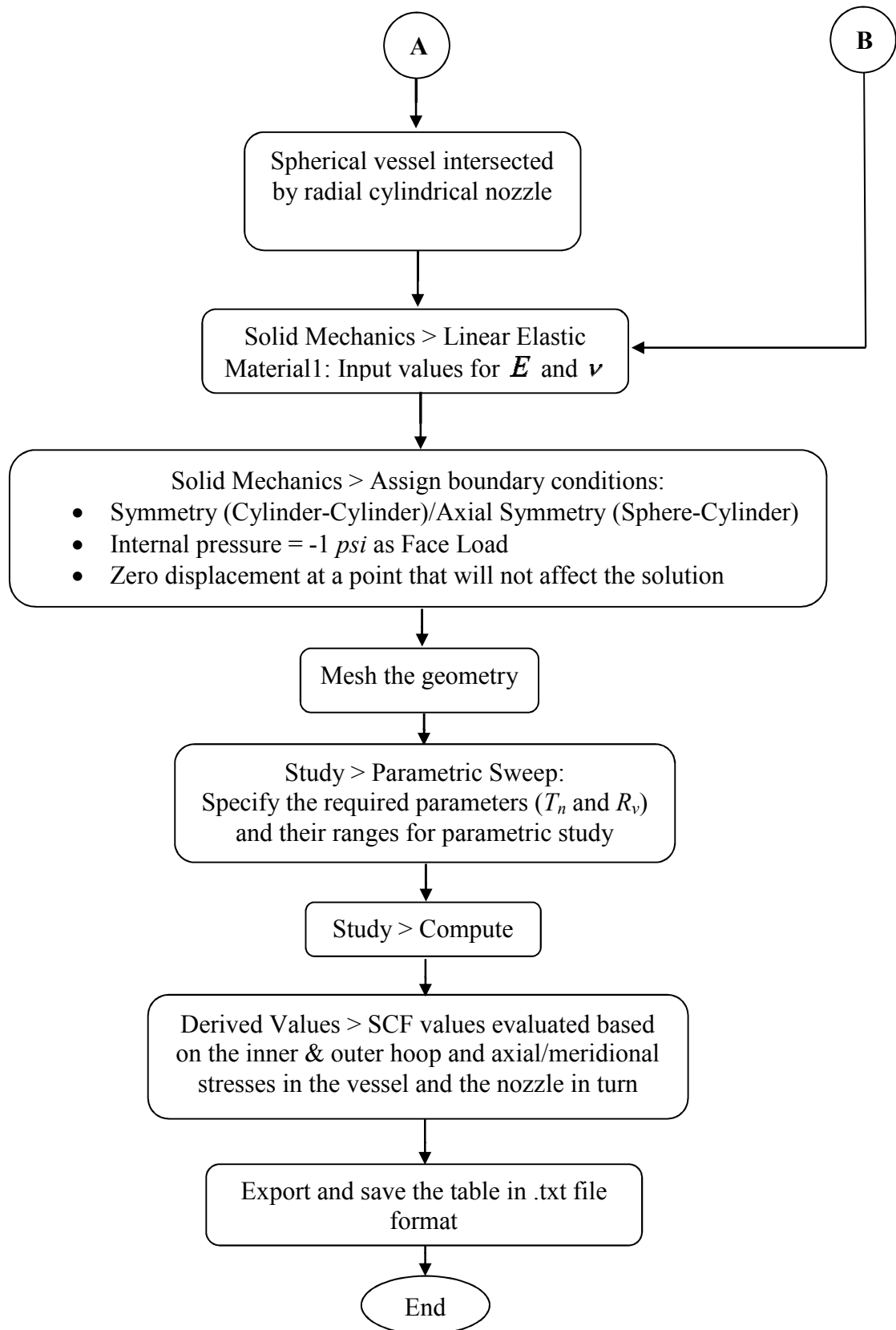


Figure 6- 7 (Cont'd): Flowchart for FEM Solution of Vessels with Small-Diameter Nozzles using COMSOL

Table 6- 1*: Coordinates Transformation in Cylindrical Vessels with Moderate-To-Large-Diameter Nozzles

	x	y	z
x1	$\cos(\text{atan2}(y,x)) * (\text{dom}==2)$ $+\cos(\text{atan2}(y,x)) * (\text{dom}==3)$ $+\cos(\text{atan2}(y,x)) * (\text{dom}==5)$ $+1 * (\text{dom}==1) + 1 * (\text{dom}==4)$ $+1 * (\text{dom}==6) + 1 * (\text{dom}==7)$ $+1 * (\text{dom}==8) + 1 * (\text{dom}==9)$	$\sin(\text{atan2}(y,x)) * (\text{dom}==2)$ $+\sin(\text{atan2}(y,x)) * (\text{dom}==3)$ $+\sin(\text{atan2}(y,x)) * (\text{dom}==5)$	0
x2	$-\sin(\text{atan2}(y,x)) * (\text{dom}==2)$ $-\sin(\text{atan2}(y,x)) * (\text{dom}==3)$ $-\sin(\text{atan2}(y,x)) * (\text{dom}==5)$	$\cos(\text{atan2}(y,x)) * (\text{dom}==2)$ $+\cos(\text{atan2}(y,x)) * (\text{dom}==3)$ $+\cos(\text{atan2}(y,x)) * (\text{dom}==5)$ $+1 * (\text{dom}==1) + 1 * (\text{dom}==4)$ $+1 * (\text{dom}==6) + 1 * (\text{dom}==7)$ $+1 * (\text{dom}==8) + 1 * (\text{dom}==9)$	0
x3	0	0	$1 * (\text{dom}==2) + 1 * (\text{dom}==3)$ $+1 * (\text{dom}==5) + 1 * (\text{dom}==1)$ $+1 * (\text{dom}==4) + 1 * (\text{dom}==6)$ $+1 * (\text{dom}==7) + 1 * (\text{dom}==8)$ $+1 * (\text{dom}==9)$

* Domains 1, 4, 6, 7, 8 and 9 represent the main cylindrical vessel, whereas domains 2, 3 and 5 refer to the cylindrical nozzle

Table 6- 2*: Coordinates Transformation in Cylindrical Vessels with Small-Diameter Nozzles

	x	y	z
x1	$\cos(\text{atan2}(x,z)) * (\text{dom}==3) +$ $\cos(\text{atan2}(x,z)) * (\text{dom}==4) +$ $1 * (\text{dom}==1) + 1 * (\text{dom}==2) +$ $1 * (\text{dom}==5)$	0	$1 * (\text{dom}==3) + 1 * (\text{dom}==4) +$ $1 * (\text{dom}==1) + 1 * (\text{dom}==2) +$ $1 * (\text{dom}==5)$
x2	0	$1 * (\text{dom}==3) + 1 * (\text{dom}==4) +$ $1 * (\text{dom}==1) + 1 * (\text{dom}==2) +$ $1 * (\text{dom}==5)$	0
x3	$\sin(\text{atan2}(x,z)) * (\text{dom}==3) +$ $\sin(\text{atan2}(x,z)) * (\text{dom}==4)$	0	$\cos(\text{atan2}(x,z)) * (\text{dom}==3) +$ $\cos(\text{atan2}(x,z)) * (\text{dom}==4) +$ $1 * (\text{dom}==1) + 1 * (\text{dom}==2) +$ $1 * (\text{dom}==5)$

* Domains 1, 2 and 5 represent the main cylindrical vessel, whereas domains 3 and 4 refer to the cylindrical nozzle

Table 6- 3*: Coordinates Transformation in Spherical Vessels with Small-Diameter Nozzles

	r	z
x1	$\sin(\text{atan2}(Z,R)) * (\text{dom} == 1)$	$-\cos(\text{atan2}(Z,R)) * (\text{dom} == 1) - 1 * (\text{dom} == 2)$
x3	$\cos(\text{atan2}(Z,R)) * (\text{dom} == 1) + 1 * (\text{dom} == 2)$	$\sin(\text{atan2}(Z,R)) * (\text{dom} == 1)$

* Domain 1 represents the main spherical vessel, whereas domain 2 refers to the cylindrical nozzle

CHAPTER SEVEN

ANALYSIS AND DEVELOPMENT OF DESIGN CHARTS FOR SPHERICAL PRESSURE VESSELS WITH MODERATE-TO-LARGE DIAMETER CYLINDRICAL NOZZLES

7.1 INTRODUCTION

The analysis presented throughout this chapter is based on shell theory. The justification being that the radius-to-thickness ratios of both the vessel and the moderate-to-large diameter nozzles are greater than the minimum required for thin shell validity (i.e.

$\frac{r}{t} \geq 10$). Consequently, the nominal stresses away from the juncture are membrane as

given in Table 7-1.

Table 7- 1: Expressions of Membrane Stresses for Internally Pressurized Vessels (Thin Shells)

Shell Type	Stress Type	Formula
Sphere	σ_r	0
	σ_θ	$\frac{pr_m}{2t}$
	σ_z	$\frac{pr_m}{2t}$
	Max σ (= $\sigma_\theta = \sigma_z$ @ $r = r_i$)	$\frac{pr_m}{2t}$
Cylinder	σ_r	0
	σ_θ	$\frac{pr_m}{t}$
	σ_z	$\frac{pr_m}{2t}$
	Max σ (= σ_θ @ $r = r_i$)	$\frac{pr_m}{t}$

The availability of exact and approximate analytical methods of solutions in addition to FEM give rise to three sources of analysis of the spherical vessel with moderate-to-large diameter nozzles at our disposal. The easiest and most appealing of the three is the approximate method. Limit for thin shell solution is denoted by $rR_{\min 1}$ as shown in Figure 7-1. The definition of vessel with moderate-to-large diameter nozzle in this research refers to such vessel-nozzle component with $rR \geq rR_{\min 1}$, and the shell-based solution by the exact analytical and the finite element methods are valid within this range. However, there exists a concern on the applicability of the approximate method for certain cases of vessel-nozzle configurations. For instance, as evident in the manner it is derived in Chapter 3, the set back of the popular Hetenyi's simplified solution is the fact that they are only applicable to spherical shells with large colatitude angle \emptyset . As reported in the literature [23], this approximate solution ceases to provide reliable results when $\rho < 2.20$. This minimum is represented equivalently as $rR_{\min 2}$ in Figure 7-1. Hence, the present chapter starts by attempting to establish the extent of applicability and reliability of the approximate solution in terms of SCF determination for varying nozzle diameter. Results of the detailed analysis by the approximate solution as well as its reliability are presented in the subsequent section.

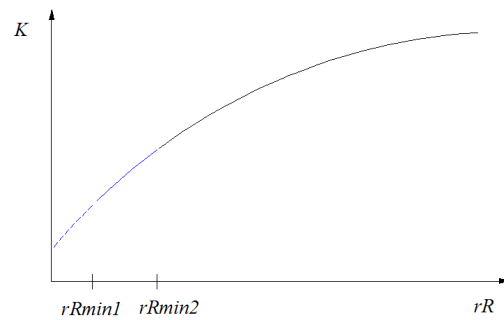


Figure 7- 1: Minimum Requirements for Validity of Shell Theory and Approximate Solution for Spherical Vessel-Cylindrical Nozzle Juncture

7.2 FINITE ELEMENT, EXACT VERSUS APPROXIMATE SOLUTIONS

The vessel-nozzle juncture is modeled using the finite element method and comparison of the results made with those of the exact and approximate solutions. Figure 7-2 shows the FEM model developed in COMSOL software.

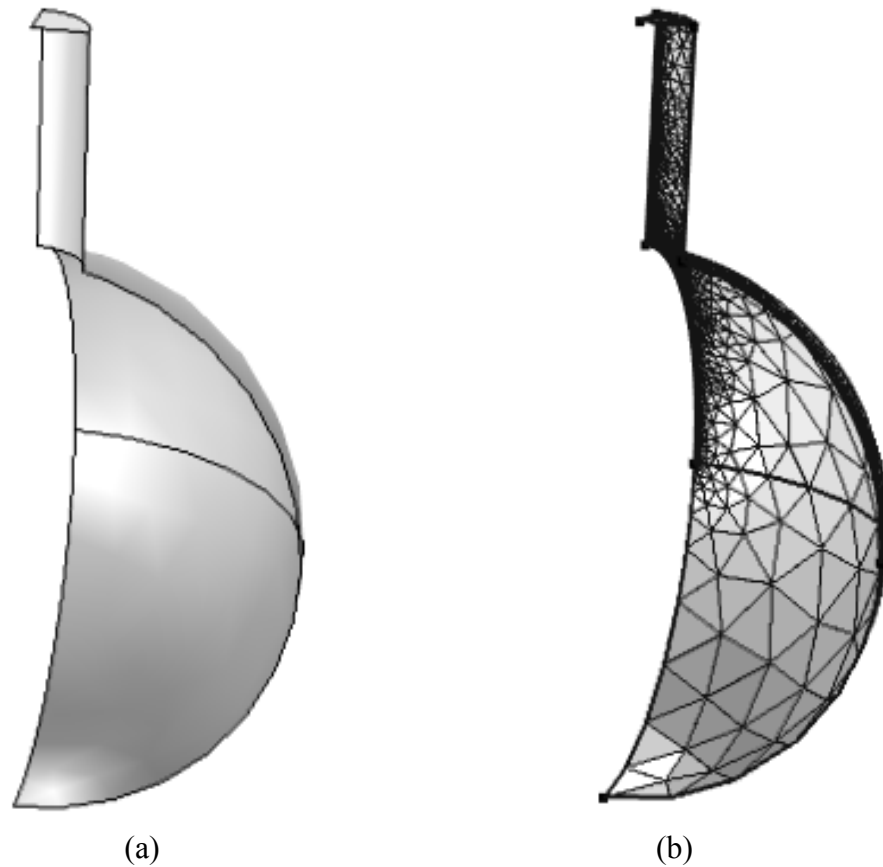


Figure 7- 2: Quarter Model for the Spherical Vessel-Nozzle Junction (a) Geometry (b) Mesh

The following ranges of non-dimensional geometric parameters were used in the simulations.

$$RT = 25 + 25i, \{i, 1, 5\}$$

$$tT = 0.25j, \{j, 1, 6\}$$

$$rR = 0.1k, \{k, 1, 5\}$$

Cases involving combination of any of the above selected values of parameters that violate the thin shell assumption are discarded, resulting into a total of 138 valid simulation runs. Throughout the analysis, the FEM and exact solutions coincide perfectly providing the confidence in their use as verification source(s) for the approximate solutions. Two typical cases were selected to be presented here; one to show relatively high deviation of the approximate solution from the exact one, and the other to show a case with better agreement between the exact and the approximate solutions. Stress variations predicted by the approximate as well as the FEM/exact solutions are as shown in Figure 2-3 for a typical vessel-nozzle geometry with $RT = 50$, $tT = 0.25$ and $rR = 0.1$. This represents a choice with low rR . Therefore, some slight deviation in the results should be expected. Despite that, however, similar trend in the behavior of the stresses are obtained by both the methods. And, still a fair prediction by the approximate solution is achieved compared to that of FEM/exact approach. Stress variations for the second case with $RT = 50$, $tT = 0.25$ and $rR = 0.2$ is shown in Figure 2-4 and it corresponds to a case with higher value of the selected rR than the previous one. Hence, the reason behind the excellent agreement between the results achieved. A choice of higher rR will even give a better result. One important point worth mentioning here is that in most cases the approximate solution provides a more conservative prediction of the maximum stress in both the nozzle and in the vessel for all the values of rR and other geometric ratios considered in this study. Since this maximum stress is the most important in design (SCF), it can be argued that the approximate analysis entails safety. This fact is clearly evident in Table 7-2.

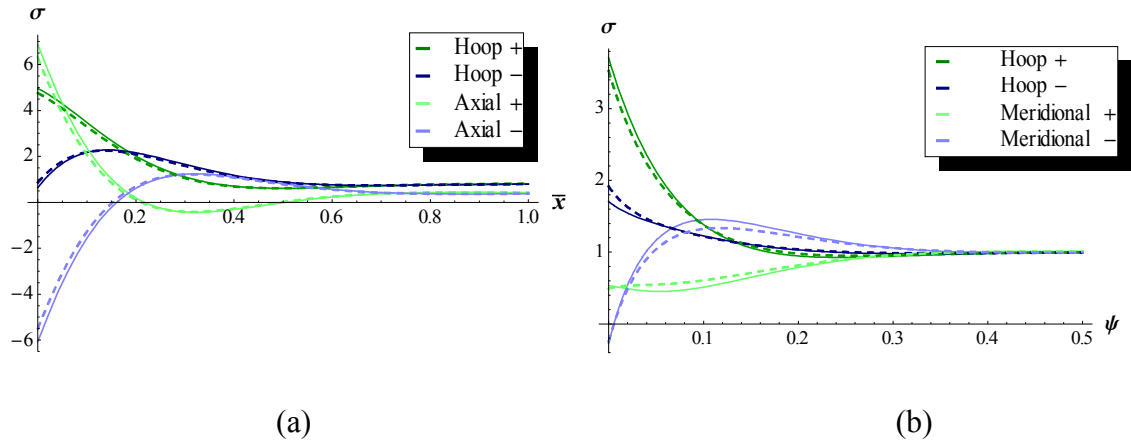


Figure 7- 3: Comparison between FEM/Exact (dashed) and Approximate (continuous) Solutions for a Vessel-Nozzle Junction with $RT = 50$, $tT = 0.25$ and $rR = 0.1$ for (a) Nozzle (b) Spherical vessel

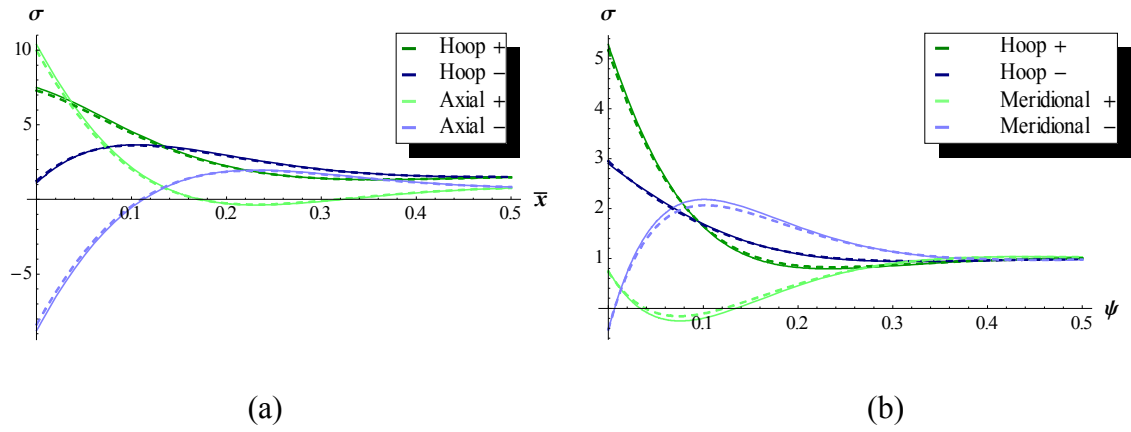


Figure 7- 4: Comparison between FEM/Exact (dashed) and Approximate (continuous) Solutions for a Vessel-Nozzle Junction with $RT = 50$, $tT = 0.25$ and $rR = 0.2$ for (a) Nozzle (b) Spherical vessel

Table 7- 2: Predictions of Vessel's and Nozzle's SCF by the Exact, FEM and Approximate Solutions

RT	tT	rR	Spherical Vessel					Cylindrical Nozzle				
			Exact	FEM	Approx.	Error (% Exact)	Error (% FEM)	Exact	FEM	Approx.	Error (% Exact)	Error (% FEM)
50	0.25	0.1	3.53	3.59	3.71	+5.2	+3.2	6.29	6.29	6.87	-0.1	+9.2
		0.2	5.17	5.27	5.28	+2.2	+0.3	9.97	10.06	10.38	+1.0	+3.1
		0.3	6.56	6.69	6.64	+1.2	-0.8	12.84	13.06	13.14	+1.7	+0.6
		0.4	7.72	7.88	7.78	+0.8	-1.3	15.03	15.33	15.25	+2.0	-0.5
		0.5	8.63	8.82	8.68	+0.5	-1.6	16.51	16.86	16.69	+2.2	-1.1
	0.5	0.1	2.67	2.76	2.69	+0.6	-2.6	4.07	4.05	4.26	-0.5	+5.4
		0.2	3.92	4.02	3.94	+0.6	-1.8	6.72	6.76	6.89	+0.5	+1.9
		0.3	4.97	5.08	4.99	+0.5	-1.8	8.87	8.95	8.99	+0.9	+0.5
		0.4	5.84	5.97	5.86	+0.4	-1.8	10.55	10.67	10.64	+1.1	-0.2
		0.5	6.52	6.66	6.54	+0.3	-1.8	11.75	11.92	11.83	+1.4	-0.8
	0.75	0.2	3.26	3.36	3.26	-0.1	-2.8	3.98	4.02	4.05	+0.9	+0.8
		0.3	4.13	4.23	4.14	+0.2	-2.2	5.39	5.44	5.44	+1.0	0.0
		0.4	4.85	4.96	4.86	+0.2	-2.0	6.51	6.58	6.56	+1.1	-0.4
		0.5	5.41	5.52	5.42	+0.3	-1.9	7.36	7.45	7.39	+1.2	-0.7
	1	0.2	2.92	3.00	2.91	-0.3	-3.1	2.97	3.14	2.95	+5.9	-6.2
		0.3	3.68	3.78	3.69	+0.1	-2.4	3.70	3.86	3.70	+4.2	-4.2
		0.4	4.32	4.42	4.33	+0.2	-2.0	4.32	4.47	4.33	+3.4	-3.2
		0.5	4.81	4.91	4.82	+0.3	-1.9	4.80	4.94	4.81	+3.0	-2.7
	1.25	0.3	3.52	3.54	3.55	+0.8	+0.4	3.06	3.23	3.05	+5.3	-5.3
		0.4	4.27	4.29	4.29	+0.5	0.0	3.54	3.69	3.54	+4.2	-4.1
		0.5	4.85	4.89	4.87	+0.4	-0.4	3.91	4.05	3.91	+3.6	-3.4
	1.5	0.3	3.42	3.44	3.45	+0.9	+0.2	2.64	2.82	2.63	+6.5	-6.5

Table 7- 2 (Cont'd): Predictions of Vessel's and Nozzle's SCF by the Exact, FEM and Approximate Solutions

RT	tT	rR	Spherical Vessel					Cylindrical Nozzle				
			Exact	FEM	Approx.	Error (% Exact)	Error (% FEM)	Exact	FEM	Approx.	Error (% Exact)	Error (% FEM)
50	1.5	0.4	4.16	4.19	4.18	+0.6	-0.2	3.03	3.19	3.03	+5.1	-5.0
		0.5	4.74	4.78	4.76	+0.4	-0.5	3.33	3.47	3.33	+4.3	-4.1
75	0.25	0.1	3.93	3.98	4.09	+4.0	+2.6	7.64	7.67	8.21	+0.4	+7.1
		0.2	5.87	5.95	5.96	+1.6	+0.1	12.24	12.40	12.62	+1.3	1.7
		0.3	7.53	7.64	7.59	+0.9	-0.7	15.83	16.09	16.09	+1.6	0.0
		0.4	8.93	9.07	8.98	+0.5	-1.0	18.59	18.92	18.78	+1.8	-0.7
		0.5	10.03	10.19	10.07	+0.4	-1.2	20.48	20.88	20.64	+1.9	-1.1
	0.5	0.1	3.00	3.06	3.01	+0.5	-1.7	4.87	4.88	5.08	+0.2	+4.1
		0.2	4.47	4.56	4.50	+0.5	-1.3	8.15	8.22	8.30	+0.8	+1.0
		0.3	5.73	5.83	5.75	+0.4	-1.4	10.77	10.89	10.88	+1.1	-0.1
		0.4	6.77	6.89	6.79	+0.3	-1.4	12.81	12.98	12.90	+1.3	-0.7
		0.5	7.58	7.71	7.60	+0.3	-1.4	14.28	14.49	14.35	+1.5	-1.0
	0.75	0.1	2.53	2.59	2.50	-0.9	-3.5	2.95	3.11	2.91	+5.3	-6.3
		0.2	3.76	3.83	3.76	0.0	-1.9	4.81	4.86	4.88	+1.1	+0.3
		0.3	4.80	4.88	4.81	+0.2	-1.6	6.51	6.58	6.56	+1.1	-0.4
		0.4	5.66	5.75	5.67	+0.2	-1.4	7.87	7.96	7.91	+1.2	-0.7
		0.5	6.31	6.42	6.33	+0.2	-1.4	8.88	8.99	8.91	+1.3	-1.0
	1	0.2	3.38	3.45	3.37	-0.1	-2.2	3.41	3.55	3.40	+4.1	-4.3
		0.3	4.30	4.38	4.30	+0.1	-1.7	4.31	4.44	4.31	+3.0	-2.9
		0.4	5.06	5.14	5.07	+0.3	-1.4	5.05	5.18	5.06	+2.5	-2.3
		0.5	5.71	5.76	5.73	+0.3	-0.5	5.64	5.75	5.66	+1.9	-1.6
	1.25	0.2	3.12	3.19	3.16	+1.2	-0.9	2.86	3.00	2.84	+5.2	-5.5
		0.3	4.21	4.24	4.24	+0.7	+0.1	3.55	3.68	3.55	+3.7	-3.7
		0.4	5.12	5.16	5.14	+0.4	-0.3	4.13	4.25	4.13	+3.0	-2.9

Table 7- 2 (Cont'd): Predictions of Vessel's and Nozzle's SCF by the Exact, FEM and Approximate Solutions

RT	tT	rR	Spherical Vessel					Cylindrical Nozzle				
			Exact	FEM	Approx.	Error (% Exact)	Error (% FEM)	Exact	FEM	Approx.	Error (% Exact)	Error (% FEM)
75	1.25	0.5	5.81	5.86	5.83	+0.3	-0.6	4.56	4.68	4.57	+2.6	-2.4
	1.5	0.2	3.02	3.04	3.06	+1.2	+0.5	2.49	2.65	2.47	+6.3	-6.7
		0.3	4.09	4.12	4.12	+0.7	-0.1	3.06	3.19	3.05	+4.5	-4.5
		0.4	4.98	5.03	5.01	+0.4	-0.5	3.53	3.65	3.52	+3.6	-3.5
		0.5	5.68	5.74	5.70	+0.3	-0.7	3.88	4.00	3.88	+3.1	-2.9
100	0.25	0.1	4.25	4.30	4.40	+3.3	+2.2	8.78	8.84	9.35	+0.7	+5.8
		0.2	6.44	6.52	6.53	+1.3	0.0	14.16	14.35	14.50	+1.3	+1.1
		0.3	8.34	8.44	8.39	+0.7	-0.6	18.35	18.64	18.59	+1.6	-0.3
		0.4	9.94	10.07	9.98	+0.4	-0.9	21.58	21.95	21.76	+1.7	-0.9
		0.5	11.21	11.35	11.24	+0.3	-1.0	23.83	24.26	23.97	+1.8	-1.2
	0.5	0.1	3.26	3.32	3.28	+0.5	-1.3	5.56	5.59	5.77	+0.5	+3.3
		0.2	4.93	5.01	4.96	+0.4	-1.1	9.35	9.44	9.49	+1.0	+0.5
		0.3	6.36	6.45	6.38	+0.3	-1.1	12.36	12.52	12.46	+1.3	-0.5
		0.4	7.55	7.66	7.57	+0.3	-1.2	14.72	14.93	14.80	+1.4	-0.9
		0.5	8.48	8.59	8.50	+0.2	-1.2	16.41	16.65	16.47	+1.5	-1.1
	0.75	0.1	2.77	2.82	2.75	-0.7	-2.7	3.22	3.36	3.23	+4.1	-3.8
		0.2	4.17	4.23	4.17	+0.1	-1.5	5.51	5.57	5.57	+1.1	0.0
		0.3	5.35	5.43	5.36	+0.2	-1.2	7.45	7.54	7.50	+1.2	-0.6
		0.4	6.33	6.42	6.35	+0.2	-1.2	9.01	9.13	9.04	+1.3	-0.9
		0.5	7.08	7.18	7.10	+0.2	-1.1	10.16	10.30	10.19	+1.4	-1.1
	1	0.1	2.51	2.57	2.48	-1.1	-3.2	2.60	2.75	2.56	+5.6	-6.9
		0.2	3.76	3.82	3.76	0.0	-1.6	3.79	3.91	3.78	+3.2	-3.3
		0.3	4.81	4.88	4.82	+0.2	-1.3	4.82	4.93	4.82	+2.4	-2.3
		0.4	5.75	5.80	5.77	+0.3	-0.4	5.67	5.79	5.68	+2.0	-1.8

Table 7- 2 (Cont'd): Predictions of Vessel's and Nozzle's SCF by the Exact, FEM and Approximate Solutions

RT	tT	rR	Spherical Vessel					Cylindrical Nozzle				
			Exact	FEM	Approx.	Error (% Exact)	Error (% FEM)	Exact	FEM	Approx.	Error (% Exact)	Error (% FEM)
100	1	0.5	6.51	6.57	6.52	+0.2	-0.7	6.44	6.53	6.46	+1.4	-1.1
	1.25	0.2	3.54	3.56	3.58	+1.0	+0.5	3.16	3.29	3.14	+4.0	-4.3
		0.3	4.80	4.83	4.82	+0.6	-0.2	3.96	4.08	3.96	+2.9	-2.9
		0.4	5.83	5.88	5.85	+0.3	-0.5	4.62	4.73	4.62	+2.4	-2.3
		0.5	6.63	6.69	6.64	+0.2	-0.7	5.12	5.23	5.13	+2.1	-1.9
	1.5	0.2	3.43	3.45	3.46	+1.1	+0.3	2.75	2.88	2.73	+4.8	-5.2
		0.3	4.66	4.70	4.69	+0.6	-0.3	3.41	3.53	3.40	+3.5	-3.6
		0.4	5.68	5.74	5.71	+0.4	-0.6	3.94	4.05	3.94	+2.8	-2.8
125	0.25	0.1	4.54	4.58	4.67	+2.9	+1.8	9.80	9.89	10.36	+0.9	+4.7
		0.2	6.95	7.03	7.02	+1.1	-0.1	15.84	16.06	16.17	+1.4	+0.6
		0.3	9.05	9.15	9.10	+0.5	-0.5	20.56	20.90	20.78	+1.6	-0.5
		0.4	10.84	10.95	10.87	+0.3	-0.7	24.22	24.62	24.39	+1.6	-0.9
		0.5	12.25	12.37	12.28	+0.2	-0.8	26.78	27.26	26.91	+1.8	-1.3
	0.5	0.1	3.49	3.54	3.51	+0.4	-1.1	6.17	6.22	6.38	+0.7	+2.7
		0.2	5.34	5.41	5.36	+0.4	-1.0	10.40	10.53	10.54	+1.2	+0.1
		0.3	6.92	7.01	6.94	+0.3	-1.0	13.77	13.96	13.86	+1.3	-0.7
		0.4	8.24	8.35	8.26	+0.2	-1.0	16.40	16.63	16.47	+1.4	-0.9
		0.5	9.27	9.38	9.29	+0.2	-1.0	18.29	18.55	18.35	+1.4	-1.1
	0.75	0.1	2.98	3.03	2.96	-0.6	-2.2	3.48	3.58	3.57	+2.8	-0.2
		0.2	4.53	4.59	4.53	+0.1	-1.3	6.12	6.20	6.18	+1.3	-0.3
		0.3	5.84	5.92	5.85	+0.2	-1.1	8.28	8.39	8.33	+1.3	-0.8
		0.4	6.93	7.01	6.94	+0.2	-1.0	10.01	10.15	10.04	+1.3	-1.0
		0.5	7.76	7.85	7.77	+0.2	-1.0	11.29	11.44	11.31	+1.4	-1.1

Table 7- 2 (Cont'd): Predictions of Vessel's and Nozzle's SCF by the Exact, FEM and Approximate Solutions

RT	tT	rR	Spherical Vessel					Cylindrical Nozzle				
			Exact	FEM	Approx.	Error (% Exact)	Error (% FEM)	Exact	FEM	Approx.	Error (% Exact)	Error (% FEM)
125	1	0.1	2.71	2.76	2.68	-0.9	-2.6	2.79	2.91	2.75	+4.6	-5.7
		0.2	4.10	4.15	4.10	0.0	-1.4	4.11	4.22	4.11	+2.7	-2.8
		0.3	5.27	5.33	5.30	+0.5	-0.7	5.26	5.37	5.27	+2.0	-1.9
		0.4	6.38	6.43	6.40	+0.3	-0.6	6.28	6.37	6.30	+1.4	-1.1
		0.5	7.21	7.29	7.22	+0.2	-0.9	7.14	7.24	7.16	+1.4	-1.2
	1.25	0.1	2.52	2.57	2.50	-0.9	-2.7	2.38	2.53	2.34	+5.9	-7.2
		0.2	3.91	3.94	3.95	+0.9	+0.3	3.43	3.54	3.41	+3.3	-3.6
		0.3	5.31	5.36	5.34	+0.5	-0.3	4.32	4.43	4.32	+2.4	-2.4
		0.4	6.47	6.53	6.48	+0.3	-0.6	5.05	5.16	5.06	+2.0	-1.9
		0.5	7.34	7.42	7.36	+0.2	-0.8	5.61	5.71	5.62	+1.8	-1.6
	1.5	0.2	3.79	3.82	3.83	+0.9	+0.1	2.98	3.10	2.96	+4.0	-4.3
		0.3	5.16	5.21	5.19	+0.5	-0.4	3.71	3.82	3.71	+2.8	-2.9
		0.4	6.30	6.37	6.32	+0.3	-0.7	4.31	4.41	4.31	+2.4	-2.3
		0.5	7.18	7.26	7.20	+0.2	-0.9	4.75	4.85	4.76	+2.1	-1.9
150	0.25	0.1	4.79	4.83	4.91	+2.5	+1.5	10.73	10.84	11.27	+1.0	+4.0
		0.2	7.41	7.48	7.47	+0.9	-0.1	17.36	17.60	17.67	+1.4	+0.4
		0.3	9.69	9.79	9.74	+0.5	-0.5	22.56	22.90	22.77	+1.5	-0.6
		0.4	11.65	11.75	11.68	+0.3	-0.6	26.60	27.02	26.76	+1.6	-1.0
		0.5	13.19	13.30	13.21	+0.2	-0.7	29.44	29.98	29.57	+1.8	-1.4
	0.5	0.1	3.70	3.75	3.71	+0.4	-0.9	6.73	6.79	6.94	+0.9	+2.2
		0.2	5.70	5.77	5.72	+0.3	-0.9	11.36	11.50	11.49	+1.2	-0.1
		0.3	7.43	7.51	7.45	+0.3	-0.9	15.04	15.25	15.13	+1.4	-0.8
		0.4	8.87	8.97	8.89	+0.2	-0.9	17.92	18.16	17.99	+1.4	-1.0
		0.5	9.98	10.09	10.00	+0.2	-0.8	19.99	20.26	20.04	+1.3	-1.1

Table 7- 2 (Cont'd): Predictions of Vessel's and Nozzle's SCF by the Exact, FEM and Approximate Solutions

RT	tT	rR	Spherical Vessel					Cylindrical Nozzle				
			Exact	FEM	Approx.	Error (% Exact)	Error (% FEM)	Exact	FEM	Approx.	Error (% Exact)	Error (% FEM)
150	0.75	0.1	3.16	3.21	3.15	-0.5	-1.9	3.80	3.85	3.88	+1.3	+1.0
		0.2	4.85	4.91	4.86	+0.1	-1.1	6.68	6.76	6.74	+1.3	-0.4
		0.3	6.28	6.35	6.30	+0.2	-0.9	9.04	9.16	9.08	+1.3	-0.9
		0.4	7.47	7.55	7.48	+0.2	-0.9	10.92	11.07	10.95	+1.3	-1.0
		0.5	8.37	8.46	8.39	+0.3	-0.8	12.31	12.48	12.33	+1.4	-1.2
	1	0.1	2.88	2.93	2.86	-0.7	-2.2	2.95	3.07	2.92	+3.9	-4.9
		0.2	4.40	4.45	4.40	+0.1	-1.1	4.41	4.51	4.41	+2.3	-2.3
		0.3	5.73	5.78	5.76	+0.4	-0.4	5.67	5.77	5.68	+1.8	-1.6
		0.4	6.94	7.01	6.96	+0.3	-0.7	6.84	6.94	6.86	+1.4	-1.1
		0.5	7.84	7.93	7.86	+0.2	-0.9	7.78	7.89	7.79	+1.4	-1.2
	1.25	0.1	2.69	2.74	2.67	-0.7	-2.3	2.52	2.65	2.49	+5.0	-6.2
		0.2	4.25	4.28	4.29	+0.8	+0.1	3.67	3.77	3.66	+2.8	-3.0
		0.3	5.78	5.83	5.81	+0.4	-0.4	4.65	4.74	4.65	+2.1	-2.0
		0.4	7.04	7.11	7.06	+0.3	-0.7	5.45	5.54	5.45	+1.8	-1.6
		0.5	7.99	8.08	8.01	+0.2	-0.9	6.05	6.14	6.06	+1.6	-1.4
	1.5	0.1	2.53	2.58	2.52	-0.6	-2.4	2.24	2.37	2.20	+6.1	-7.3
		0.2	4.12	4.15	4.15	+0.8	0.0	3.19	3.29	3.17	+3.4	-3.6
		0.3	5.62	5.67	5.65	+0.4	-0.5	3.99	4.09	3.99	+2.5	-2.5
		0.4	6.86	6.93	6.88	+0.3	-0.8	4.64	4.73	4.64	+2.0	-2.0
		0.5	7.81	7.90	7.83	+0.2	-0.9	5.12	5.22	5.13	+1.8	-1.7

7.3 ρ -SCF PLOTS VERSUS INDIVIDUAL SCF- rR PLOTS

Study on the behavior of the SCFs was carried out in this research to establish the uniqueness or otherwise of the ρ -SCF plots. Presentation of the stress analysis results in terms of ρ -SCF plots for different tT ratios is, so far, the most appealing method available. It makes possible the use of a condensed form of representation by combining the two parameters rR and RT into one, $\rho = rR\sqrt{RT}$, and plotting the ρ -SCF variation on a single set of grids for various tT ratios. This technique, developed by Leckie and Penny [9] as shown in Figure 7-5, is adopted in BS5500. These curves may, however, be inaccurate for the following reasons.

1. After running some simulations for RT and tT ranging from 50 to 150 and 0.25 to 1, respectively, it was noticed, as demonstrated in Figure 7-6, that these curves yield different SCFs for different RT and rR values corresponding to the same ρ . For e.g., a nozzle-vessel juncture with $RT = 50$, $tT = 1.0$ and $rR = 0.57$ and another nozzle-vessel juncture with $RT = 150$, $tT = 1.0$ and $rR = 0.33$ both have same $\rho = 4$ and tT values. But, whereas the former case results in $SCF \approx 5$, the later gives $SCF \approx 6$, representing an error of about 17%.
2. The curves reported in [9] cover even smaller values of the ratios r/t which contradicts the assumption of thin shell analysis ($r/t > 10$). For e.g., Figure 2-5 shows a prediction of $SCF \approx 1.75$ for a vessel-nozzle juncture with $t/T = 0.5$ and $\rho = 0.1$, whereas based on Table 7-3 the validity for thin shell assumption requires the ρ_{min} to be 0.7 and 0.4 for typical geometries with $RT = 50$ and 150, respectively. Hence, the selected vessel-nozzle geometry ($\rho = 0.1$) doesn't qualify as thin shell.

3. Location (vessel or nozzle) of the SCF may not be true in all the ratios covered in the conventional ρ -SCF plots. Dekker and Brink [23] even suggested that for $tT < 1$, one should not follow this method.

In this research, the aforementioned flaws of ρ -SCF are redressed by presenting an alternative approach, where separate charts (corresponding to different RT ratios) provide variations in SCF with the ratios tT and rR . Similar approach has been adopted by some previous researchers. The present study, however, covers a wide variety of cases in a more comprehensive manner. Figure 7-7 shows a typical example of the proposed charts verified with FEM/exact solution for the vessel and nozzle with a typical value of $RT = 100$. Prediction by the approximate solution still proves to be sufficient and conservative. Consequently, the alternative presentation shown in figures 7-8 to 7-12 is adopted. This way, the variations in SCF with the ratios tT and rR are given for a particular RT ratio. Also, both the nozzle and vessel SCF plots are indicated on the same set of grids with the nozzle's graphs on the left side while the vessel's graphs are on the right side. By making reference to Table 7-3, these plots are produced making sure that the thin shell assumption ($r/t > 10$) is not violated.

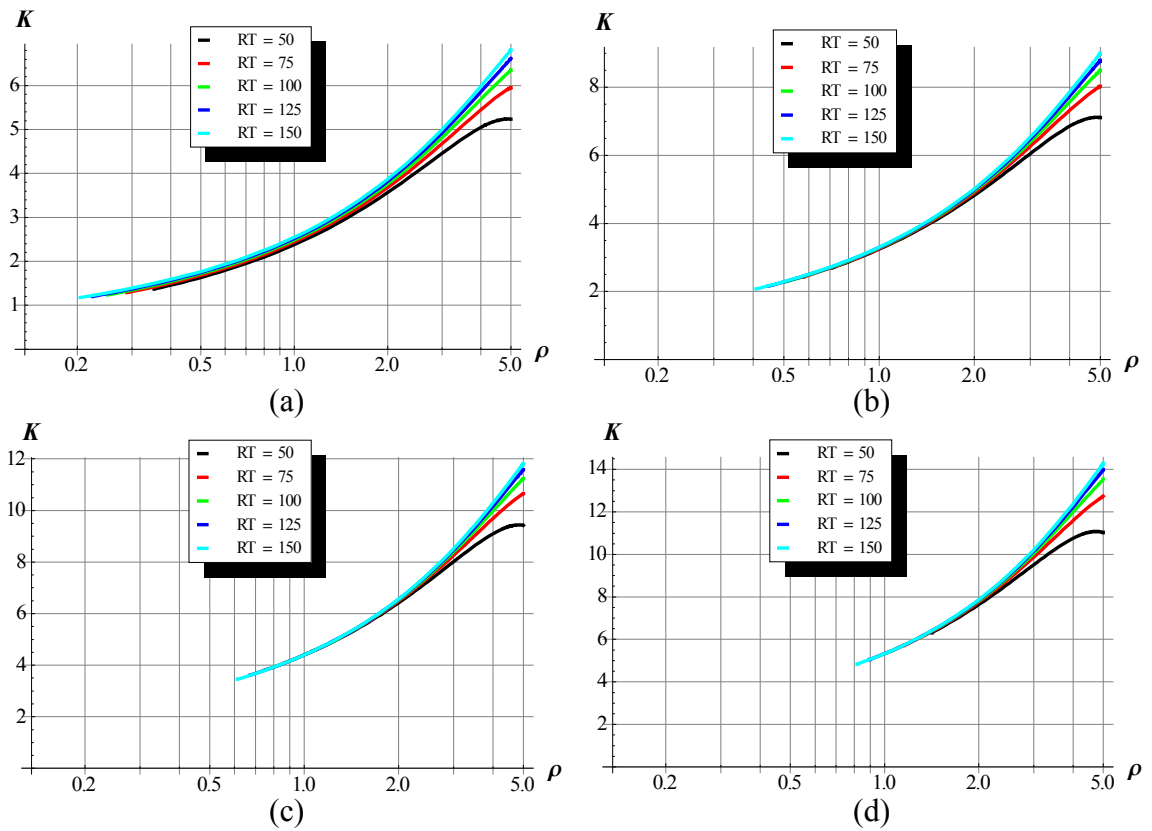
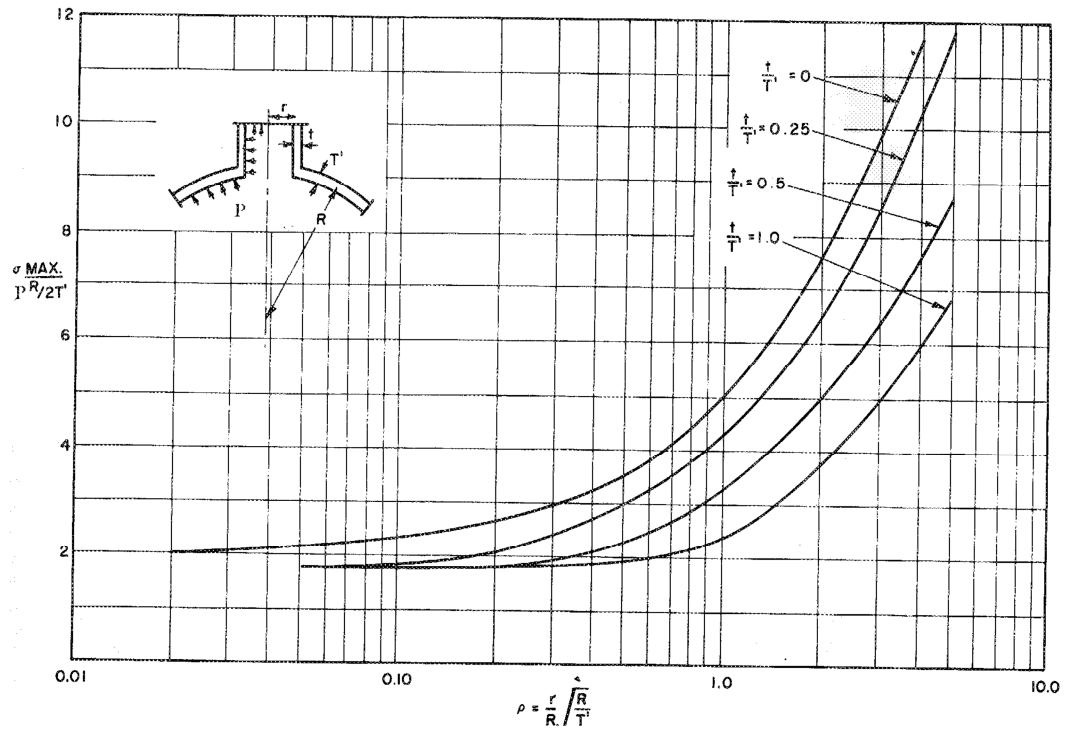
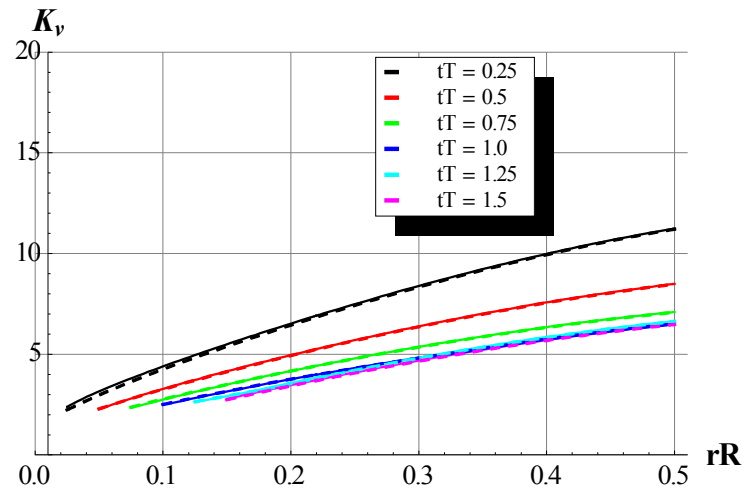
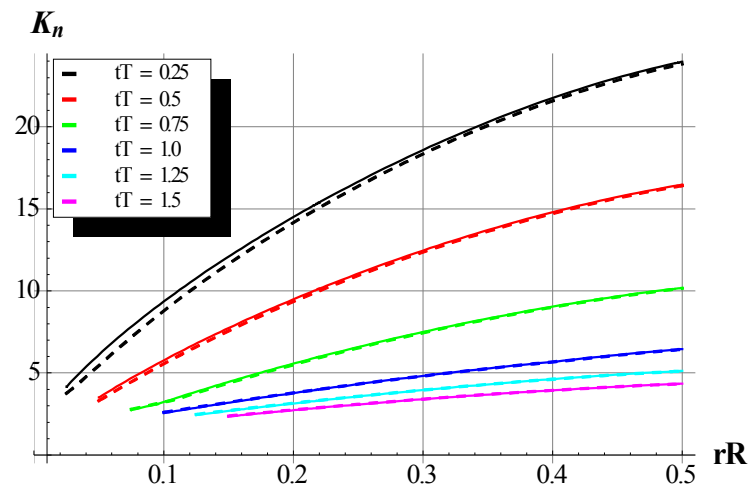


Table 7- 3: Minimum rR and ρ Values for the Validity of Thin Shell Assumption

RT	tT	rR_{min}	ρ_{min}
50	0.25	0.05	0.353553
	0.5	0.1	0.707107
	0.75	0.15	1.06066
	1	0.2	1.41421
	1.25	0.25	1.76777
	1.5	0.3	2.12132
75	0.25	0.033333	0.288675
	0.5	0.066667	0.57735
	0.75	0.1	0.866025
	1	0.133333	1.1547
	1.25	0.166667	1.44338
	1.5	0.2	1.73205
100	0.25	0.025	0.25
	0.5	0.05	0.5
	0.75	0.075	0.75
	1	0.1	1
	1.25	0.125	1.25
	1.5	0.15	1.5
125	0.25	0.02	0.223607
	0.5	0.04	0.447214
	0.75	0.06	0.67082
	1	0.08	0.894427
	1.25	0.1	1.11803
	1.5	0.12	1.34164
150	0.25	0.016667	0.204124
	0.5	0.033333	0.408248
	0.75	0.05	0.612372
	1	0.066667	0.816497
	1.25	0.083333	1.02062
	1.5	0.1	1.22474



(a)



(b)

Figure 7- 7: FEM/Exact (dashed line) and Approximate (continuous line) Variation of Maximum SCF with Geometric Ratios for $RT = 100$: (a) Vessel (b) Nozzle

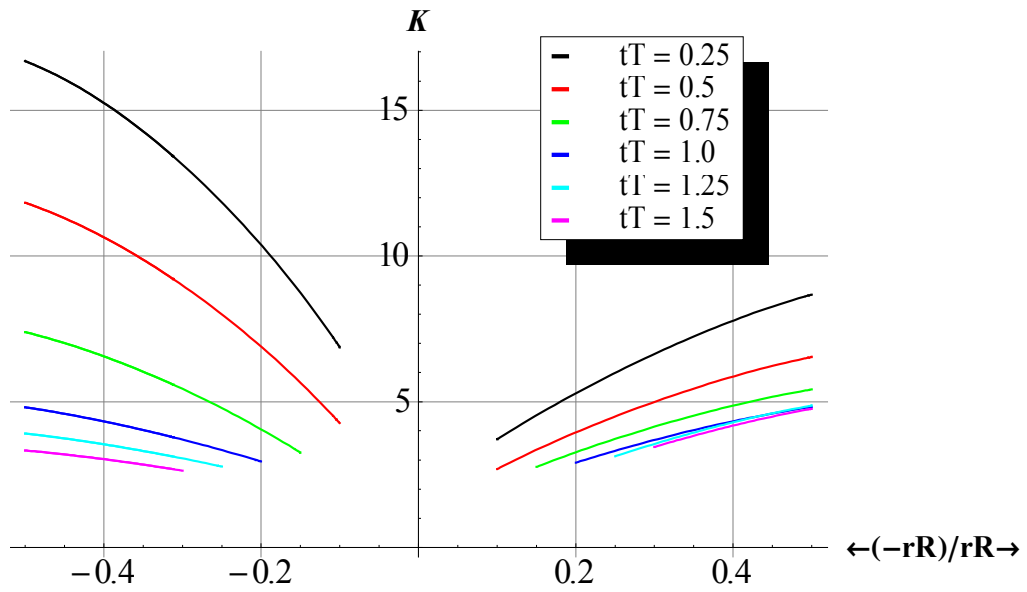


Figure 7- 8: Variation of SCF in the Spherical Vessel (right set of graphs) and Nozzle (left set of graphs) with Geometric Ratios for Constant $RT = 50$

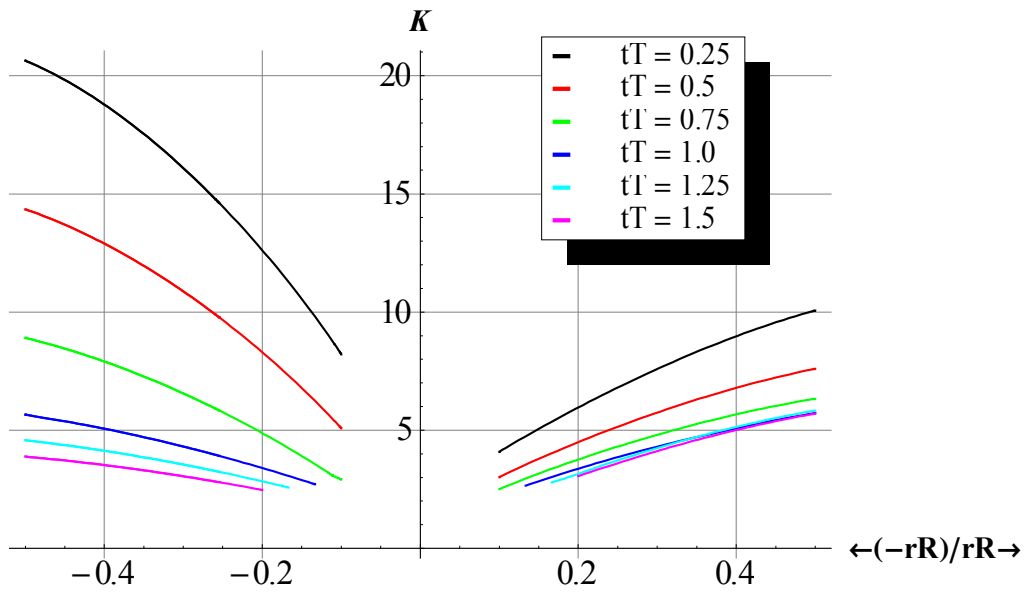


Figure 7- 9: Variation of SCF in the Spherical Vessel (right set of graphs) and Nozzle (left set of graphs) with Geometric Ratios for Constant $RT = 75$

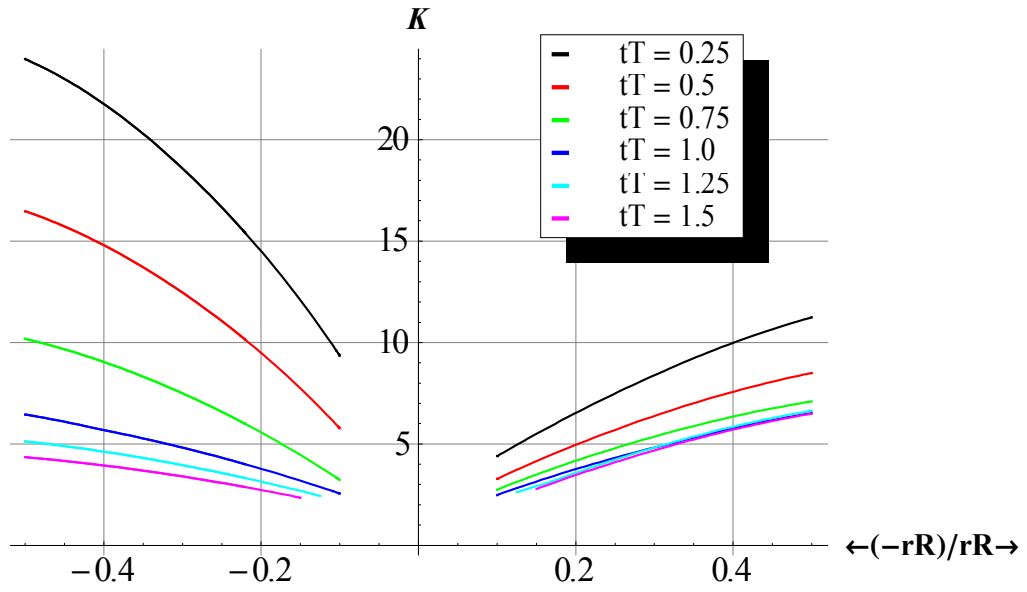


Figure 7- 10: Variation of SCF in the Spherical Vessel (right set of graphs) and Nozzle (left set of graphs) with Geometric Ratios for Constant $RT = 100$

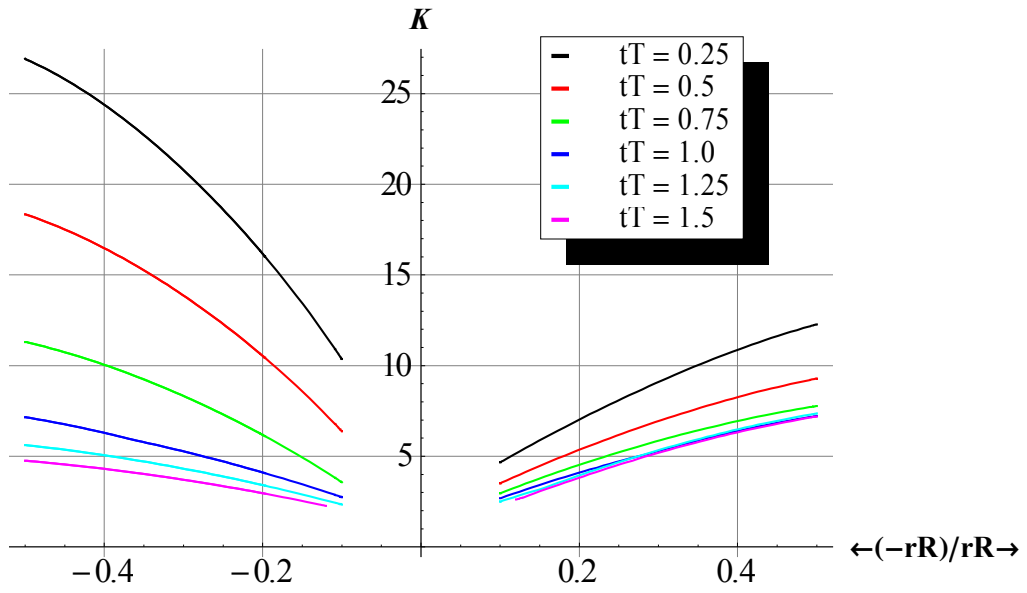


Figure 7- 11: Variation of SCF in the Spherical Vessel (right set of graphs) and Nozzle (left set of graphs) with Geometric Ratios for Constant $RT = 125$

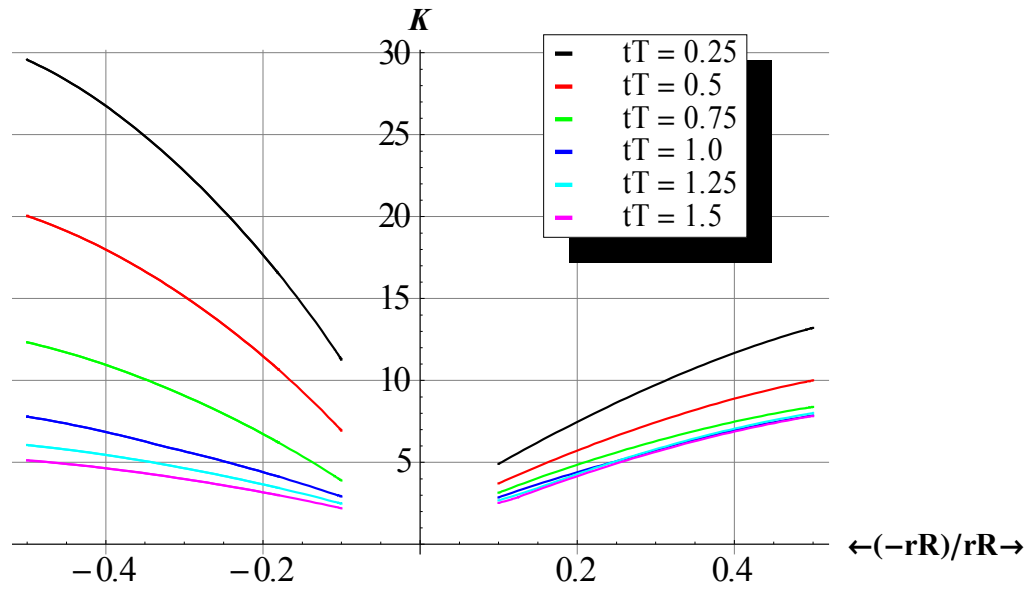


Figure 7- 12: Variation of SCF in the Spherical Vessel (right set of graphs) and Nozzle (left set of graphs) with Geometric Ratios for Constant $RT = 150$

7.4 STUDY ON THE TYPE AND LOCATION OF MAXIMUM STRESS AT THE VESSEL-NOZZLE JUNCTURE

The issue of location of maximum stresses at the vessel-nozzle juncture is addressed by the extensive analysis presented herein. It is wrong to always assume that the maximum stress occur in the vessel. This is believed to be one of the reasons behind the inaccuracies of the ρ -SCF approach [30]. While this assumption may be true for some geometrical ratios, the same may not hold in others. In fact, the outcome of the analysis conducted on all the geometric ratios considered in this work show that about 58% of the cases result in the maximum stresses occurring in the nozzle with about 42% otherwise. Some possible cases showing the difference in the location of the maximum stresses are shown in Figure 7-13. The nozzle's graphs are shown on the left side while the vessel's

graphs are on the right side of the same set of grids. Appendix B gives the behavior of such stresses for some more spherical vessel-cylindrical nozzle geometric ratios. Comprehensive information about the location and type of the stresses at the juncture for various values of the dimensionless parameters is given in Table 7-4.

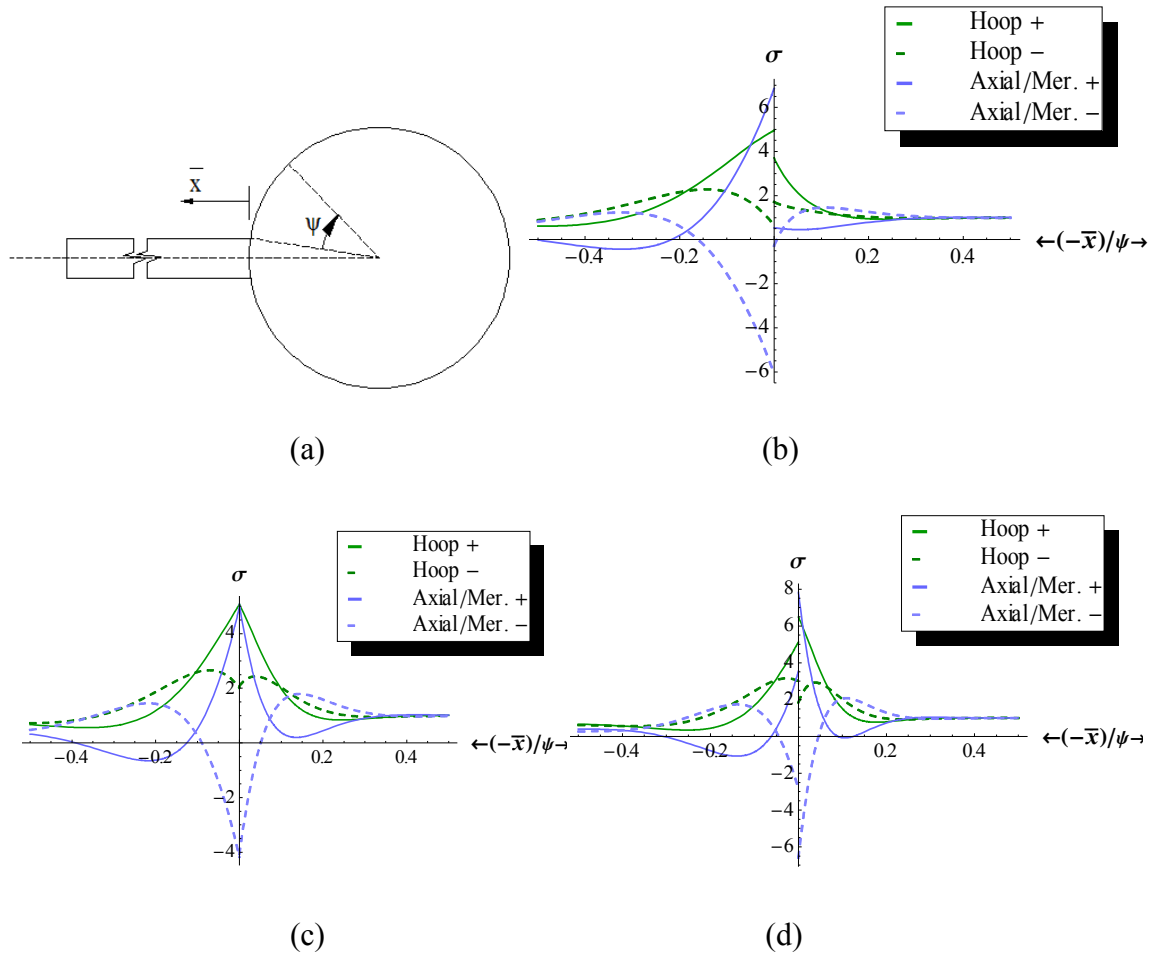


Figure 7- 13: Vessel-Nozzle Junction with Difference in the Location of the Maximum Stresses: (a) Vessel-Nozzle Orientation and Position Variables (b) $tT = 0.25$, $RT = 50$ and $rR = 0.1$ (c) $tT = 1.0$, $RT = 75$ and $rR = 0.4$ (d) $tT = 1.5$, $RT = 150$ and $rR = 0.5$

Table 7- 4: Type and Location of Maximum Stress at the Vessel-Nozzle Junction

RT	tT	rR	Type	Location	SCF
50	0.25	0.1	Axial +	Nozzle	6.87
		0.2	Axial +	Nozzle	10.38
		0.3	Axial +	Nozzle	13.14
		0.4	Axial +	Nozzle	15.25
		0.5	Axial +	Nozzle	16.69
	0.5	0.1	Axial +	Nozzle	4.26
		0.2	Axial +	Nozzle	6.89
		0.3	Axial +	Nozzle	8.99
		0.4	Axial +	Nozzle	10.64
		0.5	Axial +	Nozzle	11.83
	0.75	0.2	Axial +	Nozzle	4.05
		0.3	Axial +	Nozzle	5.44
		0.4	Axial +	Nozzle	6.56
		0.5	Axial +	Nozzle	7.39
	1	0.2	Hoop +	Nozzle	2.95
		0.3	Hoop +	Nozzle	3.7
		0.4	Hoop +	Vessel	4.33
		0.5	Hoop +	Vessel	4.82
	1.25	0.3	Meridional +	Vessel	3.55
		0.4	Meridional +	Vessel	4.29
		0.5	Meridional +	Vessel	4.87
	1.5	0.3	Meridional +	Vessel	3.45
		0.4	Meridional +	Vessel	4.18
		0.5	Meridional +	Vessel	4.76
75	0.25	0.1	Axial +	Nozzle	8.21
		0.2	Axial +	Nozzle	12.62
		0.3	Axial +	Nozzle	16.09
		0.4	Axial +	Nozzle	18.78
		0.5	Axial +	Nozzle	20.64
	0.5	0.1	Axial +	Nozzle	5.08
		0.2	Axial +	Nozzle	8.3
		0.3	Axial +	Nozzle	10.88
		0.4	Axial +	Nozzle	12.9
		0.5	Axial +	Nozzle	14.35
	0.75	0.1	Hoop +	Nozzle	2.91
		0.2	Axial +	Nozzle	4.88
		0.3	Axial +	Nozzle	6.56

Table 7- 4 (Cont'd): Type and Location of Maximum Stress at the Vessel-Nozzle Junction

RT	tT	rR	Type	Location	SCF
75	0.75	0.4	Axial +	Nozzle	7.91
		0.5	Axial +	Nozzle	8.91
	1	0.2	Hoop +	Nozzle	3.4
		0.3	Hoop +	Nozzle	4.31
		0.4	Meridional +	Vessel	5.07
		0.5	Meridional +	Vessel	5.73
	1.25	0.2	Meridional +	Vessel	3.16
		0.3	Meridional +	Vessel	4.24
		0.4	Meridional +	Vessel	5.14
		0.5	Meridional +	Vessel	5.83
	1.5	0.2	Meridional +	Vessel	3.06
		0.3	Meridional +	Vessel	4.12
		0.4	Meridional +	Vessel	5.01
		0.5	Meridional +	Vessel	5.7
100	0.25	0.1	Axial +	Nozzle	9.35
		0.2	Axial +	Nozzle	14.5
		0.3	Axial +	Nozzle	18.59
		0.4	Axial +	Nozzle	21.76
		0.5	Axial +	Nozzle	23.97
	0.5	0.1	Axial +	Nozzle	5.77
		0.2	Axial +	Nozzle	9.49
		0.3	Axial +	Nozzle	12.46
		0.4	Axial +	Nozzle	14.8
		0.5	Axial +	Nozzle	16.47
	0.75	0.1	Axial +	Nozzle	3.23
		0.2	Axial +	Nozzle	5.57
		0.3	Axial +	Nozzle	7.5
		0.4	Axial +	Nozzle	9.04
		0.5	Axial +	Nozzle	10.19
	1	0.1	Hoop +	Nozzle	2.56
		0.2	Hoop +	Nozzle	3.78
		0.3	Hoop +	Vessel	4.82
		0.4	Meridional +	Vessel	5.77
		0.5	Meridional +	Vessel	6.52
	1.25	0.2	Meridional +	Vessel	3.58
		0.3	Meridional +	Vessel	4.82
		0.4	Meridional +	Vessel	5.85
		0.5	Meridional +	Vessel	6.64

Table 7- 4 (Cont'd): Type and Location of Maximum Stress at the Vessel-Nozzle Junction

RT	tT	rR	Type	Location	SCF
100	1.5	0.2	Meridional +	Vessel	3.46
		0.3	Meridional +	Vessel	4.69
		0.4	Meridional +	Vessel	5.71
		0.5	Meridional +	Vessel	6.49
125	0.25	0.1	Axial +	Nozzle	10.36
		0.2	Axial +	Nozzle	16.17
		0.3	Axial +	Nozzle	20.78
		0.4	Axial +	Nozzle	24.39
		0.5	Axial +	Nozzle	26.91
	0.5	0.1	Axial +	Nozzle	6.38
		0.2	Axial +	Nozzle	10.54
		0.3	Axial +	Nozzle	13.86
		0.4	Axial +	Nozzle	16.47
		0.5	Axial +	Nozzle	18.35
	0.75	0.1	Axial +	Nozzle	3.57
		0.2	Axial +	Nozzle	6.18
		0.3	Axial +	Nozzle	8.33
		0.4	Axial +	Nozzle	10.04
		0.5	Axial +	Nozzle	11.31
	1	0.1	Hoop +	Nozzle	2.75
		0.2	Hoop +	Nozzle	4.11
		0.3	Meridional +	Vessel	5.3
		0.4	Meridional +	Vessel	6.4
		0.5	Meridional +	Vessel	7.22
	1.25	0.1	Hoop +	Vessel	2.5
		0.2	Meridional +	Vessel	3.95
		0.3	Meridional +	Vessel	5.34
		0.4	Meridional +	Vessel	6.48
		0.5	Meridional +	Vessel	7.36
	1.5	0.2	Meridional +	Vessel	3.83
		0.3	Meridional +	Vessel	5.19
		0.4	Meridional +	Vessel	6.32
		0.5	Meridional +	Vessel	7.2
150	0.25	0.1	Axial +	Nozzle	11.27
		0.2	Axial +	Nozzle	17.67
		0.3	Axial +	Nozzle	22.77
		0.4	Axial +	Nozzle	26.76
		0.5	Axial +	Nozzle	29.57

Table 7- 4 (Cont'd): Type and Location of Maximum Stress at the Vessel-Nozzle Junction

RT	tT	rR	Type	Location	SCF
150	0.5	0.1	Axial +	Nozzle	6.94
		0.2	Axial +	Nozzle	11.49
		0.3	Axial +	Nozzle	15.13
		0.4	Axial +	Nozzle	17.99
		0.5	Axial +	Nozzle	20.04
	0.75	0.1	Axial +	Nozzle	3.88
		0.2	Axial +	Nozzle	6.74
		0.3	Axial +	Nozzle	9.08
		0.4	Axial +	Nozzle	10.95
		0.5	Axial +	Nozzle	12.33
	1	0.1	Hoop +	Nozzle	2.92
		0.2	Hoop +	Nozzle	4.41
		0.3	Meridional +	Vessel	5.76
		0.4	Meridional +	Vessel	6.96
		0.5	Meridional +	Vessel	7.86
	1.25	0.1	Hoop +	Vessel	2.67
		0.2	Meridional +	Vessel	4.29
		0.3	Meridional +	Vessel	5.81
		0.4	Meridional +	Vessel	7.06
		0.5	Meridional +	Vessel	8.01
	1.5	0.1	Hoop +	Vessel	2.52
		0.2	Meridional +	Vessel	4.15
		0.3	Meridional +	Vessel	5.65
		0.4	Meridional +	Vessel	6.88
		0.5	Meridional +	Vessel	7.83

CHAPTER EIGHT

ANALYSIS AND DEVELOPMENT OF DESIGN CHARTS FOR CYLINDRICAL PRESSURE VESSELS WITH MODERATE-TO- LARGE DIAMETER CYLINDRICAL NOZZLES

As previously mentioned in Chapter Six, solution of the governing equations for cylindrical vessels intersected by cylindrical nozzles are obtained using finite element. This chapter presents the outcome of the finite element analysis carried out using COMSOL software. 3D Shell model was utilized because the nozzles considered in this Chapter are of moderate-to-large diameters (i.e. satisfy the assumption of shell theory).

8.1 NUMERICAL EXPERIMENTS, RESULTS AND DISCUSSIONS

The flowchart shown in Figure 6.6 gives the detailed steps used in achieving the finite element model development and the results presented herein. Advantage of symmetry was taken to arrive at the cylindrical vessel-nozzle problem as shown in Figure 8-1. Since the region of interest is the juncture between the vessel and the nozzle, the mesh within this region was refined to very fine size (Figure 8-1 (b)) in order to increase result's convergence.

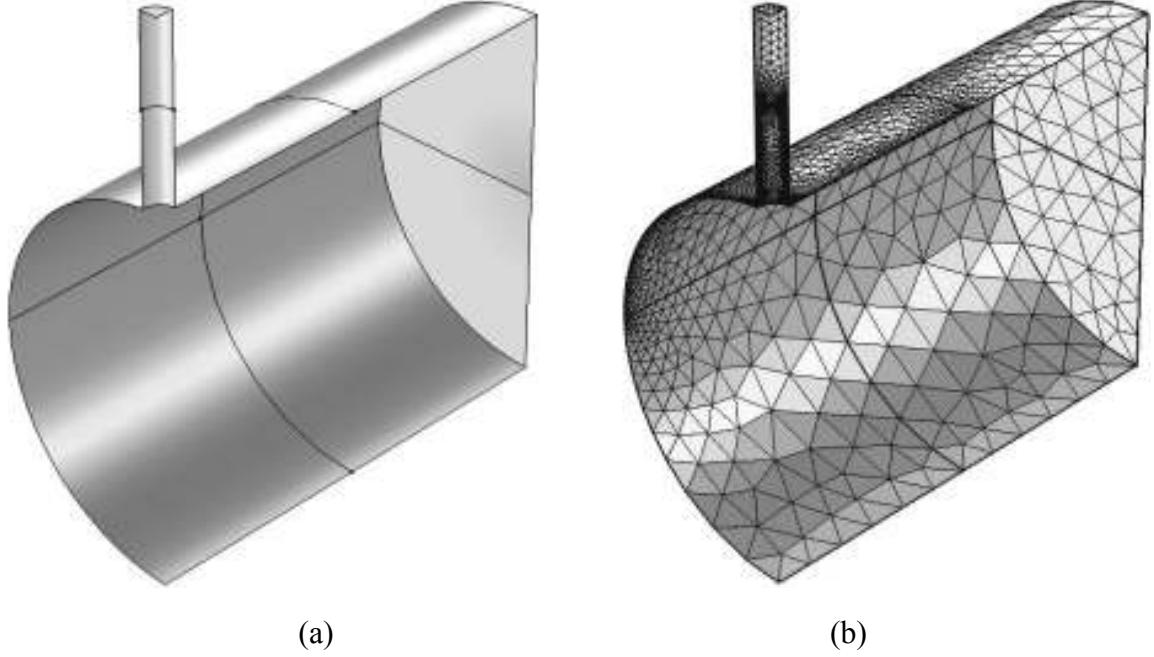


Figure 8- 1: Quarter Model for the Cylindrical Vessel-Nozzle Junction (a) Geometry (b) Mesh

Due to the absence of design-friendly exact analytical solutions of cylindrical vessel-cylindrical nozzle components compared with the case of spherical vessel-cylindrical nozzle problems, the present study intends to report more comprehensive results for the cylindrical vessel-cylindrical nozzle problem. The sole intention is to furnish the design industry with adequate and handy information on the true behavior of the SCF for such components. Consequently, the following ranges of non-dimensional geometric parameters were used in the simulations.

$$RT = 5 + 5i, \{i, 1, 29\}$$

$$tT = 0.25j, \{j, 1, 6\}$$

$$rR = 0.1k, \{k, 1, 10\}$$

Cases involving combination of any of the above selected values of parameters that violate the thin shell assumption are discarded, resulting into a total of 1526 valid numerical experiments. Based on the selected values of rR as mentioned above, it can be realized that the nozzle size is varied from moderate ($rR = 0.1$) to as large as the main vessel's size ($rR = 1$). It was ensured that enough lengths of the vessel and the nozzle were used to allow for adequate dissipation of the discontinuity stresses of interest. For that purpose, a good indicator used was when the discontinuity stresses dissipate well enough resulting in only the membrane stresses at a distance far away from the junction. This way, one is confident that there will be no interaction with other discontinuity stresses arising from adjacent junctions. This fact is evident in figures 8.2 and 8.3 for the four main non-dimensional stress types, and in Figure 8-4 for the von Mises stress distribution of a typical vessel-nozzle configuration.

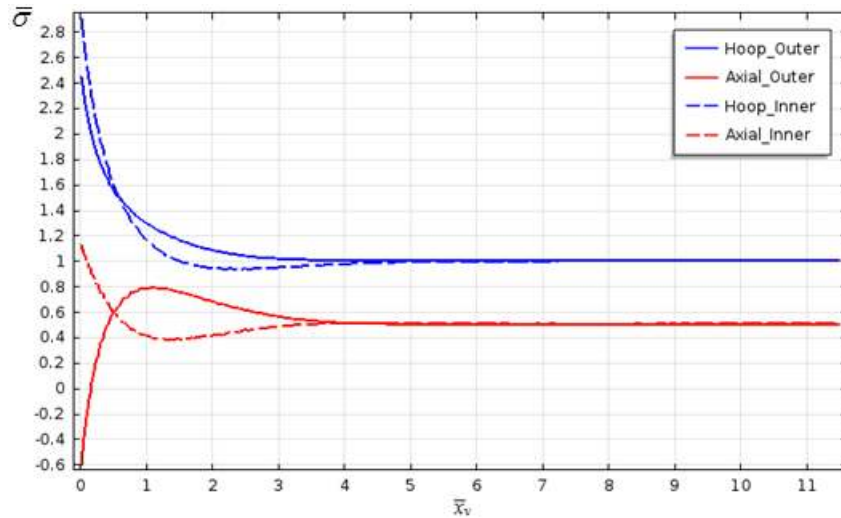


Figure 8- 2: Variation of the Four Types of Stresses in the Main Cylindrical Vessel for a Typical Vessel-Nozzle Juncture with $RT = 50$, $tT = 0.5$ and $rR = 0.1$

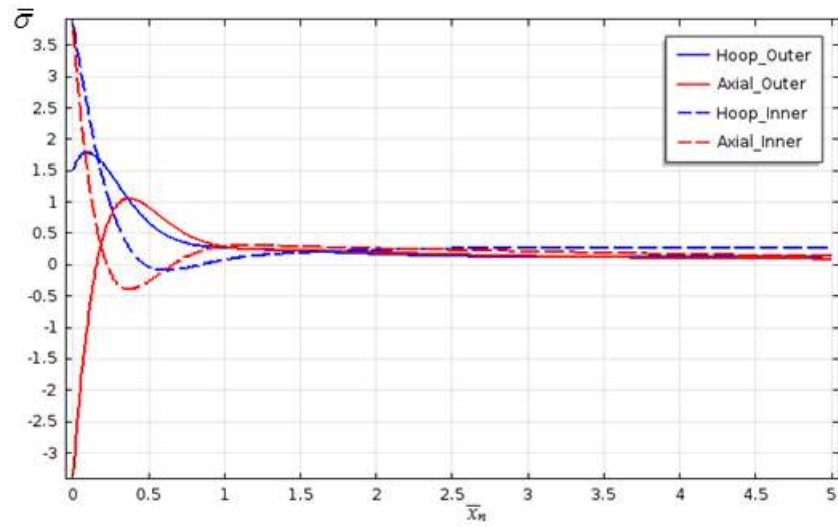


Figure 8- 3: Variation of the Four Types of Stresses in the Cylindrical Nozzle for a Typical Vessel-Nozzle Junction with $RT = 50$, $tT = 0.5$ and $rR = 0.1$

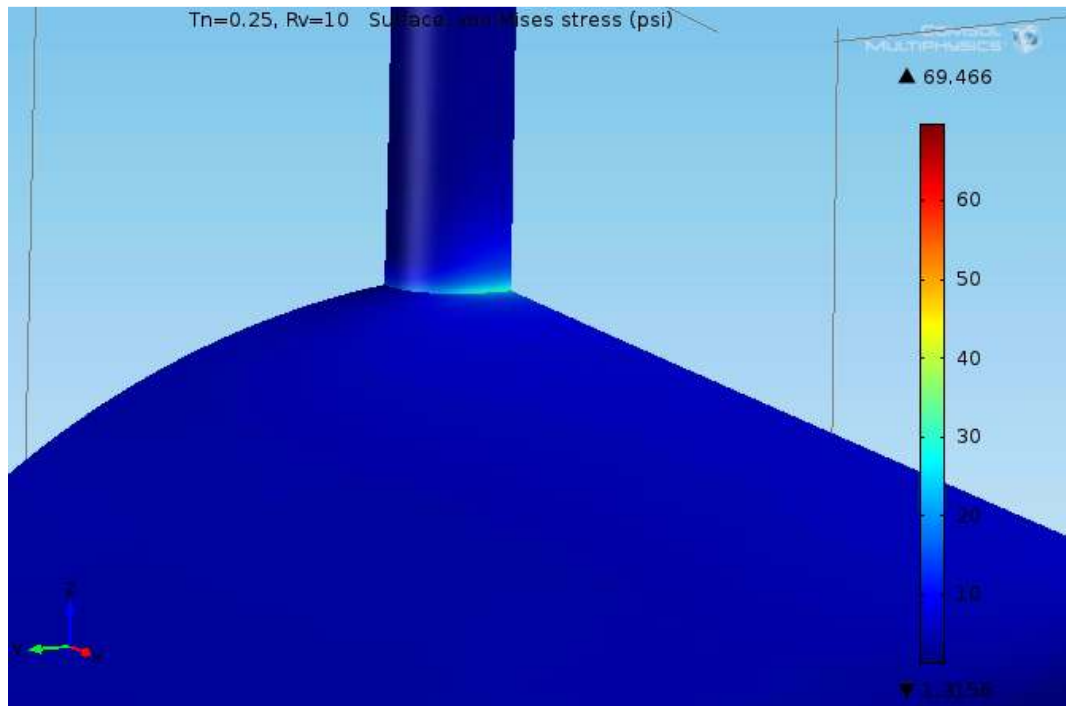


Figure 8- 4: von Mises Stress Plot for the Top Surface of a Typical Vessel-Nozzle Configuration with $RT = 50$, $tT = 0.5$ and $rR = 0.1$

Results achieved at the end of this exercise are presented in Table 8-1 for the vessel's SCF alongside with that of the nozzle for $RT = 25 + 25i$, $\{i, 1, 5\}$. Remaining set of the results achieved for other geometric ratios are given in Table C1 of Appendix C. For conciseness, Table 8-1 incorporates not only the SCF values but the idea of the location and type of the maximum stress, hence, the overall SCF of the configuration. As it can be observed in this result, the location and type of the control SCF fluctuates and in most cases happen to be in the interior of the juncture contrary to the findings in Chapter Seven for the spherical vessel-cylindrical nozzle junctures.

Table 8- 1: Predictions of Vessel's and Nozzle's SCF by the Finite Element Analysis

RT	tT	rR	Cylindrical Vessel		Cylindrical Nozzle		Overall SCF	Location	Type
			SCF	Type	SCF	Type			
50	0.25	0.1	3.61	Hoop -	6.13	Axial -	6.13	Nozzle	Axial -
		0.2	5.54	Hoop -	10.74	Axial -	10.74	Nozzle	Axial -
		0.3	7.34	Hoop -	14.92	Axial -	14.92	Nozzle	Axial -
		0.4	9.03	Hoop -	18.65	Axial -	18.65	Nozzle	Axial -
		0.5	10.48	Hoop -	21.61	Axial -	21.61	Nozzle	Axial -
		0.6	12.07	Hoop -	24.81	Axial -	24.81	Nozzle	Axial -
		0.7	13.73	Hoop -	27.98	Axial -	27.98	Nozzle	Axial -
		0.8	15.25	Hoop -	30.93	Axial -	30.93	Nozzle	Axial -
		0.9	17.14	Hoop -	34.40	Axial -	34.40	Nozzle	Axial -
		1	19.11	Hoop -	36.31	Axial -	36.31	Nozzle	Axial -
	0.5	0.1	2.91	Hoop -	3.83	Hoop -	3.83	Nozzle	Hoop -
		0.2	4.40	Hoop -	6.90	Axial -	6.90	Nozzle	Axial -
		0.3	5.76	Hoop -	9.72	Axial -	9.72	Nozzle	Axial -
		0.4	7.05	Hoop -	12.19	Axial -	12.19	Nozzle	Axial -
		0.5	8.10	Hoop -	14.11	Axial -	14.11	Nozzle	Axial -
		0.6	9.29	Hoop -	16.28	Axial -	16.28	Nozzle	Axial -
		0.7	10.53	Hoop -	18.44	Axial -	18.44	Nozzle	Axial -
		0.8	11.63	Hoop -	20.27	Axial -	20.27	Nozzle	Axial -
		0.9	13.04	Hoop -	22.36	Axial -	22.36	Nozzle	Axial -
		1	14.66	Hoop -	23.41	Axial -	23.41	Nozzle	Axial -
	0.75	0.2	3.74	Hoop -	4.28	Hoop -	4.28	Nozzle	Hoop -
		0.3	4.87	Hoop -	5.78	Axial -	5.78	Nozzle	Axial -

Table 8- 2 (cont'd): Predictions of Vessel's and Nozzle's SCF by the Finite Element Analysis

RT	tT	rR	Cylindrical Vessel		Cylindrical Nozzle		Overall SCF	Location	Type
			SCF	Type	SCF	Type			
50	0.75	0.4	5.93	Hoop -	7.33	Axial -	7.33	Nozzle	Axial -
		0.5	6.77	Hoop -	8.54	Axial -	8.54	Nozzle	Axial -
		0.6	7.74	Hoop -	9.91	Axial -	9.91	Nozzle	Axial -
		0.7	8.75	Hoop -	11.29	Axial -	11.29	Nozzle	Axial -
		0.8	9.63	Hoop -	12.46	Axial -	12.46	Nozzle	Axial -
		0.9	10.79	Hoop -	13.82	Axial -	13.82	Nozzle	Axial -
		1	12.14	Hoop -	14.45	Axial -	14.45	Nozzle	Axial -
	1	0.2	3.35	Hoop -	3.37	Hoop -	3.37	Nozzle	Hoop -
		0.3	4.33	Hoop -	4.33	Hoop -	4.33	Nozzle	Hoop -
		0.4	5.27	Hoop -	5.27	Hoop -	5.27	Nozzle	Hoop -
		0.5	6.00	Hoop -	6.01	Hoop -	6.01	Nozzle	Hoop -
		0.6	6.84	Hoop -	6.86	Hoop -	6.86	Nozzle	Hoop -
		0.7	7.73	Hoop -	7.75	Hoop -	7.75	Nozzle	Hoop -
		0.8	8.49	Hoop -	8.51	Hoop -	8.51	Nozzle	Hoop -
		0.9	9.50	Hoop -	9.51	Hoop -	9.51	Nozzle	Hoop -
		1	10.62	Hoop -	10.62	Hoop -	10.62	Nozzle	Hoop -
	1.25	0.3	3.93	Hoop -	3.56	Hoop -	3.93	Vessel	Hoop -
		0.4	4.78	Hoop -	4.32	Hoop -	4.78	Vessel	Hoop -
		0.5	5.43	Hoop -	4.91	Hoop -	5.43	Vessel	Hoop -
		0.6	6.27	Axial -	5.59	Hoop -	6.27	Vessel	Axial -
		0.7	7.17	Axial -	6.31	Hoop -	7.17	Vessel	Axial -
		0.8	7.94	Axial -	6.90	Hoop -	7.94	Vessel	Axial -
		0.9	8.82	Axial -	7.70	Hoop -	8.82	Vessel	Axial -
		1	9.52	Hoop -	8.57	Hoop -	9.52	Vessel	Hoop -
	1.5	0.3	3.59	Hoop -	3.04	Hoop -	3.59	Vessel	Hoop -
		0.4	4.41	Axial -	3.68	Hoop -	4.41	Vessel	Axial -
		0.5	5.13	Axial -	4.17	Hoop -	5.13	Vessel	Axial -
		0.6	5.98	Axial -	4.74	Hoop -	5.98	Vessel	Axial -
		0.7	6.85	Axial -	5.34	Hoop -	6.85	Vessel	Axial -
		0.8	7.60	Axial -	5.84	Hoop -	7.60	Vessel	Axial -
		0.9	8.45	Axial -	6.50	Hoop -	8.45	Vessel	Axial -
		1	8.81	Axial -	7.19	Hoop -	8.81	Vessel	Axial -
75	0.25	0.1	4.10	Hoop -	7.65	Axial -	7.65	Nozzle	Axial -
		0.2	6.41	Hoop -	13.44	Axial -	13.44	Nozzle	Axial -
		0.3	8.50	Hoop -	18.39	Axial -	18.39	Nozzle	Axial -
		0.4	10.49	Hoop -	22.85	Axial -	22.85	Nozzle	Axial -
		0.5	12.25	Hoop -	26.65	Axial -	26.65	Nozzle	Axial -

Table 8- 3 (cont'd): Predictions of Vessel's and Nozzle's SCF by the Finite Element Analysis

RT	tT	rR	Cylindrical Vessel		Cylindrical Nozzle		Overall SCF	Location	Type
			SCF	Type	SCF	Type			
75	0.25	0.6	14.15	Hoop -	30.43	Axial -	30.43	Nozzle	Axial -
		0.7	16.17	Hoop -	34.46	Axial -	34.46	Nozzle	Axial -
		0.8	18.05	Hoop -	38.18	Axial -	38.18	Nozzle	Axial -
		0.9	20.33	Hoop -	42.23	Axial -	42.23	Nozzle	Axial -
		1	23.10	Hoop -	45.87	Axial -	45.87	Nozzle	Axial -
	0.5	0.1	3.32	Hoop -	4.79	Axial -	4.79	Nozzle	Axial -
		0.2	5.06	Hoop -	8.64	Axial -	8.64	Nozzle	Axial -
		0.3	6.65	Hoop -	11.96	Axial -	11.96	Nozzle	Axial -
		0.4	8.15	Hoop -	14.89	Axial -	14.89	Nozzle	Axial -
		0.5	9.41	Hoop -	17.27	Axial -	17.27	Nozzle	Axial -
		0.6	10.83	Hoop -	19.91	Axial -	19.91	Nozzle	Axial -
		0.7	12.33	Hoop -	22.59	Axial -	22.59	Nozzle	Axial -
		0.8	13.66	Hoop -	24.94	Axial -	24.94	Nozzle	Axial -
		0.9	15.37	Hoop -	27.60	Axial -	27.60	Nozzle	Axial -
		1	17.54	Hoop -	29.43	Axial -	29.43	Nozzle	Axial -
	0.75	0.1	2.87	Hoop -	3.32	Hoop -	3.32	Nozzle	Hoop -
		0.2	4.32	Hoop -	5.08	Axial -	5.08	Nozzle	Axial -
		0.3	5.63	Hoop -	7.11	Axial -	7.11	Nozzle	Axial -
		0.4	6.87	Hoop -	8.93	Axial -	8.93	Nozzle	Axial -
		0.5	7.88	Hoop -	10.43	Axial -	10.43	Nozzle	Axial -
		0.6	9.03	Hoop -	12.11	Axial -	12.11	Nozzle	Axial -
		0.7	10.25	Hoop -	13.83	Axial -	13.83	Nozzle	Axial -
		0.8	11.31	Hoop -	15.30	Axial -	15.30	Nozzle	Axial -
		0.9	12.71	Hoop -	17.04	Axial -	17.04	Nozzle	Axial -
		1	14.49	Hoop -	18.08	Axial -	18.08	Nozzle	Axial -
	1	0.2	3.88	Hoop -	3.90	Hoop -	3.90	Nozzle	Hoop -
		0.3	5.04	Hoop -	5.05	Hoop -	5.05	Nozzle	Hoop -
		0.4	6.13	Hoop -	6.15	Hoop -	6.15	Nozzle	Hoop -
		0.5	7.00	Hoop -	7.02	Hoop -	7.02	Nozzle	Hoop -
		0.6	8.02	Hoop -	8.04	Hoop -	8.04	Nozzle	Hoop -
		0.7	9.09	Hoop -	9.11	Hoop -	9.11	Nozzle	Hoop -
		0.8	10.00	Hoop -	10.02	Hoop -	10.02	Nozzle	Hoop -
		0.9	11.22	Hoop -	11.23	Hoop -	11.23	Nozzle	Hoop -
		1	12.72	Hoop -	12.71	Hoop -	12.72	Vessel	Hoop -
	1.25	0.2	3.55	Hoop -	3.24	Hoop -	3.55	Vessel	Hoop -
		0.3	4.60	Hoop -	4.16	Hoop -	4.60	Vessel	Hoop -
		0.4	5.63	Axial -	5.05	Hoop -	5.63	Vessel	Axial -

Table 8- 4 (cont'd): Predictions of Vessel's and Nozzle's SCF by the Finite Element Analysis

RT	tT	rR	Cylindrical Vessel		Cylindrical Nozzle		Overall SCF	Location	Type
			SCF	Type	SCF	Type			
75	1.25	0.5	6.59	Axial -	5.74	Hoop -	6.59	Vessel	Axial -
		0.6	7.69	Axial -	6.54	Hoop -	7.69	Vessel	Axial -
		0.7	8.83	Axial -	7.39	Hoop -	8.83	Vessel	Axial -
		0.8	9.82	Axial -	8.10	Hoop -	9.82	Vessel	Axial -
		0.9	10.98	Axial -	9.07	Hoop -	10.98	Vessel	Axial -
		1	11.57	Axial -	10.23	Hoop -	11.57	Vessel	Axial -
	1.5	0.2	3.26	Hoop -	2.78	Hoop -	3.26	Vessel	Hoop -
		0.3	4.28	Axial -	3.56	Hoop -	4.28	Vessel	Axial -
		0.4	5.37	Axial -	4.31	Hoop -	5.37	Vessel	Axial -
		0.5	6.30	Axial -	4.88	Hoop -	6.30	Vessel	Axial -
		0.6	7.37	Axial -	5.56	Hoop -	7.37	Vessel	Axial -
		0.7	8.50	Axial -	6.27	Hoop -	8.50	Vessel	Axial -
		0.8	9.48	Axial -	6.86	Hoop -	9.48	Vessel	Axial -
		0.9	10.62	Axial -	7.65	Hoop -	10.62	Vessel	Axial -
		1	11.18	Axial -	8.59	Hoop -	11.18	Vessel	Axial -
100	0.25	0.1	4.51	Hoop -	8.94	Axial -	8.94	Nozzle	Axial -
		0.2	7.10	Hoop -	15.65	Axial -	15.65	Nozzle	Axial -
		0.3	9.45	Hoop -	21.36	Axial -	21.36	Nozzle	Axial -
		0.4	11.68	Hoop -	26.27	Axial -	26.27	Nozzle	Axial -
		0.5	13.66	Hoop -	30.60	Axial -	30.60	Nozzle	Axial -
		0.6	15.90	Hoop -	35.37	Axial -	35.37	Nozzle	Axial -
		0.7	18.21	Hoop -	39.80	Axial -	39.80	Nozzle	Axial -
		0.8	20.45	Hoop -	44.89	Axial -	44.89	Nozzle	Axial -
		0.9	23.01	Hoop -	48.76	Axial -	48.76	Nozzle	Axial -
		1	26.38	Hoop -	53.91	Axial -	53.91	Nozzle	Axial -
	0.5	0.1	3.64	Hoop -	5.64	Axial -	5.64	Nozzle	Axial -
		0.2	5.61	Hoop -	10.06	Axial -	10.06	Nozzle	Axial -
		0.3	7.38	Hoop -	13.76	Axial -	13.76	Nozzle	Axial -
		0.4	9.06	Hoop -	17.09	Axial -	17.09	Nozzle	Axial -
		0.5	10.49	Hoop -	19.88	Axial -	19.88	Nozzle	Axial -
		0.6	12.10	Hoop -	22.89	Axial -	22.89	Nozzle	Axial -
		0.7	13.81	Hoop -	25.97	Axial -	25.97	Nozzle	Axial -
		0.8	15.35	Hoop -	28.75	Axial -	28.75	Nozzle	Axial -
		0.9	17.31	Hoop -	31.88	Axial -	31.88	Nozzle	Axial -
		1	19.93	Hoop -	34.47	Axial -	34.47	Nozzle	Axial -
	0.75	0.1	3.16	Hoop -	3.65	Hoop -	3.65	Nozzle	Hoop -
		0.2	4.79	Hoop -	5.90	Axial -	5.90	Nozzle	Axial -

Table 8- 5 (cont'd): Predictions of Vessel's and Nozzle's SCF by the Finite Element Analysis

RT	tT	rR	Cylindrical Vessel		Cylindrical Nozzle		Overall SCF	Location	Type
			SCF	Type	SCF	Type			
100	0.75	0.3	6.26	Hoop -	8.17	Axial -	8.17	Nozzle	Axial -
		0.4	7.65	Hoop -	10.24	Axial -	10.24	Nozzle	Axial -
		0.5	8.79	Hoop -	11.98	Axial -	11.98	Nozzle	Axial -
		0.6	10.10	Hoop -	13.92	Axial -	13.92	Nozzle	Axial -
		0.7	11.50	Hoop -	15.92	Axial -	15.92	Nozzle	Axial -
		0.8	12.73	Hoop -	17.70	Axial -	17.70	Nozzle	Axial -
		0.9	14.33	Hoop -	19.74	Axial -	19.74	Nozzle	Axial -
		1	16.46	Hoop -	21.16	Axial -	21.16	Nozzle	Axial -
	1	0.1	2.87	Hoop -	2.94	Hoop -	2.94	Nozzle	Hoop -
		0.2	4.32	Hoop -	4.34	Hoop -	4.34	Nozzle	Hoop -
		0.3	5.62	Hoop -	5.63	Hoop -	5.63	Nozzle	Hoop -
		0.4	6.85	Hoop -	6.87	Hoop -	6.87	Nozzle	Hoop -
		0.5	7.84	Hoop -	7.86	Hoop -	7.86	Nozzle	Hoop -
		0.6	8.99	Hoop -	9.01	Hoop -	9.01	Nozzle	Hoop -
		0.7	10.22	Hoop -	10.23	Hoop -	10.23	Nozzle	Hoop -
		0.8	11.29	Hoop -	11.29	Hoop -	11.29	Nozzle	Hoop -
		0.9	12.68	Hoop -	12.68	Hoop -	12.68	Vessel	Hoop -
		1	14.47	Hoop -	14.46	Hoop -	14.47	Vessel	Hoop -
	1.25	0.2	3.96	Hoop -	3.60	Hoop -	3.96	Vessel	Hoop -
		0.3	5.14	Hoop -	4.64	Hoop -	5.14	Vessel	Hoop -
		0.4	6.44	Axial -	5.63	Hoop -	6.44	Vessel	Axial -
		0.5	7.57	Axial -	6.41	Hoop -	7.57	Vessel	Axial -
		0.6	8.85	Axial -	7.32	Hoop -	8.85	Vessel	Axial -
		0.7	10.20	Axial -	8.28	Hoop -	10.20	Vessel	Axial -
		0.8	11.40	Axial -	9.11	Hoop -	11.40	Vessel	Axial -
		0.9	12.78	Axial -	10.20	Hoop -	12.78	Vessel	Axial -
		1	13.56	Axial -	11.60	Hoop -	13.56	Vessel	Axial -
	1.5	0.2	3.65	Hoop -	3.10	Hoop -	3.65	Vessel	Hoop -
		0.3	4.90	Axial -	3.98	Hoop -	4.90	Vessel	Axial -
		0.4	6.16	Axial -	4.82	Hoop -	6.16	Vessel	Axial -
		0.5	7.26	Axial -	5.46	Hoop -	7.26	Vessel	Axial -
		0.6	8.53	Axial -	6.22	Hoop -	8.53	Vessel	Axial -
		0.7	9.86	Axial -	7.02	Hoop -	9.86	Vessel	Axial -
		0.8	11.06	Axial -	7.70	Hoop -	11.06	Vessel	Axial -
		0.9	12.42	Axial -	8.61	Hoop -	12.42	Vessel	Axial -
		1	13.15	Axial -	9.74	Hoop -	13.15	Vessel	Axial -
125	0.25	0.1	4.86	Hoop -	10.09	Axial -	10.09	Nozzle	Axial -

Table 8- 6 (cont'd): Predictions of Vessel's and Nozzle's SCF by the Finite Element Analysis

RT	tT	rR	Cylindrical Vessel		Cylindrical Nozzle		Overall SCF	Location	Type
			SCF	Type	SCF	Type			
125	0.25	0.2	7.69	Hoop -	17.55	Axial -	17.55	Nozzle	Axial -
		0.3	10.22	Hoop -	23.57	Axial -	23.57	Nozzle	Axial -
		0.4	12.69	Hoop -	29.24	Axial -	29.24	Nozzle	Axial -
		0.5	14.90	Hoop -	34.05	Axial -	34.05	Nozzle	Axial -
		0.6	17.37	Hoop -	39.25	Axial -	39.25	Nozzle	Axial -
		0.7	19.96	Hoop -	44.42	Axial -	44.42	Nozzle	Axial -
		0.8	22.50	Hoop -	49.78	Axial -	49.78	Nozzle	Axial -
		0.9	25.38	Hoop -	55.17	Axial -	55.17	Nozzle	Axial -
		1	29.24	Hoop -	60.94	Axial -	60.94	Nozzle	Axial -
	0.5	0.1	3.92	Hoop -	6.38	Axial -	6.38	Nozzle	Axial -
		0.2	6.06	Hoop -	11.25	Axial -	11.25	Nozzle	Axial -
		0.3	7.99	Hoop -	15.30	Axial -	15.30	Nozzle	Axial -
		0.4	9.84	Hoop -	18.98	Axial -	18.98	Nozzle	Axial -
		0.5	11.44	Hoop -	22.16	Axial -	22.16	Nozzle	Axial -
		0.6	13.23	Hoop -	25.52	Axial -	25.52	Nozzle	Axial -
		0.7	15.15	Hoop -	29.03	Axial -	29.03	Nozzle	Axial -
		0.8	16.86	Hoop -	32.15	Axial -	32.15	Nozzle	Axial -
		0.9	19.03	Hoop -	35.69	Axial -	35.69	Nozzle	Axial -
		1	22.01	Hoop -	38.91	Axial -	38.91	Nozzle	Axial -
	0.75	0.1	3.41	Hoop -	3.94	Hoop -	3.94	Nozzle	Hoop -
		0.2	5.19	Hoop -	6.59	Axial -	6.59	Nozzle	Axial -
		0.3	6.80	Hoop -	9.08	Axial -	9.08	Nozzle	Axial -
		0.4	8.32	Hoop -	11.37	Axial -	11.37	Nozzle	Axial -
		0.5	9.60	Hoop -	13.34	Axial -	13.34	Nozzle	Axial -
		0.6	11.06	Hoop -	15.51	Axial -	15.51	Nozzle	Axial -
		0.7	12.61	Hoop -	17.77	Axial -	17.77	Nozzle	Axial -
		0.8	13.98	Hoop -	19.74	Axial -	19.74	Nozzle	Axial -
		0.9	15.75	Hoop -	22.09	Axial -	22.09	Nozzle	Axial -
		1	18.18	Hoop -	23.87	Axial -	23.87	Nozzle	Axial -
	1	0.1	3.10	Hoop -	3.16	Hoop -	3.16	Nozzle	Hoop -
		0.2	4.69	Hoop -	4.71	Hoop -	4.71	Nozzle	Hoop -
		0.3	6.11	Hoop -	6.13	Hoop -	6.13	Nozzle	Hoop -
		0.4	7.47	Hoop -	7.49	Hoop -	7.49	Nozzle	Hoop -
		0.5	8.58	Hoop -	8.60	Hoop -	8.60	Nozzle	Hoop -
		0.6	9.86	Hoop -	9.88	Hoop -	9.88	Nozzle	Hoop -
		0.7	11.25	Axial -	11.23	Hoop -	11.25	Vessel	Axial -
		0.8	12.54	Axial -	12.48	Axial -	12.54	Vessel	Axial -

Table 8- 7 (cont'd): Predictions of Vessel's and Nozzle's SCF by the Finite Element Analysis

RT	tT	rR	Cylindrical Vessel		Cylindrical Nozzle		Overall SCF	Location	Type
			SCF	Type	SCF	Type			
125	1	0.9	14.03	Axial -	13.99	Axial -	14.03	Vessel	Axial -
		1	16.00	Hoop -	15.99	Hoop -	16.00	Vessel	Hoop -
	1.25	0.1	2.86	Hoop -	2.66	Hoop -	2.86	Vessel	Hoop -
		0.2	4.31	Hoop -	3.91	Hoop -	4.31	Vessel	Hoop -
		0.3	5.69	Axial -	5.05	Hoop -	5.69	Vessel	Axial -
		0.4	7.15	Axial -	6.14	Hoop -	7.15	Vessel	Axial -
		0.5	8.43	Axial -	7.00	Hoop -	8.43	Vessel	Axial -
		0.6	9.89	Axial -	8.01	Hoop -	9.89	Vessel	Axial -
		0.7	11.41	Axial -	9.07	Hoop -	11.41	Vessel	Axial -
		0.8	12.78	Axial -	9.99	Hoop -	12.78	Vessel	Axial -
		0.9	14.32	Axial -	11.20	Hoop -	14.32	Vessel	Axial -
		1	15.30	Axial -	12.81	Hoop -	15.30	Vessel	Axial -
	1.5	0.2	3.98	Hoop -	3.37	Hoop -	3.98	Vessel	Hoop -
		0.3	5.43	Axial -	4.34	Hoop -	5.43	Vessel	Axial -
		0.4	6.84	Axial -	5.25	Hoop -	6.84	Vessel	Axial -
		0.5	8.11	Axial -	5.97	Hoop -	8.11	Vessel	Axial -
		0.6	9.55	Axial -	6.80	Hoop -	9.55	Vessel	Axial -
		0.7	11.06	Axial -	7.68	Hoop -	11.06	Vessel	Axial -
		0.8	12.42	Axial -	8.43	Hoop -	12.42	Vessel	Axial -
		0.9	13.96	Axial -	9.43	Hoop -	13.96	Vessel	Axial -
		1	14.86	Axial -	10.74	Hoop -	14.86	Vessel	Axial -
150	0.25	0.1	5.16	Hoop -	11.13	Axial -	11.13	Nozzle	Axial -
		0.2	8.20	Hoop -	19.24	Axial -	19.24	Nozzle	Axial -
		0.3	10.92	Hoop -	25.77	Axial -	25.77	Nozzle	Axial -
		0.4	13.62	Hoop -	31.96	Axial -	31.96	Nozzle	Axial -
		0.5	15.99	Hoop -	37.04	Axial -	37.04	Nozzle	Axial -
		0.6	18.71	Hoop -	43.12	Axial -	43.12	Nozzle	Axial -
		0.7	21.54	Hoop -	48.55	Axial -	48.55	Nozzle	Axial -
		0.8	24.37	Hoop -	54.75	Axial -	54.75	Nozzle	Axial -
		0.9	27.52	Hoop -	60.79	Axial -	60.79	Nozzle	Axial -
		1	31.82	Hoop -	67.33	Axial -	67.33	Nozzle	Axial -
	0.5	0.1	4.16	Hoop -	7.04	Axial -	7.04	Nozzle	Axial -
		0.2	6.47	Hoop -	12.32	Axial -	12.32	Nozzle	Axial -
		0.3	8.55	Hoop -	16.67	Axial -	16.67	Nozzle	Axial -
		0.4	10.55	Hoop -	20.69	Axial -	20.69	Nozzle	Axial -
		0.5	12.28	Hoop -	24.16	Axial -	24.16	Nozzle	Axial -
		0.6	14.23	Hoop -	27.84	Axial -	27.84	Nozzle	Axial -

Table 8- 8 (cont'd): Predictions of Vessel's and Nozzle's SCF by the Finite Element Analysis

RT	tT	rR	Cylindrical Vessel		Cylindrical Nozzle		Overall SCF	Location	Type
			SCF	Type	SCF	Type			
150	0.5	0.7	16.28	Hoop -	31.59	Axial -	31.59	Nozzle	Axial -
		0.8	18.22	Hoop -	35.28	Axial -	35.28	Nozzle	Axial -
		0.9	20.57	Hoop -	39.21	Axial -	39.21	Nozzle	Axial -
		1	23.88	Hoop -	42.90	Axial -	42.90	Nozzle	Axial -
	0.75	0.1	3.63	Hoop -	4.20	Hoop -	4.20	Nozzle	Hoop -
		0.2	5.56	Hoop -	7.21	Axial -	7.21	Nozzle	Axial -
		0.3	7.28	Hoop -	9.88	Axial -	9.88	Nozzle	Axial -
		0.4	8.93	Hoop -	12.40	Axial -	12.40	Nozzle	Axial -
		0.5	10.32	Hoop -	14.55	Axial -	14.55	Nozzle	Axial -
		0.6	11.91	Hoop -	16.93	Axial -	16.93	Nozzle	Axial -
		0.7	13.59	Hoop -	19.39	Axial -	19.39	Nozzle	Axial -
		0.8	15.10	Hoop -	21.63	Axial -	21.63	Nozzle	Axial -
		0.9	17.02	Hoop -	24.16	Axial -	24.16	Nozzle	Axial -
		1	19.73	Hoop -	26.32	Axial -	26.32	Nozzle	Axial -
	1	0.1	3.31	Hoop -	3.36	Hoop -	3.36	Nozzle	Hoop -
		0.2	5.03	Hoop -	5.05	Hoop -	5.05	Nozzle	Hoop -
		0.3	6.56	Hoop -	6.58	Hoop -	6.58	Nozzle	Hoop -
		0.4	8.03	Hoop -	8.05	Hoop -	8.05	Nozzle	Hoop -
		0.5	9.24	Hoop -	9.25	Hoop -	9.25	Nozzle	Hoop -
		0.6	10.68	Axial -	10.65	Hoop -	10.68	Vessel	Axial -
		0.7	12.28	Axial -	12.19	Axial -	12.28	Vessel	Axial -
		0.8	13.75	Axial -	13.69	Axial -	13.75	Vessel	Axial -
		0.9	15.37	Axial -	15.33	Axial -	15.37	Vessel	Axial -
		1	17.37	Hoop -	17.36	Hoop -	17.37	Vessel	Hoop -
	1.25	0.1	3.06	Hoop -	2.83	Hoop -	3.06	Vessel	Hoop -
		0.2	4.63	Hoop -	4.19	Hoop -	4.63	Vessel	Hoop -
		0.3	6.18	Axial -	5.42	Hoop -	6.18	Vessel	Axial -
		0.4	7.79	Axial -	6.59	Hoop -	7.79	Vessel	Axial -
		0.5	9.19	Axial -	7.53	Hoop -	9.19	Vessel	Axial -
		0.6	10.80	Axial -	8.62	Hoop -	10.80	Vessel	Axial -
		0.7	12.48	Axial -	9.77	Hoop -	12.48	Vessel	Axial -
		0.8	14.03	Axial -	10.80	Hoop -	14.03	Vessel	Axial -
		0.9	15.72	Axial -	12.10	Hoop -	15.72	Vessel	Axial -
		1	16.88	Axial -	13.89	Hoop -	16.88	Vessel	Axial -
	1.5	0.1	2.83	Hoop -	2.46	Hoop -	2.83	Vessel	Hoop -
		0.2	4.31	Axial -	3.61	Hoop -	4.31	Vessel	Axial -
		0.3	5.91	Axial -	4.66	Hoop -	5.91	Vessel	Axial -

Table 8- 9 (cont'd): Predictions of Vessel's and Nozzle's SCF by the Finite Element Analysis

RT	tT	rR	Cylindrical Vessel		Cylindrical Nozzle		Overall SCF	Location	Type
			SCF	Type	SCF	Type			
150	1.5	0.4	7.47	Axial -	5.64	Hoop -	7.47	Vessel	Axial -
		0.5	8.85	Axial -	6.41	Hoop -	8.85	Vessel	Axial -
		0.6	10.45	Axial -	7.32	Hoop -	10.45	Vessel	Axial -
		0.7	12.11	Axial -	8.27	Hoop -	12.11	Vessel	Axial -
		0.8	13.66	Axial -	9.10	Hoop -	13.66	Vessel	Axial -
		0.9	15.33	Axial -	10.18	Hoop -	15.33	Vessel	Axial -
		1	16.40	Axial -	11.64	Hoop -	16.40	Vessel	Axial -

8.2 COMPARISON WITH THE PREDICTION BY OTHER MODELS

In order to establish more confidence in the analysis carried out, results achieved in this study are compared with some well-recognized models of SCF for cylindrical vessel intersected by cylindrical nozzles. These models are developed by: Lind [93] based on the Area Replacement Method, Money [95] based on statistical analysis on many pressurized cylindrical vessel-nozzle junctions, and Decock [96] based on the consideration that forces acting on a longitudinal plane of symmetry must be balanced by the hoop stresses in shell and nozzle within restricted surface limits.

Figures 8.5 to 8.7 show how the FEM predictions in this study perform relative to such models. However, since these models and many other similar ones in the literature concentrate on the vessel's SCF alone, these comparisons are carried out with only the vessel's SCF of the present study. It can be observed that in majority of the cases, the other three models sandwich the model used in this research. At tT values higher than 0.5, predictions by the present work are more conservative than those of Money [95] and Decock [96], but less conservative than that of Lind [93]. At lower tT values, however, the present work is more conservative than all the other three models. Hence, it can be

argued that, safety-wise, the adopted finite element model performs consistently and that it is very reliable. In terms of giving consideration to the possibility of having higher values of SCF in the nozzle, the present work clearly exposes the shortcoming of several models reported in the literature (including the above mentioned three) on their lack of consideration to the stresses developed in the nozzles itself.

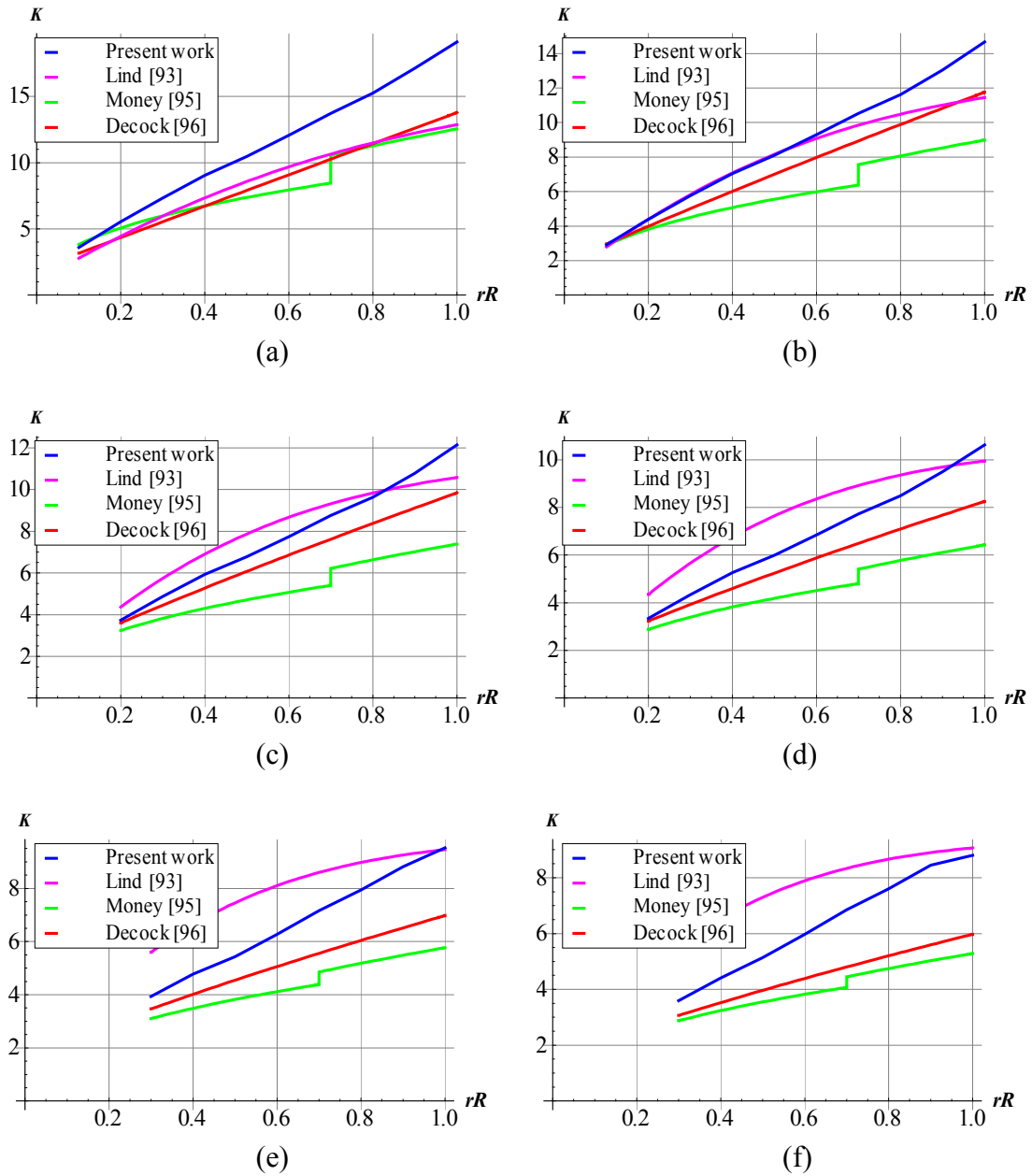


Figure 8- 5: Comparison between Predictions of the Present Work with other Established SCF Models for $RT = 50$ and (a) $tT = 0.25$ (b) $tT = 0.5$ (c) $tT = 0.75$ (d) $tT = 1.0$ (e) $tT = 1.25$ (f) $tT = 1.5$

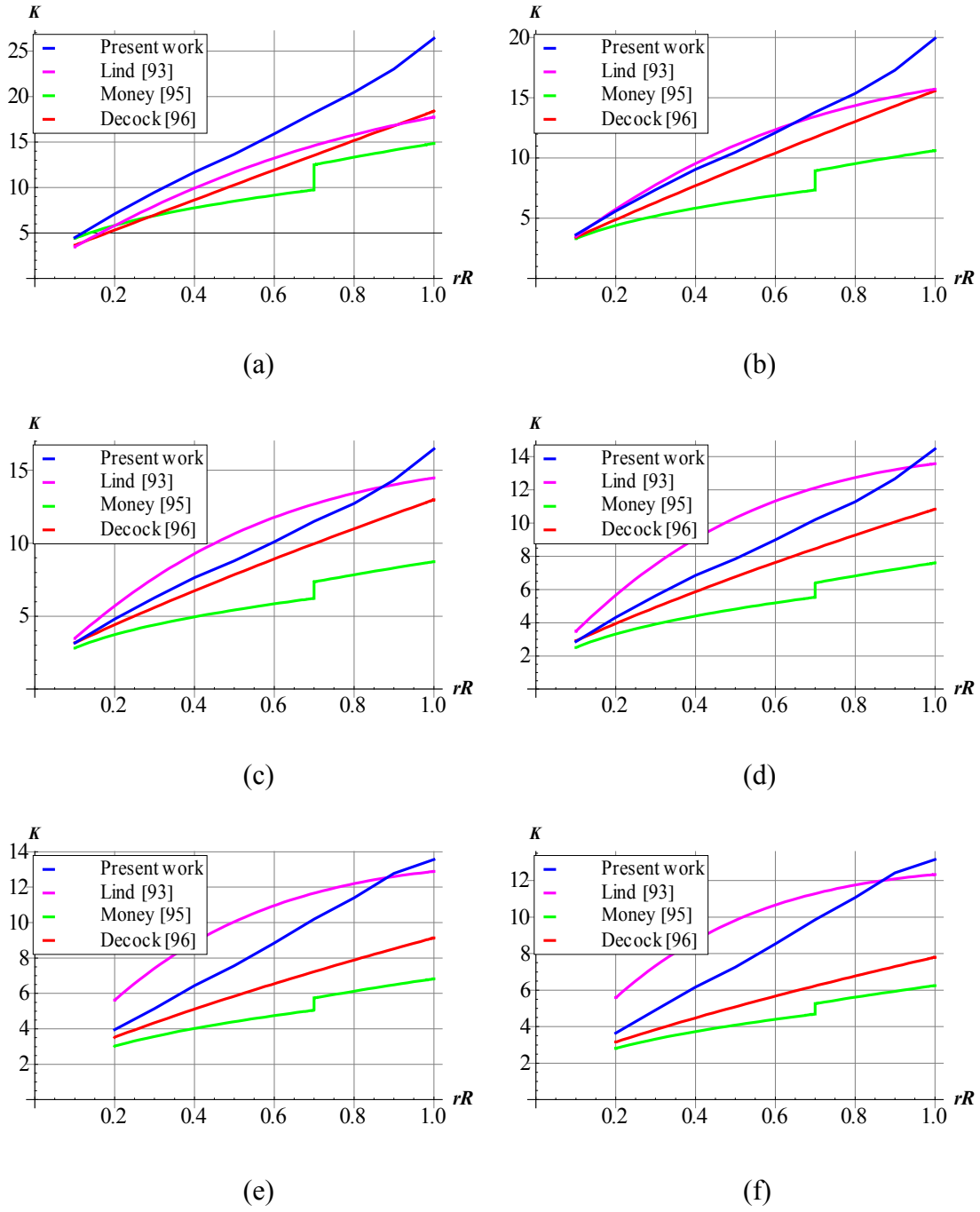


Figure 8- 6: Comparison between Predictions of the Present Work with other Established SCF Models for $RT = 100$ and (a) $tT = 0.25$ (b) $tT = 0.5$ (c) $tT = 0.75$ (d) $tT = 1.0$ (e) $tT = 1.25$ (f) $tT = 1.5$

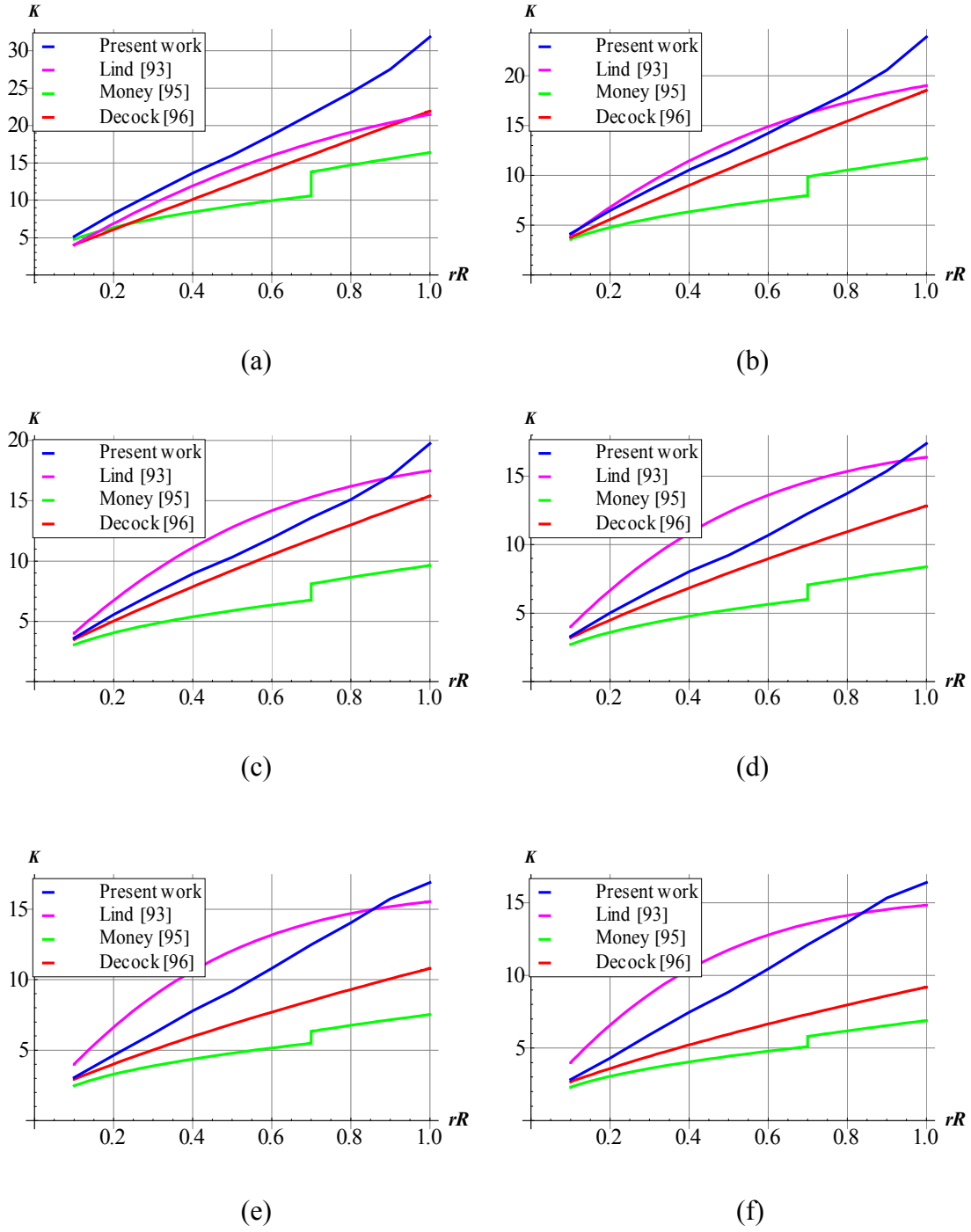


Figure 8- 7: Comparison between Predictions of the Present Work with other Established SCF Models for $RT = 150$ and (a) $tT = 0.25$ (b) $tT = 0.5$ (c) $tT = 0.75$ (d) $tT = 1.0$ (e) $tT = 1.25$ (f) $tT = 1.5$

8.3 DESIGN CHARTS FOR CYLINDRICAL VESSELS INTERSECTED BY MODERATE-TO-LARGE-DIAMETER NOZZLES

Based on the analysis present in the previous subsections, design charts for cylindrical vessel-cylindrical nozzle junctures are proposed in this study as shown in figures 8.8 to 8.12. As it applies to the spherical vessel-cylindrical nozzle case, the SCF representation presented in these figures overcome two major shortcomings of the conventional ρ -SCF plots. First, individual plots are devised to enable prediction of unique SCF values for specific combinations of the vessel-nozzle geometric ratios in contrast to the ρ -SCF plots that may result in certain error for some geometries (see [23]). Second, the outcome of the analysis conducted on all the cylindrical vessel-cylindrical nozzle geometric ratios considered in this chapter show that about 64% of the cases result in the maximum stresses occurring in the nozzle with about 36% otherwise. Hence, consideration is given to the possibility of having higher values of SCF in the nozzle. Therefore, the charts corresponding to the SCF in the nozzle are equally plotted. Based on the outcome of the location (in the vessel or in the nozzle) of higher value of SCF, the designer is left with an alternative to choose the appropriate plots presented here-in.

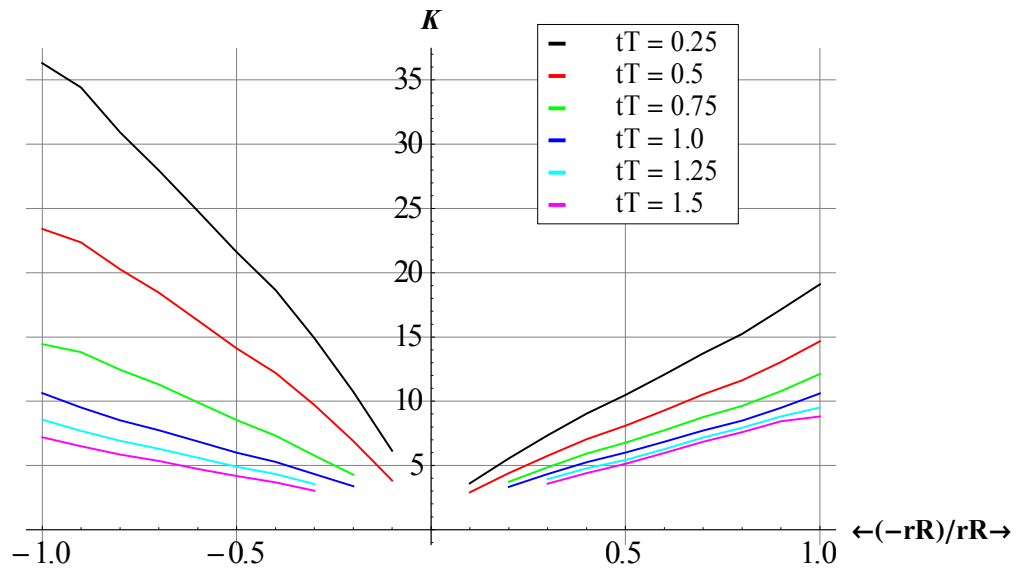


Figure 8- 8: Variation of SCF in the Cylindrical Vessel (left set of graphs) and Nozzle (right set of graphs) with Geometric Ratios for Constant $RT = 50$ as predicted by the FEM

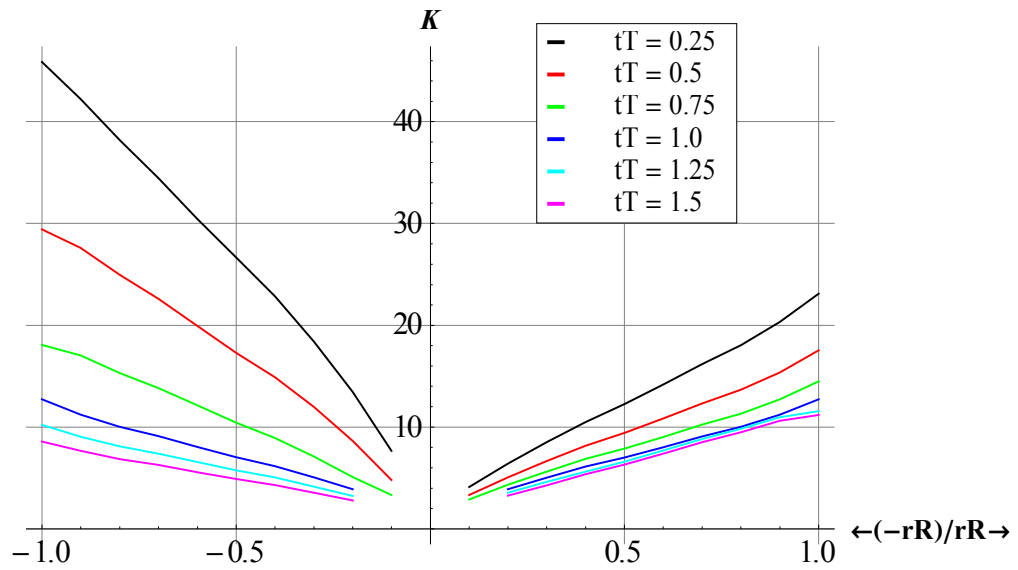


Figure 8- 9: Variation of SCF in the Cylindrical Vessel (left set of graphs) and Nozzle (right set of graphs) with Geometric Ratios for Constant $RT = 75$ as predicted by the FEM

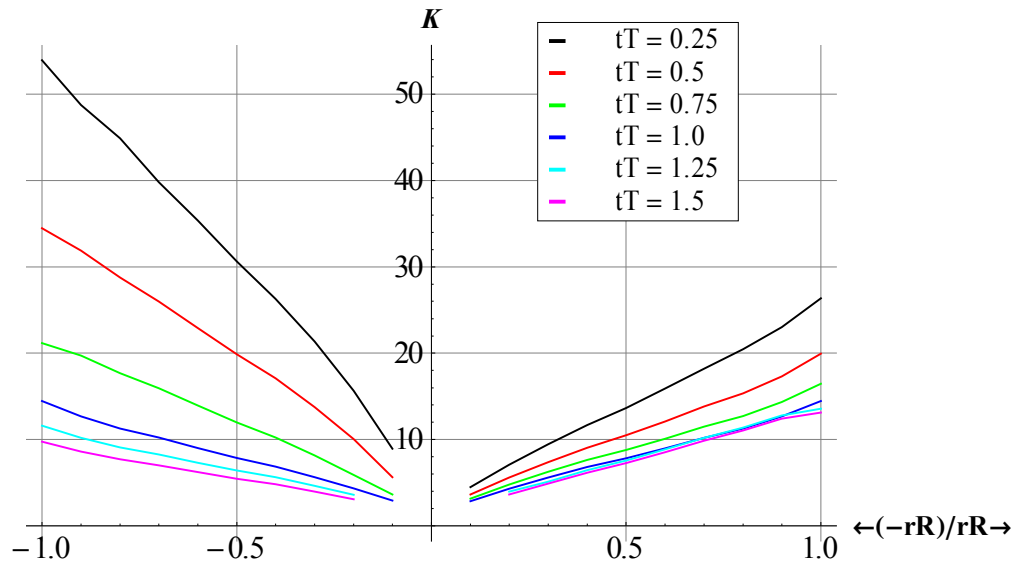


Figure 8- 10: Variation of SCF in the Cylindrical Vessel (left set of graphs) and Nozzle (right set of graphs) with Geometric Ratios for Constant $RT = 100$ as predicted by the FEM

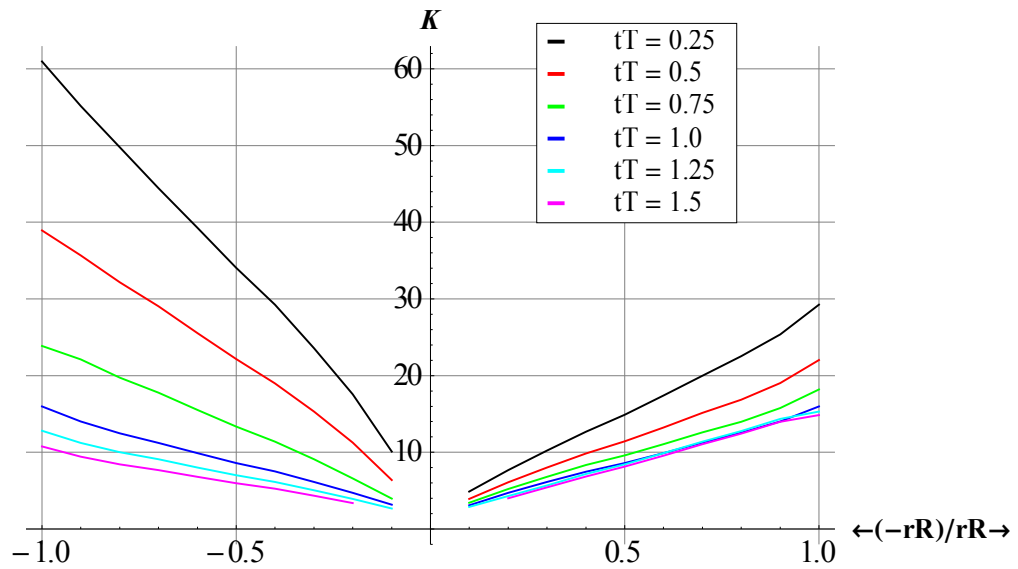


Figure 8- 11: Variation of SCF in the Cylindrical Vessel (left set of graphs) and Nozzle (right set of graphs) with Geometric Ratios for Constant $RT = 125$ as predicted by the FEM

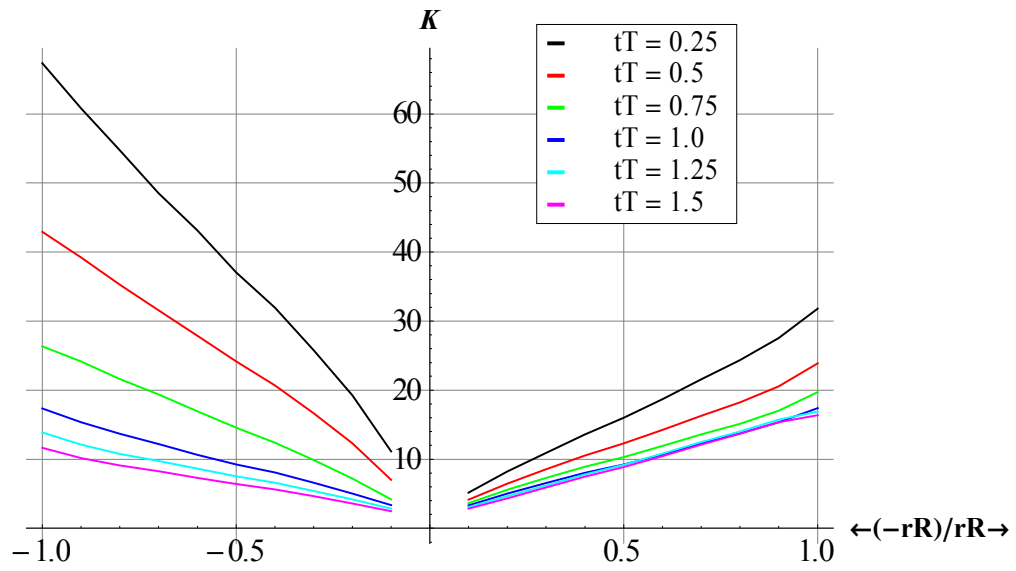


Figure 8- 12: Variation of SCF in the Cylindrical Vessel (left set of graphs) and Nozzle (right set of graphs) with Geometric Ratios for Constant $RT = 150$ as predicted by the FEM

CHAPTER NINE

MODELING AND ANALYSIS OF SCF FOR SPHERICAL PRESSURE VESSELS WITH SMALL DIAMETER NOZZLES

9.1 USE OF SOLID VERSUS SHELL ELEMENTS

The analysis presented in Chapter Seven is based on the consideration that the intersecting nozzle sizes are moderate-to-large. As a result, the thin shell theory is not violated. In that case both solid and shell elements will give reliable results of the stress analysis. Hence, the reason behind adopting the thin shell analytical models for the spherical vessel-cylindrical nozzle problems and finite element models for the spherical and cylindrical vessels intersected by cylindrical nozzles in those chapters. In practice, however, there appear many instances in which the intersecting nozzles are required to be small in sizes. Some of those cases result in nozzle elements whose configuration violates the assumption of shell theory. In such instances the analyst is left with no other option than to adopt the use of solid elements in modeling the vessel-nozzle problems. Unlike the shell model, the solid model is based on theory of elasticity and, therefore, expressions for the membrane stresses given in Table 7-1 ceases to hold. Instead, those given in Table 9-1 will be applicable.

This chapter presents the modeling and analysis of spherical pressure vessels with small-diameter nozzles. The numerical experiments and results achieved are discussed followed by comparison with the prediction by the method of area replacement. Finally, the design charts presented in Chapter Seven are augmented with those of spherical vessels having

small-diameters to arrive at the overall design charts that cover all the possible ranges of nozzle-to-vessel diameter ratios.

Table 9- 1: Expressions of Membrane Stresses for Internally Pressurized Vessels

Vessel Type	Stress Type	Formula
Sphere	σ_r	$\frac{pr_i^3}{r_o^3 - r_i^3} \times \left(\frac{r_o^3}{r^3} - 1 \right)$
	σ_θ	$\frac{pr_i^3}{r_o^3 - r_i^3} \times \left(\frac{r_o^3}{2r^3} + 1 \right)$
	σ_z	$\frac{pr_i^3}{r_o^3 - r_i^3} \times \left(\frac{r_o^3}{2r^3} + 1 \right)$
	Max σ ($= \sigma_\theta = \sigma_z$ @ $r = r_i$)	$\frac{p(r_o^3 + 2r_i^3)}{2(r_o^3 - r_i^3)}$
Cylinder	σ_r	$\frac{pr_i^2}{r_o^2 - r_i^2} \times \left(\frac{r_o^2}{r^2} + 1 \right)$
	σ_θ	$\frac{pr_i^2}{r_o^2 - r_i^2} \times \left(1 - \frac{r_o^2}{r^2} \right)$
	σ_z	$\frac{pr_i^2}{r_o^2 - r_i^2}$
	Max σ ($= \sigma_\theta$ @ $r = r_i$)	$p \times \left(\frac{r_o^2 + r_i^2}{r_o^2 - r_i^2} \right)$

9.2 NUMERICAL EXPERIMENTS, RESULTS AND DISCUSSIONS

The required steps needed to set-up the model and solve the problem of spherical vessels with small-diameter nozzles are explained in the flowchart shown in Figure 6.7. The problem is modeled as an axisymmetric model which reduces, to a very large extent, computational time and efforts as well as minimizes memory resources. In order to avoid the effect of singularity, a fillet radius $\rho_f = 0.00215R_v$ is used at the external junction

between the main vessel and the nozzle. This radius is arrived at by carrying out several simulation runs of spherical vessel-nozzle problem of very large diameter and, each time, verifying against the solution obtained using shell theory in which the effect of singularity does not manifest. Length of the nozzle is chosen large enough to allow for the dissipation of discontinuity stresses. The final model achieved is shown in Figure 9-1. Figure 9-1 (b) shows location of the fillet and the lines (shown in dark) on which the stress solution is evaluated to avoid singularity effect. Discretization of the problem is shown in Figure 9-2.

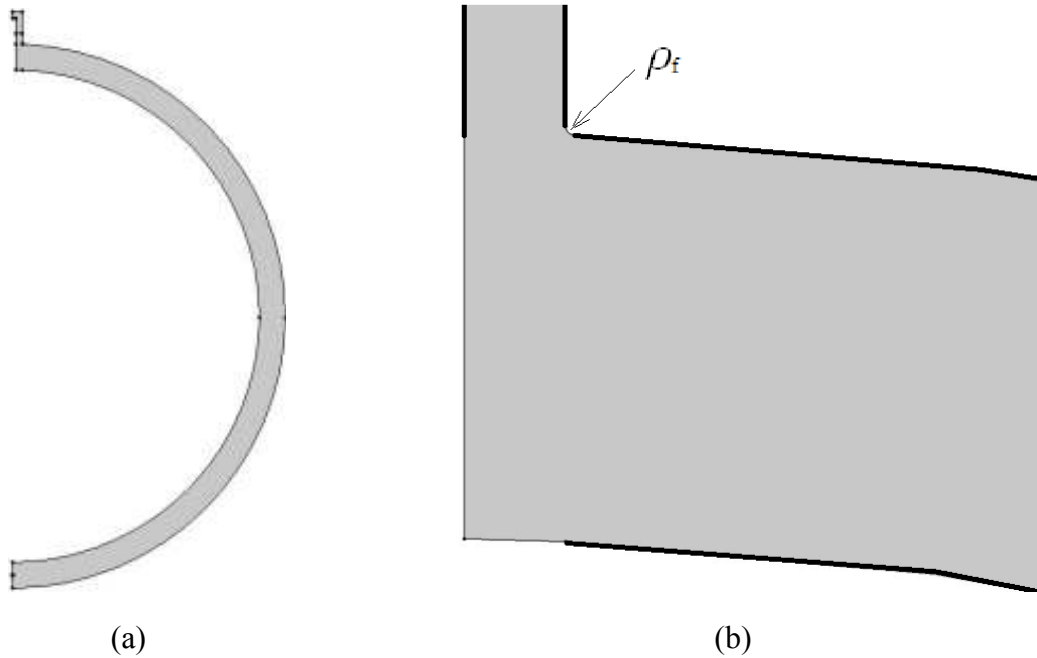


Figure 9- 1: Axi-Symmetric Model for the Spherical Vessel-Nozzle Junction (a) Geometry (b) Corner Fillet and Lines (shown in dark) for Stress Evaluation

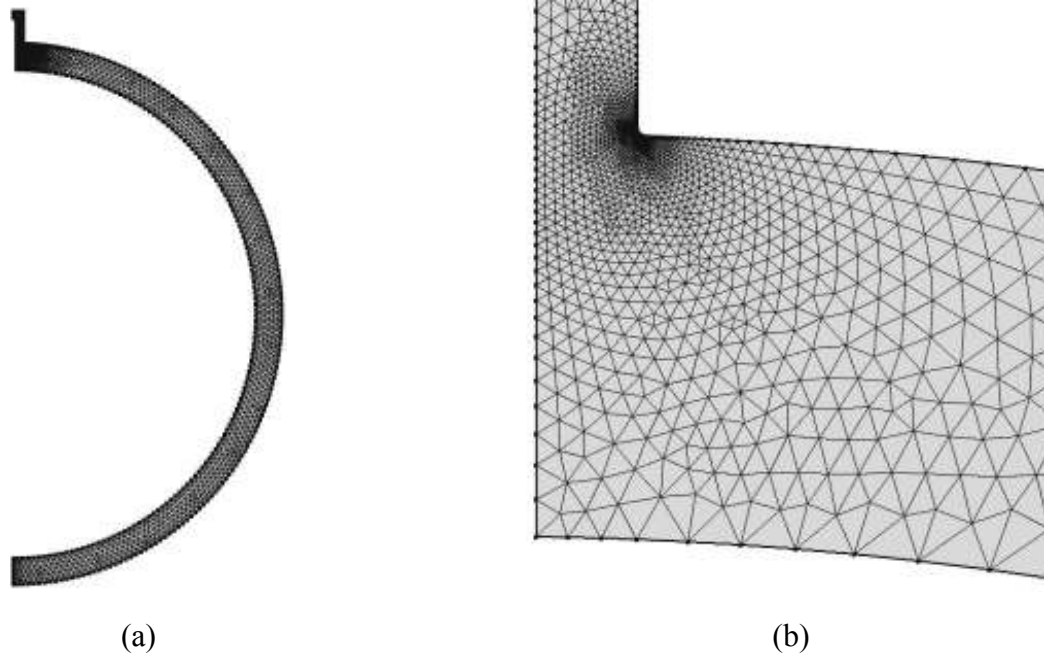


Figure 9- 2: Geometry Discretization (a) Overall mesh (b) Refined Mesh at the Junction

The following ranges of non-dimensional geometric parameters were used in the simulations.

$$RT = 5 + 5i, \{i, 1, 29\}$$

$$tT = 0.25j, \{j, 1, 6\}$$

$$rR = T_n/R_v \text{ and } 0.05$$

Hence, a total of 335 numerical experiments were conducted. Figures 9.3 to 9.5 show typical non-dimensional stress behaviors along the vessel's and nozzle's geometry.

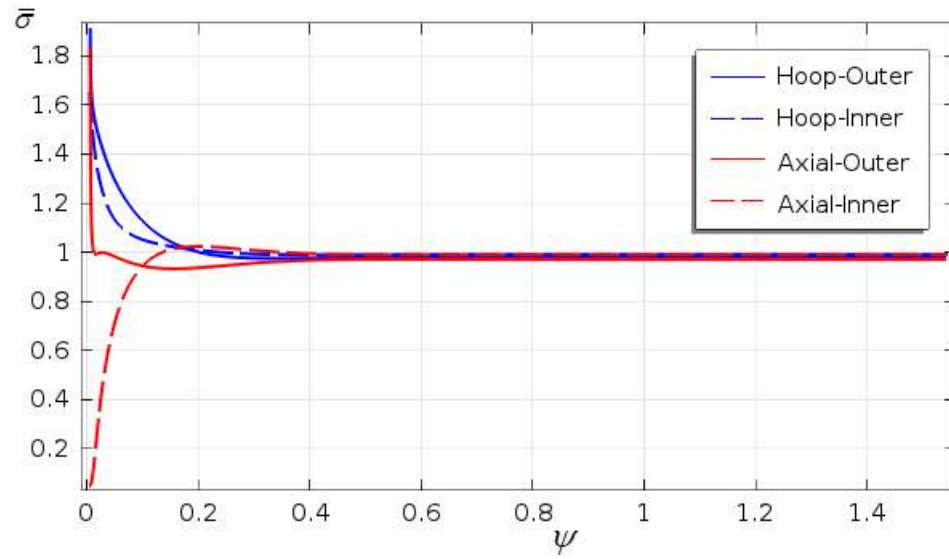


Figure 9- 3: Variation of the Four Types of Stresses in the Main Spherical Vessel for a Typical Vessel-Nozzle Junction with $RT = 50$, $tT = 0.5$ and $rR = 0.05$

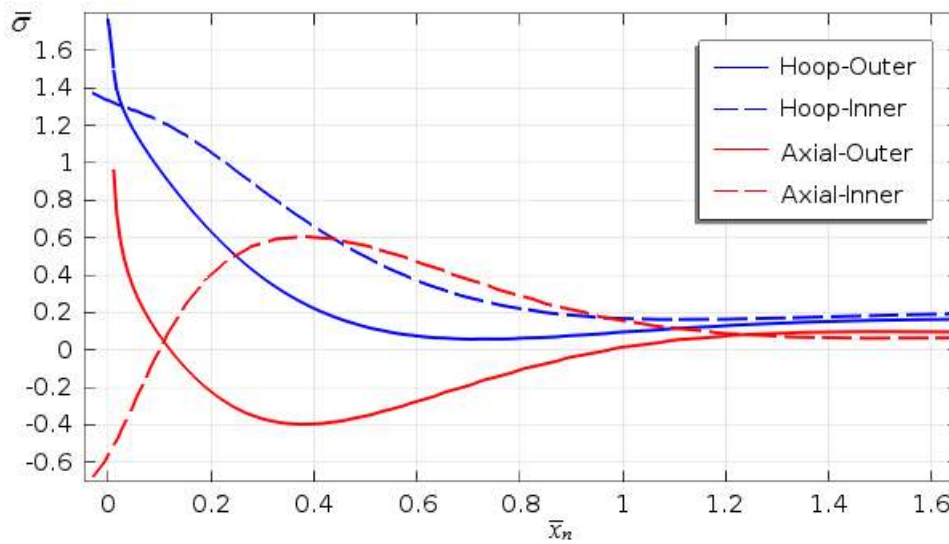


Figure 9- 4: Variation of the Four Types of Stresses in the Main Spherical Vessel for a Typical Vessel-Nozzle Junction with $RT = 50$, $tT = 0.5$ and $rR = 0.05$

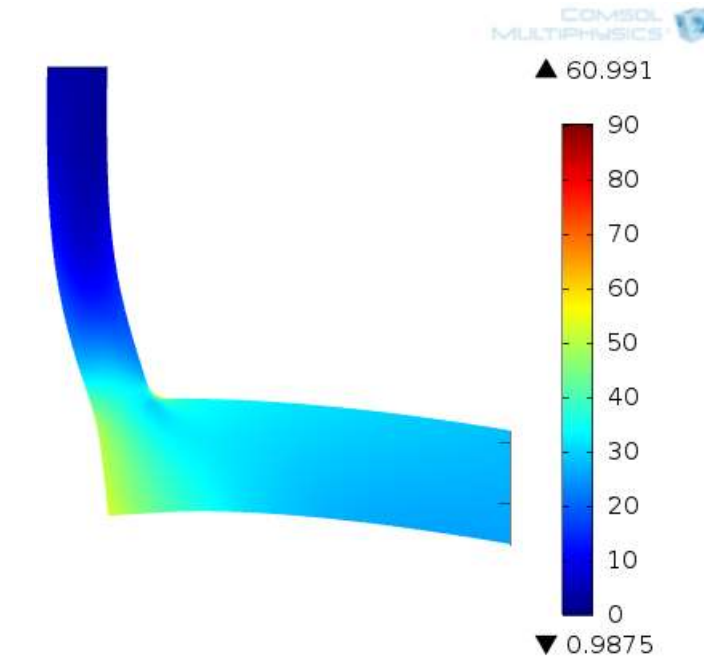


Figure 9- 5: von Mises Stress Plot for a Typical Vessel-Nozzle Configuration with $RT = 50$, $tT = 0.5$, $rR = 0.05$

Table 9-2 presents results for the vessel's SCF alongside with that of the nozzle for $RT = 25 + 25i$, $\{i, 1, 5\}$. Table C2 of Appendix C provides the remaining set of the results for other geometric ratios. Table 9-2 includes result of the study on type and location of the maximum stress of the configuration. It was learnt that, in terms of location of the maximum stress, about 87% of the spherical vessel with small-diameter nozzles dealt with in this chapter have the maximum SCF occurring in the vessel while the remaining of only about 13% have maximum SCF occurring in the nozzle. Hence, since most of the literature SCF models for such components concentrate on the vessels rather than the nozzles, it can be claimed that the percentage validity of many of such reported models are higher when the nozzles are of small diameters.

Table 9- 2: FEM Predictions of SCF for Spherical Vessels with Small-Diameter Nozzles

RT	tT	rR	Spherical Vessel		Cylindrical Nozzle		Overall SCF	Location	Type
			SCF	Type	SCF	Type			
50	0.25	0.005	1.46	Axial +	1.14	Hoop -	1.46	Vessel	Axial +
		0.05	2.39	Hoop +	2.81	Hoop +	2.81	Nozzle	Hoop +
	0.5	0.01	1.60	Axial +	1.10	Hoop -	1.60	Vessel	Axial +
		0.05	1.89	Hoop +	1.77	Hoop +	1.89	Vessel	Hoop +
	0.75	0.015	1.67	Axial +	1.09	Hoop -	1.67	Vessel	Axial +
		0.05	1.85	Axial +	1.32	Hoop -	1.85	Vessel	Axial +
	1	0.02	1.71	Axial +	1.11	Hoop -	1.71	Vessel	Axial +
		0.05	1.86	Axial +	1.31	Hoop -	1.86	Vessel	Axial +
	1.25	0.025	1.75	Axial +	1.15	Hoop -	1.75	Vessel	Axial +
		0.05	1.87	Axial +	1.29	Hoop -	1.87	Vessel	Axial +
	1.5	0.03	1.78	Axial +	1.18	Hoop -	1.78	Vessel	Axial +
		0.05	1.86	Axial +	1.27	Hoop -	1.86	Vessel	Axial +
75	0.25	0.003	1.38	Axial +	1.13	Hoop -	1.38	Vessel	Axial +
		0.05	2.58	Hoop +	3.25	Hoop +	3.25	Nozzle	Hoop +
	0.5	0.007	1.48	Axial +	1.09	Hoop -	1.48	Vessel	Axial +
		0.05	2.07	Hoop +	2.06	Hoop +	2.07	Vessel	Hoop +
	0.75	0.01	1.53	Axial +	1.08	Hoop -	1.53	Vessel	Axial +
		0.05	1.81	Hoop +	1.46	Hoop +	1.81	Vessel	Hoop +
	1	0.013	1.57	Axial +	1.10	Hoop -	1.57	Vessel	Axial +
		0.05	1.80	Axial +	1.38	Hoop -	1.80	Vessel	Axial +
	1.25	0.017	1.60	Axial +	1.14	Hoop -	1.60	Vessel	Axial +
		0.05	1.80	Axial +	1.37	Hoop -	1.80	Vessel	Axial +
	1.5	0.02	1.62	Axial +	1.17	Hoop -	1.62	Vessel	Axial +
		0.05	1.78	Axial +	1.34	Hoop -	1.78	Vessel	Axial +
100	0.25	0.003	1.33	Axial +	1.14	Hoop -	1.33	Vessel	Axial +
		0.05	2.72	Hoop +	3.63	Axial +	3.63	Nozzle	Axial +
	0.5	0.005	1.41	Axial +	1.08	Hoop -	1.41	Vessel	Axial +
		0.05	2.20	Hoop +	2.27	Hoop +	2.27	Nozzle	Hoop +
	0.75	0.008	1.45	Axial +	1.07	Hoop -	1.45	Vessel	Axial +
		0.05	1.94	Hoop +	1.62	Hoop +	1.94	Vessel	Hoop +
	1	0.01	1.48	Axial +	1.09	Hoop -	1.48	Vessel	Axial +
		0.05	1.79	Axial +	1.44	Hoop -	1.79	Vessel	Axial +
	1.25	0.013	1.51	Axial +	1.13	Hoop -	1.51	Vessel	Axial +
		0.05	1.77	Axial +	1.42	Hoop -	1.77	Vessel	Axial +
	1.5	0.015	1.53	Axial +	1.16	Hoop -	1.53	Vessel	Axial +
		0.05	1.76	Axial +	1.40	Hoop -	1.76	Vessel	Axial +
125	0.25	0.002	1.29	Axial +	1.13	Hoop -	1.29	Vessel	Axial +

Table 9- 3 (Cont'd): FEM Predictions of SCF for Spherical Vessels with Small-Diameter Nozzles

RT	tT	rR	Spherical Vessel		Cylindrical Nozzle		Overall SCF	Location	Type
			SCF	Type	SCF	Type			
125	0.25	0.05	2.84	Hoop +	3.99	Axial +	3.99	Nozzle	Axial +
	0.5	0.004	1.36	Axial +	1.08	Hoop -	1.36	Vessel	Axial +
		0.05	2.30	Hoop +	2.46	Hoop +	2.46	Nozzle	Hoop +
	0.75	0.006	1.40	Axial +	1.07	Hoop -	1.40	Vessel	Axial +
		0.05	2.04	Hoop +	1.74	Hoop +	2.04	Vessel	Hoop +
	1	0.008	1.43	Axial +	1.09	Hoop -	1.43	Vessel	Axial +
		0.05	1.89	Hoop +	1.48	Hoop -	1.89	Vessel	Hoop +
	1.25	0.01	1.45	Axial +	1.13	Hoop -	1.45	Vessel	Axial +
		0.05	1.78	Axial +	1.47	Hoop -	1.78	Vessel	Axial +
	1.5	0.012	1.47	Axial +	1.15	Hoop -	1.47	Vessel	Axial +
		0.05	1.75	Axial +	1.45	Hoop -	1.75	Vessel	Axial +
150	0.25	0.002	1.27	Axial +	1.13	Hoop -	1.27	Vessel	Axial +
		0.05	2.93	Hoop +	4.30	Axial +	4.30	Nozzle	Axial +
	0.5	0.003	1.32	Axial +	1.08	Hoop -	1.32	Vessel	Axial +
		0.05	2.40	Hoop +	2.61	Hoop +	2.61	Nozzle	Hoop +
	0.75	0.005	1.36	Axial +	1.07	Hoop -	1.36	Vessel	Axial +
		0.05	2.14	Hoop +	1.85	Hoop +	2.14	Vessel	Hoop +
	1	0.007	1.39	Axial +	1.09	Hoop -	1.39	Vessel	Axial +
		0.05	1.98	Hoop +	1.52	Hoop -	1.98	Vessel	Hoop +
	1.25	0.008	1.40	Axial +	1.13	Hoop -	1.40	Vessel	Axial +
		0.05	1.86	Hoop +	1.52	Hoop -	1.86	Vessel	Hoop +
	1.5	0.01	1.42	Axial +	1.16	Hoop -	1.42	Vessel	Axial +
		0.05	1.77	Axial +	1.49	Hoop -	1.77	Vessel	Axial +

9.3 COMPARISON WITH AREA REPLACEMENT METHOD

Results of the finite element analysis for spherical vessels with small-diameter nozzles in this study are compared against those predicted by the Area Replacement Method reported by Lind [92]. The Area Replacement Method makes use of geometric dimensions to arrive at a very compact form of SCF expression as given in Equation (2.1). The main challenge in using Equation (2.1) lies in the determination of the areas F and G indicated in Figure 2.8 particularly when parametric analysis needs to be carried

out as in the present case. In this study, the built-in integration function available in COMSOL package was used to evaluate these areas by assigning unity as the expression whose integration needs to be computed over F and over G in turn. The effect of fillet (bending correction) is accounted as given in Equation (2.3) to arrive at the total stress concentration factor K . Where, the parameter K_s is determined from Figure 9-6, $\rho = \rho_f$ and $H = \max (T_n, T_v)$.

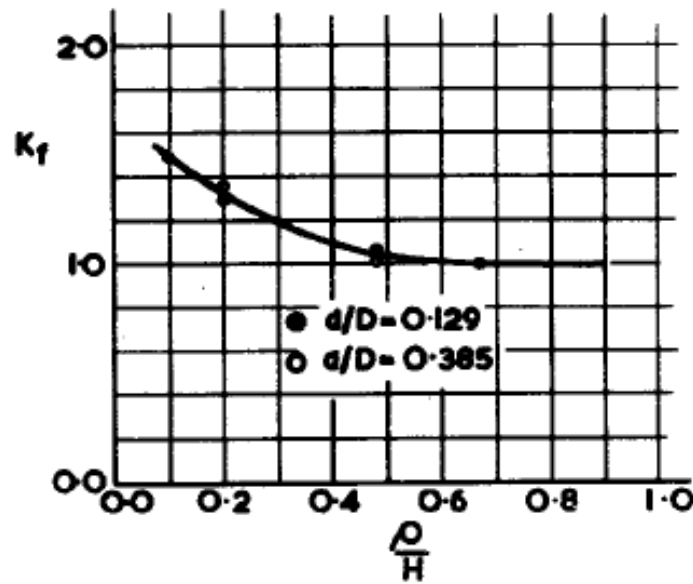


Figure 9- 6: Stress Raising Effect of Fillet in Area Replacement Method (adopted from [92])

Table 9-3 gives the comparison between SCF values predicted by FEM in this study and those obtained using the method of area replacement. It can be observed that the two predictions agree closely. While, in some instances, the FEM results appear to be more conservative than those by Area Replacement Method, the reverse is the case in others. However, as seen in Table 9-2 the possibility of having the maximum SCF occurring in either the vessel or the nozzle is taken into consideration, it can be argued that the FEM

model presented in this work is more comprehensive and more reliable to be used in the overall design of the junctions between spherical vessels and small-diameter nozzles.

Table 9- 4: Predictions of SCF for Spherical Vessels with Small-Diameter Nozzles: FEM versus Area Replacement Method [92]

RT	tT	rR	H	ρ/H	F	G	K_s	K_f	K	FEM	Deviation (%)
50	0.25	0.005	1	0.11	0.40	12.27	1.24	1.47	1.82	1.46	-19.5
		0.05	1	0.11	2.66	124.34	1.87	1.47	2.75	2.39	-13.1
	0.5	0.01	1	0.11	0.84	24.56	1.17	1.47	1.72	1.60	-6.8
		0.05	1	0.11	2.92	124.47	1.70	1.47	2.5	1.89	-24.3
	0.75	0.015	1	0.11	1.33	36.88	1.11	1.47	1.63	1.67	+2.5
		0.05	1	0.11	3.23	124.50	1.54	1.47	2.27	1.85	-18.5
	1	0.02	1	0.11	1.87	49.22	1.05	1.47	1.55	1.71	+10.9
		0.05	1	0.11	3.56	124.47	1.40	1.47	2.05	1.86	-9.3
	1.25	0.025	1.25	0.09	2.46	61.58	1.00	1.51	1.52	1.75	+15.3
		0.05	1.25	0.09	3.92	124.41	1.27	1.51	1.92	1.87	-2.8
	1.5	0.03	1.5	0.07	3.08	73.97	0.96	1.54	1.48	1.78	+20.1
		0.05	1.5	0.07	4.31	124.32	1.15	1.54	1.78	1.86	+4.5
75	0.25	0.003	1	0.16	0.40	18.52	1.25	1.37	1.7	1.38	-19.2
		0.05	1	0.16	3.64	270.01	1.98	1.37	2.71	2.58	-4.6
	0.5	0.007	1	0.16	0.85	37.06	1.17	1.37	1.6	1.48	-7.3
		0.05	1	0.16	3.94	270.39	1.83	1.37	2.51	2.07	-17.5
	0.75	0.01	1	0.16	1.34	55.62	1.11	1.37	1.51	1.53	+1.4
		0.05	1	0.16	4.29	270.60	1.68	1.37	2.31	1.81	-21.6
	1	0.013	1	0.16	1.88	74.21	1.05	1.37	1.44	1.57	+9.5
		0.05	1	0.16	4.67	270.73	1.55	1.37	2.12	1.80	-15.0
	1.25	0.017	1.25	0.13	2.47	92.83	1.00	1.43	1.43	1.60	+12.2
		0.05	1.25	0.13	5.09	270.79	1.42	1.43	2.03	1.80	-11.3
	1.5	0.02	1.5	0.11	3.11	111.46	0.96	1.47	1.4	1.62	+15.6
		0.05	1.5	0.11	5.54	270.80	1.30	1.47	1.92	1.78	-6.9
100	0.25	0.003	1	0.22	0.40	24.76	1.25	1.28	1.6	1.33	-17.0
		0.05	1	0.22	4.20	450.02	2.14	1.28	2.75	2.72	-1.0
	0.5	0.005	1	0.22	0.85	49.55	1.16	1.28	1.49	1.41	-5.7
		0.05	1	0.22	4.52	450.71	1.99	1.28	2.56	2.20	-14.1
	0.75	0.008	1	0.22	1.35	74.37	1.10	1.28	1.41	1.45	+2.8
		0.05	1	0.22	4.91	451.15	1.84	1.28	2.36	1.94	-18.0
	1	0.01	1	0.22	1.89	99.21	1.05	1.28	1.35	1.48	+10.4
		0.05	1	0.22	5.33	451.46	1.69	1.28	2.17	1.79	-17.7

Table 9- 5 (Cont'd): Predictions of SCF for Spherical Vessels with Small-Diameter Nozzles: FEM versus Area Replacement Method [92]

RT	tT	rR	H	ρ/H	F	G	Ks	Kf	K	FEM	Deviation (%)
100	1.25	0.013	1.25	0.17	2.49	124.07	1.00	1.35	1.35	1.51	+12.0
		0.05	1.25	0.17	5.80	451.68	1.56	1.35	2.1	1.77	-15.7
	1.5	0.015	1.5	0.14	3.13	148.96	0.95	1.4	1.34	1.53	+14.3
		0.05	1.5	0.14	6.30	451.83	1.43	1.4	2.01	1.76	-12.6
125	0.25	0.002	1	0.27	0.40	31.01	1.25	1.21	1.51	1.29	-14.3
		0.05	1	0.27	4.69	670.82	2.29	1.21	2.77	2.84	+2.3
	0.5	0.004	1	0.27	0.85	62.05	1.17	1.21	1.42	1.36	-4.5
		0.05	1	0.27	5.04	671.85	2.13	1.21	2.58	2.30	-10.8
	0.75	0.006	1	0.27	1.36	93.12	1.10	1.21	1.33	1.40	+5.1
		0.05	1	0.27	5.45	672.56	1.97	1.21	2.39	2.04	-14.5
	1	0.008	1	0.27	1.90	124.21	1.04	1.21	1.27	1.43	+12.7
		0.05	1	0.27	5.92	673.08	1.82	1.21	2.2	1.89	-14.3
	1.25	0.01	1.25	0.22	2.50	155.32	1.00	1.28	1.28	1.45	+13.3
		0.05	1.25	0.22	6.43	673.49	1.68	1.28	2.15	1.78	-17.1
	1.5	0.012	1.5	0.18	3.14	186.46	0.95	1.34	1.27	1.47	+15.3
		0.05	1.5	0.18	6.97	673.80	1.55	1.34	2.07	1.75	-15.4
150	0.25	0.002	1	0.32	0.40	37.26	1.25	1.15	1.44	1.27	-11.7
		0.05	1	0.32	5.14	931.36	2.42	1.15	2.78	2.93	+5.3
	0.5	0.003	1	0.32	0.85	74.55	1.17	1.15	1.35	1.32	-2.2
		0.05	1	0.32	5.51	932.79	2.26	1.15	2.6	2.40	-7.9
	0.75	0.005	1	0.32	1.36	111.87	1.09	1.15	1.26	1.36	+7.8
		0.05	1	0.32	5.95	933.79	2.09	1.15	2.41	2.14	-11.3
	1	0.007	1	0.32	1.91	149.21	1.04	1.15	1.2	1.39	+15.5
		0.05	1	0.32	6.45	934.55	1.93	1.15	2.23	1.98	-10.9
	1.25	0.008	1.25	0.26	2.51	186.57	0.99	1.23	1.22	1.40	+15.4
		0.05	1.25	0.26	7.00	935.16	1.78	1.23	2.18	1.86	-14.7
	1.5	0.01	1.5	0.22	3.15	223.96	0.95	1.28	1.22	1.42	+16.3
		0.05	1.5	0.22	7.58	935.66	1.64	1.28	2.11	1.77	-16.2

9.4 OVERALL DESIGN CHARTS: SPHERICAL VESSEL-CYLINDRICAL NOZZLE JUNCTURES

As previously claimed, the design charts presented in chapter seven are valid only for spherical vessels intersected by moderate-to-large-diameter nozzles that do not violate the thin shell assumption. Results of the analysis of spherical vessels having small-diameters

presented in section 9.2 are used to augment those of vessels with moderate-to-large-diameters to arrive at the overall design charts that cover all the possible ranges of nozzle-to-vessel diameter ratios as shown in figures 9.7 to 9.11.

By adopting these individual plots, some likely errors are minimized because they enable prediction of unique SCF values for specific combinations of the vessel-nozzle geometric ratios in contrast to some literature approaches that combines and shows the effect of all the geometric parameters in a single plot. In addition, consideration is given to the possibility of having higher values of SCF in the nozzle.

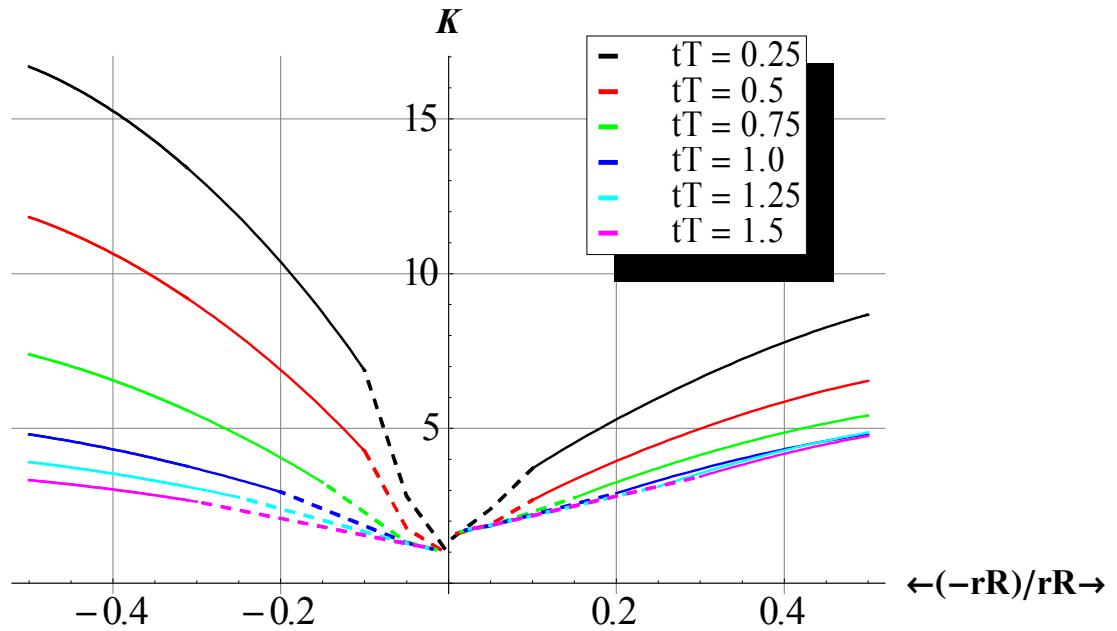


Figure 9- 7: Variation of SCF in the Spherical Vessel (left set of graphs) and Nozzle (right set of graphs) with Geometric Ratios for Constant $RT = 50$ as predicted by the FEM

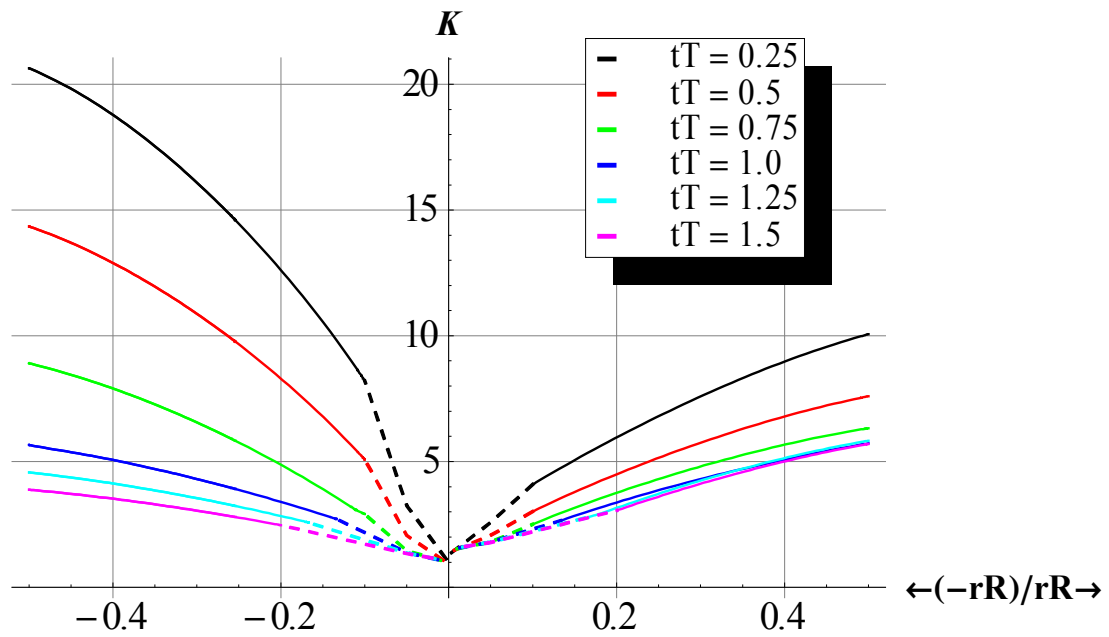


Figure 9- 8: Variation of SCF in the Spherical Vessel (left set of graphs) and Nozzle (right set of graphs) with Geometric Ratios for Constant $RT = 75$ as predicted by the FEM

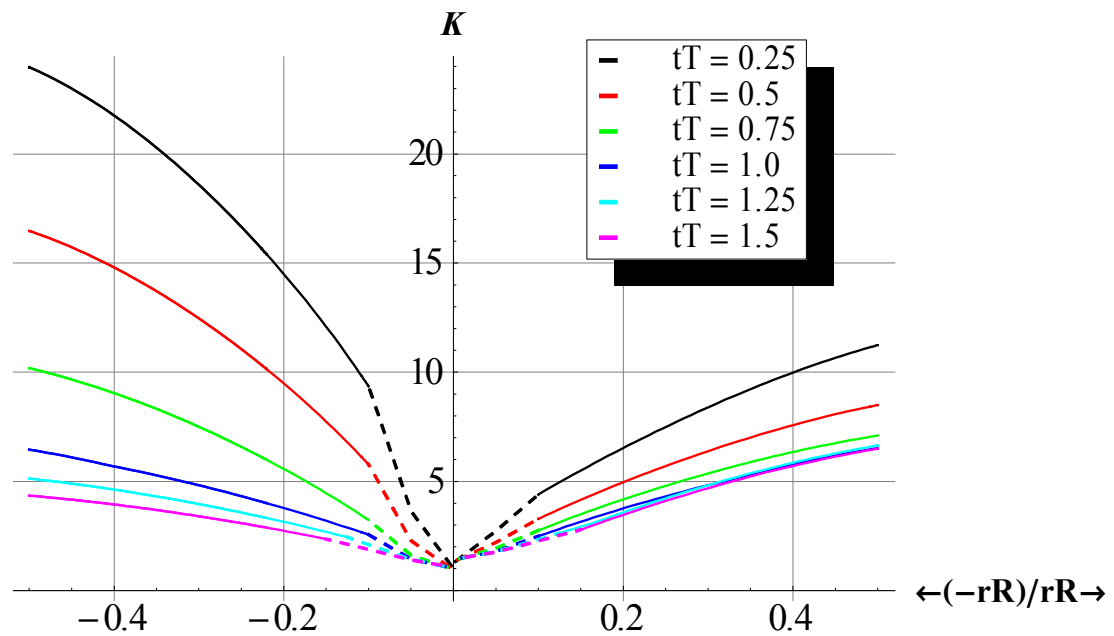


Figure 9- 9: Variation of SCF in the Spherical Vessel (left set of graphs) and Nozzle (right set of graphs) with Geometric Ratios for Constant $RT = 100$ as predicted by the FEM

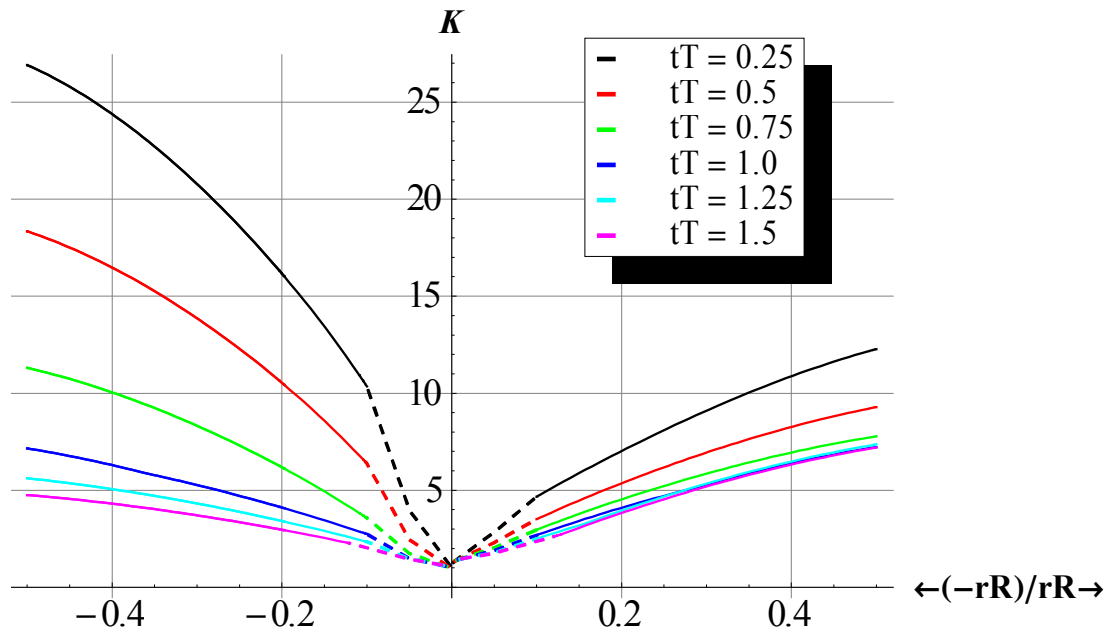


Figure 9- 10: Variation of SCF in the Spherical Vessel (left set of graphs) and Nozzle (right set of graphs) with Geometric Ratios for Constant $RT = 125$ as predicted by the FEM

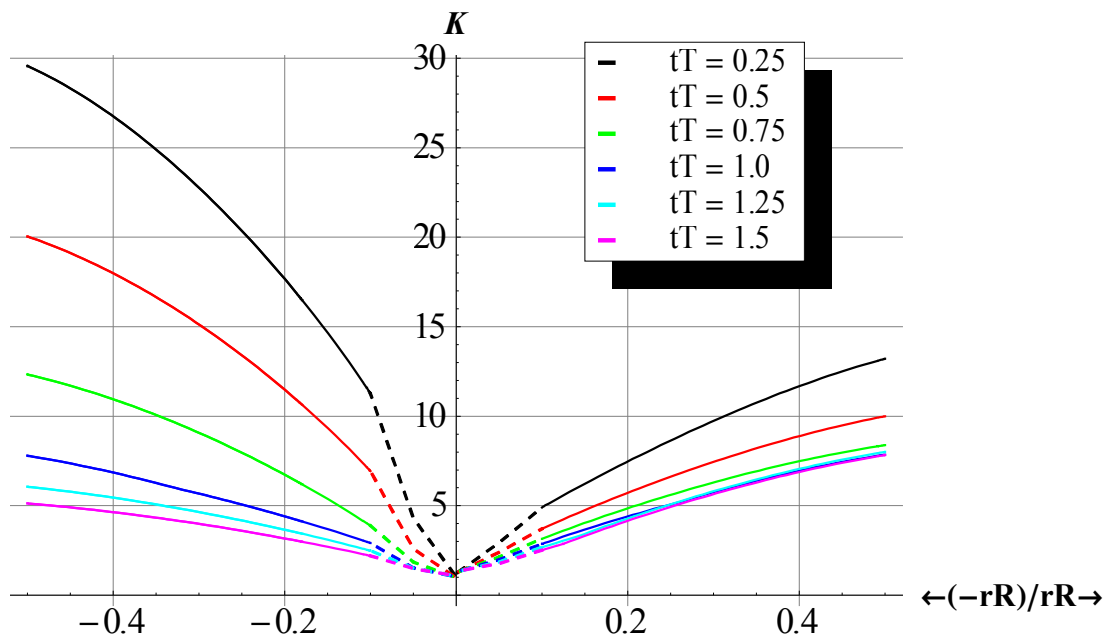


Figure 9- 11: Variation of SCF in the Spherical Vessel (left set of graphs) and Nozzle (right set of graphs) with Geometric Ratios for Constant $RT = 150$ as predicted by the FEM

CHAPTER TEN

MODELING AND ANALYSIS OF SCF FOR CYLINDRICAL PRESSURE VESSELS WITH SMALL DIAMETER NOZZLES

10.1 INTRODUCTION

This chapter aims at complementing the analysis presented in Chapter Eight that is based on the use of thin shell theory due to the fact that the intersecting nozzle sizes are moderate-to-large. Such analysis becomes invalid in instances when the nozzles are small in sizes which may result in nozzles whose configuration violates the assumption of shell theory. As a result, use of solid elements (based on theory of elasticity) in modeling the cylindrical vessels with small-diameter nozzles is presented in the present chapter. Expressions for the membrane stresses in cylindrical vessels given in Table 9-1 holds for both the main vessel and the nozzle. Discussions of the numerical experiments and the results achieved are, first, given. The results are then compared with the prediction by other models reported in the literature. In order to arrive at the overall design charts that cover all the possible ranges of nozzle-to-vessel diameter ratio, the charts presented in Chapter Eight are augmented with those of cylindrical vessels intersected by small-diameter nozzles developed in this chapter.

10.2 NUMERICAL EXPERIMENTS, RESULTS AND DISCUSSIONS

Shown in Figure 10-1 is the solid model developed for cylindrical vessel with small-diameter nozzles based on the steps outlined in Figure 6.7. Since a 3D fillet is not available in COMSOL Version 4.3b, the effect of singularity at the junction between the

main vessel and the nozzle is avoided by evaluating the stresses at an offset distance of $0.0005375R_v$ from the external intersection point. This distance is arrived at by carrying out several simulation runs of cylindrical vessel-nozzle problem of very large diameter and, each time, verifying the solution against that obtained using shell theory in which the effect of singularity does not manifest. Evaluation of the results at internal surfaces was done along the dark lines shown in Figure 10-1 (b). The meshed geometry and the juncture mesh details are shown in Figure 10-2.

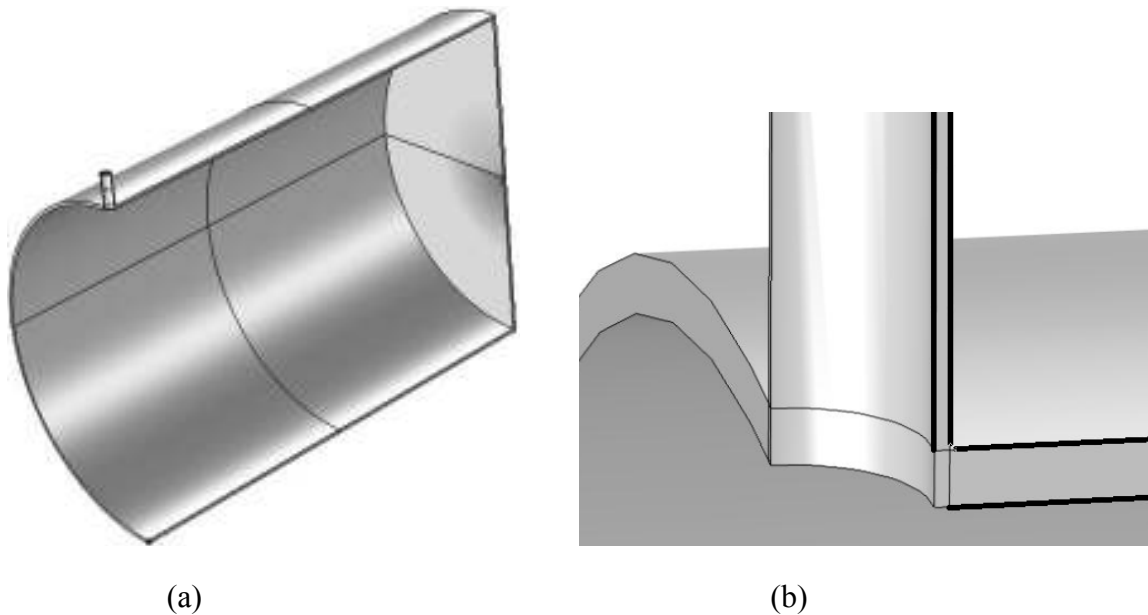


Figure 10- 1: Quarter Model for the Cylindrical Vessel-Nozzle Junction (a) Geometry (b) Lines (shown in dark) for Stress Evaluation to avoid Singularity

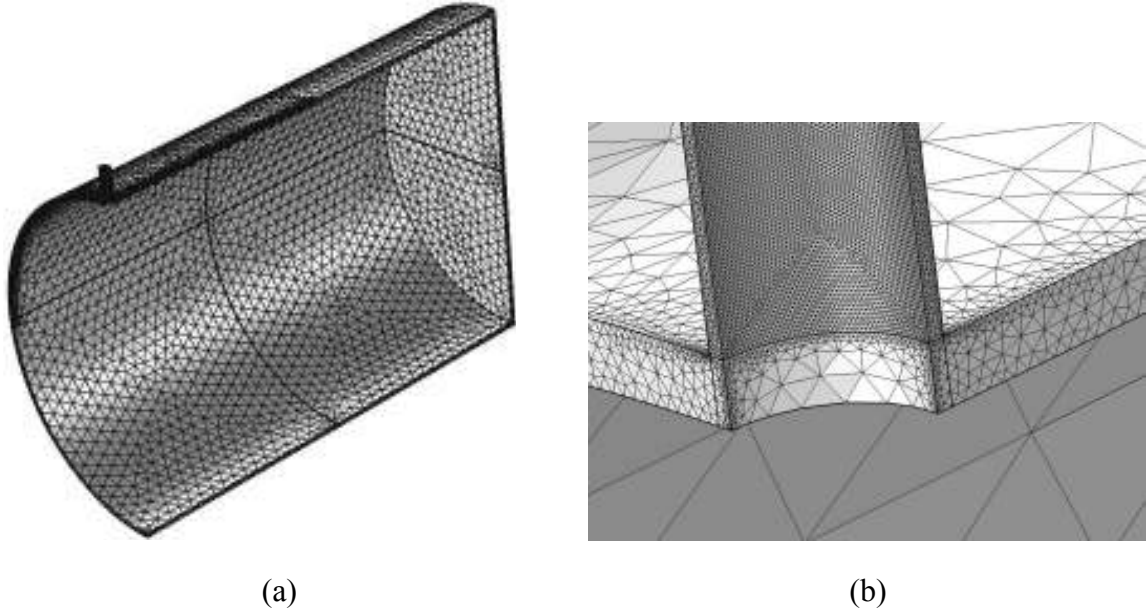


Figure 10- 2: Geometry Discretization (a) Overall Mesh (b) Refined Mesh at the Junction

A total of 335 numerical experiments were conducted, corresponding to the following ranges of non-dimensional geometric parameters.

$$RT = 5 + 5i, \{i, 1, 29\}$$

$$tT = 0.25j, \{j, 1, 6\}$$

$$rR = T_n/R_v \text{ and } 0.05$$

Figures 9.3 to 9.5 show typical stress behaviors along the vessel's and nozzle's geometry. It can be observed how both the non-dimensional hoop and axial discontinuity stresses in both the cylindrical vessel and the nozzle dissipates, leaving behind only the non-dimensional membrane stresses at some distances away from the juncture. This behavior reinforces the claim that care was taken in choosing dimensions of both the vessel and nozzle to give rise to a configuration with no interaction between the discontinuity stresses arising from adjacent junctions.

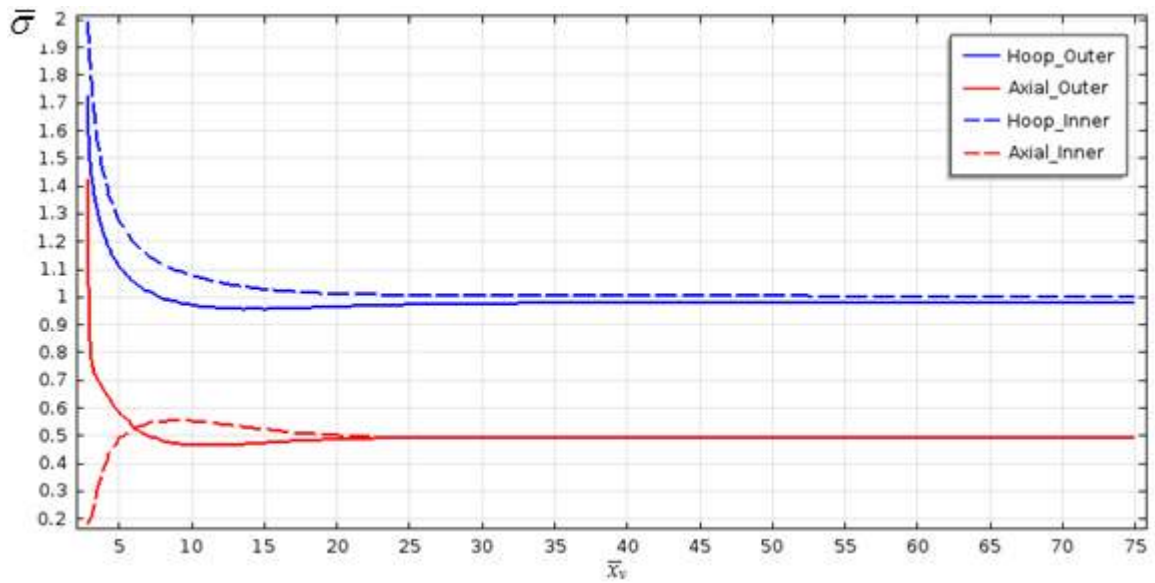


Figure 10- 3: Variation of the Four Types of Stresses in the Main Cylindrical Vessel for a Typical Vessel-Nozzle Junction with $RT = 50$, $tT = 0.5$ and $rR = 0.05$

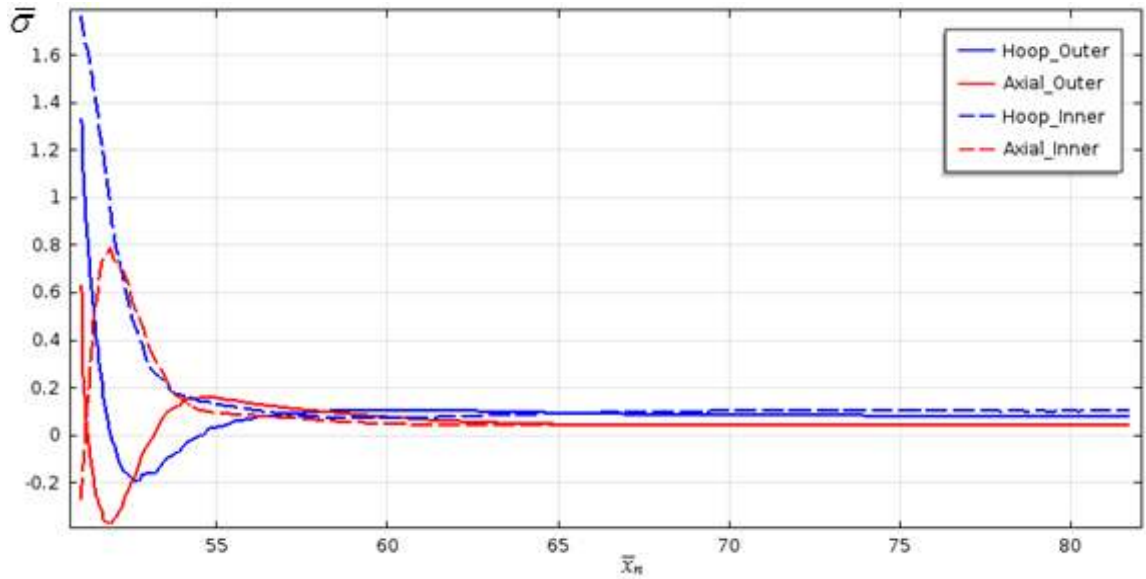


Figure 10- 4: Variation of the Four Types of Stresses in the Cylindrical Nozzle for a Typical Vessel-Nozzle Junction with $RT = 50$, $tT = 0.5$ and $rR = 0.05$

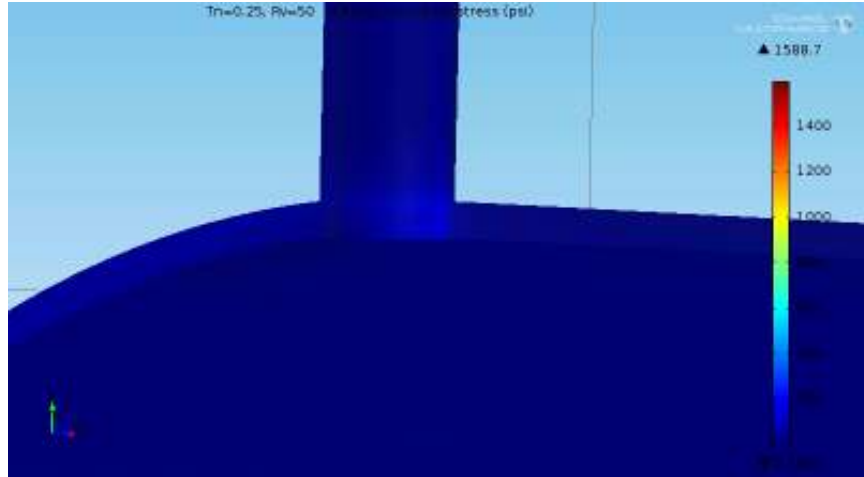


Figure 10- 5: von Mises Stress Plot for a Typical Vessel-Nozzle Configuration with $RT = 50$, $tT = 0.5$ and $rR = 0.05$

Results obtained for the mentioned ranges of the non-dimensional parameters tT and rR are given in Table 10-1 for the cylindrical vessel's SCF alongside with that of the nozzle for $RT = 25 + 25i$, $\{i, 1, 5\}$. Table C2 of Appendix C lists remaining set of the results for other geometric ratios. Study on the location and type of maximum stresses, hence the overall SCF values are also incorporated. In most cases, the interior part of the juncture happens to have higher stresses than the exterior part of the configurations considered.

Table 10- 1: FEM Predictions of SCF for Cylindrical Vessels with Small-Diameter Nozzles

RT	tT	rR	Cylindrical Vessel		Cylindrical Nozzle		Overall SCF	Location	Type
			SCF	Type	SCF	Type			
50	0.25	0.005	1.08	Hoop -	1.47	Hoop -	1.47	Nozzle	Hoop -
		0.05	2.32	Hoop +	2.33	Hoop +	2.33	Nozzle	Hoop +
	0.5	0.01	1.16	Hoop -	1.47	Hoop -	1.47	Nozzle	Hoop -
		0.05	1.99	Hoop -	1.77	Hoop -	1.99	Vessel	Hoop -
	0.75	0.015	1.21	Hoop -	1.44	Hoop -	1.44	Nozzle	Hoop -
		0.05	1.74	Hoop -	1.75	Hoop -	1.75	Nozzle	Hoop -
	1	0.02	1.23	Hoop -	1.44	Hoop -	1.44	Nozzle	Hoop -
		0.05	1.57	Hoop -	1.71	Hoop -	1.71	Nozzle	Hoop -
	1.25	0.025	1.24	Hoop -	1.38	Hoop -	1.38	Nozzle	Hoop -

Table 10- 2 (Cont'd): FEM Predictions of SCF for Cylindrical Vessels with Small-Diameter Nozzles

RT	tT	rR	Cylindrical Vessel		Cylindrical Nozzle		Overall SCF	Location	Type
			SCF	Type	SCF	Type			
50	1.25	0.05	1.43	Hoop -	1.66	Hoop -	1.66	Nozzle	Hoop -
	1.5	0.03	1.22	Hoop -	1.45	Hoop -	1.45	Nozzle	Hoop -
		0.05	1.33	Hoop -	1.61	Hoop -	1.61	Nozzle	Hoop -
75	0.25	0.003	1.06	Hoop -	1.36	Hoop -	1.36	Nozzle	Hoop -
		0.05	2.57	Hoop +	2.94	Hoop +	2.94	Nozzle	Hoop +
	0.5	0.007	1.16	Hoop -	1.52	Hoop -	1.52	Nozzle	Hoop -
		0.05	2.13	Hoop -	1.80	Hoop -	2.13	Vessel	Hoop -
	0.75	0.01	1.21	Hoop -	1.36	Hoop -	1.36	Nozzle	Hoop -
		0.05	1.87	Hoop -	1.80	Hoop -	1.87	Vessel	Hoop -
	1	0.013	1.24	Hoop -	1.30	Hoop -	1.30	Nozzle	Hoop -
		0.05	1.68	Hoop -	1.78	Hoop -	1.78	Nozzle	Hoop -
	1.25	0.017	1.24	Hoop -	1.39	Hoop -	1.39	Nozzle	Hoop -
		0.05	1.53	Hoop -	1.75	Hoop -	1.75	Nozzle	Hoop -
	1.5	0.02	1.23	Hoop -	1.50	Hoop -	1.50	Nozzle	Hoop -
		0.05	1.42	Hoop -	1.69	Hoop -	1.69	Nozzle	Hoop -
100	0.25	0.003	1.06	Hoop -	1.44	Hoop -	1.44	Nozzle	Hoop -
		0.05	2.82	Hoop +	3.37	Hoop +	3.37	Nozzle	Hoop +
	0.5	0.005	1.16	Hoop -	1.54	Hoop -	1.54	Nozzle	Hoop -
		0.05	2.24	Hoop +	2.08	Hoop +	2.24	Vessel	Hoop +
	0.75	0.008	1.21	Hoop -	1.43	Hoop -	1.43	Nozzle	Hoop -
		0.05	1.94	Hoop -	1.83	Hoop -	1.94	Vessel	Hoop -
	1	0.01	1.24	Hoop -	1.37	Hoop -	1.37	Nozzle	Hoop -
		0.05	1.74	Hoop -	1.82	Hoop -	1.82	Nozzle	Hoop -
	1.25	0.013	1.24	Hoop -	1.40	Hoop -	1.40	Nozzle	Hoop -
		0.05	1.60	Hoop -	1.79	Hoop -	1.79	Nozzle	Hoop -
	1.5	0.015	1.23	Hoop -	1.41	Hoop -	1.41	Nozzle	Hoop -
		0.05	1.47	Hoop -	1.74	Hoop -	1.74	Nozzle	Hoop -
125	0.25	0.002	1.08	Hoop -	1.45	Hoop -	1.45	Nozzle	Hoop -
		0.05	3.10	Hoop +	3.63	Hoop +	3.63	Nozzle	Hoop +
	0.5	0.004	1.16	Hoop -	1.38	Hoop -	1.38	Nozzle	Hoop -
		0.05	2.44	Hoop +	2.41	Hoop +	2.44	Vessel	Hoop +
	0.75	0.006	1.21	Hoop -	1.38	Hoop -	1.38	Nozzle	Hoop -
		0.05	2.10	Hoop +	1.85	Hoop -	2.10	Vessel	Hoop +
	1	0.008	1.24	Hoop -	1.35	Hoop -	1.35	Nozzle	Hoop -
		0.05	1.85	Hoop +	1.85	Hoop -	1.85	Vessel	Hoop +
	1.25	0.01	1.24	Hoop -	1.44	Hoop -	1.44	Nozzle	Hoop -
		0.05	1.70	Hoop +	1.82	Hoop -	1.82	Nozzle	Hoop -

Table 10- 3 (Cont'd): FEM Predictions of SCF for Cylindrical Vessels with Small-Diameter Nozzles

RT	tT	rR	Cylindrical Vessel		Cylindrical Nozzle		Overall SCF	Location	Type
			SCF	Type	SCF	Type			
125	1.5	0.012	1.22	Hoop -	1.42	Hoop -	1.42	Nozzle	Hoop -
		0.05	1.52	Hoop -	1.78	Hoop -	1.78	Nozzle	Hoop -
150	0.25	0.002	1.06	Hoop -	1.82	Hoop -	1.82	Nozzle	Hoop -
		0.05	3.16	Hoop +	4.00	Hoop +	4.00	Nozzle	Hoop +
	0.5	0.003	1.16	Hoop -	1.37	Hoop -	1.37	Nozzle	Hoop -
		0.05	2.58	Hoop +	2.57	Hoop +	2.58	Vessel	Hoop +
	0.75	0.005	1.21	Hoop -	1.44	Hoop -	1.44	Nozzle	Hoop -
		0.05	2.26	Hoop +	1.88	Hoop +	2.26	Vessel	Hoop +
	1	0.007	1.24	Hoop -	1.38	Hoop -	1.38	Nozzle	Hoop -
		0.05	2.05	Hoop +	1.87	Hoop -	2.05	Vessel	Hoop +
	1.25	0.008	1.24	Hoop -	1.39	Hoop -	1.39	Nozzle	Hoop -
		0.05	1.83	Hoop +	1.84	Hoop -	1.84	Nozzle	Hoop -
	1.5	0.01	1.23	Hoop -	1.39	Hoop -	1.39	Nozzle	Hoop -
		0.05	1.67	Hoop +	1.80	Hoop -	1.80	Nozzle	Hoop -

10.3 COMPARISON WITH THE PREDICTION BY OTHER MODELS

To have an idea about how results of the FEM analysis for cylindrical vessels intersected by small-diameter nozzles achieved in this chapter perform, comparisons are made with three established SCF models available in the literature [93, 95, 96]. These models require no further introduction as they are the same models against which the findings in Chapter Eight are compared.

Figures 10-6 to 10-8 show a relative performance of the FEM predictions in this chapter to the three other models. It would be reiterated here that since these models and many other similar ones in the literature concentrate on the vessel's SCF alone, the comparisons are carried out with only the vessel's SCF of the present study. As seen in the mentioned figures, the FEM results agree well with these other models especially the model proposed by Money [95] based on several experimental observations. Hence, reliability

of the FEM model is established. Such agreement seems better than the one realized in case of cylindrical vessels with moderate-to-large-diameter nozzles. Robustness of the present model is further attributed to its consideration to the possibility of having higher values of SCF in the nozzle as seen in Table 10-1.

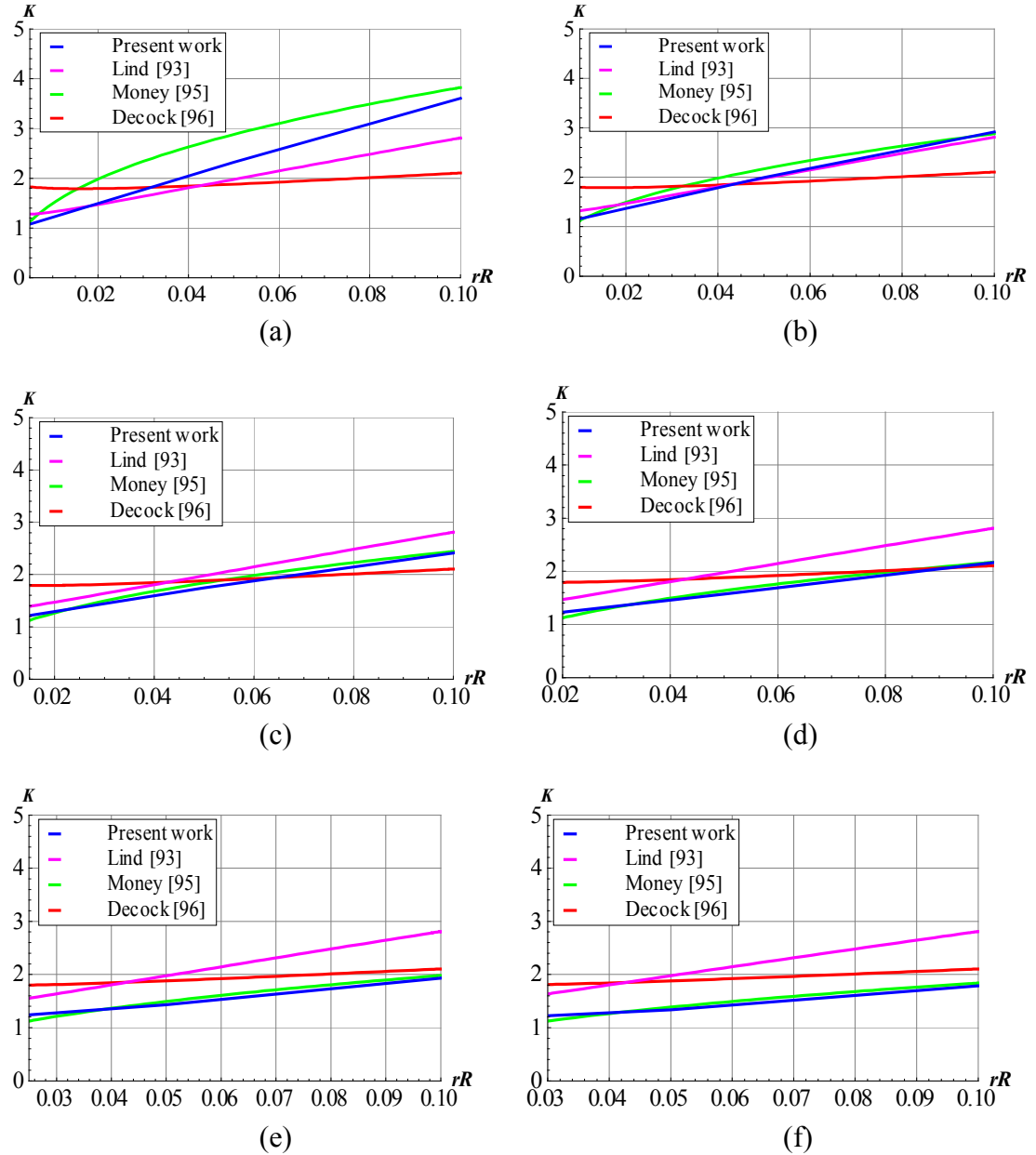


Figure 10- 6: Comparison between Prediction of the Present Work with other Established SCF Models for $RT = 50$ and (a) $tT = 0.25$ (b) $tT = 0.5$ (c) $tT = 0.75$ (d) $tT = 1.0$ (e) $tT = 1.25$ (f) $tT = 1.5$

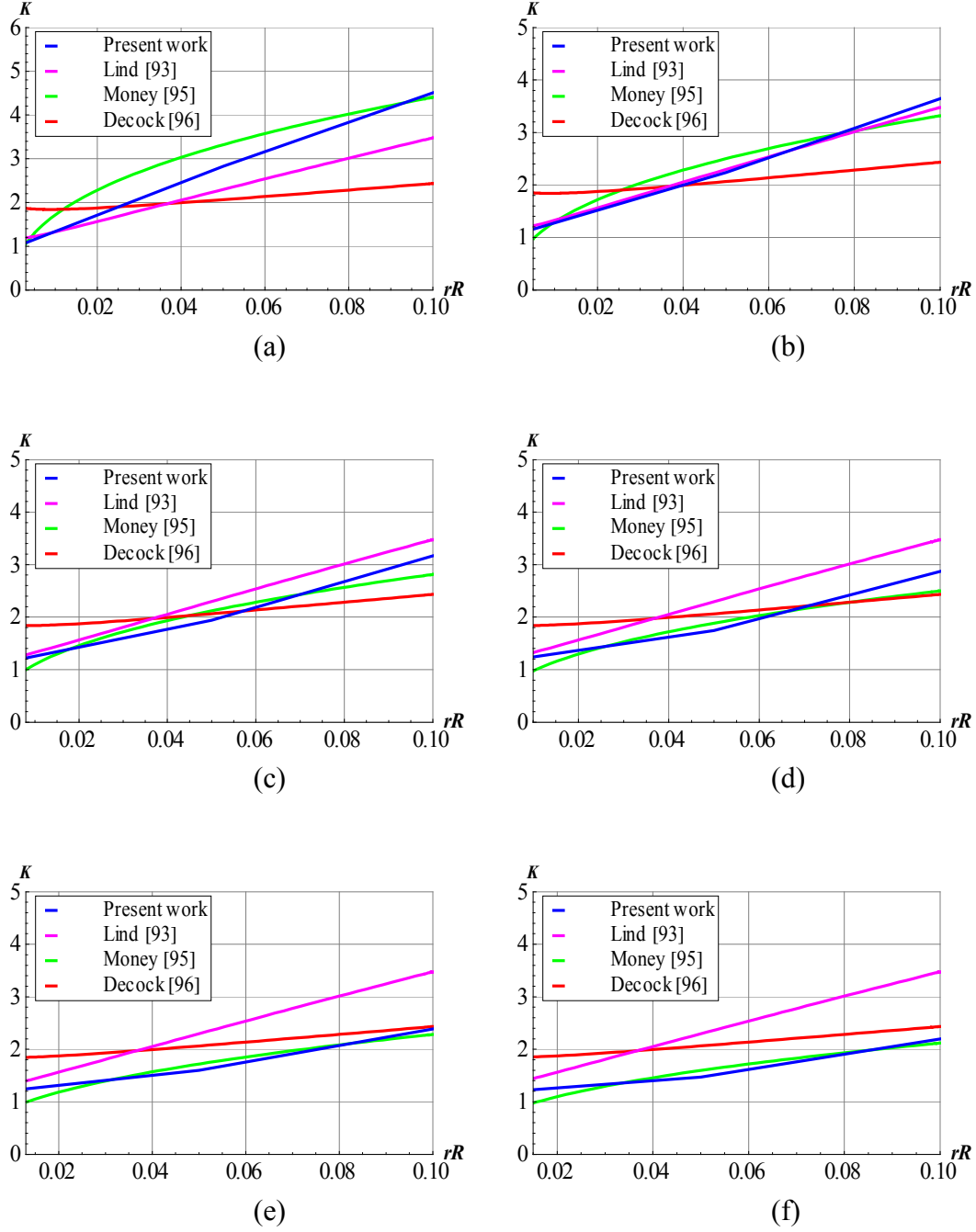


Figure 10- 7: Comparison between Prediction of the Present Work with other Established SCF Models for $RT = 100$ and (a) $tT = 0.25$ (b) $tT = 0.5$ (c) $tT = 0.75$ (d) $tT = 1.0$ (e) $tT = 1.25$ (f) $tT = 1.5$

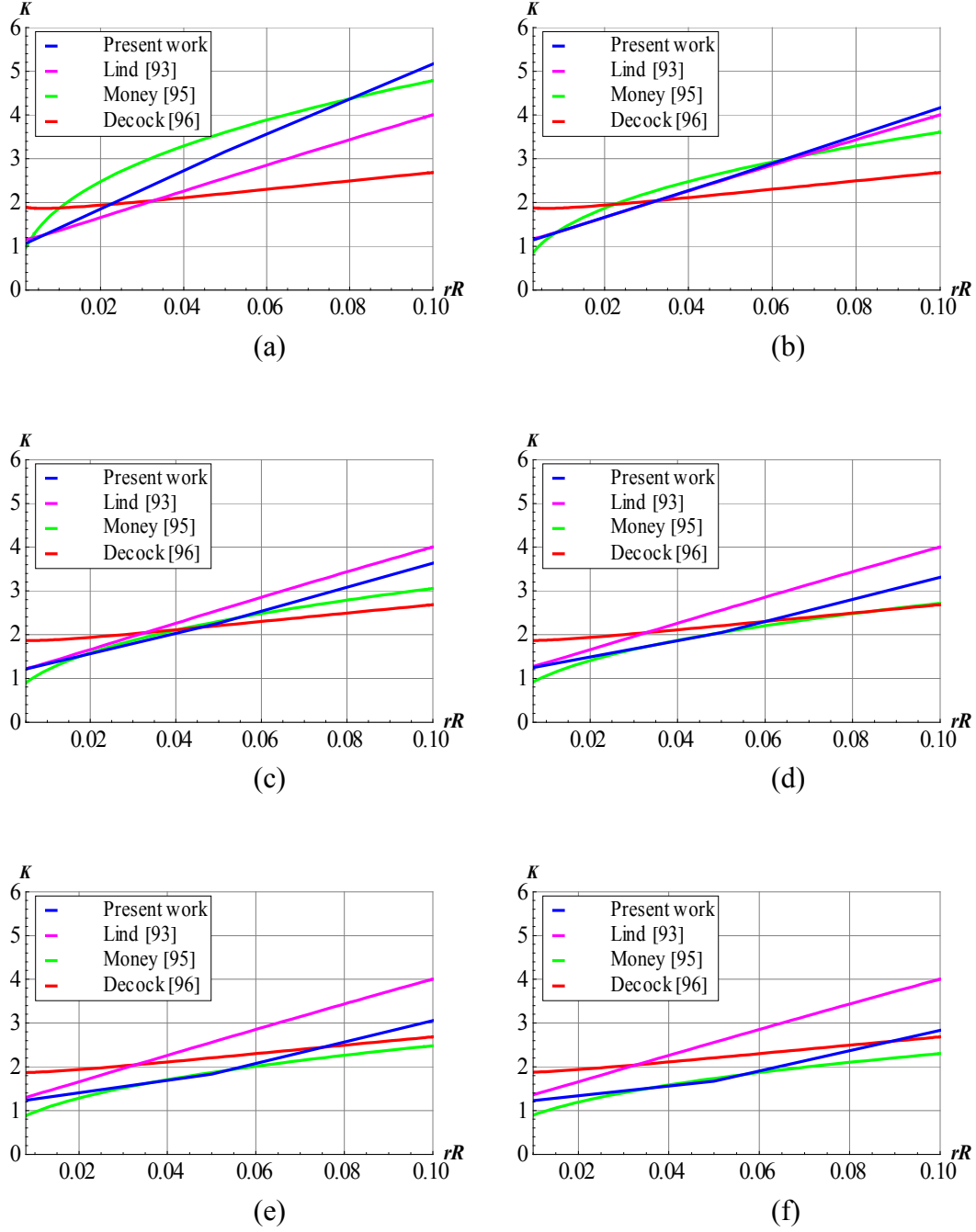


Figure 10- 8: Comparison between Prediction of the Present Work with other Established SCF Models for $RT = 150$ and (a) $tT = 0.25$ (b) $tT = 0.5$ (c) $tT = 0.75$ (d) $tT = 1.0$ (e) $tT = 1.25$ (f) $tT = 1.5$

10.4 OVERALL DESIGN CHARTS: CYLINDRICAL VESSEL-CYLINDRICAL NOZZLE JUNCTURES

Since the analysis presented in Chapter Eight is based on thin shell theory, its validity only holds for cylindrical vessels intersected by moderate-to-large-diameter nozzles. Hence, results of the analysis carried out in section 10.2 is used here to develop design charts applicable to cylindrical vessels with small-diameter nozzles that will be, subsequently, used to augment those presented in Chapter Eight. This way, the overall design charts covering all the possible ranges of nozzle-to-vessel diameter ratios as shown in figures 10-9 to 10-13 are obtained for cylindrical vessel-cylindrical nozzle junctures.

About 83% of the geometric ratios for cylindrical vessel with small-diameter nozzles dealt with in this chapter have the maximum stress occurring in the nozzle while the remaining of only about 17% have maximum stress in the vessel. This fact tenders the adoption of combined SCF charts of the vessel and the nozzle presented here more robust than even the models against which comparison was made in section 10.3.

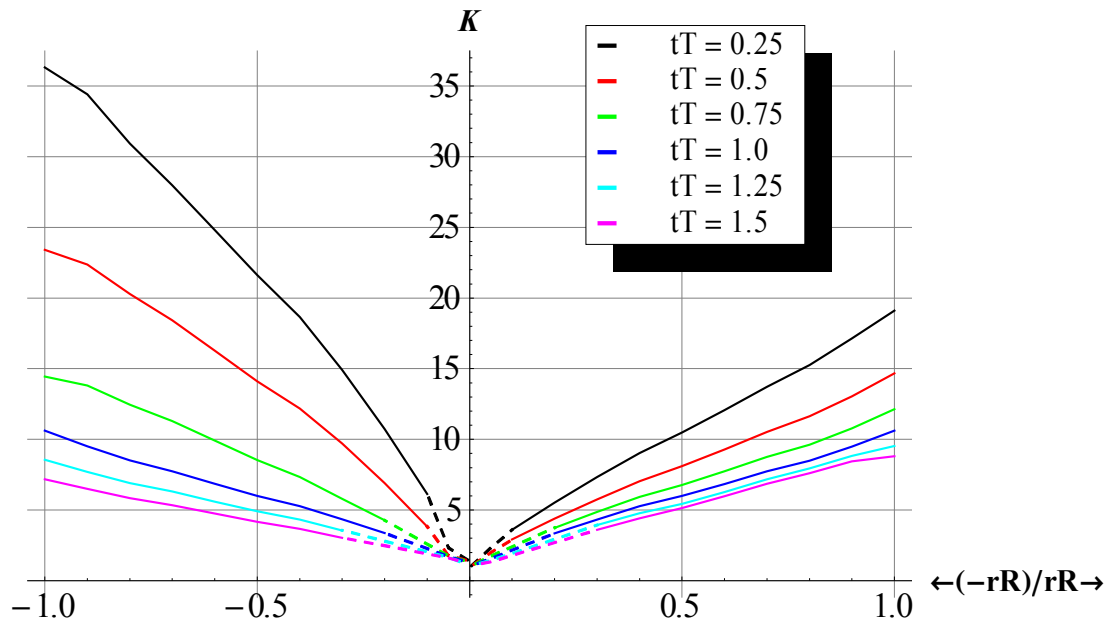


Figure 10- 9: Variation of SCF in the Cylindrical Vessel (left set of graphs) and Nozzle (right set of graphs) with Geometric Ratios for Constant $RT = 50$ as predicted by the FEM

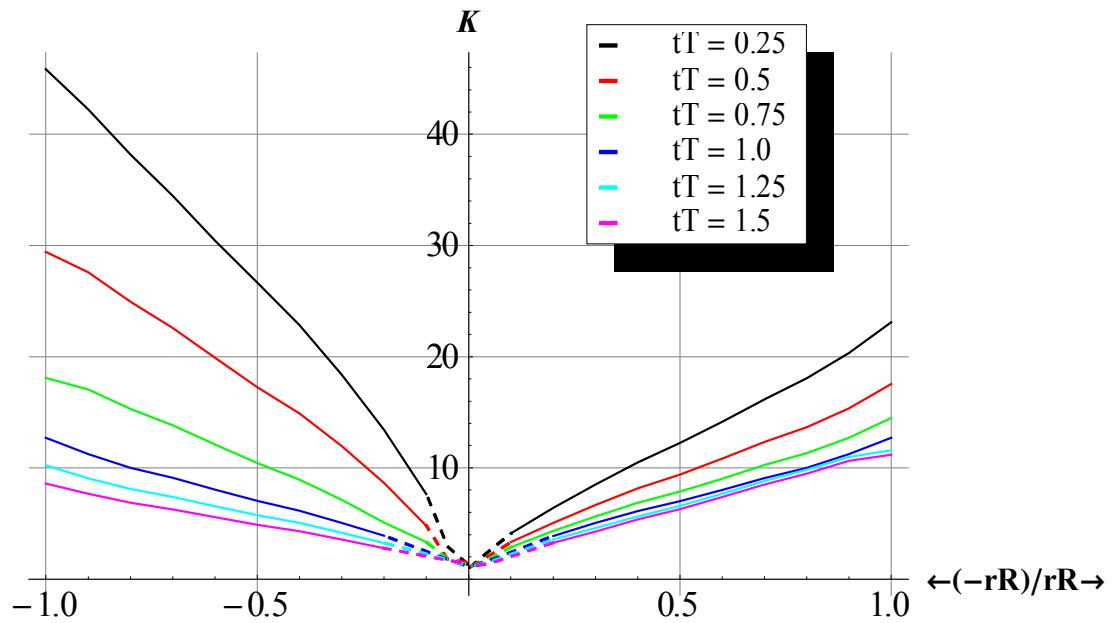


Figure 10- 10: Variation of SCF in the Cylindrical Vessel (left set of graphs) and Nozzle (right set of graphs) with Geometric Ratios for Constant $RT = 75$ as predicted by the FEM

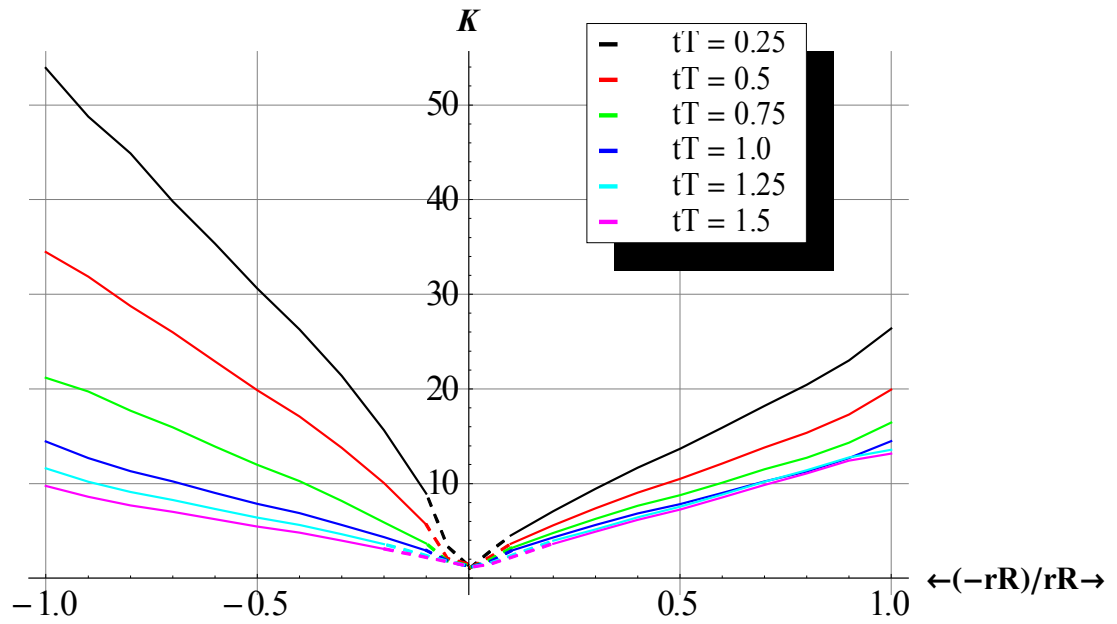


Figure 10- 11: Variation of SCF in the Cylindrical Vessel (left set of graphs) and Nozzle (right set of graphs) with Geometric Ratios for Constant $RT=100$ as predicted by the FEM

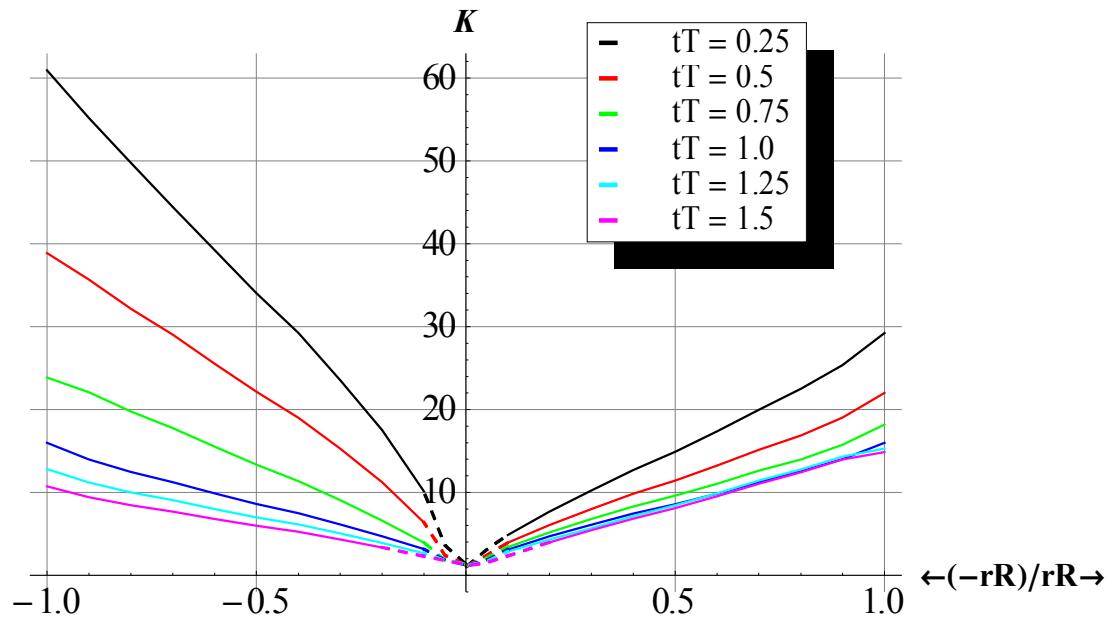


Figure 10- 12: Variation of SCF in the Cylindrical Vessel (left set of graphs) and Nozzle (right set of graphs) with Geometric Ratios for Constant $RT=125$ as predicted by the FEM

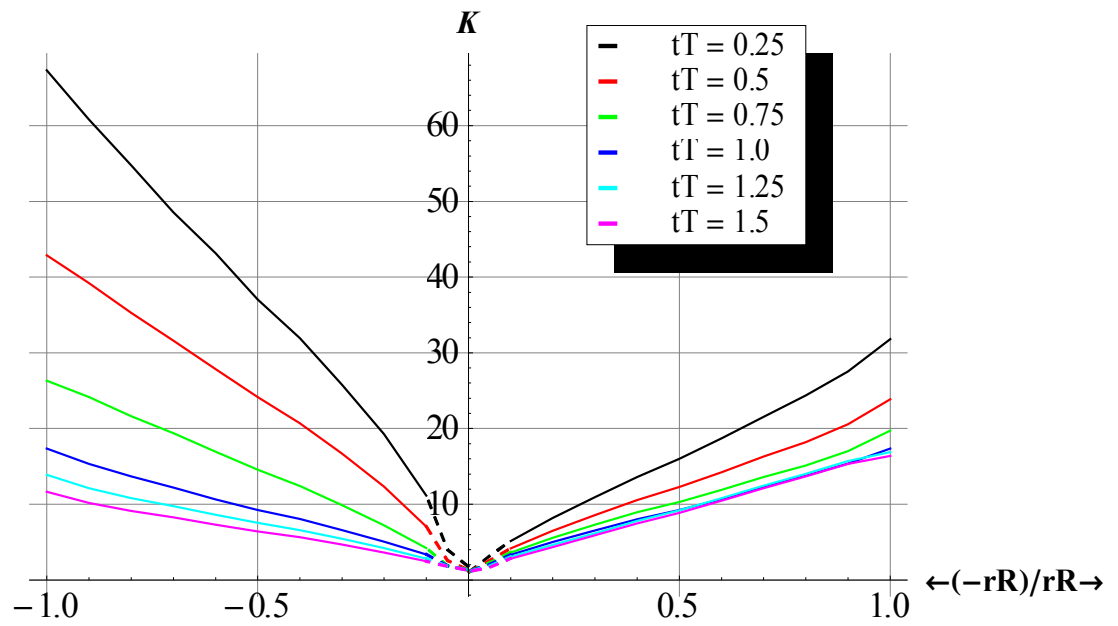


Figure 10- 13: Variation of SCF in the Cylindrical Vessel (left set of graphs) and Nozzle (right set of graphs) with Geometric Ratios for Constant $RT=150$ as predicted by the FEM

CHAPTER ELEVEN

DEVELOPMENT OF SIMPLIFIED EXPRESSIONS OF SCF

Results of the analytical and numerical analyses presented in the previous chapters are used to arrive at symbolic expressions of SCF for both cylindrical and spherical vessels with nozzle diameters ranging from small to large. Efforts are put to ensure the compactness and ease of use of the developed expressions. Their accuracy is verified as the percentage deviations from the actual numerical experimental results from which they are derived.

11.1 SPHERICAL VESSELS

11.1.1 Spherical Vessels with Moderate-To-Large-Diameter Nozzles

Two forms of SCF symbolic expressions are presented for spherical vessels intersected by moderate-to-large-diameter nozzles. The first (presented in subsection 11.1.1.1) is derived based on the Hetenyi's solution that was proved, in Chapter Seven, to be sufficient for SCF determination. The second (presented in subsection 11.1.1.2) is obtained as an empirical relation via extensive parametric analysis.

11.1.1.1 Closed-Form Analytical Expressions of SCF

The approximate analytical solution used in the analysis of Chapter Seven is derived here in a closed-form. The two compatibility conditions (equations (6.31) and (6.32)) are solved to provide the required expressions for the non-dimensionalized discontinuity force and moment given by Equation (11.1).

$$\begin{aligned}
\bar{Q} &= - \frac{tT \left(\theta_v \cdot tT + \sqrt{\frac{rR RT}{tT}} (2tT w_v + \bar{p} \cdot rR \cdot RT (\nu - 2)) \sqrt[4]{3(1 - \nu^2)} \right)}{2 \cdot rR^2 \cdot RT^2 \sqrt{3(1 - \nu^2)}} \\
\bar{M} &= - \frac{\bar{p} \left(\frac{rR RT}{tT} \right)^{3/2} tT (\nu - 2) \sqrt[4]{3(1 - \nu^2)} + 2tT \left(\theta_v + \sqrt{\frac{rR RT}{tT}} w_v \sqrt[4]{3(1 - \nu^2)} \right)}{4 \left(\frac{rR RT}{tT} \right)^{5/2} tT \sqrt[4]{(3 - 3\nu^2)^{3/4}}}
\end{aligned} \tag{11.1}$$

With \bar{Q} and \bar{M} at hand, their values can be easily substituted into the expressions for the dimensionless membrane forces and moments given, respectively, in equations (6.15) and (6.16) for the vessel and in equations (6.26) and (6.27) for the nozzle. These are, in turn, substituted into expressions for stresses both in the vessel (equations (6.33) and (6.34)) and in the nozzle (equations (6.35) and (6.36)) to arrive at the non-dimensional outer/inner axial and hoop stresses (membrane plus discontinuity effects) in the vessel and nozzle.

Consequently, the non-dimensional outer and inner stresses (membrane plus discontinuity effects) along the meridional and circumferential/hoop directions in the spherical vessel are obtained as follows.

$$\bar{\sigma}_{\varphi(+/-)} = \frac{RT}{2} (\bar{p} \mp 12\bar{M} \cdot rR^2 RT - 2\bar{H} \cdot rR \cdot \cos \varphi_0) \tag{11.2}$$

$$\begin{aligned}
\bar{\sigma}_{\theta(+/-)} &= \frac{RT}{2k_{01}\nu} \left[\left(k_{01} \cdot \bar{p} \cdot \nu \mp 2\bar{M} \cdot rR^2 RT \left(3(k_{01} - k_{02}) + 3(k_{01} + k_{02})\nu^2 \mp 2\nu \sqrt{3(1 - \nu^2)} \right) \right) \right. \\
&\quad \left. + \frac{1.32\bar{H} \cdot rR \cdot RT^{3/2}}{2k_{01}\nu \sqrt[4]{(1 - \nu^2)}} \left[\pm 3.46 k_{01} \nu^2 + \nu \sqrt{1 - \nu^2} (2 + k_{01}^2 + k_{01} k_{02}) \right. \right. \\
&\quad \left. \left. \mp 1.73 (k_{01} + k_{02} + (k_{01} + k_{02})\nu^2) \sin \varphi_0 \right] \right] \tag{11.3}
\end{aligned}$$

Similarly, the final expressions for the outer and inner stresses (membrane plus discontinuity effects) in non-dimensional form along the axial and hoop directions in the cylindrical nozzle are given in equations (11.4) and (11.5) as functions of the vessel-nozzle geometrical ratios.

$$\bar{\sigma}_{a(+/-)} = \frac{\bar{p}.rR.RT.tT^4 \pm 144\bar{D}_n.rR^5.RT^5(\nu^2 - 1)\bar{M}}{2tT^5} \quad (11.4)$$

$$\bar{\sigma}_{h(+/-)} = \frac{rR.RT}{tT^5} \left[\pm 72\bar{D}_n.\bar{M}.rR^4.RT^4\nu(\nu^2 - 1) + tT^3 \left(\bar{p}.tT - 2\sqrt{\frac{rR.RT}{tT}} tT\sqrt[4]{3(1 - \nu^2)}\bar{Q} + 2\bar{M}.rR.RT\sqrt{3(1 - \nu^2)} \right) \right] \quad (11.5)$$

Finally, based on equations (6.37) and (6.38), the closed-form expressions of SCF for the spherical vessel and the nozzle are given in equations (11.6) and (11.7), respectively.

$$K_v = \max \left\{ \begin{array}{l} \frac{1}{\bar{p}} (\bar{p} \mp 12\bar{M}.rR^2.RT - 2\bar{H}.rR.\cos\varphi_0) \\ \frac{1}{k_{01}\bar{p}\nu} \left[\left(k_{01}.\bar{p}.\nu \mp 2\bar{M}.rR^2.RT \left(3(k_{01} - k_{02}) + 3(k_{01} + k_{02})\nu^2 \mp 2\nu\sqrt{3(1 - \nu^2)} \right) \right) \right. \\ \left. + \frac{2.64\bar{H}.rR.\sqrt{RT}}{2k_{01}\bar{p}\nu\sqrt[4]{(1 - \nu^2)}} \left[\pm 3.46k_{01}\nu^2 + \nu\sqrt{1 - \nu^2} (2 + k_{01}^2 + k_{01}k_{02}) \right. \right. \\ \left. \left. \mp 1.73(k_{01} + k_{02})(1 + \nu^2)\sin\varphi_0 \right] \right] \end{array} \right. \quad (11.6)$$

$$K_n = \max \left\{ \begin{array}{l} \frac{\bar{p}.rR.tT^4 \pm 144\bar{D}_n.rR^5.RT^4(\nu^2 - 1)\bar{M}}{tT^5.\bar{p}} \\ \frac{2rR}{tT^5.\bar{p}} \left[\pm 72\bar{D}_n.\bar{M}.rR^4.RT^4\nu(\nu^2 - 1) + tT^3 \left(\bar{p}.tT - 2\sqrt{\frac{rR.RT}{tT}} tT^4\sqrt{3(1 - \nu^2)}\bar{Q} \right. \right. \\ \left. \left. + 2\bar{M}.rR.RT\sqrt{3(1 - \nu^2)} \right) \right] \end{array} \right. \quad (11.7)$$

11.1.1.2 Closed-Form Empirical Expressions of SCF

In order to develop more simplified closed-form formulas for the SCF and discontinuity forces and moments, parametric analysis of the stresses, edge forces and moments based on the Hetenyi's analytical method (that is proved to be sufficient in Chapter Seven) have been carried out.

The following ranges of non-dimensional parameters are selected for the study.

$$RT = 45 + 5i, \{i, 1, 21\}$$

$$tT = 0.25j, \{j, 1, 6\}$$

$$rR = 0.08 + 0.02k, \{k, 1, 21\}$$

where, the index $\{i, i_{min}, i_{max}\}$ signifies i runs from i_{min} to i_{max} . The same applies to the remaining two indices j and k . Hence, RT ranges between 50 and 150, tT between 0.25 and 1.5 and rR between 0.1 and 0.5 resulting into a total of 2,646 analytical experiments.

In each experiment, the SCF values for the vessel and nozzle were determined as the ratio of the maximum discontinuity stress to the nominal stress in the component.

In this study, the SCF data is 3-D (i.e. functions of rR , RT and tT). Consequently, a preliminary work has been carried out to study different trial functions for each of the 1-

D trend lines. This is done by fixing all but one of the independent variables constant for each of rR , RT and tT in turn. The study found out that \bar{Q} , \bar{M} , SCF_V and SCF_N are proportional to both rR and RT raised to some powers. Typical plots for SCF_V and SCF_N are shown in Figure 11-1 generated based on the single-term polynomial of the form $y = c_1 x_1^{c_2} x_2^{c_3}$. Where, $x_1 = rR$, $x_2 = RT$ and $x_3 = tT$, y stands for \bar{Q} , \bar{M} , SCF_V or SCF_N and c_1 , c_2 and c_3 are unknown constants to be determined in order to provide the best fit for the generated data points. The proposed 2-D fitting was found to be very sufficient at discrete values of x_3 . The 1-D fitting for the remaining parameter tT , however, suggests a decreasing function of the form $SCF = \frac{c_1 tT^{c_2}}{c_3 + c_4 tT^{c_5}}$ for both the vessel and nozzle SCF as typically shown in Figure 11-2 for the nozzle. Going by the foregoing discussion, the 3-D fitting $y = c_0 + \frac{c_1 + c_2 x_1^{c_3} x_2^{c_4} x_3^{c_5}}{c_6 + c_7 x_3^{c_8}}$ for SCF data of both the vessel and nozzle is proposed. Interestingly, this overall best-fit correlation expression seems to be in form of product of the best-fit 1-D analytical trend lines. Finally, the unknown constants are determined by the method of least squares.

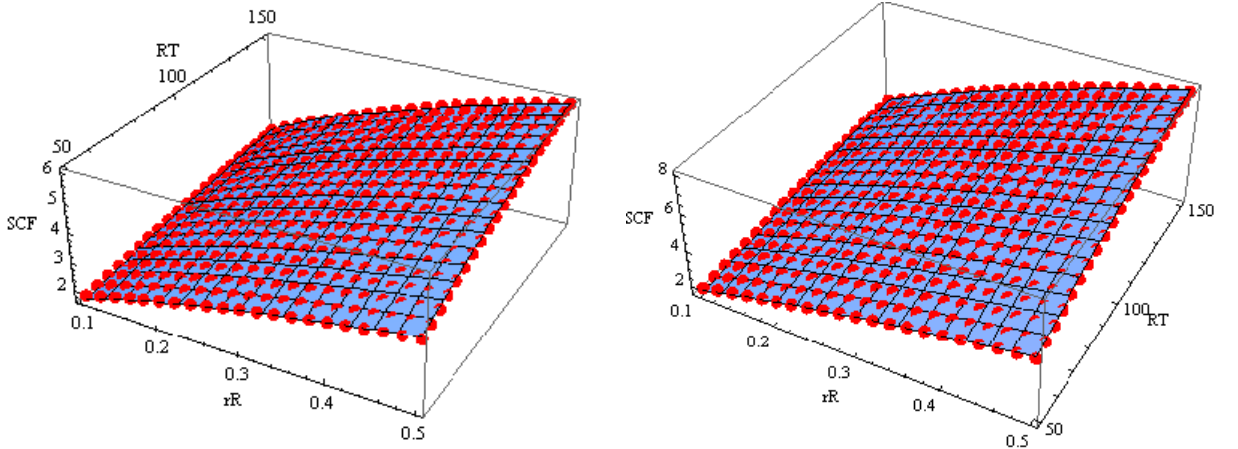


Figure 11- 1: Typical Variation of SCF with rR and RT for $tT = 1.25$ and the Corresponding 2-D Fit for the (a) Vessel, and (b) Nozzle

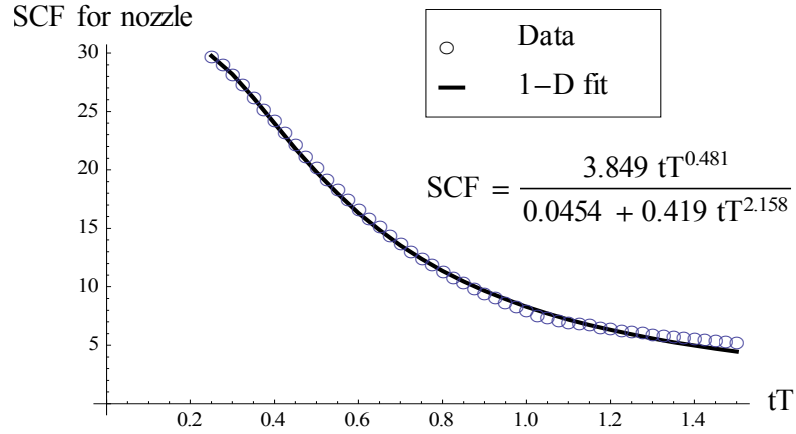


Figure 11- 2: Typical 1-D Fitting of the SCF in the Nozzle for $rR = 0.5$ and $RT = 150$

Results of the estimated values of the constants are flogged back in to the correlation equations to give the final models of the edge forces and moments, and the vessel's and nozzle's SCF as shown in Table 11-1 for the 2-parameter models. The benefit of having such expression for \bar{Q} and \bar{M} is for use in instances when other variables need to be studied in addition to the SCF. For example, the stresses and displacements for both the vessel and the nozzle are functions of \bar{Q} and \bar{M} . Hence, having their closed-form expressions will aid in faster computation of any other variable that depends on them.

Because SCF prediction is the main objective of the present study, the subsequent discussion will focus more on the SCF analysis, apart from the validation of the 2-parameter models of \bar{Q} and \bar{M} . Consequently, the 3-parameter models are constructed for the SCF only in accordance with the approach explained earlier. These models are given in equations (11.8) and (11.9) for the vessel and nozzle, respectively. Similar method can be used to arrive at 3-parameter expressions for \bar{Q} and \bar{M} . A good correlation exists between these developed models and the original data, giving rise to R^2 values of 0.991 and 0.998 for equations (11.8) and (11.9), respectively.

$$SCF_V = 0.44 + \frac{0.138 + 115 r R^{0.7} R T^{0.43} t T^{4.17}}{78.23 t T^{4.48}} \quad (11.8)$$

$$SCF_N = 0.656 + \frac{0.09 + 87.273 r R^{0.665} R T^{0.533} t T^{4.241}}{0.037 + 103.05 t T^{5.646}} \quad (11.9)$$

Table 11- 1: 2-Parameter Models for the Discontinuity Forces, Moments and SCF for Spherical Vessel-Cylindrical Nozzle Intersection

tT	\bar{Q}	\bar{M}	SCF_V	SCF_N
0.25	$0.071 r R^{-0.918} R T^{-0.03}$	$0.018 r R^{-1.415} R T^{-0.504}$	$3.3 r R^{0.6} R T^{0.36}$	$3.59 r R^{0.58} R T^{0.5}$
0.5	$0.185 r R^{-0.89} R T^{-0.05}$	$0.061 r R^{-1.33} R T^{-0.524}$	$2.37 r R^{0.6} R T^{0.37}$	$2.94 r R^{0.63} R T^{0.48}$
0.75	$0.252 r R^{-0.905} R T^{-0.073}$	$0.088 r R^{-1.263} R T^{-0.52}$	$1.84 r R^{0.6} R T^{0.39}$	$1.97 r R^{0.69} R T^{0.47}$
1.0	$0.296 r R^{-0.94} R T^{-0.09}$	$0.096 r R^{-1.214} R T^{-0.507}$	$1.44 r R^{0.6} R T^{0.42}$	$1.48 r R^{0.59} R T^{0.41}$
1.25	$0.331 r R^{-0.977} R T^{-0.103}$	$0.093 r R^{-1.178} R T^{-0.491}$	$1.39 r R^{0.68} R T^{0.45}$	$1.28 r R^{0.54} R T^{0.39}$
1.5	$0.363 r R^{-1.009} R T^{-0.111}$	$0.084 r R^{-1.149} R T^{-0.472}$	$1.36 r R^{0.7} R T^{0.45}$	$1.1 r R^{0.51} R T^{0.38}$

Figure 11-3 shows typical surface plots for Q and M based on the developed 2-parameter models for $tT = 0.75$. Shown in dots are the generated data points computed using the actual Hetenyi's analytical solution. Excellent agreement is evident between the proposed simplified equations and the actual predictions. Table 11-2 shows results of the SCF predicted by the proposed formulas validated against the actual analytical predictions from which they are derived. Acceptable percentage deviations, as indicated alongside the SCF values, are achieved for both the 2-parameter and 3-parameter models. The relatively higher deviation in the 3-parameter model results due to the increase in independent variables present in comparison to the 2-parameter model; total error

increases with increase in the parameters involved due to contributions from the individual errors.

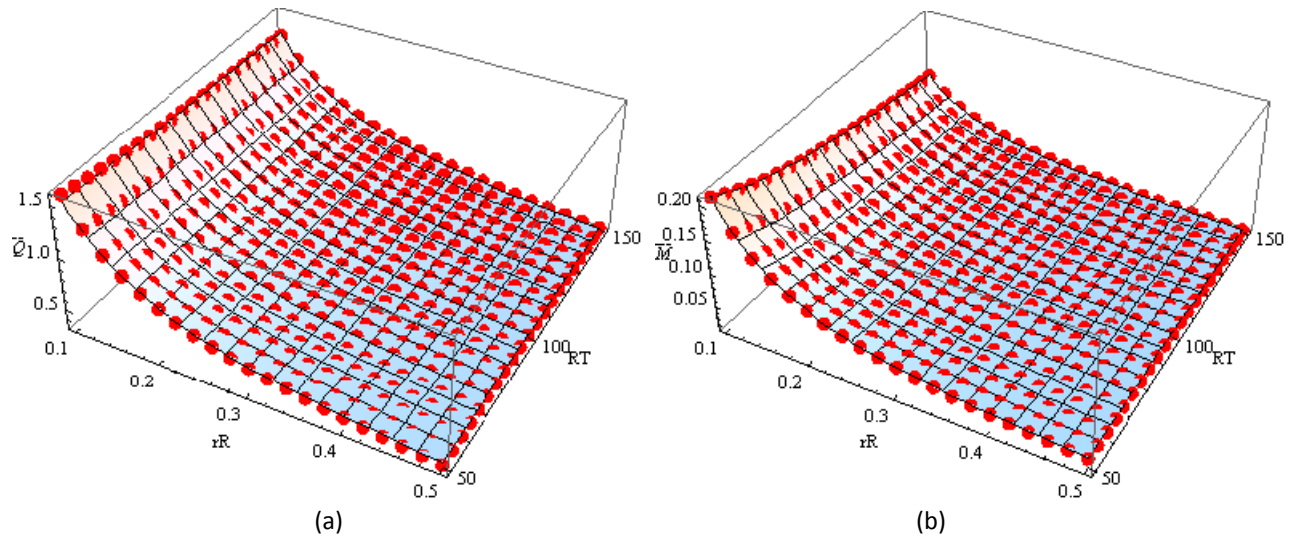


Figure 11- 3: Comparison between Predictions by the Actual Analytical Solution and the Proposed Models for (a) Q , and (b) M

Table 11- 2: Predictions of SCF by the Simplified Models for Spherical Vessels with Moderate-to-Large-Diameter Nozzles

RT	tT	rR	Spherical Vessel					Cylindrical Nozzle				
			Analy.	3-Para Model: Equation (11.8)	Deviation (% FEM)	2-Para Model: (Table 11-1)	Deviation (% FEM)	Analy.	3-Para Model: Equation (11.9)	Deviation (% FEM)	2-Para Model: (Table 11-1)	Deviation (% FEM)
50	0.25	0.1	3.71	3.74	0.9	3.39	-8.6	6.87	6.59	-4.1	6.68	-2.8
		0.2	5.28	5.26	-0.5	5.14	-2.8	10.38	9.39	-9.6	9.98	-3.8
		0.3	6.64	6.55	-1.3	6.55	-1.3	13.14	11.73	-10.7	12.63	-3.9
		0.4	7.78	7.72	-0.8	7.79	0.1	15.25	13.82	-9.4	14.92	-2.2
		0.5	8.68	8.80	1.4	8.90	2.6	16.69	15.75	-5.6	16.98	1.8
	0.5	0.2	3.94	3.66	-7.3	3.84	-2.7	6.89	6.04	-12.3	6.97	1.2
		0.3	4.99	4.70	-5.9	4.89	-2.0	8.99	7.69	-14.4	9.00	0.1
		0.4	5.86	5.64	-3.8	5.82	-0.8	10.64	9.17	-13.8	10.79	1.4
		0.5	6.54	6.51	-0.4	6.65	1.7	11.83	10.52	-11.0	12.42	5.0
	0.75	0.2	3.26	3.25	-0.5	3.22	-1.3	4.05	3.73	-7.9	4.08	0.7
		0.3	4.14	4.17	0.6	4.11	-0.8	5.44	4.68	-13.9	5.40	-0.8
		0.4	4.86	5.00	2.7	4.88	0.4	6.56	5.53	-15.7	6.58	0.4
		0.5	5.42	5.77	6.4	5.58	3.0	7.39	6.31	-14.6	7.68	3.9
	1	0.3	3.69	3.84	4.3	3.62	-1.9	3.70	3.34	-9.6	3.62	-2.2
		0.4	4.33	4.60	6.4	4.30	-0.7	4.33	3.91	-9.6	4.29	-0.9
		0.5	4.82	5.31	10.1	4.91	1.9	4.81	4.43	-7.8	4.89	1.7
	1.25	0.3	3.55	3.62	1.8	3.56	0.4	3.05	2.62	-14.2	3.07	0.6
		0.4	4.29	4.32	0.8	4.33	1.0	3.54	3.04	-14.2	3.59	1.4
		0.5	4.87	4.98	2.3	5.04	3.6	3.91	3.42	-12.6	4.05	3.5
	1.5	0.4	4.18	4.11	-1.6	4.16	-0.4	3.03	2.50	-17.5	3.05	0.7
		0.5	4.76	4.73	-0.5	4.87	2.4	3.33	2.79	-16.1	3.42	2.6

Table 11- 3 (Cont'd): Predictions of SCF by the Simplified Models for Spherical Vessels with Moderate-to-Large-Diameter Nozzles

RT	tT	rR	Spherical Vessel					Cylindrical Nozzle				
			Analy.	3-Para Model: Equation (11.8)	Deviation (% FEM)	2-Para Model: (Table 11-1)	Deviation (% FEM)	Analy.	3-Para Model: Equation (11.9)	Deviation (% FEM)	2-Para Model: (Table 11-1)	Deviation (% FEM)
100	0.25	0.1	4.40	4.58	4.3	4.35	-1.0	9.35	8.57	-8.4	9.44	1.0
		0.2	6.53	6.62	1.5	6.59	1.0	14.50	12.53	-13.6	14.12	-2.7
		0.3	8.39	8.36	-0.3	8.41	0.2	18.59	15.84	-14.8	17.86	-3.9
		0.4	9.98	9.94	-0.5	9.99	0.1	21.76	18.80	-13.6	21.10	-3.0
		0.5	11.24	11.39	1.4	11.43	1.7	23.97	21.52	-10.2	24.02	0.2
	0.5	0.1	3.28	3.11	-5.0	3.27	-0.2	5.77	5.46	-5.4	6.29	8.9
		0.2	4.96	4.76	-4.0	4.96	0.1	9.49	8.25	-13.0	9.73	2.5
		0.3	6.38	6.16	-3.4	6.32	-0.9	12.46	10.59	-15.0	12.56	0.8
		0.4	7.57	7.43	-1.9	7.52	-0.8	14.80	12.68	-14.3	15.05	1.7
		0.5	8.50	8.61	1.3	8.59	1.1	16.47	14.59	-11.4	17.33	5.2
	0.75	0.1	2.75	2.77	0.8	2.78	1.3	3.23	3.40	5.3	3.50	8.5
		0.2	4.17	4.22	1.2	4.22	1.2	5.57	5.00	-10.2	5.65	1.5
		0.3	5.36	5.46	1.8	5.38	0.4	7.50	6.35	-15.3	7.48	-0.3
		0.4	6.35	6.58	3.6	6.40	0.8	9.04	7.55	-16.6	9.12	0.8
		0.5	7.10	7.61	7.3	7.31	3.0	10.19	8.65	-15.1	10.64	4.4
	1	0.2	3.76	3.89	3.6	3.79	0.9	3.78	3.56	-5.7	3.78	0.2
		0.3	4.82	5.03	4.2	4.84	0.3	4.82	4.46	-7.5	4.81	-0.3
		0.4	5.77	6.05	4.8	5.75	-0.4	5.68	5.26	-7.4	5.69	0.2
		0.5	6.52	7.00	7.3	6.57	0.8	6.46	6.00	-7.1	6.50	0.6
	1.25	0.2	3.58	3.66	2.4	3.70	3.3	3.14	2.78	-11.6	3.23	2.9

Table 11- 4 (Cont'd): Predictions of SCF by the Simplified Models for Spherical Vessels with Moderate-to-Large-Diameter Nozzles

RT	tT	rR	Spherical Vessel					Cylindrical Nozzle				
			Analy.	3-Para Model: Equation (11.8)	Deviation (% FEM)	2-Para Model: (Table 11-1)	Deviation (% FEM)	Analy.	3-Para Model: Equation (11.9)	Deviation (% FEM)	2-Para Model: (Table 11-1)	Deviation (% FEM)
100	1.25	0.3	4.82	4.72	-2.2	4.87	0.9	3.96	3.44	-13.2	4.03	1.7
		0.4	5.85	5.67	-3.1	5.92	1.2	4.62	4.02	-13.0	4.70	1.7
		0.5	6.64	6.56	-1.3	6.89	3.7	5.13	4.56	-11.1	5.30	3.5
	1.5	0.2	3.46	3.48	0.6	3.50	1.1	2.73	2.30	-15.9	2.79	1.9
		0.3	4.69	4.48	-4.3	4.65	-0.8	3.40	2.81	-17.4	3.43	0.8
		0.4	5.71	5.39	-5.6	5.69	-0.3	3.94	3.26	-17.3	3.97	0.6
		0.5	6.49	6.22	-4.2	6.65	2.4	4.35	3.68	-15.4	4.44	2.3
150	0.25	0.1	4.91	5.21	6.1	5.03	2.6	11.27	10.09	-10.5	11.56	2.6
		0.2	7.47	7.63	2.2	7.63	2.1	17.67	14.93	-15.5	17.29	-2.2
		0.3	9.74	9.71	-0.3	9.73	-0.1	22.77	19.00	-16.6	21.87	-4.0
		0.4	11.68	11.58	-0.9	11.56	-1.0	26.76	22.62	-15.5	25.84	-3.4
		0.5	13.21	13.31	0.8	13.22	0.1	29.57	25.95	-12.2	29.41	-0.5
	0.5	0.1	3.71	3.62	-2.6	3.80	2.4	6.94	6.53	-5.8	7.64	10.1
		0.2	5.72	5.57	-2.6	5.76	0.7	11.49	9.95	-13.4	11.82	2.9
		0.3	7.45	7.25	-2.7	7.35	-1.3	15.13	12.82	-15.3	15.26	0.8
		0.4	8.89	8.76	-1.5	8.73	-1.7	17.99	15.37	-14.6	18.29	1.7
		0.5	10.00	10.15	1.5	9.98	-0.2	20.04	17.72	-11.6	21.05	5.0
	0.75	0.1	3.15	3.21	2.0	3.26	3.6	3.88	4.01	3.4	4.24	9.1
		0.2	4.86	4.94	1.7	4.94	1.8	6.74	5.98	-11.2	6.84	1.5
		0.3	6.30	6.41	1.8	6.31	0.1	9.08	7.63	-16.0	9.05	-0.3
		0.4	7.48	7.74	3.5	7.49	0.1	10.95	9.09	-17.0	11.03	0.7
		0.5	8.39	8.98	7.1	8.57	2.2	12.33	10.44	-15.3	12.87	4.4

Table 11- 5 (Cont'd): Predictions of SCF by the Simplified Models for Spherical Vessels with Moderate-to-Large-Diameter Nozzles

RT	tT	rR	Spherical Vessel					Cylindrical Nozzle				
			Analy.	3-Para Model: Equation (11.8)	Deviation (% FEM)	2-Para Model: (Table 11-1)	Deviation (% FEM)	Analy.	3-Para Model: Equation (11.9)	Deviation (% FEM)	2-Para Model: (Table 11-1)	Deviation (% FEM)
150	1	0.1	2.86	2.97	3.7	2.97	3.6	2.92	2.90	-0.6	2.97	1.7
		0.2	4.40	4.55	3.4	4.50	2.2	4.41	4.21	-4.4	4.47	1.3
		0.3	5.76	5.90	2.5	5.74	-0.4	5.68	5.31	-6.5	5.67	-0.1
		0.4	6.96	7.12	2.3	6.82	-2.0	6.86	6.29	-8.2	6.72	-2.0
		0.5	7.86	8.25	4.9	7.79	-0.8	7.79	7.20	-7.7	7.67	-1.6
	1.25	0.1	2.67	2.80	4.8	2.77	3.6	2.49	2.30	-7.6	2.61	4.8
		0.2	4.29	4.28	-0.3	4.44	3.5	3.66	3.26	-11.0	3.79	3.6
		0.3	5.81	5.53	-4.7	5.84	0.7	4.65	4.06	-12.6	4.72	1.5
		0.4	7.06	6.67	-5.5	7.11	0.7	5.45	4.78	-12.4	5.51	1.0
		0.5	8.01	7.72	-3.5	8.27	3.3	6.06	5.44	-10.3	6.21	2.5
	1.5	0.2	4.15	4.06	-2.2	4.20	1.2	3.17	2.67	-15.9	3.25	2.4
		0.3	5.65	5.25	-6.9	5.58	-1.1	3.99	3.29	-17.4	4.00	0.3
		0.4	6.88	6.33	-8.1	6.83	-0.8	4.64	3.85	-17.1	4.63	-0.3
		0.5	7.83	7.32	-6.5	7.98	1.9	5.13	4.36	-15.0	5.19	1.1

11.1.2 Spherical Vessels with Small-Diameter Nozzles

Result of the parametric analysis carried out in Chapter Nine for spherical vessels with small-diameter nozzles are used to obtain the simplified formulas given in equations (11.10) and (11.11) for the vessel and nozzle, respectively. It is decided to adopt the 3-parameter model approach based on its accuracy and more convenience than having different 2-parameter models for different tT ratios. All the 335 data points generated in the mentioned chapter are used in arriving at these compact models with values of R^2 equal to 0.869 and 0.991 for equations (11.10) and (11.11), respectively. Results predicted by these models are shown in Table 11-3 for $RT = 50i$, $\{i, 1, 3\}$.

$$SCF_V = 6.105 + \frac{-3.37 + 1.87 \sqrt{\frac{rR}{tT}} RT^{0.052}}{0.266 + 0.417 tT^{0.05}} \quad (11.10)$$

$$SCF_N = 1.094 + \frac{0.006 + 1920 rR^{2.6} RT^{0.69} tT^{3.06}}{0.027 + 50 tT^{4.62}} \quad (11.11)$$

Table 11- 6: Predictions of SCF by the Simplified Models for Spherical Vessels with Small-Diameter Nozzles

RT	tT	rR	Spherical Vessel SCF			Cylindrical Nozzle SCF		
			FEM	Model Equation (11.10)	Deviation (%)	FEM	Model Equation (11.11)	Deviation (%)
50	0.25	0.005	1.46	1.46	-0.4	1.14	1.15	1.5
		0.05	2.39	2.53	5.6	2.81	2.70	-3.9
	0.5	0.01	1.60	1.55	-3.1	1.10	1.11	0.9
		0.05	1.89	2.15	13.4	1.77	1.79	0.7
	0.75	0.015	1.67	1.61	-3.7	1.09	1.11	2.1
		0.05	1.85	2.00	8.3	1.32	1.46	10.8
	1	0.02	1.71	1.65	-4.0	1.11	1.12	0.5
		0.05	1.86	1.92	3.1	1.31	1.33	1.9
	1.25	0.025	1.75	1.68	-4.3	1.15	1.12	-2.1

Table 11- 7 (Cont'd): Predictions of SCF by the Simplified Models for Spherical Vessels with Small-Diameter Nozzles

RT	tT	rR	Spherical Vessel SCF			Cylindrical Nozzle SCF		
			FEM	Model Equation (11.10)	Deviation (%)	FEM	Model Equation (11.11)	Deviation (%)
50	1.25	0.05	1.87	1.87	0.2	1.29	1.26	-2.4
	1.5	0.03	1.78	1.70	-4.4	1.18	1.13	-4.3
		0.05	1.86	1.84	-1.5	1.27	1.22	-4.3
100	0.25	0.003	1.33	1.32	-0.4	1.14	1.15	1.2
		0.05	2.72	2.58	-5.2	3.63	3.65	0.4
	0.5	0.005	1.41	1.42	1.1	1.08	1.10	1.6
		0.05	2.20	2.19	-0.4	2.27	2.21	-2.8
	0.75	0.008	1.45	1.48	1.7	1.07	1.10	2.5
		0.05	1.94	2.03	5.1	1.62	1.69	4.7
	1	0.01	1.48	1.52	2.3	1.09	1.10	0.6
		0.05	1.79	1.95	9.0	1.44	1.48	2.8
	1.25	0.013	1.51	1.55	2.6	1.13	1.10	-2.5
		0.05	1.77	1.90	6.8	1.42	1.36	-4.3
	1.5	0.015	1.53	1.58	3.2	1.16	1.10	-5.1
		0.05	1.76	1.86	5.9	1.40	1.30	-7.3
150	0.25	0.002	1.27	1.26	-0.5	1.13	1.15	1.3
		0.05	2.93	2.62	-10.7	4.30	4.46	3.6
	0.5	0.003	1.32	1.36	3.0	1.08	1.10	2.1
		0.05	2.40	2.21	-7.6	2.61	2.57	-1.5
	0.75	0.005	1.36	1.42	4.6	1.07	1.10	2.9
		0.05	2.14	2.05	-3.9	1.85	1.88	1.7
	1	0.007	1.39	1.46	5.5	1.09	1.10	0.6
		0.05	1.98	1.97	-0.9	1.52	1.60	5.0
	1.25	0.008	1.40	1.49	6.3	1.13	1.10	-2.8
		0.05	1.86	1.91	2.5	1.52	1.45	-4.3
	1.5	0.01	1.42	1.52	7.2	1.16	1.10	-5.3
		0.05	1.77	1.87	5.8	1.49	1.36	-8.5

11.2 CYLINDRICAL VESSELS

11.2.1 Cylindrical Vessels with Moderate-To-Large-Diameter Nozzles

Empirical Expressions of SCF

The outcome of fitting the 1526 data points generated by the numerical analysis of cylindrical vessels with moderate-to-large-diameter nozzles presented in Chapter Eight result in equations (11.12) and (11.13) for the main vessel and nozzle, respectively. Relatively, high R^2 values are obtained for the fittings: 0.993 and 0.999 for equations (11.12) and (11.13), respectively. Interestingly, a common radical applies to RT in both the two equations. This behavior agrees with that of presenting SCF in terms of the single parameter ρ (function of the same radical as observed here).

$$SCF_V = 1.4 + \frac{1.15 + 1.99rR^{1.05}tT^{-0.36}\sqrt{RT}}{0.064 + 1.52tT^{0.095}} \quad (11.12)$$

$$SCF_N = 0.58 + \frac{0.045 + 4248rR^{0.81}tT^{5.77}\sqrt{RT}}{0.0992 + 3050tT^{7.07}} \quad (11.13)$$

Performance of the above expressions, relative to the data from which they are derived, is illustrated in Table 11-4 for $RT = 50i$, $\{i, 1, 3\}$. Percentage deviations for both the vessel and nozzle SCF expressions are also indicated.

Table 11- 8: Predictions of SCF by the Simplified Models for Cylindrical Vessels with Moderate-to-Large-Diameter Nozzles

RT	tT	rR	Cylindrical Vessel SCF			Cylindrical Nozzle SCF		
			FEM	Model Equation (11.12)	Deviation (%)	FEM	Model Equation (11.13)	Deviation (%)
50	0.25	0.1	3.61	3.70	2.7	6.13	6.57	7.2
		0.2	5.54	5.29	-4.5	10.74	10.96	2.1
		0.3	7.34	6.91	-5.8	14.92	14.93	0.1
		0.4	9.03	8.57	-5.2	18.65	18.66	0.0
		0.5	10.48	10.24	-2.3	21.61	22.21	2.7
		0.6	12.07	11.93	-1.1	24.81	25.62	3.3
		0.7	13.73	13.64	-0.6	27.98	28.93	3.4
		0.8	15.25	15.35	0.7	30.93	32.15	3.9
		0.9	17.14	17.08	-0.3	34.40	35.29	2.6
		1	19.11	18.82	-1.5	36.31	38.37	5.7
	0.5	0.1	2.91	3.26	11.7	3.83	4.32	12.7
		0.2	4.40	4.41	0.4	6.90	7.14	3.5
		0.3	5.76	5.60	-2.7	9.72	9.69	-0.3
		0.4	7.05	6.81	-3.4	12.19	12.08	-0.9
		0.5	8.10	8.04	-0.7	14.11	14.35	1.7
		0.6	9.29	9.28	-0.2	16.28	16.55	1.6
		0.7	10.53	10.52	-0.1	18.44	18.67	1.2
		0.8	11.63	11.78	1.3	20.27	20.73	2.3
		0.9	13.04	13.05	0.1	22.36	22.75	1.7
		1	14.66	14.32	-2.4	23.41	24.73	5.6
	0.75	0.2	3.74	4.01	7.2	4.28	4.47	4.4
		0.3	4.87	5.00	2.8	5.78	5.98	3.3
		0.4	5.93	6.01	1.4	7.33	7.39	0.9
		0.5	6.77	7.03	3.8	8.54	8.74	2.4
		0.6	7.74	8.06	4.2	9.91	10.04	1.3
		0.7	8.75	9.10	4.0	11.29	11.30	0.1
		0.8	9.63	10.15	5.4	12.46	12.53	0.5
		0.9	10.79	11.20	3.8	13.82	13.72	-0.7
		1	12.14	12.26	1.0	14.45	14.89	3.0
	1	0.2	3.35	3.77	12.5	3.37	3.25	-3.6
		0.3	4.33	4.64	7.1	4.33	4.29	-0.9
		0.4	5.27	5.52	4.8	5.27	5.27	-0.1
		0.5	6.00	6.42	7.0	6.01	6.20	3.2
		0.6	6.84	7.32	7.0	6.86	7.09	3.4
		0.7	7.73	8.23	6.5	7.75	7.96	2.6

Table 11- 9 (Cont'd): Predictions of SCF by the Simplified Models for Cylindrical Vessels with Moderate-to-Large-Diameter Nozzles

RT	tT	rR	Cylindrical Vessel SCF			Cylindrical Nozzle SCF		
			FEM	Model Equation (11.12)	Deviation (%)	FEM	Model Equation (11.13)	Deviation (%)
50	1	0.8	8.49	9.15	7.8	8.51	8.80	3.4
		0.9	9.50	10.08	6.1	9.51	9.62	1.2
		1	10.62	11.01	3.7	10.62	10.43	-1.8
	1.25	0.3	3.93	4.38	11.4	3.56	3.36	-5.8
		0.4	4.78	5.18	8.4	4.32	4.09	-5.4
		0.5	5.43	5.99	10.3	4.91	4.78	-2.5
		0.6	6.27	6.81	8.5	5.59	5.45	-2.5
		0.7	7.17	7.63	6.5	6.31	6.10	-3.3
		0.8	7.94	8.47	6.6	6.90	6.73	-2.5
		0.9	8.82	9.30	5.5	7.70	7.35	-4.6
		1	9.52	10.14	6.5	8.57	7.95	-7.2
		0.3	3.59	4.19	16.7	3.04	2.77	-8.7
		0.4	4.41	4.93	11.8	3.68	3.35	-9.0
		0.5	5.13	5.67	10.5	4.17	3.90	-6.5
		0.6	5.98	6.43	7.5	4.74	4.42	-6.7
		0.7	6.85	7.19	4.9	5.34	4.93	-7.7
		0.8	7.60	7.95	4.6	5.84	5.43	-7.0
		0.9	8.45	8.72	3.2	6.50	5.92	-8.9
		1	8.81	9.50	7.9	7.19	6.39	-11.0
100	0.25	0.1	4.51	4.32	-4.2	8.94	8.99	0.5
		0.2	7.10	6.56	-7.7	15.65	15.19	-2.9
		0.3	9.45	8.85	-6.4	21.36	20.81	-2.6
		0.4	11.68	11.19	-4.1	26.27	26.08	-0.7
		0.5	13.66	13.56	-0.7	30.60	31.09	1.6
		0.6	15.90	15.95	0.3	35.37	35.92	1.6
		0.7	18.21	18.36	0.9	39.80	40.60	2.0
		0.8	20.45	20.79	1.7	44.89	45.15	0.6
		0.9	23.01	23.24	1.0	48.76	49.60	1.7
		1	26.38	25.70	-2.6	53.91	53.95	0.1
	0.5	0.1	3.64	3.70	1.6	5.64	5.87	4.0
		0.2	5.61	5.34	-4.7	10.06	9.85	-2.0
		0.3	7.38	7.02	-4.8	13.76	13.46	-2.2
		0.4	9.06	8.74	-3.6	17.09	16.84	-1.5
		0.5	10.49	10.47	-0.2	19.88	20.06	0.9
		0.6	12.10	12.22	1.0	22.89	23.16	1.1
		0.7	13.81	13.98	1.2	25.97	26.16	0.7

Table 11- 10 (Cont'd): Predictions of SCF by the Simplified Models for Cylindrical Vessels with Moderate-to-Large-Diameter Nozzles

RT	tT	rR	Cylindrical Vessel SCF			Cylindrical Nozzle SCF		
			FEM	Model Equation (11.12)	Deviation (%)	FEM	Model Equation (11.13)	Deviation (%)
100	0.5	0.8	15.35	15.76	2.7	28.75	29.08	1.2
		0.9	17.31	17.55	1.4	31.88	31.93	0.2
		1	19.93	19.35	-2.9	34.47	34.73	0.8
	0.75	0.1	3.16	3.42	8.1	3.65	3.71	1.7
		0.2	4.79	4.78	-0.2	5.90	6.08	2.9
		0.3	6.26	6.19	-1.2	8.17	8.21	0.5
		0.4	7.65	7.61	-0.5	10.24	10.22	-0.3
		0.5	8.79	9.05	3.0	11.98	12.12	1.2
		0.6	10.10	10.51	4.0	13.92	13.96	0.3
		0.7	11.50	11.98	4.2	15.92	15.74	-1.1
		0.8	12.73	13.46	5.8	17.70	17.47	-1.3
		0.9	14.33	14.95	4.3	19.74	19.16	-2.9
		1	16.46	16.45	-0.1	21.16	20.82	-1.6
	1	0.1	2.87	3.25	13.2	2.94	2.74	-6.8
		0.2	4.32	4.44	3.0	4.34	4.36	0.6
		0.3	5.62	5.67	1.1	5.63	5.83	3.5
		0.4	6.85	6.93	1.1	6.87	7.21	4.9
		0.5	7.84	8.19	4.5	7.86	8.52	8.5
		0.6	8.99	9.47	5.3	9.01	9.79	8.6
		0.7	10.22	10.76	5.4	10.23	11.01	7.7
		0.8	11.29	12.07	6.9	11.29	12.20	8.1
		0.9	12.68	13.37	5.5	12.68	13.37	5.4
		1	14.47	14.69	1.5	14.46	14.51	0.3
	1.25	0.2	3.96	4.21	6.3	3.60	3.41	-5.3
		0.3	5.14	5.32	3.4	4.64	4.51	-2.8
		0.4	6.44	6.45	0.1	5.63	5.54	-1.6
		0.5	7.57	7.60	0.4	6.41	6.52	1.8
		0.6	8.85	8.76	-1.1	7.32	7.47	2.0
		0.7	10.20	9.92	-2.7	8.28	8.39	1.3
		0.8	11.40	11.10	-2.7	9.11	9.28	1.9
		0.9	12.78	12.28	-3.9	10.20	10.15	-0.6
		1	13.56	13.47	-0.7	11.60	11.00	-5.2
	1.5	0.2	3.65	4.03	10.4	3.10	2.81	-9.2
		0.3	4.90	5.06	3.1	3.98	3.68	-7.5
		0.4	6.16	6.10	-1.0	4.82	4.49	-6.7
		0.5	7.26	7.15	-1.4	5.46	5.27	-3.5

Table 11- 11 (Cont'd): Predictions of SCF by the Simplified Models for Cylindrical Vessels with Moderate-to-Large-Diameter Nozzles

RT	tT	rR	Cylindrical Vessel SCF			Cylindrical Nozzle SCF		
			FEM	Model Equation (11.12)	Deviation (%)	FEM	Model Equation (11.13)	Deviation (%)
100	1.5	0.6	8.53	8.22	-3.6	6.22	6.02	-3.3
		0.7	9.86	9.29	-5.8	7.02	6.74	-4.0
		0.8	11.06	10.38	-6.2	7.70	7.44	-3.3
		0.9	12.42	11.47	-7.7	8.61	8.13	-5.5
		1	13.15	12.56	-4.5	9.74	8.80	-9.6
150	0.25	0.1	5.16	4.79	-7.3	11.13	10.84	-2.6
		0.2	8.20	7.53	-8.2	19.24	18.44	-4.2
		0.3	10.92	10.34	-5.3	25.77	25.32	-1.7
		0.4	13.62	13.21	-3.0	31.96	31.77	-0.6
		0.5	15.99	16.11	0.7	37.04	37.91	2.3
		0.6	18.71	19.04	1.8	43.12	43.83	1.7
		0.7	21.54	21.99	2.1	48.55	49.56	2.1
		0.8	24.37	24.97	2.5	54.75	55.13	0.7
		0.9	27.52	27.96	1.6	60.79	60.58	-0.4
		1	31.82	30.97	-2.7	67.33	65.91	-2.1
	0.5	0.1	4.16	4.05	-2.8	7.04	7.06	0.3
		0.2	6.47	6.05	-6.5	12.32	11.94	-3.1
		0.3	8.55	8.11	-5.1	16.67	16.35	-1.9
		0.4	10.55	10.21	-3.2	20.69	20.49	-0.9
		0.5	12.28	12.33	0.4	24.16	24.43	1.1
		0.6	14.23	14.48	1.7	27.84	28.23	1.4
		0.7	16.28	16.64	2.2	31.59	31.91	1.0
		0.8	18.22	18.81	3.2	35.28	35.49	0.6
		0.9	20.57	21.00	2.1	39.21	38.98	-0.6
		1	23.88	23.21	-2.8	42.90	42.40	-1.2
	0.75	0.1	3.63	3.71	2.1	4.20	4.42	5.2
		0.2	5.56	5.38	-3.2	7.21	7.31	1.4
		0.3	7.28	7.09	-2.6	9.88	9.93	0.5
		0.4	8.93	8.84	-1.1	12.40	12.38	-0.1
		0.5	10.32	10.61	2.8	14.55	14.72	1.2
		0.6	11.91	12.39	4.1	16.93	16.97	0.2
		0.7	13.59	14.19	4.4	19.39	19.15	-1.2
		0.8	15.10	16.00	6.0	21.63	21.27	-1.7
		0.9	17.02	17.83	4.8	24.16	23.34	-3.4
		1	19.73	19.66	-0.3	26.32	25.37	-3.6
	1	0.1	3.31	3.50	5.7	3.36	3.22	-4.1

Table 11- 12 (Cont'd): Predictions of SCF by the Simplified Models for Cylindrical Vessels with Moderate-to-Large-Diameter Nozzles

RT	tT	rR	Cylindrical Vessel SCF			Cylindrical Nozzle SCF		
			FEM	Model Equation (11.12)	Deviation (%)	FEM	Model Equation (11.13)	Deviation (%)
150	1	0.2	5.03	4.97	-1.2	5.05	5.21	3.3
		0.3	6.56	6.47	-1.4	6.58	7.01	6.5
		0.4	8.03	8.01	-0.3	8.05	8.70	8.1
		0.5	9.24	9.56	3.5	9.25	10.31	11.4
		0.6	10.68	11.13	4.1	10.65	11.86	11.4
		0.7	12.28	12.71	3.5	12.19	13.36	9.6
		0.8	13.75	14.30	4.0	13.69	14.82	8.2
		0.9	15.37	15.90	3.5	15.33	16.24	5.9
		1	17.37	17.51	0.8	17.36	17.64	1.6
	1.25	0.1	3.06	3.35	9.7	2.83	2.56	-9.8
		0.2	4.63	4.68	1.1	4.19	4.05	-3.4
		0.3	6.18	6.04	-2.2	5.42	5.39	-0.5
		0.4	7.79	7.43	-4.6	6.59	6.66	1.0
		0.5	9.19	8.83	-3.9	7.53	7.86	4.4
		0.6	10.80	10.25	-5.1	8.62	9.02	4.6
		0.7	12.48	11.68	-6.4	9.77	10.14	3.8
		0.8	14.03	13.12	-6.5	10.80	11.23	4.0
		0.9	15.72	14.57	-7.3	12.10	12.30	1.6
		1	16.88	16.02	-5.1	13.89	13.34	-3.9
	1.5	0.1	2.83	3.24	14.4	2.46	2.14	-13.2
		0.2	4.31	4.46	3.5	3.61	3.31	-8.3
		0.3	5.91	5.72	-3.2	4.66	4.38	-6.0
		0.4	7.47	7.00	-6.4	5.64	5.37	-4.8
		0.5	8.85	8.29	-6.4	6.41	6.32	-1.4
		0.6	10.45	9.59	-8.2	7.32	7.24	-1.1
		0.7	12.11	10.91	-9.9	8.27	8.12	-1.8
		0.8	13.66	12.24	-10.4	9.10	8.98	-1.3
		0.9	15.33	13.57	-11.5	10.18	9.83	-3.5
		1	16.40	14.91	-9.0	11.64	10.65	-8.5

11.2.2 Cylindrical Vessels with Small-Diameter Nozzles

For cylindrical vessels with small-diameter nozzles, 335 data points have already been generated based on the numerical experiments carried out using FEM in Chapter Ten. This result is used, in this sub-section, to fit SCF models for the main vessel and nozzle given by equations (11.15) and (11.16), respectively, by the method of least squares. Appreciable values of R^2 are obtained as 0.988 and 0.969, respectively, for the vessel and nozzle equations. The success of these fittings is illustrated in Table 11-5 for selected values of RT . The compactness achieved for the nozzle's SCF model is interesting (Equation (11.15)). In fact, of all the fitted 3-parameter models for spherical and cylindrical vessels with nozzles of any size, Equation 11.15 is the shortest and, hence, less sophisticated.

$$SCF_V = 0.377 + \frac{-0.256 + 0.296rR^{0.056}tT^{0.0044}RT^{0.057}}{0.01 + 0.04tT^{0.59}} \quad (11.14)$$

$$SCF_N = 1.41 + 6.87rR^{2.46}tT^{-1.16}RT^{0.95} \quad (11.15)$$

Table 11- 13: Predictions of SCF by the Simplified Models for Cylindrical Vessels with Small-Diameter Nozzles

RT	tT	rR	Cylindrical Vessel SCF			Cylindrical Nozzle SCF		
			FEM	Model Equation (11.14)	Deviation (%)	FEM	Model Equation (11.15)	Deviation (%)
50	0.25	0.005	1.08	1.00	-7.0	1.47	1.41	-4.1
		0.05	2.32	2.36	1.8	2.33	2.30	-1.2
	0.5	0.01	1.16	1.17	0.9	1.47	1.42	-3.5
		0.05	1.99	1.90	-4.5	1.77	1.81	2.3
	0.75	0.015	1.21	1.20	-1.1	1.44	1.42	-1.3
		0.05	1.74	1.67	-4.3	1.75	1.66	-5.0
	1	0.02	1.23	1.20	-2.5	1.44	1.43	-0.7

Table 11- 14 (Cont'd): Predictions of SCF by the Simplified Models for Cylindrical Vessels with Small-Diameter Nozzles

RT	tT	rR	Cylindrical Vessel SCF			Cylindrical Nozzle SCF		
			FEM	Model Equation (11.14)	Deviation (%)	FEM	Model Equation (11.15)	Deviation (%)
50	1	0.05	1.57	1.51	-3.5	1.71	1.59	-7.1
	1.25	0.025	1.24	1.19	-4.1	1.38	1.43	4.3
		0.05	1.43	1.40	-2.0	1.66	1.55	-6.5
	1.5	0.03	1.22	1.18	-4.0	1.45	1.44	-0.7
		0.05	1.33	1.32	-1.1	1.61	1.52	-5.7
100	0.25	0.003	1.06	1.01	-5.0	1.44	1.41	-2.0
		0.05	2.82	2.82	-0.3	3.37	3.13	-7.2
	0.5	0.005	1.16	1.17	1.5	1.54	1.41	-8.5
		0.05	2.24	2.25	0.5	2.08	2.18	4.7
	0.75	0.008	1.21	1.21	-0.7	1.43	1.41	-0.8
		0.05	1.94	1.95	0.7	1.83	1.89	3.5
	1	0.01	1.24	1.20	-2.9	1.37	1.42	3.6
		0.05	1.74	1.77	1.2	1.82	1.75	-3.8
	1.25	0.013	1.24	1.19	-4.0	1.40	1.42	1.2
		0.05	1.60	1.63	2.2	1.79	1.68	-6.5
	1.5	0.015	1.23	1.18	-4.0	1.41	1.42	0.5
		0.05	1.47	1.53	3.8	1.74	1.62	-6.8
150	0.25	0.002	1.06	1.01	-4.0	1.82	1.41	-22.5
		0.05	3.16	3.09	-2.4	4.00	3.93	-1.8
	0.5	0.003	1.16	1.18	1.9	1.37	1.41	2.7
		0.05	2.58	2.46	-4.7	2.57	2.54	-1.0
	0.75	0.005	1.21	1.21	-0.5	1.44	1.41	-2.2
		0.05	2.26	2.13	-6.0	1.88	2.12	12.3
	1	0.007	1.24	1.21	-2.7	1.38	1.41	2.4
		0.05	2.05	1.92	-6.3	1.87	1.92	2.7
	1.25	0.008	1.24	1.20	-3.6	1.39	1.41	1.6
		0.05	1.83	1.77	-3.6	1.84	1.80	-2.4
	1.5	0.01	1.23	1.18	-3.6	1.39	1.42	1.9
		0.05	1.67	1.65	-1.1	1.80	1.73	-4.4

11.3 SUMMARIZED EXPRESSIONS OF SCF FOR SPHERICAL AND CYLINDRICAL VESSELS

This sub-section is dedicated to provide a summary of the simplified closed-form expressions of SCF developed in the previous sections. However, instead of stuffing the designer with the lengthy list of such formulas, a more brief presentation would be more appealing. Interestingly, it can be recalled that all the developed SCF models for spherical and cylindrical vessels with all ranges of nozzle diameters assumes the general expression of the form given in Equation (11.16). This makes it convenient, to present a table of the unknown constants for different cases considered in this study. This is done as shown in Table 11-6.

$$SCF = c_0 + \frac{c_1 + c_2 r R^{c_3} t T^{c_4} R T^{c_5}}{c_6 + c_7 t T^{c_8}} \quad (11.16)$$

Table 11- 15: Summary of the Unknown Constants Appearing in the Simplified General Expression of SCF (Equation (11.16)) for Spherical and Cylindrical Vessels Intersected by Cylindrical Nozzles

Constant	SPHERICAL VESSEL				CYLINDRICAL VESSEL			
	Small-Dia. Nozzles		Moderate-to-Large Dia. Nozzles		Small-Dia. Nozzles		Moderate-to-Large Dia. Nozzles	
	Vessel	Nozzle	Vessel	Nozzle	Vessel	Nozzle	Vessel	Nozzle
c_0	6.105	1.094	0.44	0.656	0.377	1.41	1.4	0.58
c_1	-3.37	0.006	0.138	0.09	-0.256	0	1.15	0.045
c_2	1.87	1920	115	87.273	0.296	6.8	1.99	4248
c_3	0.5	2.6	0.7	0.665	0.0056	2.46	1.05	0.81
c_4	0.5	3.06	4.17	0.533	0.0044	-1.16	-0.36	5.77
c_5	0.052	0.69	0.43	4.241	0.057	0.95	0.5	0.5
c_6	0.266	0.027	0	0.037	0.01	0	0.064	0.0992
c_7	0.417	50	78.23	103.05	0.04	1	1.52	3050
c_8	0.05	4.62	4.48	5.646	0.59	0	0.095	7.07

CHAPTER TWELVE

CONCLUSIONS AND RECOMMENDATIONS

12.1 CONCLUSIONS

Based on the extensive analytical and numerical analyses of spherical and cylindrical pressure vessels intersected by radial nozzles carried out in this research, a comprehensive evaluation of SCF around the vessel-nozzle junctures was carried out and the following conclusions can be drawn.

1. By means of pure analytical approach, the study developed the dimensionless closed-form expressions of SCF as functions of the three key geometric ratios (R_v/T_v , T_n/T_v , and R_n/R_v) of the spherical vessel-nozzle juncture. This is an improvement over the conventional ways of deriving such expressions as either empirical or semi-empirical in nature developed by fitting experimental and/or numerical simulation results as reported in the literature.
2. Results achieved by the approximate method (Hetenyi's solution) for the spherical vessel-nozzle junctures are acceptable and conservative within the validity of thin shell assumption; conservative prediction of the maximum stress in both the nozzle and in the vessel. Since this maximum stress is the most important one in design (SCF), it can be argued that the approximate analysis entails safety.
3. Using shell theory, FEM-based numerical models are developed for both spherical and cylindrical pressure vessels and exact analytical models implemented for spherical pressure vessels intersected by moderate-to-large-diameter nozzles.

4. The limitation of the shell solution for spherical and cylindrical pressure vessels with small-diameter nozzles is addressed by the use of solid elements based on the theory of elasticity to generate the overall design curves for the mentioned vessels with nozzle diameters of any size (small to large).
5. Contrary to the use of one unique graph as adopted by many researchers, the present study has proved that the ρ -SCF plots are not unique. Limitations and incorrectness of this approach are exposed and addressed in this research. There exist significant variations in the SCF for junctions with different RT and rR values corresponding to the same ρ . Hence, alternative presentations, that are believed to be more accurate and all-encompassing, where separate charts (corresponding to different RT ratios) provide variations in SCF with the ratios tT and rR are adopted.
6. The location (either in the vessel or in the nozzle) of maximum stresses at the vessel-nozzle juncture plays a significant role in the design of such components. And, as demonstrated by the analysis carried out, the type and location of the said stresses are not always the same.
7. Knowledge of the location and type of the maximum stresses can be very vital in many instances such as in case of decision-making about the material variation for non-homogeneous vessel/nozzle material types.
8. Parametric study of the thin shell and solid solutions for the internally pressurized spherical and cylindrical vessels intersected by radial cylindrical nozzles has been used to develop simplified closed-form formulas of SCF in terms of the vessel-nozzle geometric ratios. Maximum stresses in both the vessel and in the nozzle

have been assessed and the corresponding SCF formulas reported individually. This makes it possible to arrive at a reliable prediction depending on which component has a controlling SCF. Hence, the possible mistake of concentrating on the vessels SCF alone (by wrongly assuming that its stresses are higher than those in the nozzle), as is the case with many famous literature closed-form SCF formulas, is avoided.

9. High degree of correlation exists between the simplified formulas and the actual numerical and/or numerical data from which the models are developed.
10. A large database is generated for pressurized vessel-nozzle components comprising of the SCF results for different combinations of the geometric ratios as follows:
 - i. 1,526 SCF data points for spherical vessels intersected by moderate-to-large-diameter nozzles
 - ii. 335 SCF data points for cylindrical vessels intersected by small-diameter nozzles
 - iii. 1,526 SCF data points for cylindrical vessels intersected by moderate-to-large-diameter nozzles
 - iv. 335 SCF data points for cylindrical vessels intersected by small-diameter nozzles
11. Such large collection of comprehensive SCF results that takes into account both the vessel and nozzle stresses has been missing in the previous collection of literature. Hence, it becomes handy for possible usage by any other interested researcher for future studies.

12.2 RECOMMENDATIONS

1. The present study conducts a thorough analysis of spherical and cylindrical pressure vessels with no reinforcement of any sort at the juncture. Similar study can be conducted for the said pressure vessels with pad reinforcements
2. Since in practice there exists a possibility of having various shapes of the vessel and/or nozzle. Other types of vessel and/or nozzle geometries can be studied in a similar manner followed in this research.
3. Use of single discontinuity analysis for the analytical solution of the spherical vessels has been adopted in this research due to the fact that the literature proves its sufficiency. However, double discontinuity analysis can be used in such a comprehensive manner followed here to access and appraise its performance.
4. The presented analysis in this research assumes a homogeneous material for both the vessel and the nozzle. It is recommended to extend similar approach to non-homogeneous vessel or nozzle materials or both. These materials can be functionally graded, orthotropic, etc.
5. Future study is recommended to extend such comprehensive analysis with vessel-nozzle junctures with both pressure and external loading types (such as external moments, forces, etc.).
6. Because the parametric tool available in COMSOL package has been used in the analysis, the major challenge became that of dealing with the effect of stress singularity at the juncture in case of the Solid Model. Fixing the fillet radius or the offset distance result in SCF values that are valid for some vessel-nozzle

configurations and invalid for others. Hence, a great deal of time has been spent to overcome such challenge. However, future work to come up with a more formal and general approach of dealing with the singularity of the juncture stresses is recommended. Such approach may present needed expressions for the fillet radius and/or offset distances from the juncture as functions of the three important geometric ratios (R_v/T_v , T_n/T_v , and R_n/R_v) that will result in avoiding the singularity effect.

REFERENCES

1. COMSOL Inc., *COMSOL Ver. 4.3*, 2013: Burlington, MA, U.S.A.
2. Wolfram Research Inc., *MATHEMATICA Ver. 9*, 2012: Champaign, IL, U.S.A.
3. Timoshenko, S.P. and Woinowsky-Krieger, S., *Theory of Plates and Shells*. 1970, New York: McGraw-Hill Book Company.
4. Leckie, F.A., *Localized Loads Applied to Spherical Shells*. *Int. Mech. Eng. Sci.*, 1961. **3**(2): p. 111-118.
5. Langer, R.E., *On the Asymptotic Solutions of Ordinary Differential Equations, with Reference to the Stokes' Phenomenon About a Singular Point*. *Trans. Am. Soc.*, 1935. **37**: p. 397-416.
6. Leckie, F.A., *Asymptotic Solutions for the Spherical Shell Subjected to Axially Symmetric Loading*, in *Symp. On Nuclear Reactor Containment Buildings and Pressure Vessels* 1960: Butterworths, London. p. 286 -297.
7. Leckie, F.A. and Penny, R. K., *A critical Study of the Solutions for the Axisymmetric Bending of Spherical Shells*. *Welding Research Council Bulletin* 1961. **90**.
8. Penny, R.K. and Leckie, F. A., *Solutions for the Stresses at Nozzles in Pressure Vessels, A critical Study of the Solutions for the Axisymmetric Bending of Spherical Shells*. *Welding Research Council Bulletin* 1961. **90**.
9. Leckie, F.A. and Penny, R. K., *Stress Concentration Factors for the Stresses at Nozzle Intersections in Pressure Vessels*. *Welding Research Council Bulletin*, 1963. **90**.
10. Dawoud, R.H., *Symmetrically Loaded Shallow Shells of Revolution*. *Mathematika* 1960. **7**(23 - 35).
11. Reissner, E., *Stresses and Small Displacements of Shallow Spherical Shells*. *J. Math. Phys.*, 1946. **25**: p. 80 - 85.
12. Wan, F.Y.M., *Membrane and Bending Stresses in Shallow Spherical Shells*. *Int. J. Solids Structures*, 1967. **3**: p. 353 - 366.
13. Gill, S.S., *The Stress Analysis of Pressure Vessels and Pressure Vessel Components*. 1970, New York: Pergamon Press.
14. Mackerle, J., *Finite elements in the analysis of pressure vessels and piping – a bibliography (1976-1996)*. *Int. J. Pressure Vessel Piping*, 1997. **69**: p. 279 - 339.

15. Mackerle, J., *Finite elements in the analysis of pressure vessels and piping, an Addendum: a bibliography (1996-1998)*. Int. J. Pressure Vessel Piping, 1999. **76**: p. 461- 485.
16. Mackerle, J., *Finite elements in the analysis of pressure vessels and piping, an addendum: a bibliography (1998-2001)*. Int. J. Pressure Vessel Piping, 2002. **79**: p. 1-26.
17. Mackerle, J., *Finite elements in the analysis of pressure vessels and piping, an addendum: a bibliography (2001-2004)*. Int. J. Pressure Vessel Piping, 2005. **82**: p. 571-592.
18. Mackerle, J., *Finite and Boundary Element Linear and Nonlinear Analyses of Shells and Shell-like Structures: A Bibliography (1999-2001)*. Finite Elements in Analysis and Design, 2002. **38**: p. 765-782.
19. Penny, R.K., *Symmetric Bending of the General Shell of Revolution by Finite Difference Methods*. Jnl. Mech. Eng. Sci., 1961. **3**(4): p. 369-377.
20. Prasad, M.M.S., *Nozzle on Spherical Shell Under Internal Pressure and Edge Loadings Analysed by FEM and Thin Shell Theory*, in *Mechanical Engineering 2011*, SRM University: India.
21. Hardik, A., Nayak, B., and Trivedi, B. R. R. *Stress Analysis of Reactor Nozzle to Head Junction*. in *International Conference on Current Trends in Technology, 'NUiCONE-2011'*. 2011. India.
22. Al-Gahtani, H., et al., *Local Pressure Testing of Spherical Vessels*. International Journal of Pressure Vessels and Piping, 2014. **114-115**: p. 61-68.
23. Dekker, C.J. and Brink, H.J., *Nozzles on Spheres with Outward Weld Area under Internal Pressure analyzed by FEM and Thin Shell Theory*. Int. J. Pressure Vessel Piping, 2000. **77**: p. 399-415.
24. Attwater, I.J.S., Anderson, J., and Findlay, G.E., *Three-dimensional Finite Element Analysis of Sphere/Cylinder Intersections under Axisymmetric Loading*. Int. J. Pressure Vessel Piping, 1994. **57**: p. 231-235.
25. Schindler, S. and Zeman, J. L., *Stress Concentration Factors of Nozzle-Sphere Connections*. Int. J. Pressure Vessel Piping, 2003. **80**: p. 87-95.
26. Chaudhari, S.S. and Jadhav, D. N., *A Suggested Stress Analysis Procedure for Nozzle to Head Shell Element Model – A Case Study*. Int. J. Theoretical Appl. Res. Mech. Engr., 2012. **1** (2): p. 92-98.
27. Naderan-Tahan, K., *Stress Concentration Factors in Spherical Vessels with Single Oblique Nozzle*. Journal of Engineering, Islamic Republic of Iran, 1995. **8**(2): p. 95-105

28. Luo, C. and Song, S., *Finite Element Analysis of Spherical Shell with Opening Nozzle*. Information Technology Journal, 2012. **11**(4): p. 426-430.
29. Liu, J.-S., Parks, G. T., and Clarkson, P. J. , *Shape Optimization of Axisymmetric Cylindrical Nozzles in Spherical Pressure Vessels Subject to Stress Constraints*. Int. J. Pressure Vessel Piping, 2001. **78**: p. 1-9.
30. Qadir, M. and Redekop, D. *SCF and Fatigue Analysis of Sphere-Nozzle Intersections With LTA*. in *ASME Pressure Vessels and Piping Conference*. 2008. Chicago, Illinois, USA.
31. Fuad, K., et al. *Stress Concentration Factors of Various Adjacent Holes Configurations in a Spherical Pressure Vessel*. in *5th Australian Congress on Applied Mechanics (ACAM)*. 2007. Brisbane, Australia.
32. Naghdi, A.K., *An Approximate Solution to the Problem of a Circular Cylindrical Shell with a Circular Hole Subjected to an Arbitrary Self-Equilibrating Edge Loading*. Archive of Applied Mechanics, 1969. **38**(6): p. 380-388.
33. Dyke, P.V., *Stresses about a Circular Hole in a Cylindrical Shell*. AIAA Journal, 1965. **3**(9): p. 1733-1742.
34. Lekkerkerker, J.G. *Stress Concentration around circular holes in Cylindrical Shells*. in *Eleventh International Congress Applied Mechanics*. 1964. Munich.
35. Lekkerkerker, J.G., *The Determination of Elastic Stresses near Cylinder-to-Cylinder Intersections*. Nuclear Engineering and Design, 1972. **20**: p. 57-84.
36. Eringen, A.C. and Suhubi, E. S. , *Stress Distribution at Two Normally Intersecting Cylindrical Shells*. Nuclear Structural Engineering, 1965. **2**: p. 253-270.
37. Maye, R.F. and Eringen, A. C. , *Further Analysis of Two Normally Intersecting Cylindrical Shells subjected to Internal Pressure*. Nuclear Engineering and Design, 1970. **12**: p. 457-474.
38. Naghdi, A.K. and Eringen, A. C. , *Stress Distribution in a Circular Cylindrical Shell with a Circular Cutout*. Archive of Applied Mechanics, 1965. **34**(3): p. 161-172.
39. Diankui, L. and Chao, H., *The General Solution for the Stress Problem of Circular Cylindrical Shells with an Arbitrary Cutout*. Applied Mathematics and Mechanics, 1997. **18** (7): p. 629-646.
40. Dekker, C.J. and Stikvoort, W. J. , *Pressure Stress Intensity at Nozzles on Cylindrical Vessels: A Comparison of Calculation Methods*. Int. J. Pres. Ves. & Piping, 1997. **74**: p. 121-128.
41. Xue, M.D., Chen, W., and Hwang, K.C., *Stresses at the Intersection of Two Cylindrical Shells*. Nucl. Eng. Des. , 1995. **154**: p. 231-238.

42. Xue, M.D., Wang, H. H., and Hwang, K.C. , *Stress Analysis of Cylindrical Shells with Nozzles due to External Run Pipe Moments*. Journal of Strain Analysis, 2000. **35**(3): p. 159-170.
43. Xue, M.D., Li, D. F., and Hwang, K.C. , *Analytical Solution of Two Intersecting Cylindrical Shells Subjected to Transverse Moment on Nozzle*. International Journal of Solids and Structures, 2004. **41**: p. 6949-6962.
44. Xue, M.D., Li, D. F., and Hwang, K.C., *A Thin Shell Theoretical Solution for Two Intersecting Cylindrical Shells Due to External Branch Pipe Moments*. Journal of Pressure Vessel Technology, 2005. **127**: p. 357-368.
45. Xue, M.D., Deng, Y., and Hwang, K. C. , *Some Results on Analytical Solution of Cylindrical Shells with Large Opening*. ASME J. Pressure Vessel Technol., 1991. **113**: p. 297–307.
46. Deng, Y., Hwang, K. C. , and Xue, M. D. *The Stress Analysis of Cylindrical Shells with Rigid Inclusions having a Large Ratio of Radii*. in *SMiRT 11 Transactions* 1991.
47. Xue, M.D., et al., *The Thin Shell Theoretical Solution for Cylindrical Shells with Large Openings*. Acta Mech. Sin., 1995. **27**(4): p. 482 – 488.
48. Xue, M.D., et al., *A Reinforcement Design Method Based on Analysis of Large Openings in Cylindrical Pressure Vessels*. ASME J. Pressure Vessel Technol., 1996. **118**: p. 502–506.
49. Xue, M.D., et al., *Analytical Solution for Cylindrical Thin Shells with Normally Intersecting Nozzles Due to External Moments on the Ends of Shells*. Sci. China, Ser. A: Math., Phys., Aston., 1999. **42**(3): p. 293–304.
50. Xue, M.D., Li, D. F., and Hwang, K. C. , *Theoretical Stress Analysis of Two Intersecting Cylindrical Shells Subjected to External Loads Transmitted Through Branch Pipes*. Int.J. Solids Struct., 2005. **42**: p. 3299–3319.
51. Xue, M.D., et al., *An Analytical Method for Cylindrical Shells with Nozzles Due to Internal Pressure and External Loads – Part I: Theoretical Foundation*. Journal of Pressure Vessel Technology, 2010. **132**(3).
52. Xue, M.D., et al., *An Analytical Method for Cylindrical Shells with Nozzles Due to Internal Pressure and External Loads – Part II: Design Method*. Journal of Pressure Vessel Technology, 2010. **132**(3).
53. Pattabiraman, J. and Ramamurti, V. , *Stresses around a Small Circular Cutout in a Cylindrical Shell subjected to Asymmetric Bending*. Journal of Strain Analysis, 1977. **12**(1): p. 53-61.
54. Dekker, C.J. and Bos, H. J. , *Nozzles – On External Loads and Internal Pressure*. Int. J. Pres. Ves. & Piping, 1997. **72**: p. 1–18.

55. Campen, D.H.V. and Spaas, A. C. M. , *On the Stress Distribution in Nozzle-to-Cylinder Connections for Small Diameter Ratios*. Nuclear Engineering and Design, 1972. **21**: p. 368-395.
56. Campen, D.H.V., *On the Stress Distribution in an Arbitrary Loaded Nozzle-to-Flat Plate Connection*. Nuclear Engineering and Design, 1970. **11**: p. 495.
57. Campen, D.H.V., Kroon, J. P. , and Latzko, D. G. H. *The Nozzle-to-Flat Plate Approach in the Stress Concentration Problem of Nozzle-to-Cylinder Intersections*. in *Proc. First Internat. Conf. Struct. Mechan. In Reactor Technol.* 1971. Berlin, Germany.
58. Ha, J.L., Sun, B. C. , and Koplik, B. , *Local Stress Factors of a Pipe-Nozzle Under Internal Pressure*. Nuclear Engineering and Design, 1995 **157**: p. 81–91.
59. Lu, M.H., Yu, J. S. , and Chen, J. J. , *The Effect of Analysis Model on the Stress Intensity Calculation for the Nozzle attached to Pressure Vessel under Internal Pressure Loading*. Int. J. Pres. Ves. & Piping, 2013.
60. Liang, C.C., Hsu, C. Y. , and Chen, W., *Curvature Effect on Stress Concentrations around Circular Hole in Opened Shallow Cylindrical Shell under External Pressure*. Int. J. Pres. Ves. & Piping, 1998. **75**: p. 749-763.
61. Xue, M.D., et al., *Stress and Strength Analysis by FEM of Fibre Reinforced Plastic Pipe Tees Subjected to Internal Pressure*. Int.J. Pres. Ves. & Piping. , 1996. **67**: p. 11-15.
62. Skopinsky, V.N., *A Comparative Study of Three-Dimensional and Two-Dimensional Finite Element Analyses for Intersecting Shells*. Journal of Strain Analysis, 2001. **36**(3): p. 313-322.
63. Xu, J.J., Sun, B. C., and Koplik, B. , *Local Pressure Stresses on Lateral Pipe-Nozzle with Various Angles of Intersection*. Nuclear Engineering and Design, 2000. **199**: p. 335-340.
64. Petrovic, A., *Stress Analysis in Cylindrical Pressure Vessels with Loads Applied to the Free End of a Nozzle*. International Journal of Pressure Vessels and Piping, 2001. **78**: p. 485-493.
65. Qadir, M. and Redekop, D., *SCF Analysis of a Pressurized Vessel-Nozzle Intersection With Wall Thinning Damage*. International Journal of Pressure Vessels and Piping, 2009. **86**: p. 541-549.
66. Kacmarcik, J., Vukojevic, N. , and Hadzikadunic, F. *Comparison of Numerically and Experimentally Determined SCF for Nozzle in Cylindrical Pressure Vessel*. in *14th International Research/Expert Conference "Trends in the Development of Machinery and Associated Technology" (TMT)*. 2010. Mediterranean Cruise.

67. Calladine, C.R., *On the Design of Reinforcement for Openings and Nozzles in Thin Spherical Pressure Vessels*. Journal of Mechanical Engineering Science, 1966. **8**(1): p. 1–14.
68. Kitching, R. and Kannas, A. , *An Alternative to Current Practice in Design of Pad Reinforcement of Spherical Pressure Vessels*. Int. J. Pres. Ves. & Piping, 1977. **5**: p. 287–307.
69. Yeo, K.T. and Robinson, M., *Minimum Weight Designs for Reinforcement of Spherical Pressure Vessels with Flush Radial Nozzles*. Int. J. Pres. Ves. & Piping, 1978. **6**: p. 53–83.
70. Kannas, A., Kitching, R. , and Gill, S. S. , *A Design Procedure for Pad Reinforced Flush Nozzles in Spherical Pressure Vessels*. Int. J. Pres. Ves. & Piping, 1978. **6**: p. 147–163.
71. Soliman, S.F. and Gill, S. S. , *Stresses Due to a Moment Applied to a Pad Reinforced Nozzle in a Spherical Pressure Vessel – A Theoretical Analysis and Experimental Investigation*. Int. J. Pres. Ves. & Piping, 1979. **7**: p. 133–161.
72. Soliman, S.F. and Gill, S. S. , *Stress Concentration Factors for Integral and Pad Reinforced Nozzles in Spherical Pressure Vessels Subjected to Radial Load and Moment*. Int. J. Pres. Ves. & Piping, 1979: p. 275–307.
73. Hsu, I.M., Kettlewell, J. , and Gill, S. S. , *Shear Loading of Pad Reinforced Nozzles in Spherical Pressure Vessels – A Theoretical Investigation*. Int. J. Pres. Ves. & Piping, 1980. **8**: p. 461–486.
74. Lee, Y.S. and Sohn, Y. S., *Modified Solution of Radial Nozzle with Thick Reinforcement in Spherical Vessel Head Subjected to Radial Load*. Nuclear Engineering and Design, 1997. **178**: p. 185–194.
75. Chattopadhyay, S., *Pressure Vessels: Design and Practice*. 2005, Boca Raton, Florida, USA: CRC Press.
76. Miranda, J.R. and Werneck, H. S. . *Stress Analysis on Vessel/Nozzle Intersections With/Without Pad Reinforcements for Cylindrical Pressure Vessels*. in *19th International Congress of Mechanical Engineering*. 2007. Brasilia, DF.
77. Chien, H. and Tu, S. , *The Contact Stress Analysis of Pad-Reinforced Structures*. J. Pressure Vessel Technol., 1988. **110**: p. 182–187.
78. Chen, H. and Chao, Y. –J. , *Contact Between Vessel Shell and Welded Pad in Nozzle Reinforcement*. J. Pressure Vessel Technol., 1993. **115**(4): p. 364–372.
79. Wu, B.H. and Sang, Z. F., *Contact Behavior Between Reinforcement Pad and Vessel Shell Due to Longitudinal Moment [J]*. Pressure Vessel Technology, 2004. **6**.

80. Sang, Z.F., et al., *Effect of Geometric Gap Between Cylinder and Reinforcement Pad on Local Stresses (Axial Thrust Load on Nozzle)*. Int. J. Pres. Ves. & Piping, 1997. **71**: p. 113–120.
81. Sang, Z.F., et al., *Effect of Gap Between Pad and Vessel for Moment Loading on Nozzle*. J. Pressure Vessel Technol., 1999. **121**: p. 225–231.
82. Skopinsky, V.N., *Comparative Study of Reinforced Nozzle Connections*. Nuclear Engineering and Design, 1998. **180**: p. 175–179.
83. Skopinsky, V.N. and Smetankin, A. B., *Parametric Study of Reinforcement of Pressure Vessel Head with Offset Nozzle*. Int. J. Pres. Ves. & Piping, 2003. **80**: p. 333–343.
84. Finlay, J.P., et al., *Effective Stress Factors for Reinforced Butt-Welded Branch Outlets Subjected to Internal Pressure or External Moment Loads*. Int. J. Pres. Ves. & Piping, 2003. **80**: p. 311–331.
85. Nash, D.H. and Hitchen, J. *Effects of Local Reinforcement on Nozzles in Dished Ends*. in *12th International Conference on Pressure Vessel Technology (ICPVT-12)*. 2009. Jeju Island, South Korea.
86. Liang, L.L., et al. *Analysis and Comparison of Pad Reinforcement of Pressure Vessel by Elastic and Elastoplastic FEM*. in *ASME Pressure Vessels and Piping Conference*. 2007. San Antonio, Texas, USA.
87. Xue, L., Widera, G. E. O. , and Sang, Z. F., *Influence of Pad Reinforcement on the Limit and Burst Pressures of a Cylinder-Cylinder Intersection*. ASME Pressure Vessels and Piping, 2003. **125**: p. 182–187.
88. Sang, Z.F., et al., *Reinforced Cylindrical Vessels Under Out-of-Plane Moement of Nozzle*. ASME Pressure Vessels and Piping, 2006. **128**: p. 49–56.
89. Fang, J., Tang, Q. H., and Sang, Z. F., *A Comparative Study of Usefulness For Pad Reinforcement in Cylindrical Vessels Under External Load on Nozzle*. Int. J. Pres. Ves. & Piping, 2009. **86**: p. 273–279.
90. Kim, Y.-J., Myeong, M.-S. , and Yoon, K.-B. , *Effect of Reinforcement on Plastic Limit Loads of Branch Junctions*. Int. J. Pres. Ves. & Piping, 2009. **86**: p. 508–516.
91. Skopinskii, V.N., et al., *Effect of Paramaters of Local Reinforcement of Connection Between Pressure-Vessel and Nozzle on Limiting Plastic Load*. Chemical and Petroleum Engineering, 2013. **49**((3-4)): p. 214-218.
92. Lind, N.C., *A Rapid Method to Estimate the Elastic Stress Concentration of a Nozzle in a Spherical Pressure Vessel*. Nuclear Structural Engineering 2, 1965: p. 159-168.

93. Lind, N.C., *Approximate Stress-Concentration Analysis for Pressurized Branch Pipe Connections*. ASME Paper 67-WA/PVP-7, ASME Pressure Vessels and Piping: Design and Analysis, 1967: p. 951-958.
94. Leckie, F.A., Paine, D. J. , and Penny, R. K. , *Elliptical Discontinuities in Spherical Shells*. J. Strain Anal., 1967. **2**: p. 34-42.
95. Money, H.A., *Designing Flush Cylinder-to-Cylinder Intersections to Withstand Pressure*. ASME PVP-17, ASME Pressure Vessels and Piping, 1968.
96. Decock, J., *Reinforcement Method of Openings in Cylindrical Pressure Vessels Subjected to Internal Pressure*. Weld. Res. Abroad, 1975. **21**(9): p. 9-36.
97. Xie, D.S. and Lu, Y. G. , *Prediction of Stress Concentration Factors for Cylindrical Pressure Vessels with Nozzles*. Int. J. Pres. Ves. & Piping, 1985. **21**: p. 1–20.
98. Moffat, D.G., Misty, J. , and Moore, S. E. , *Effective Stress Factor Correlation Equations for Piping Branch Junctions Under Internal Pressure Loading*. J. Pressure Vessel Technol., 1999. **121**(2): p. 121-126.
99. Gurumurthy, K., Jain, R., and Salpekar, V. Y., *Simplified Formula for Stress Concentration Factor in Radial Nozzle Shell Junctions Under Internal Pressure Loading*. ASME PVP-430, 2001: p. 3-6.
100. de Carvalho, E.A., *Stress Concentration Factors for an Internally Pressurized Circular Vessel Containing a Radial U-notch*. Int. J. Pres. Ves. & Piping, 2005. **82**: p. 517–521.
101. Lotsberg, I., *Stress Concentration Factors at Welds in Pipelines and Tanks Subjected to Internal Pressure and Axial Force*. Marine Structures, 2008. **21**: p. 138–159.
102. Oliveira, S.C., Deus, E. P. , and Mont'Alverne, A. M. *Finite Element Analysis of Pipes Considering The Effects of Stress Concentration Factors Due to Dents*. in COMSOL Conference 2010. Boston, USA.
103. Pilkey, W.D. and Pilkey, D. F. , *Peterson's Stress Concentration Factors*. 3rd ed. 2008: John Wiley & Sons Ltd.
104. Pinheiro, B., Pasqualino, L. , and de Azevedo, N. . *Stress Concentration Factors of Dented Rigid Risers*. in ASME 32nd International Conference on Ocean, Offshore and Arctic Engineering. 2013. Nantes, France.
105. Donnell, L.H., *Stability of Thin-walled Tubes under Torsion*. National Advisory Committee for Aeronautics Report (NACA-R-479), 1933.
106. Hoff, N.J., *Boundary-Value Problems of the Thin-Walled Circular Cylinder*. ASME J. Appl. Mechanics, 1954. **21**: p. 343-350.

107. Geckeler, J.W., *Über die Festigkeit achsen-symmetrischer Schalen*. Forsch. Arb. Ingwes. H. 276, Berlin, 1926.
108. Hetenyi, M., *Spherical Shells Subjected to Axial Symmetric Bending*. Bull. Int. Assoc. Bridge Eng., 1938. **5**: p. 173-184.

APPENDIX A:

MATHEMATICA CODES FOR ANALYTICAL SOLUTIONS OF SPHERICAL VESSEL-CYLINDRICAL NOZZLE JUNCTURES

Exact Analytical Solution for Spherical Vessel Intersected by Nozzle: Langer Asymptotic Solution

■ Input the geometric data and calculate properties and parameters

`Clear["Global`*"]`

`ee = 30 × 106; v = 0.33; p = 1;`

$$\mu = \left(\frac{3 (1 - v^2)}{Rn^2 Tn^2} \right)^{1/4}; Dn = \frac{ee Tn^3}{12 (1 - v^2)}; Dv = \frac{ee Tv^3}{12 (1 - v^2)}; \lambda = \left(3 (1 - v^2) (Rv^2 / Tv^2) \right)^{1/4};$$

■ Nozzle Solution (circular cylindrical shell)

$$Wnp = \frac{p Rn^2}{2 ee Tn} (2 - v);$$

$$WnQM = -\text{Exp}[-\mu x] / (2 \mu^3 Dn) (Q \text{Cos}[\mu x] + \mu (M) (\text{Sin}[\mu x] - \text{Cos}[\mu x]));$$

$$Wn = Wnp + WnQM;$$

$$\Theta n = \text{Exp}[-\mu x] / (2 \mu^2 Dn) (-Q (\text{Cos}[\mu x] + \text{Sin}[\mu x]) + 2 \mu (M) \text{Cos}[\mu x]);$$

$$\Theta n1 = -D[Wn, x];$$

$$Mx = -Dn D[Wn, \{x, 2\}];$$

$$Wn0 = Wn /. x \rightarrow 0;$$

$$\Theta n0 = \Theta n /. x \rightarrow 0;$$

■ Vessel Edge Solution (spherical shell)

$$\phi 0 = \text{ArcSin}[Rn / Rv];$$

$$DDv = \frac{ee Tv}{(1 - v^2)};$$

$$\kappa = \left(\frac{3 (1 - v^2) Rv^2}{Tv^2} - \frac{v^2}{4} \right)^{(1/4)};$$

$$T1 = \sqrt{\frac{\phi}{\text{Sin}[\phi]}} D[\text{KelvinBer}[z], z];$$

$$T2 = \sqrt{\frac{\phi}{\sin[\phi]}} D[\text{KelvinBei}[z], z];$$

$$T3 = \sqrt{\frac{\phi}{\sin[\phi]}} D[\text{KelvinKer}[z], z];$$

$$T4 = \sqrt{\frac{\phi}{\sin[\phi]}} D[\text{KelvinKei}[z], z];$$

$$dT1 = -\sqrt{2} \kappa \sqrt{\frac{\phi}{\sin[\phi]}} \left(\text{KelvinBei}[z] + \frac{1}{2\sqrt{2}\kappa} \left(\frac{1}{\phi} + \cot[\phi] \right) D[\text{KelvinBer}[z], z] \right);$$

$$dT2 = \sqrt{2} \kappa \sqrt{\frac{\phi}{\sin[\phi]}} \left(\text{KelvinBer}[z] - \frac{1}{2\sqrt{2}\kappa} \left(\frac{1}{\phi} + \cot[\phi] \right) D[\text{KelvinBei}[z], z] \right);$$

$$dT3 = -\sqrt{2} \kappa \sqrt{\frac{\phi}{\sin[\phi]}} \left(\text{KelvinKei}[z] + \frac{1}{2\sqrt{2}\kappa} \left(\frac{1}{\phi} + \cot[\phi] \right) D[\text{KelvinKer}[z], z] \right);$$

$$dT4 = \sqrt{2} \kappa \sqrt{\frac{\phi}{\sin[\phi]}} \left(\text{KelvinKer}[z] - \frac{1}{2\sqrt{2}\kappa} \left(\frac{1}{\phi} + \cot[\phi] \right) D[\text{KelvinKei}[z], z] \right);$$

$$z = \sqrt{2} \kappa \phi;$$

$$A1 = A2 = 0;$$

$$Q\phi = \left(\frac{DDv}{Rv} \right) (A1 T1 + A2 T2 + B1 T3 + B2 T4);$$

$$N\phi2 = - \left(\frac{DDv}{Rv} \right) \cot[\phi] (A1 T1 + A2 T2 + B1 T3 + B2 T4);$$

$$N\theta2 = - \left(\frac{DDv}{Rv} \right) (A1 dT1 + A2 dT2 + B1 dT3 + B2 dT4);$$

$$V =$$

$$- \frac{2\kappa^2}{Rv(1-v^2)} \left(A1 \left(T2 - \frac{v}{2\kappa^2} T1 \right) - A2 \left(T1 + \frac{v}{2\kappa^2} T2 \right) + B1 \left(T4 - \frac{v}{2\kappa^2} T3 \right) - B2 \left(T3 + \frac{v}{2\kappa^2} T4 \right) \right);$$

$$M\phi2 = - \left(\frac{Dv}{Rv^2} \right) \left(\frac{2\kappa^2}{(1-v^2)} \right) \left(A1 \left(dT2 + v \cot[\phi] T2 - \frac{v}{2\kappa^2} (dT1 + v \cot[\phi] T1) \right) - \right.$$

$$A2 \left(dT1 + v \cot[\phi] T1 + \frac{v}{2\kappa^2} (dT2 + v \cot[\phi] T2) \right) +$$

$$\begin{aligned}
& B1 \left(dT4 + v \cot[\phi] T4 - \frac{v}{2 \kappa^2} (dT3 + v \cot[\phi] T3) \right) - \\
& B2 \left(dT3 + v \cot[\phi] T3 + \frac{v}{2 \kappa^2} (dT4 + v \cot[\phi] T4) \right) \Bigg); \\
M\theta 2 = & - \left(\frac{Dv}{Rv^2} \right) \left(\frac{2 \kappa^2}{(1 - v^2)} \right) \left(A1 \left(v dT2 + \cot[\phi] T2 - \frac{v}{2 \kappa^2} (v dT1 + \cot[\phi] T1) \right) - \right. \\
& A2 \left(v dT1 + \cot[\phi] T1 + \frac{v}{2 \kappa^2} (v dT2 + \cot[\phi] T2) \right) + \\
& B1 \left(v dT4 + \cot[\phi] T4 - \frac{v}{2 \kappa^2} (v dT3 + \cot[\phi] T3) \right) - \\
& \left. B2 \left(v dT3 + \cot[\phi] T3 + \frac{v}{2 \kappa^2} (v dT4 + \cot[\phi] T4) \right) \right) \Bigg); \\
del = & \frac{Rv \sin[\phi]}{ee Tv} (N\theta 2 - v N\phi 2); \\
eq1 = & M\phi 2 == -M /. \phi \rightarrow \phi 0; \\
eq2 = & N\phi 2 == 0 /. \phi \rightarrow \phi 0; \\
eq3 = & M\phi 2 == 0 /. \phi \rightarrow \phi 0; \\
eq4 = & N\phi 2 == -H \cos[\phi 0] /. \phi \rightarrow \phi 0; \\
sol1 = & \text{Solve}[\{eq1, eq2\}, \{B1, B2\}]; \\
sol12 = & \text{Solve}[\{eq3, eq4\}, \{B1, B2\}]; \\
wv = & \frac{(1 - v) Rv^2 \sin[\phi 0]}{2 ee Tv} p + (del /. sol1[[1]] /. \phi \rightarrow \phi 0) + (del /. sol12[[1]] /. \phi \rightarrow \phi 0); \\
\theta v = & (V /. sol1[[1]] /. \phi \rightarrow \phi 0) + (V /. sol12[[1]] /. \phi \rightarrow \phi 0); \\
H = & Q + p / 2 \left(Rv^2 - Rn^2 \right)^{1/2};
\end{aligned}$$

■ Compatibility Equations at the juncture

$$\begin{aligned}
eq1 = & Wn0 == wv; \\
eq2 = & \theta n0 == -\theta v; \\
sol = & \text{Solve}[\{eq1, eq2\}, \{Q, M\}];
\end{aligned}$$

■ Stresses in the nozzle

$$M\theta = v Mx;$$

$$\sigma_{xout} = \left(\frac{T_n}{R_n} \right) \left(\frac{p R_n}{2 T_n} + \frac{6 Mx}{T_n^2} \right);$$

$$\sigma_{xin} = \left(\frac{T_n}{R_n} \right) \left(\frac{p R_n}{2 T_n} - \frac{6 Mx}{T_n^2} \right);$$

$$\sigma_{\theta out} = \left(\frac{T_n}{R_n} \right) \left(\frac{p R_n}{T_n} + \frac{ee}{R_n} WnQM + \frac{6 M\theta}{T_n^2} \right);$$

$$\sigma_{\theta in} = \left(\frac{T_n}{R_n} \right) \left(\frac{p R_n}{T_n} + \frac{ee}{R_n} WnQM - \frac{6 M\theta}{T_n^2} \right);$$

$$\sigma_{xout} = \sigma_{xout} /. sol[[1]];$$

$$\sigma_{xin} = \sigma_{xin} /. sol[[1]];$$

$$\sigma_{\theta out} = \sigma_{\theta out} /. sol[[1]];$$

$$\sigma_{\theta in} = \sigma_{\theta in} /. sol[[1]];$$

■ Stresses in the Spherical Vessel (Approx. II)

$$\psi = 0;$$

$$\lambda = \left(3 \left(1 - v^2 \right) \left(Rv^2 / Tv^2 \right) \right)^{1/4};$$

$$\phi = \psi + \phi 0;$$

$$N\phi_{apr} = (N\phi 2 /. sol1[[1]] /. sol[[1]]) + (N\phi 2 /. sol12[[1]] /. sol[[1]]);$$

$$N\theta_{apr} = (N\theta 2 /. sol1[[1]] /. sol[[1]]) + (N\theta 2 /. sol12[[1]] /. sol[[1]]);$$

$$M\phi_{apr} = (M\phi 2 /. sol1[[1]] /. sol[[1]]) + (M\phi 2 /. sol12[[1]] /. sol[[1]]);$$

$$M\theta_{apr} = (M\theta 2 /. sol1[[1]] /. sol[[1]]) + (M\theta 2 /. sol12[[1]] /. sol[[1]]);$$

$$\delta_{apr} = (\delta 1 /. sol1[[1]] /. sol[[1]]) + (\delta 1 /. sol12[[1]] /. sol[[1]]);$$

$$\sigma_{\phi t} = (2 Tv / Rv) \left((p Rv / (2 Tv)) + N\phi_{apr} / Tv + (6 M\phi_{apr} / Tv^2) \right);$$

$$\sigma_{\phi b} = (2 Tv / Rv) \left((p Rv / (2 Tv)) + N\phi_{apr} / Tv - (6 M\phi_{apr} / Tv^2) \right);$$

$$\sigma_{\theta t} = (2 Tv / Rv) \left((p Rv / (2 Tv)) + N\theta_{apr} / Tv + (6 M\theta_{apr} / Tv^2) \right);$$

$$\sigma_{\theta b} = (2 Tv / Rv) \left((p Rv / (2 Tv)) + N\theta_{apr} / Tv - (6 M\theta_{apr} / Tv^2) \right);$$

```
(*Example on plotting the stress variations along the nozzle geometry*)
Rv = 144 × 25.4; Rn = 26 × 25.4; Tv = 0.5 × 25.4; Tn = 0.25 × 25.4;
p1 = Plot[σxout /. sol[[1]], {x, 0, 10 × 25.4}, AxesOrigin → {0, 0},
  PlotRange → {-30, 30}, PlotStyle → {Darker[Green, 0.4], Thick}];
p2 = Plot[σxin /. sol[[1]], {x, 0, 10 × 25.4}, AxesOrigin → {0, 0},
  PlotRange → {-30, 30}, PlotStyle → {Lighter[Green, 0.5], Thick}];
p3 = Plot[σθout /. sol[[1]], {x, 0, 10 × 25.4}, AxesOrigin → {0, 0},
  PlotRange → {-30, 30}, PlotStyle → {Blue, Thick}];
p4 = Plot[σθin /. sol[[1]], {x, 0, 10 × 25.4}, AxesOrigin → {0, 0},
  PlotRange → {-30, 30}, PlotStyle → {Lighter[Blue, 0.6], Thick}];
Print["Exact Analytical nozzle Solution:"]
```

```
Show[p1, p2, p3, p4]
```

```
(*Example on plotting the normal forces and bending
moments variations along the spherical vessel geometry*)
pp1 = Plot[Nφapr, {ψ, 0, π / 10}, PlotRange → All,
  PlotStyle → {Darker[Green, 0.4], Thick}];
pp2 = Plot[Nθapr, {ψ, 0, π / 10}, PlotRange → All,
  PlotStyle → {Lighter[Green, 0.4], Thick}];
pp3 = Plot[Mφapr, {ψ, 0, π / 10}, PlotRange → All,
  PlotStyle → {Lighter[Blue, 0.5], Thick}];
pp4 = Plot[Mθapr, {ψ, 0, π / 10}, PlotRange → All, PlotStyle → {Blue, Thick}];
pp5 = Plot[δapr, {ψ, 0, π / 10},
  PlotRange → All, PlotStyle → {Lighter[Blue, 0.6], Thick}];

Show[pp1, pp2, pp3, pp4, pp5];
```

```
(*Example on plotting the stress
variations along the spherical vessel geometry*)
ppp1 = Plot[σφt, {ψ, 0, π / 8}, PlotRange → All,
  PlotStyle → {Darker[Green, 0.4], Thick}];
ppp2 = Plot[σφb, {ψ, 0, π / 8}, PlotRange → All,
  PlotStyle → {Lighter[Green, 0.5], Thick}];
ppp3 = Plot[σθt, {ψ, 0, π / 8}, PlotRange → All, PlotStyle → {Blue, Thick}];
ppp4 =
  Plot[σθb, {ψ, 0, π / 8}, PlotRange → All, PlotStyle → {Lighter[Blue, 0.6], Thick}];
Print["Exact Analytical Solution for the Spherical Shell:"]

Show[ppp1, ppp2, ppp3, ppp4]
```

```
(*Minimum nozzle radius required for validity of shell assumption*)
```

```
sol1 = Solve[ $\frac{Rn}{Tn} == 10$ , Rn];
```

```
rmin1 = Rn /. sol1[[1]];
```

```
(*Minimum nozzle radius required for validity of approximate solution*)
```

```
sol2 = Solve[ $\sqrt{(Rv / Tv)} (Rn / Rv) == 2.2$ , Rn];
```

```
rmin2 = FullSimplify[Rn /. sol2[[1]]];
```

```
(*Example on plotting the SCF for selected values of geometrical ratios*)
```

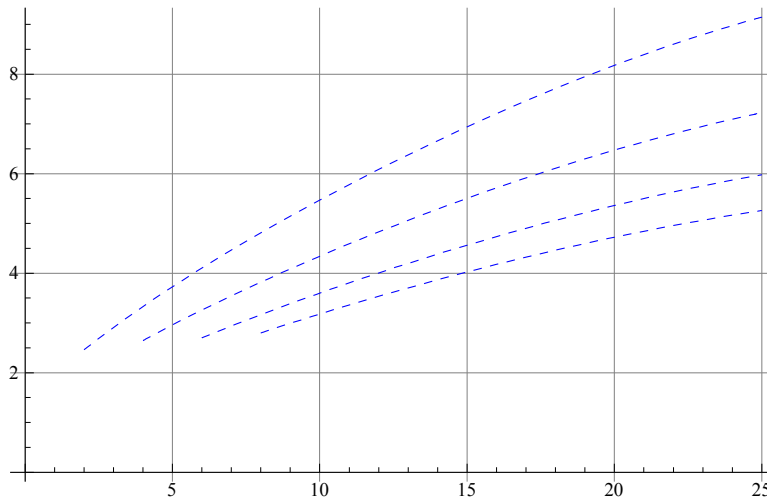
```
 $\gamma = \{1, 0.5, 0.25, 0.000001\};$ 
```

```
Do[omax1[i, j] = Max[ $\sigma_{\theta t}$ ,  $\sigma_{\phi t}$ ] /. {Tn  $\rightarrow$  0.2 i, Rv  $\rightarrow$  50 j, Tv  $\rightarrow$  1}, {i, 1, 4}, {j, 1, 6}]
```

```
Do[p1[i, j] = Plot[omax1[i, j], {Rn, rmin1 /. Tn  $\rightarrow$  0.2 i, 25 j}, AxesOrigin  $\rightarrow$  {0.01, 0},  
GridLines -> Automatic, PlotStyle  $\rightarrow$  {Blue, Dashed}], {i, 1, 4}, {j, 1, 6}]
```

```
Do[pp1[j] = Show[Table[p1[i, j], {i, 1, 4}], PlotRange  $\rightarrow$  All], {j, 1, 6}]
```

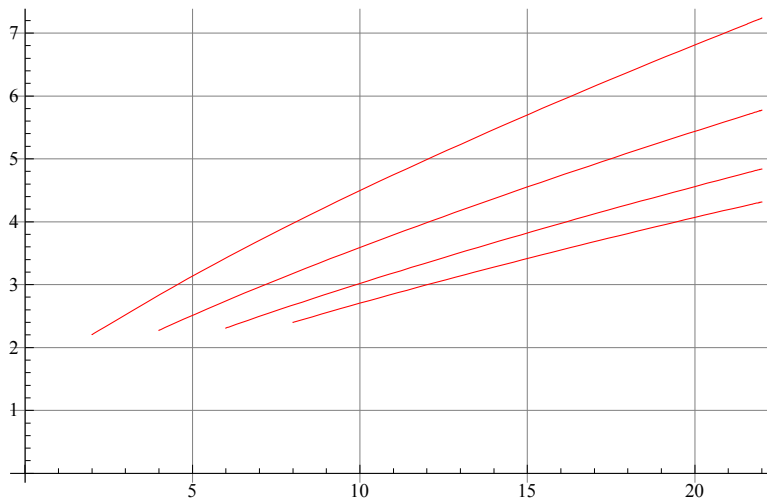
```
Show[pp1[1]]
```



```
(*Example on plotting the SCF for selected values of geometrical ratios
between the validity limits of the shell theory and approximate solution*)
γ = {1, 0.5, 0.25, 0.000001};
Do[σmax1[i, j] = Max[σθt, σφt] /. {Tn → 0.2 i, Rv → 50 j, Tv → 1}, {i, 1, 4}, {j, 1, 6}]
Do[p1[i, j] = Plot[σmax1[i, j],
  {Rn, rmin1 /. Tn → 0.2 i, rmin2 /. {Rv → 50 j, Tv → 1}}, AxesOrigin → {0.01, 0},
  GridLines -> Automatic, PlotStyle -> Red], {i, 1, 4}, {j, 1, 6}]

Do[pp1[j] = Show[Table[p1[i, j], {i, 1, 4}], PlotRange -> All], {j, 1, 6}]

Show[pp1[2]]
```



Approximate Analytical Approach for Spherical Vessel Intersected by Nozzle based on Hetenyi's Solution (Approximation II)

Minimum rR

- rRmin1 is the minimum r/R corresponding to $r/t = 10$ (validity of thin shell assumption)
rRmin2 is the minimum r/R corresponding to $\rho = 2.2$ (validity of the approximate solution) where $\rho = rR \sqrt{RT}$

```
Clear["Global`*"]

sol1 = Solve[ $\frac{RT}{tT} rR == 10, rR$ ];
rRmin1 = rR /. sol1[[1]];
sol2 = Solve[ $\sqrt{RT} rR == 2.2, rR$ ];
rRmin2 = rR /. sol2[[1]];
tT1 = {0.25, 0.5, 0.75, 1., 1.25, 1.5};
RT1 = Table[25 + 25 i, {i, 1, 5}];
rR1 = Table[0.1 i, {i, 1, 5}];
i1 = Length[tT1];
j1 = Length[RT1];
k1 = Length[rR1];

Do[Rmin[j] = Table[{RT1[[j]], tT1[[i]], rRmin1 /. {tT -> tT1[[i]], RT -> RT1[[j]]},
 $\sqrt{RT} rRmin1 /. {tT -> tT1[[i]], RT -> RT1[[j]]},$ 
rRmin2 /. {RT -> RT1[[j]]}, 2.2}, {i, 1, i1}], {j, 1, j1}]
RRmin = Join[Rmin[1], Rmin[2], Rmin[3], Rmin[4], Rmin[5]];
TableForm[RRmin,
TableHeadings -> {None, {"RT ", "tT", "rRmin1", " $\rho_1$ ", "rRmin2", " $\rho_2$ "}}]
```

RT	tT	rRmin1	ρ_1	rRmin2	ρ_2
50	0.25	0.05	0.353553	0.311127	2.2
50	0.5	0.1	0.707107	0.311127	2.2
50	0.75	0.15	1.06066	0.311127	2.2
50	1.	0.2	1.41421	0.311127	2.2
50	1.25	0.25	1.76777	0.311127	2.2
50	1.5	0.3	2.12132	0.311127	2.2
75	0.25	0.0333333	0.288675	0.254034	2.2
75	0.5	0.0666667	0.57735	0.254034	2.2
75	0.75	0.1	0.866025	0.254034	2.2
75	1.	0.133333	1.1547	0.254034	2.2
75	1.25	0.166667	1.44338	0.254034	2.2
75	1.5	0.2	1.73205	0.254034	2.2
100	0.25	0.025	0.25	0.22	2.2
100	0.5	0.05	0.5	0.22	2.2
100	0.75	0.075	0.75	0.22	2.2
100	1.	0.1	1.	0.22	2.2
100	1.25	0.125	1.25	0.22	2.2
100	1.5	0.15	1.5	0.22	2.2
125	0.25	0.02	0.223607	0.196774	2.2
125	0.5	0.04	0.447214	0.196774	2.2
125	0.75	0.06	0.67082	0.196774	2.2
125	1.	0.08	0.894427	0.196774	2.2
125	1.25	0.1	1.11803	0.196774	2.2
125	1.5	0.12	1.34164	0.196774	2.2
150	0.25	0.0166667	0.204124	0.179629	2.2
150	0.5	0.0333333	0.408248	0.179629	2.2
150	0.75	0.05	0.612372	0.179629	2.2
150	1.	0.0666667	0.816497	0.179629	2.2
150	1.25	0.0833333	1.02062	0.179629	2.2
150	1.5	0.1	1.22474	0.179629	2.2

Dicontinuity Analysis (Q & M)

```

v = 1 / 3;

phi0 = ArcSin[rR];
beta = (3 (1 - v^2))^(1/4) sqrt[rt];

lambda = (3 (1 - v^2))^(1/4) sqrt[RT];
Dbn = 1 / (12 rt^3 (1 - v^2));
Wnp = (pb rt) / 2 (2 - v);
WnFM = - (6 (1 - v^2) rt^3) / (beta^3) Exp[-beta xb] (Qb Cos[beta xb] + beta Mb (Sin[beta xb] - Cos[beta xb]));
Wn = Wnp + WnFM;
theta_n = (6 (1 - v^2) rt^3) / (beta^2) Exp[-beta xb] (-Qb (Cos[beta xb] + Sin[beta xb]) + 2 beta Mb Cos[beta xb]);
Wn0 = Wn /. xb -> 0;
theta_n0 = theta_n /. xb -> 0;
Hb = Qb + pb / 2 ((1 / rR)^2 - 1)^(1/2);
kk1 = 1 + ((1 - 2 v) Cot[phi0]) / (2 lambda);
kk2 = 1 + ((1 + 2 v) Cot[phi0]) / (2 lambda);
Wv = ((1 - v) RT Sin[phi0]) / (2 rR) pb + lambda RT Sin[phi0]^2 ((1 / kk1) + kk2) Hb + (2 lambda^2 RT rR Sin[phi0]) / kk1 Mb;
theta_v = (2 lambda^2 RT rR Sin[phi0]) / kk1 Hb + (4 lambda^3 RT rR^2) / kk1 Mb;
eq1 = Wn0 == Wv;
eq2 = theta_n0 == -theta_v;
sol = Simplify[Solve[{eq1, eq2}, {Qb, Mb}]];

```

Stresses in the Nozzle

```

Mbx = -Dbn D[Wn, {xb, 2}];
Mbtheta = v Mbx;
sigma_out = rt / RT + 12 Mbx rt^2 / RT;
sigma_in = rt / RT - 12 Mbx rt^2 / RT;
sigma_out_theta = 2 rt / RT + 2 WnFM / RT + 12 Mbtheta rt^2 / RT;
sigma_in_theta = 2 rt / RT + 2 WnFM / RT - 12 Mbtheta rt^2 / RT;

```

```

xb1 = -0.5;
Do[s1[i, j, k] =  $\sigma_{hout}$  /. sol[[1]] /.  $\mathbf{x}b \rightarrow -\mathbf{x}b$  /.  $\mathbf{rt} \rightarrow (\mathbf{rRRT} / \mathbf{tT})$  /.
  {tT  $\rightarrow$  tT1[[i]], RT  $\rightarrow$  RT1[[j]], rR  $\rightarrow$  rR1[[k]], pb  $\rightarrow$  1},
  {i, 1, i1}, {j, 1, j1}, {k, 1, k1}]
Do[p1[i, j, k] = Plot[s1[i, j, k], {xb, 0, xb1}, AxesOrigin  $\rightarrow$  {0, 0}, PlotRange  $\rightarrow$  All,
  PlotStyle  $\rightarrow$  {Darker[Green, 0.4]}], {i, 1, i1}, {j, 1, j1}, {k, 1, k1}]
Do[s2[i, j, k] =  $\sigma_{hin}$  /. sol[[1]] /.  $\mathbf{x}b \rightarrow -\mathbf{x}b$  /.  $\mathbf{rt} \rightarrow (\mathbf{rRRT} / \mathbf{tT})$  /.
  {tT  $\rightarrow$  tT1[[i]], RT  $\rightarrow$  RT1[[j]], rR  $\rightarrow$  rR1[[k]], pb  $\rightarrow$  1},
  {i, 1, i1}, {j, 1, j1}, {k, 1, k1}]
Do[p2[i, j, k] = Plot[s2[i, j, k], {xb, 0, xb1}, AxesOrigin  $\rightarrow$  {0, 0}, PlotRange  $\rightarrow$  All,
  PlotStyle  $\rightarrow$  {Darker[Green, 0.5], Dashed}], {i, 1, i1}, {j, 1, j1}, {k, 1, k1}]
Do[s3[i, j, k] =  $\sigma_{xout}$  /. sol[[1]] /.  $\mathbf{x}b \rightarrow -\mathbf{x}b$  /.  $\mathbf{rt} \rightarrow (\mathbf{rRRT} / \mathbf{tT})$  /.
  {tT  $\rightarrow$  tT1[[i]], RT  $\rightarrow$  RT1[[j]], rR  $\rightarrow$  rR1[[k]], pb  $\rightarrow$  1},
  {i, 1, i1}, {j, 1, j1}, {k, 1, k1}]
Do[p3[i, j, k] = Plot[s3[i, j, k], {xb, 0, xb1}, AxesOrigin  $\rightarrow$  {0, 0}, PlotRange  $\rightarrow$  All,
  PlotStyle  $\rightarrow$  {Lighter[Blue, 0.4]}], {i, 1, i1}, {j, 1, j1}, {k, 1, k1}]
Do[s4[i, j, k] =  $\sigma_{xin}$  /. sol[[1]] /.  $\mathbf{x}b \rightarrow -\mathbf{x}b$  /.  $\mathbf{rt} \rightarrow (\mathbf{rRRT} / \mathbf{tT})$  /.
  {tT  $\rightarrow$  tT1[[i]], RT  $\rightarrow$  RT1[[j]], rR  $\rightarrow$  rR1[[k]], pb  $\rightarrow$  1},
  {i, 1, i1}, {j, 1, j1}, {k, 1, k1}]
Do[p4[i, j, k] = Plot[s4[i, j, k], {xb, 0, xb1}, AxesOrigin  $\rightarrow$  {0, 0}, PlotRange  $\rightarrow$  All,
  PlotStyle  $\rightarrow$  {Lighter[Blue, 0.5], Dashed}], {i, 1, i1}, {j, 1, j1}, {k, 1, k1}]
Do[pn[i, j, k] = Show[p1[i, j, k], p2[i, j, k], p3[i, j, k], p4[i, j, k]],
  {i, 1, i1}, {j, 1, j1}, {k, 1, k1}]

```

Stresses in the Spherical Vessel

$\psi = .$;

$\mathbf{rT} = \mathbf{rRRT}$;

$\phi = \psi + \phi_0$;

$$\lambda = \left(3 \left(1 - \nu^2 \right) \right)^{1/4} \sqrt{\mathbf{RT}};$$

$$\mathbf{K1} = 1 + \left((1 - 2\nu) / (2\lambda) \right) \text{Cot}[\phi_0 + \psi];$$

$$\mathbf{K2} = 1 + \left((1 + 2\nu) / (2\lambda) \right) \text{Cot}[\phi_0 + \psi];$$

$$\gamma_1 = 0;$$

$$\gamma_2 = -\text{ArcCos}\left[\frac{1}{\sqrt{1 + \mathbf{k}k_1^2}}\right];$$

$$\mathbf{N}\phi\mathbf{b} = \text{Cot}[\phi] \left(\frac{2\lambda \sqrt{\text{Sin}[\phi_0]}}{\mathbf{k}k_1} \mathbf{Mb} \mathbf{rR} \right) \frac{e^{-\lambda \psi}}{\sqrt{\text{Sin}[\phi]}} \text{Sin}[\gamma_1 + \lambda \psi] +$$

$$\begin{aligned}
& \text{Cot}[\phi] \left(\frac{\text{Sin}[\phi 0] \sqrt{\text{Sin}[\phi 0]} \sqrt{1 + \text{kk}1^2}}{\text{kk}1} \text{Hb} \right) \frac{e^{-\lambda \psi}}{\sqrt{\text{Sin}[\phi]}} \text{Sin}[\gamma 2 + \lambda \psi]; \\
\text{N}\theta\text{b} = & \left(\frac{2 \lambda \sqrt{\text{Sin}[\phi 0]}}{\text{kk}1} \text{Mb rR} \right) \frac{\lambda e^{-\lambda \psi}}{2 \sqrt{\text{Sin}[\phi]}} (2 \text{Cos}[\gamma 1 + \lambda \psi] - (\text{K}1 + \text{K}2) \text{Sin}[\gamma 1 + \lambda \psi]) + \\
& \left(\frac{\text{Sin}[\phi 0] \sqrt{\text{Sin}[\phi 0]} \sqrt{1 + \text{kk}1^2}}{\text{kk}1} \text{Hb} \right) \frac{\lambda e^{-\lambda \psi}}{2 \sqrt{\text{Sin}[\phi]}} \\
& (2 \text{Cos}[\gamma 2 + \lambda \psi] - (\text{K}1 + \text{K}2) \text{Sin}[\gamma 2 + \lambda \psi]); \\
\text{M}\phi\text{b} = & \left(\left(\frac{\sqrt{\text{Sin}[\phi 0]}}{\text{kk}1} \text{Mb} \right) \frac{e^{-\lambda \psi}}{\sqrt{\text{Sin}[\phi]}} (\text{K}1 \text{Cos}[\gamma 1 + \lambda \psi] + \text{Sin}[\gamma 1 + \lambda \psi]) + \right. \\
& \left. \left(\frac{\text{Sin}[\phi 0] \sqrt{\text{Sin}[\phi 0]} \sqrt{1 + \text{kk}1^2}}{\text{kk}1 \text{rR}} \text{Hb} \right) \frac{e^{-\lambda \psi}}{2 \lambda \sqrt{\text{Sin}[\phi]}} (\text{K}1 \text{Cos}[\gamma 2 + \lambda \psi] + \text{Sin}[\gamma 2 + \lambda \psi]) \right); \\
\text{M}\theta\text{b} = & \left(\left(\frac{\sqrt{\text{Sin}[\phi 0]}}{\text{kk}1} \text{Mb} \right) \frac{e^{-\lambda \psi}}{2 \nu \sqrt{\text{Sin}[\phi]}} ((\text{K}1 + \text{K}2) (1 + \nu^2) - 2 \text{K}2) \text{Cos}[\gamma 1 + \lambda \psi] + \right. \\
& 2 \nu^2 \text{Sin}[\gamma 1 + \lambda \psi]) + \left(\frac{\text{Sin}[\phi 0] \sqrt{\text{Sin}[\phi 0]} \sqrt{1 + \text{kk}1^2}}{\text{kk}1 \text{rR}} \text{Hb} \right) \frac{e^{-\lambda \psi}}{4 \nu \lambda \sqrt{\text{Sin}[\phi]}} \\
& ((\text{K}1 + \text{K}2) (1 + \nu^2) - 2 \text{K}2) \text{Cos}[\gamma 2 + \lambda \psi] + 2 \nu^2 \text{Sin}[\gamma 2 + \lambda \psi] \Big); \\
\delta\text{b} = & \text{RT rR Sin}[\phi] \left(\frac{2 \lambda \sqrt{\text{Sin}[\phi 0]}}{\text{kk}1} \text{Mb} \right) \frac{\lambda e^{-\lambda \psi}}{\sqrt{\text{Sin}[\phi]}} (\text{Cos}[\gamma 1 + \lambda \psi] - \text{K}2 \text{Sin}[\gamma 1 + \lambda \psi]) + \\
& \text{RT Sin}[\phi] \left(\frac{\text{Sin}[\phi 0] \sqrt{\text{Sin}[\phi 0]} \sqrt{1 + \text{kk}1^2}}{\text{kk}1} \text{Hb} \right) \\
& \frac{\lambda e^{-\lambda \psi}}{\sqrt{\text{Sin}[\phi]}} (\text{Cos}[\gamma 2 + \lambda \psi] - \text{K}2 \text{Sin}[\gamma 2 + \lambda \psi]); \\
\sigma\phi\text{out} = & (2 / (\text{pb RT})) ((\text{pb RT} / 2) + \text{N}\phi\text{b rT} - (6 \text{M}\phi\text{b rT}^2)); \\
\sigma\phi\text{in} = & (2 / (\text{pb RT})) ((\text{pb RT} / 2) + \text{N}\phi\text{b rT} + (6 \text{M}\phi\text{b rT}^2)); \\
\sigma\theta\text{out} = & (2 / (\text{pb RT})) ((\text{pb RT} / 2) + \text{N}\theta\text{b rT} - (6 \text{M}\theta\text{b rT}^2)); \\
\sigma\theta\text{in} = & (2 / (\text{pb RT})) ((\text{pb RT} / 2) + \text{N}\theta\text{b rT} + (6 \text{M}\theta\text{b rT}^2));
\end{aligned}$$

```

ψ1 = 0.5;
Do[S1[i, j, k] = σθout /. sol[[1]] /. rt → (rR RT / tT) /.
  {tT → tT1[[i]], RT → RT1[[j]], rR → rR1[[k]], pb → 1},
  {i, 1, i1}, {j, 1, j1}, {k, 1, k1}]
Do[P1[i, j, k] = Plot[S1[i, j, k], {ψ, 0, ψ1}, AxesOrigin → {0, 0}, PlotRange → All,
  PlotStyle → {Darker[Green, 0.4]}], {i, 1, i1}, {j, 1, j1}, {k, 1, k1}]
Do[S2[i, j, k] = σθin /. sol[[1]] /. rt → (rR RT / tT) /.
  {tT → tT1[[i]], RT → RT1[[j]], rR → rR1[[k]], pb → 1},
  {i, 1, i1}, {j, 1, j1}, {k, 1, k1}]
Do[P2[i, j, k] = Plot[S2[i, j, k], {ψ, 0, ψ1}, AxesOrigin → {0, 0}, PlotRange → All,
  PlotStyle → {Darker[Green, 0.5], Dashed}], {i, 1, i1}, {j, 1, j1}, {k, 1, k1}]

Do[S3[i, j, k] = σφout /. sol[[1]] /. rt → (rR RT / tT) /.
  {tT → tT1[[i]], RT → RT1[[j]], rR → rR1[[k]], pb → 1},
  {i, 1, i1}, {j, 1, j1}, {k, 1, k1}]
Do[P3[i, j, k] = Plot[S3[i, j, k], {ψ, 0, ψ1}, AxesOrigin → {0, 0}, PlotRange → All,
  PlotStyle → {Lighter[Blue, 0.4]}], {i, 1, i1}, {j, 1, j1}, {k, 1, k1}]
Do[S4[i, j, k] = σφin /. sol[[1]] /. rt → (rR RT / tT) /.
  {tT → tT1[[i]], RT → RT1[[j]], rR → rR1[[k]], pb → 1},
  {i, 1, i1}, {j, 1, j1}, {k, 1, k1}]
Do[P4[i, j, k] = Plot[S4[i, j, k], {ψ, 0, ψ1}, AxesOrigin → {0, 0}, PlotRange → All,
  PlotStyle → {Lighter[Blue, 0.5], Dashed}], {i, 1, i1}, {j, 1, j1}, {k, 1, k1}]

Do[pv[i, j, k] = Show[P1[i, j, k], P2[i, j, k], P3[i, j, k], P4[i, j, k]],
  {i, 1, i1}, {j, 1, j1}, {k, 1, k1}]

(*Example on plotting stress variations in both the spherical vessel and
cylindrical nozzle for various combinations of the geometric ratios*)
Needs["PlotLegends`"]
legend0 =
  {{{Graphics[{Darker[Green, 0.4], Thick, Line[{{0, 0}, {1, 0}}]}], "Hoop +"},
   {Graphics[{Darker[Green, 0.5], Dashed, Line[{{0, 0}, {1, 0}}]}], "Hoop -"},
   {Graphics[{Lighter[Blue, 0.4], Thick, Line[{{0, 0}, {1, 0}}]}],
    "Axial/Mer. +"}, {Graphics[
    {Lighter[Blue, 0.5], Dashed, Line[{{0, 0}, {1, 0}}]}], "Axial/Mer. -"}],
  LegendSize → {0.7, 0.4}, LegendPosition → {0.15, 0.2}];
Table[{tT1[[i]], RT1[[j]], rR1[[k]], ShowLegend[
  Show[pn[i, j, k], pv[i, j, k], TicksStyle → Directive[12], AxesLabel →
    {Style["←(-x̄)/ψ→", FontSize → 14, Bold], Style[σ, FontSize → 14, Bold]}],
  legend0}], {i, 1, i1}, {j, 1, j1}, {k, 1, k1}]

```

Types & Location of Maximum stresses

```

Do[test[i, j, k] =
  Position[{S1[i, j, k], S3[i, j, k], s1[i, j, k], s3[i, j, k]} /. {ψ → 0, xb → 0},
    Max[{S1[i, j, k], S3[i, j, k], s1[i, j, k], s3[i, j, k]} /. {ψ → 0, xb → 0}]],
  {i, 1, i1}, {j, 1, j1}, {k, 1, k1}]

Do[If[test[i, j, k] == {{1}}, Print["RT=", RT1[[j]], " ", "rR1=",
  rR1[[k]], " ", "tT1=", tT1[[i]], " ", "hoop out in vessel",
  " ", S1[i, j, k] /. {ψ → 0, xb → 0}], If[test[i, j, k] == {{2}},
  Print["RT=", RT1[[j]], " ", "rR1=", rR1[[k]], " ", "tT1=", tT1[[i]],
  " ", "meridional out in vessel", " ", S3[i, j, k] /. {ψ → 0, xb → 0}],
  If[test[i, j, k] == {{3}}, Print["RT=", RT1[[j]], " ", "rR1=",
  rR1[[k]], " ", "tT1=", tT1[[i]], " ", "hoop out in nozzle", " ",
  s1[i, j, k] /. {ψ → 0, xb → 0}], Print["RT=", RT1[[j]], " ", "rR1=",
  rR1[[k]], " ", "tT1=", tT1[[i]], " ", "axial out in nozzle", " ",
  s3[i, j, k] /. {ψ → 0, xb → 0}]]], {i, 1, i1}, {j, 1, j1}, {k, 1, k1}]

```

(*Sample output for the type and location of maximum stresses*)

```

RT=50  rR1=0.1  tT1=0.25  axial out in nozzle 6.86629
RT=50  rR1=0.3  tT1=0.25  axial out in nozzle 13.1373
RT=50  rR1=0.5  tT1=0.25  axial out in nozzle 16.6859
RT=75  rR1=0.1  tT1=0.25  axial out in nozzle 8.21347
RT=75  rR1=0.3  tT1=0.25  axial out in nozzle 16.0937
RT=75  rR1=0.5  tT1=0.25  axial out in nozzle 20.6399
RT=100 rR1=0.1  tT1=0.25  axial out in nozzle 9.3527
RT=100 rR1=0.3  tT1=0.25  axial out in nozzle 18.587
RT=100 rR1=0.5  tT1=0.25  axial out in nozzle 23.974

```

SCF in the Nozzle

```
Needs["PlotLegends`"]

legendn = {{Graphics[Black, Thick, Line[{{0, 0}, {1, 0}}]], "tT = 0.25"},
  {Graphics[Red, Thick, Line[{{0, 0}, {1, 0}}]], "tT = 0.5"},
  {Graphics[Green, Thick, Line[{{0, 0}, {1, 0}}]], "tT = 0.75"},
  {Graphics[Blue, Thick, Line[{{0, 0}, {1, 0}}]], "tT = 1.0"},
  {Graphics[Cyan, Thick, Line[{{0, 0}, {1, 0}}]], "tT = 1.25"},
  {Graphics[Magenta, Thick, Line[{{0, 0}, {1, 0}}]], "tT = 1.5"}},
  LegendSize -> {0.4, 0.4}, LegendPosition -> {-0.9, 0.08}};

color = {Black, Red, Green, Blue, Cyan, Magenta};

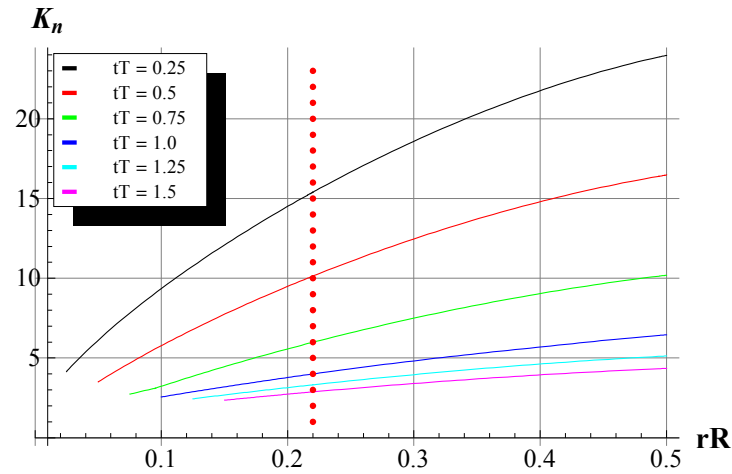
Do[omaxn[i, j] = Max[oxout, ohout] /. sol[[1]] /. xb -> 0 /. rt -> (rRRT / tT) /.
  {tT -> tT1[[i]], RT -> RT1[[j]], pb -> 1}, {i, 1, i1}, {j, 1, j1}]
Do[Pn1[i, j] = Plot[omaxn[i, j], {rR, rRmin1 /. {RT -> RT1[[j]], tT -> tT1[[i]]},
  rRmin2 /. {RT -> RT1[[j]], tT -> tT1[[i]]}, AxesOrigin -> {0.01, 0},
  GridLines -> Automatic, PlotStyle -> {color[[i]]}, {i, 1, i1}, {j, 1, j1}]
Do[Pn2[i, j] = Plot[omaxn[i, j], {rR, rRmin2 /. {RT -> RT1[[j]], tT -> tT1[[i]]}, 0.5},
  AxesOrigin -> {0.01, 0}, GridLines -> Automatic,
  PlotStyle -> {color[[i]]}, {i, 1, i1}, {j, 1, j1}]

(*rRmin2 limit plot*)

Do[Rmin2[j] =
  ListPlot[Table[{rRmin2 /. RT -> RT1[[j]], i}, {i, 1, omaxn[1, j] /. rR -> 0.5}],
  PlotStyle -> {Red, Dashed}], {j, 1, j1}]
Do[Rmin22[j] = ListPlot[Table[{-rRmin2 /. RT -> RT1[[j]], i},
  {i, 1, omaxn[1, j] /. rR -> 0.5}], PlotStyle -> {Red, Dashed}], {j, 1, j1}]

Do[
  Pn[j] = ShowLegend[Show[{Join[Table[{Pn1[i, j], Pn2[i, j]}, {i, 1, i1}]], Rmin2[j]},
  TicksStyle -> Directive[12], AxesLabel -> {Style["rR", FontSize -> 14, Bold],
  Style[Kn, FontSize -> 14, Bold]}, PlotRange -> All], legendn, {j, 1, j1}]
```

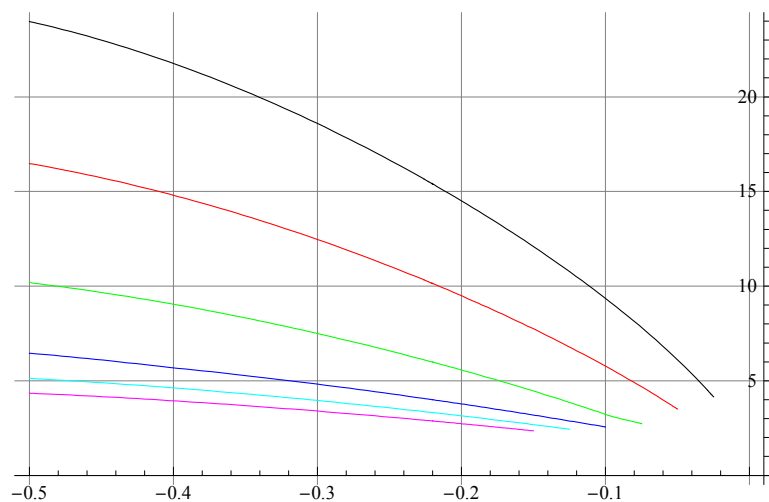

Pn[3]



```
(*Example on plotting the nozzle SCF on the left side of the grids*)
Do[omaxn[i, j] = Max[oxout, ohout] /. sol[[1]] /. xb -> 0 /. rt -> (rRRT / tT) /.
  {tT -> tT1[[i]], RT -> RT1[[j]], pb -> 1} /. {rR -> -rR}, {i, 1, i1}, {j, 1, j1}]
Do[Pn1[i, j] = Plot[omaxn[i, j], {rR, -rRmin1 /. {RT -> RT1[[j]], tT -> tT1[[i]]},
  -rRmin2 /. {RT -> RT1[[j]], tT -> tT1[[i]]}], AxesOrigin -> {0.01, 0},
  GridLines -> Automatic, PlotStyle -> {color[[i]]}, {i, 1, i1}, {j, 1, j1}]
Do[Pn2[i, j] = Plot[omaxn[i, j], {rR, -rRmin2 /. {RT -> RT1[[j]], tT -> tT1[[i]]},
  -0.5}, AxesOrigin -> {-0.01, 0}, GridLines -> Automatic,
  PlotStyle -> {color[[i]]}, {i, 1, i1}, {j, 1, j1}]

Do[Pn[j] = Show[{Join[Table[{Pn1[i, j], Pn2[i, j]}, {i, 1, i1}]}], PlotRange -> All],
  {j, 1, j1}]
```

Show[Pn[3]]



SCF in the Vessel

```

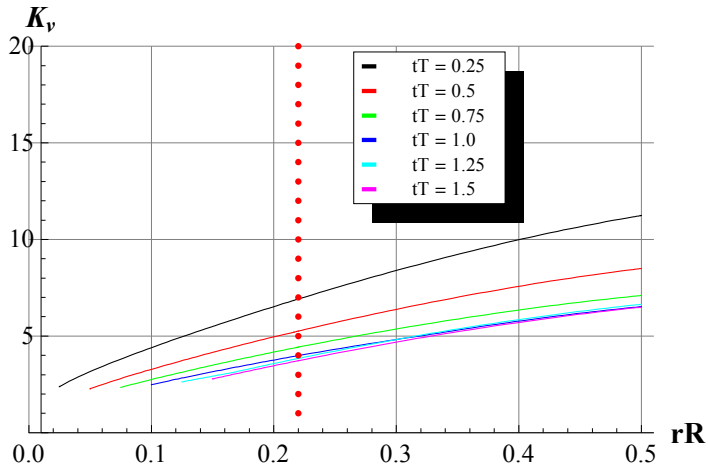
legendv = {{Graphics[{Black, Thick, Line[{0, 0}, {1, 0}]}], "tT = 0.25"},
  {Graphics[{Red, Thick, Line[{0, 0}, {1, 0}]}], "tT = 0.5"},
  {Graphics[{Green, Thick, Line[{0, 0}, {1, 0}]}], "tT = 0.75"},
  {Graphics[{Blue, Thick, Line[{0, 0}, {1, 0}]}], "tT = 1.0"},
  {Graphics[{Cyan, Thick, Line[{0, 0}, {1, 0}]}], "tT = 1.25"},
  {Graphics[{Magenta, Thick, Line[{0, 0}, {1, 0}]}], "tT = 1.5"}},
LegendSize -> {0.4, 0.4}, LegendPosition -> {-0.09, 0.08};

Do[omaxv[i, j] = Max[σθout, σφout] /. sol[[1]] /. ψ -> 0 /. rt -> (rR RT / tT) /.
  {tT -> tT1[[i]], RT -> RT1[[j]], pb -> 1}, {i, 1, i1}, {j, 1, j1}]
Do[Pv1[i, j] = Plot[omaxv[i, j], {rR, rRmin1 /. {RT -> RT1[[j]], tT -> tT1[[i]]},
  rRmin2 /. {RT -> RT1[[j]], tT -> tT1[[i]]}}, AxesOrigin -> {0.01, 0},
  GridLines -> Automatic, PlotStyle -> {color[[i]]},
  PlotRange -> {0, 20}], {i, 1, i1}, {j, 1, j1}]
Do[Pv2[i, j] = Plot[omaxv[i, j], {rR, rRmin2 /. {RT -> RT1[[j]], tT -> tT1[[i]]}, 0.5},
  AxesOrigin -> {0.01, 0}, GridLines -> Automatic,
  PlotStyle -> {color[[i]]}, PlotRange -> {0, 20}], {i, 1, i1}, {j, 1, j1}]
Do[Pv[j] = ShowLegend[Show[{Join[Table[{Pv1[i, j], Pv2[i, j]}, {i, 1, i1}]],
  Rmin2[j]], TicksStyle -> Directive[12],
  AxesLabel -> {Style["rR", FontSize -> 14, Bold], Style[Kv, FontSize -> 14, Bold]},
  PlotRange -> {{0.01, 0.5}, {0, 20}}], legendv], {j, 1, j1}]

```

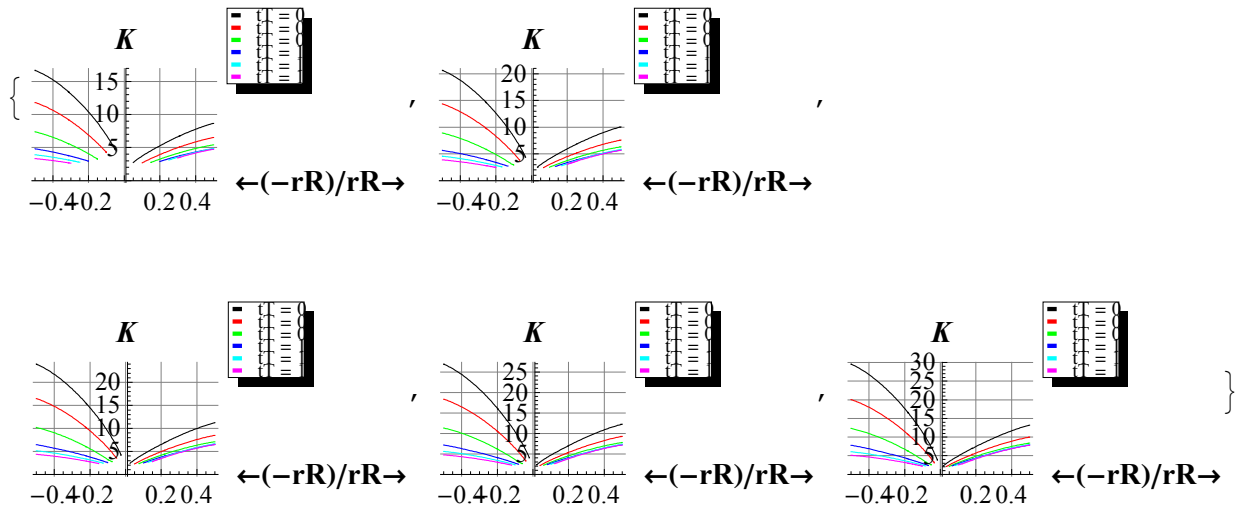
(*Example on plotting the vessel SCF*)

Pv[3]



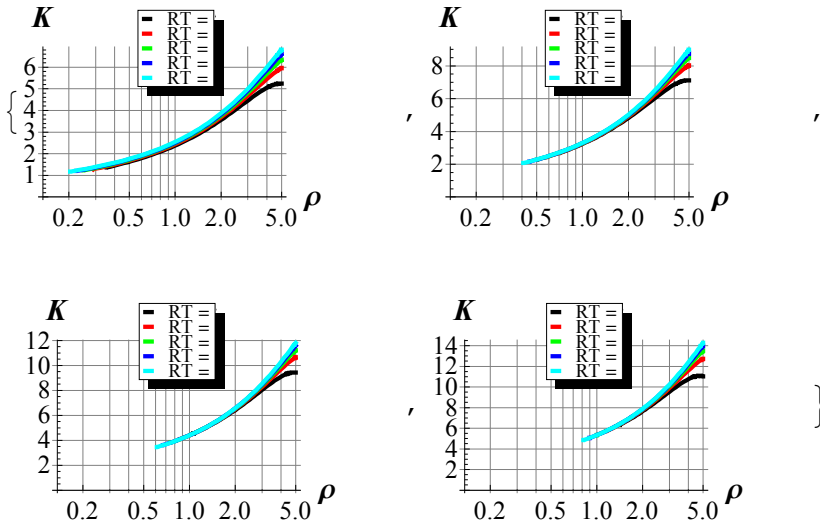
```
(*Combined plots for RT ratios ranging from 50 to 150 at intervals of 25*)
Do[Pv[j] = Show[Join[Table[{Pv1[i, j], Pv2[i, j]}, {i, 1, i1}]]],
  PlotRange -> {{0.01, 0.5}, {0, 20}}, {j, 1, j1}]
Needs["PlotLegends`"]
legend = {{Graphics[{Black, Thick, Line[{{0, 0}, {1, 0}}]}], "tT = 0.25"},
  {Graphics[{Red, Thick, Line[{{0, 0}, {1, 0}}]}], "tT = 0.5"},
  {Graphics[{Green, Thick, Line[{{0, 0}, {1, 0}}]}], "tT = 0.75"},
  {Graphics[{Blue, Thick, Line[{{0, 0}, {1, 0}}]}], "tT = 1.0"},
  {Graphics[{Cyan, Thick, Line[{{0, 0}, {1, 0}}]}], "tT = 1.25"},
  {Graphics[{Magenta, Thick, Line[{{0, 0}, {1, 0}}]}], "tT = 1.5"}},
  LegendSize -> {0.4, 0.4}, LegendPosition -> {0.05, 0.08}};

Table[ShowLegend[Show[Pn[j], Pv[j], TicksStyle -> Directive[12],
  AxesLabel -> {Style[" $\leftarrow(-rR)/rR\rightarrow$ ", FontSize -> 14, Bold],
    Style[K, FontSize -> 14, Bold]}], legend], {j, 1, j1}]
```



Prove for Non-uniqueness of Leckie & Penny's ρ - SCF curves

```
Needs["PlotLegends`"]
legend $\rho$  = {{Graphics[{Black, Thick, Line[{0, 0}, {1, 0}]}]}, "RT = 50"},
  {Graphics[{Red, Thick, Line[{0, 0}, {1, 0}]}]}, "RT = 75"},
  {Graphics[{Green, Thick, Line[{0, 0}, {1, 0}]}]}, "RT = 100"},
  {Graphics[{Blue, Thick, Line[{0, 0}, {1, 0}]}]}, "RT = 125"},
  {Graphics[{Cyan, Thick, Line[{0, 0}, {1, 0}]}]}, "RT = 150"}},
  LegendSize  $\rightarrow$  {0.4, 0.4}, LegendPosition  $\rightarrow$  {-0.4, 0.15}};
color2 = {Black, Red, Green, Blue, Cyan};
 $\gamma$  = {1, 0.5, 0.25, 0.0001};
Do[ $\sigma_{\max 2}[i, j] = \sigma_{\theta \text{out}} /. \text{sol}[[1]] /. \psi \rightarrow 0 /. \{rt \rightarrow rR RT / tT\} /. \{RT \rightarrow RT1[[j]], tT \rightarrow \gamma[[i]], pb \rightarrow 1\}, \{i, 1, 4\}, \{j, 1, j1\}$ 
Do[PV[i, j] = LogLinearPlot[ $\sigma_{\max 2}[i, j] /. \{rR \rightarrow \frac{\rho}{\sqrt{RT1[[j]]}}\}, \{\rho, (rR_{\min 1} \sqrt{RT}) /. \{tT \rightarrow tT1[[i]], RT \rightarrow RT1[[j]]\}, 5\}, \text{AxesOrigin} \rightarrow \{-2, 0\}, \text{GridLines} \rightarrow \text{Automatic}, \text{Ticks} \rightarrow \text{Automatic}, \text{PlotStyle} \rightarrow \{\text{color2}[[j]], \text{Thick}\}, \text{PlotRange} \rightarrow \text{All}], \{i, 1, 4\}, \{j, 1, j1\}$ 
Table[ShowLegend[Show[Table[PV[i, j], {j, 1, j1}], PlotRange  $\rightarrow$  All, AxesOrigin  $\rightarrow$  {-2, 0}, TicksStyle  $\rightarrow$  Directive[12], AxesLabel  $\rightarrow$  {Style[" $\rho$ ", FontSize  $\rightarrow$  14, Bold], Style[K, FontSize  $\rightarrow$  14, Bold]}], legend $\rho$ ], {i, 1, 4}]
```



APPENDIX B:

BEHAVIOUR OF THE MEMBRANE STRESSES IN SPHERICAL VESSEL-CYLINDRICAL NOZZLE JUNCTURES

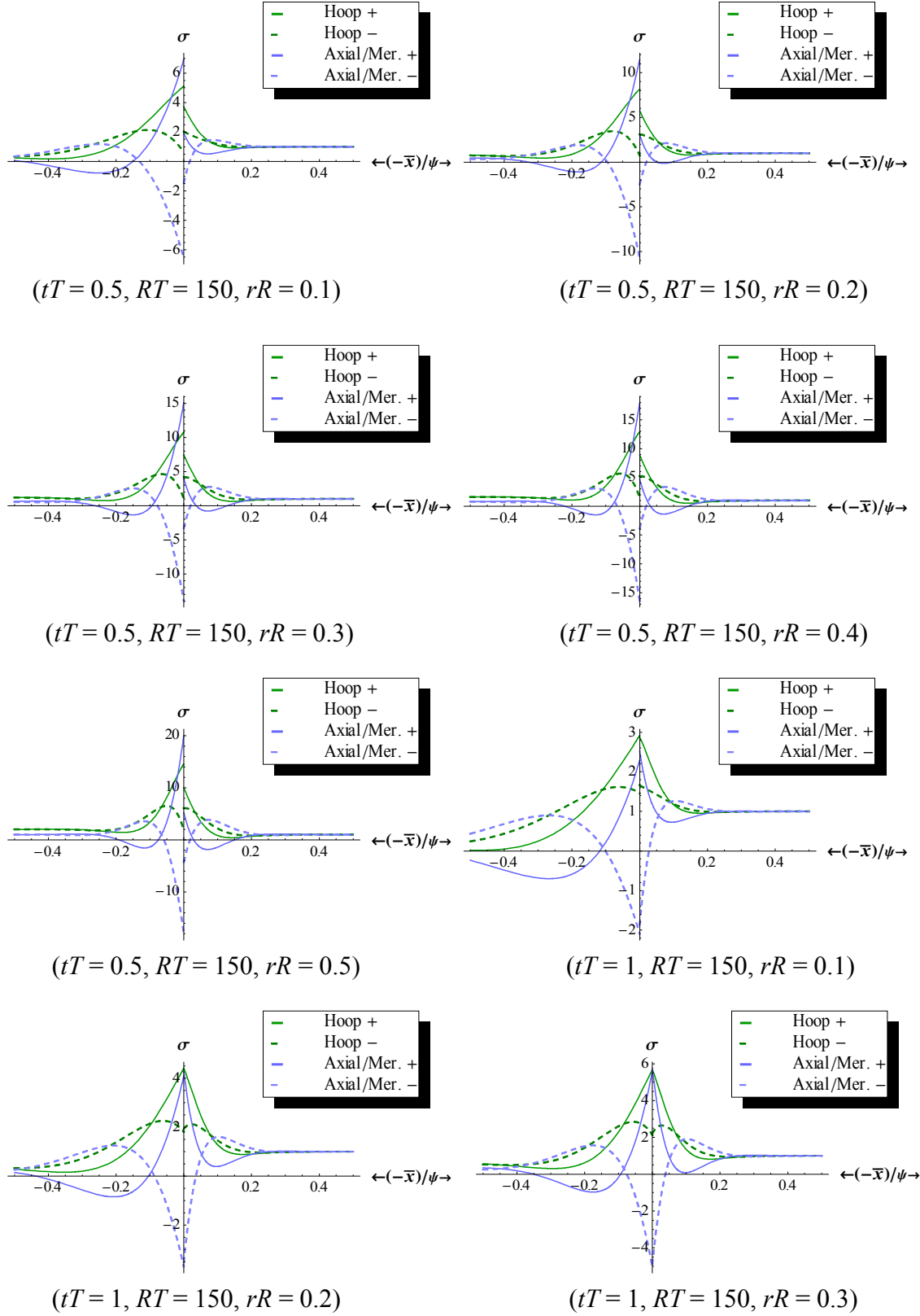
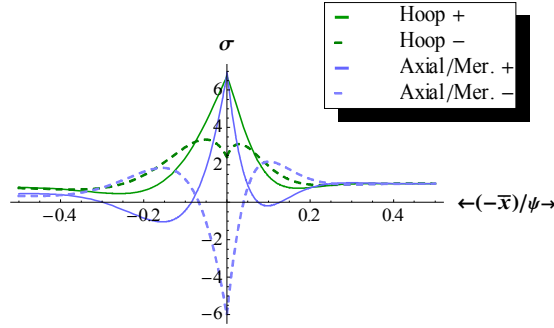
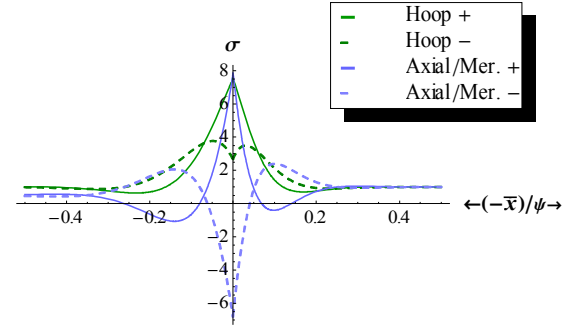


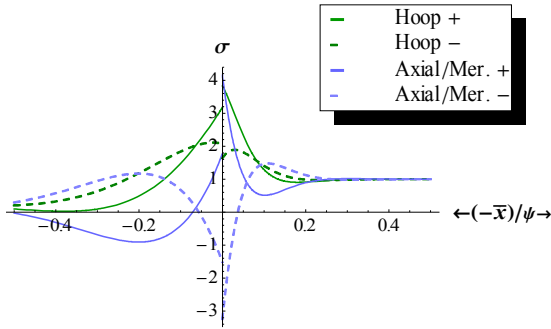
Figure B1: Variation in the Location of the Maximum Stresses for Different Selected Geometric Ratios



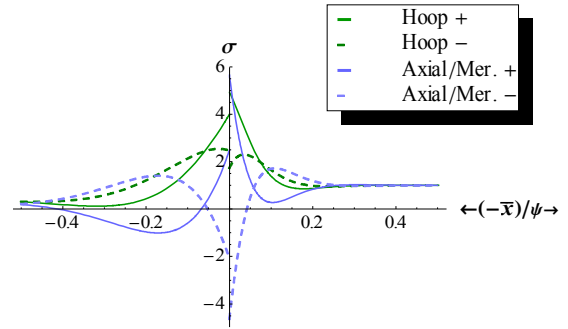
$(tT = 1, RT = 150, rR = 0.4)$



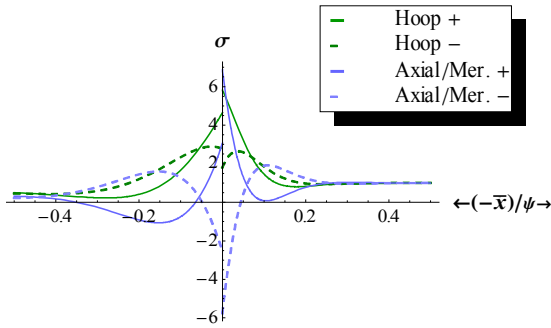
$(tT = 1, RT = 150, rR = 0.5)$



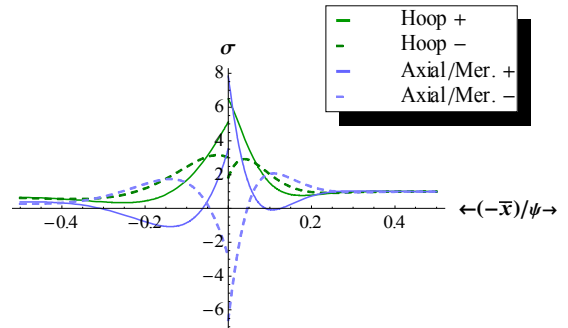
$(tT = 1.5, RT = 150, rR = 0.2)$



$(tT = 1.5, RT = 150, rR = 0.3)$



$(tT = 1.5, RT = 150, rR = 0.4)$



$(tT = 1.5, RT = 150, rR = 0.5)$

Figure B1 (Cont'd): Variation in the Location of the Maximum Stresses for Different Selected Geometric Ratios

APPENDIX C:

FINITE ELEMENT SOLUTION OF SCF FOR CASES WITH NO HANDY ANALYTICAL SOLUTIONS

Table C1: SCF Results for Cylindrical Vessels with Moderate-To-Large-Diameter Nozzles

RT	tT	rR	Cylindrical Vessel		Cylindrical Nozzle		Overall SCF	Location	Type
			SCF	Type	SCF	Type			
10	0.25	0.3	4.09	Hoop -	5.58	Axial -	5.58	Nozzle	Axial -
		0.4	4.90	Hoop -	7.20	Axial -	7.20	Nozzle	Axial -
		0.5	5.55	Hoop -	8.20	Axial -	8.20	Nozzle	Axial -
		0.6	6.29	Hoop -	9.56	Axial -	9.56	Nozzle	Axial -
		0.7	7.00	Hoop -	10.78	Axial -	10.78	Nozzle	Axial -
		0.8	7.52	Hoop -	11.47	Axial -	11.47	Nozzle	Axial -
		0.9	8.00	Hoop -	11.97	Axial -	11.97	Nozzle	Axial -
		1	8.50	Hoop +	11.85	Hoop -	11.85	Nozzle	Hoop -
	0.5	0.5	4.52	Hoop -	5.67	Hoop -	5.67	Nozzle	Hoop -
		0.6	5.14	Hoop -	6.49	Hoop -	6.49	Nozzle	Hoop -
		0.7	5.74	Hoop -	7.30	Axial -	7.30	Nozzle	Axial -
		0.8	6.21	Hoop -	7.93	Hoop -	7.93	Nozzle	Hoop -
		0.9	6.67	Hoop -	8.58	Hoop -	8.58	Nozzle	Hoop -
		1	6.94	Hoop -	8.97	Hoop -	8.97	Nozzle	Hoop -
	0.75	0.8	5.23	Hoop -	5.81	Hoop -	5.81	Nozzle	Hoop -
		0.9	5.64	Hoop -	6.31	Hoop -	6.31	Nozzle	Hoop -
		1	5.94	Hoop -	6.67	Hoop -	6.67	Nozzle	Hoop -
	1	1	5.19	Hoop -	5.14	Hoop -	5.19	Vessel	Hoop -
15	0.25	0.2	3.65	Hoop -	5.16	Axial -	5.16	Nozzle	Axial -
		0.3	4.69	Hoop -	7.35	Axial -	7.35	Nozzle	Axial -
		0.4	5.72	Hoop -	9.45	Axial -	9.45	Nozzle	Axial -
		0.5	6.53	Hoop -	10.73	Axial -	10.73	Nozzle	Axial -
		0.6	7.47	Hoop -	12.52	Axial -	12.52	Nozzle	Axial -
		0.7	8.38	Hoop -	14.15	Axial -	14.15	Nozzle	Axial -
		0.8	9.09	Hoop -	15.16	Axial -	15.16	Nozzle	Axial -
		0.9	9.83	Hoop -	16.08	Axial -	16.08	Nozzle	Axial -
		1	10.22	Hoop -	15.55	Axial -	15.55	Nozzle	Axial -
	0.5	0.4	4.58	Hoop -	6.15	Axial -	6.15	Nozzle	Axial -
		0.5	5.25	Hoop -	7.17	Axial -	7.17	Nozzle	Axial -
		0.6	5.99	Hoop -	8.39	Axial -	8.39	Nozzle	Axial -
		0.7	6.73	Hoop -	9.53	Axial -	9.53	Nozzle	Axial -
		0.8	7.32	Hoop -	10.36	Axial -	10.36	Nozzle	Axial -
		0.9	7.98	Hoop -	11.13	Axial -	11.13	Nozzle	Axial -
		1	8.45	Hoop -	11.09	Axial -	11.09	Nozzle	Axial -
	0.75	0.5	4.40	Hoop -	4.91	Hoop -	4.91	Nozzle	Hoop -
		0.6	5.02	Hoop -	5.59	Hoop -	5.59	Nozzle	Hoop -

Table C1 (Cont'd): SCF Results for Cylindrical Vessels with Moderate-To-Large-Diameter Nozzles

RT	tT	rR	Cylindrical Vessel		Cylindrical Nozzle		Overall SCF	Location	Type
			SCF	Type	SCF	Type			
15	0.75	0.7	5.63	Hoop -	6.30	Hoop -	6.30	Nozzle	Hoop -
		0.8	6.12	Hoop -	6.88	Hoop -	6.88	Nozzle	Hoop -
		0.9	6.70	Hoop -	7.54	Hoop -	7.54	Nozzle	Hoop -
		1	7.15	Hoop -	8.06	Hoop -	8.06	Nozzle	Hoop -
	1	0.7	4.91	Hoop -	4.85	Hoop -	4.91	Vessel	Hoop -
		0.8	5.34	Hoop -	5.30	Hoop -	5.34	Vessel	Hoop -
		0.9	5.84	Hoop -	5.80	Hoop -	5.84	Vessel	Hoop -
		1	6.24	Hoop -	6.21	Hoop -	6.24	Vessel	Hoop -
	1.25	0.9	5.16	Hoop -	4.65	Hoop -	5.16	Vessel	Hoop -
		1	5.50	Hoop -	4.97	Hoop -	5.50	Vessel	Hoop -
	1.5	1	4.87	Hoop -	4.08	Hoop -	4.87	Vessel	Hoop -
20	0.25	0.2	4.00	Hoop -	6.21	Axial -	6.21	Nozzle	Axial -
		0.3	5.22	Hoop -	8.84	Axial -	8.84	Nozzle	Axial -
		0.4	6.40	Hoop -	11.27	Axial -	11.27	Nozzle	Axial -
		0.5	7.33	Hoop -	12.85	Axial -	12.85	Nozzle	Axial -
		0.6	8.41	Hoop -	14.96	Axial -	14.96	Nozzle	Axial -
		0.7	9.47	Hoop -	16.90	Axial -	16.90	Nozzle	Axial -
		0.8	10.34	Hoop -	18.28	Axial -	18.28	Nozzle	Axial -
		0.9	11.31	Hoop -	19.58	Axial -	19.58	Nozzle	Axial -
		1	11.98	Hoop -	19.44	Axial -	19.44	Nozzle	Axial -
	0.5	0.3	4.16	Hoop -	5.69	Axial -	5.69	Nozzle	Axial -
		0.4	5.09	Hoop -	7.38	Axial -	7.38	Nozzle	Axial -
		0.5	5.83	Hoop -	8.56	Axial -	8.56	Nozzle	Axial -
		0.6	6.66	Hoop -	9.98	Axial -	9.98	Nozzle	Axial -
		0.7	7.50	Hoop -	11.32	Axial -	11.32	Nozzle	Axial -
		0.8	8.18	Hoop -	12.33	Axial -	12.33	Nozzle	Axial -
		0.9	9.01	Hoop -	13.36	Axial -	13.36	Nozzle	Axial -
		1	9.69	Hoop -	13.41	Axial -	13.41	Nozzle	Axial -
	0.75	0.4	4.27	Hoop -	4.79	Hoop -	4.79	Nozzle	Hoop -
		0.5	4.88	Hoop -	5.48	Hoop -	5.48	Nozzle	Hoop -
		0.6	5.56	Hoop -	6.26	Hoop -	6.26	Nozzle	Hoop -
		0.7	6.26	Hoop -	7.07	Hoop -	7.07	Nozzle	Hoop -
		0.8	6.82	Hoop -	7.73	Hoop -	7.73	Nozzle	Hoop -
		0.9	7.52	Hoop -	8.53	Hoop -	8.53	Nozzle	Hoop -
		1	8.13	Hoop -	9.20	Hoop -	9.20	Nozzle	Hoop -
	1	0.5	4.29	Hoop -	4.25	Hoop -	4.29	Vessel	Hoop -

Table C1 (cont'd): SCF Results for Cylindrical Vessels with Moderate-To-Large-Diameter Nozzles

RT	tT	rR	Cylindrical Vessel		Cylindrical Nozzle		Overall SCF	Location	Type
			SCF	Type	SCF	Type			
20	1	0.6	4.87	Hoop -	4.83	Hoop -	4.87	Vessel	Hoop -
		0.7	5.47	Hoop -	5.44	Hoop -	5.47	Vessel	Hoop -
		0.8	5.96	Hoop -	5.94	Hoop -	5.96	Vessel	Hoop -
		0.9	6.56	Hoop -	6.55	Hoop -	6.56	Vessel	Hoop -
		1	7.09	Hoop -	7.08	Hoop -	7.09	Vessel	Hoop -
	1.25	0.7	4.88	Hoop -	4.41	Hoop -	4.88	Vessel	Hoop -
		0.8	5.31	Hoop -	4.81	Hoop -	5.31	Vessel	Hoop -
		0.9	5.83	Hoop -	5.28	Hoop -	5.83	Vessel	Hoop -
		1	6.27	Hoop -	5.69	Hoop -	6.27	Vessel	Hoop -
	1.5	0.8	4.76	Hoop -	4.01	Hoop -	4.76	Vessel	Hoop -
		0.9	5.20	Hoop -	4.39	Hoop -	5.20	Vessel	Hoop -
		1	5.57	Hoop -	4.70	Hoop -	5.57	Vessel	Hoop -
25	0.25	0.1	2.98	Hoop -	4.14	Axial -	4.14	Nozzle	Axial -
		0.2	4.31	Hoop -	7.12	Axial -	7.12	Nozzle	Axial -
		0.3	5.68	Hoop -	10.12	Axial -	10.12	Nozzle	Axial -
		0.4	6.97	Hoop -	12.86	Axial -	12.86	Nozzle	Axial -
		0.5	8.01	Hoop -	14.70	Axial -	14.70	Nozzle	Axial -
		0.6	9.20	Hoop -	17.06	Axial -	17.06	Nozzle	Axial -
		0.7	10.39	Hoop -	19.28	Axial -	19.28	Nozzle	Axial -
		0.8	11.40	Hoop -	20.99	Axial -	20.99	Nozzle	Axial -
		0.9	12.56	Hoop -	22.65	Axial -	22.65	Nozzle	Axial -
		1	13.51	Hoop -	22.96	Axial -	22.96	Nozzle	Axial -
	0.5	0.2	3.46	Hoop -	4.51	Axial -	4.51	Nozzle	Axial -
		0.3	4.51	Hoop -	6.56	Axial -	6.56	Nozzle	Axial -
		0.4	5.51	Hoop -	8.41	Axial -	8.41	Nozzle	Axial -
		0.5	6.32	Hoop -	9.75	Axial -	9.75	Nozzle	Axial -
		0.6	7.22	Hoop -	11.33	Axial -	11.33	Nozzle	Axial -
		0.7	8.14	Hoop -	12.83	Axial -	12.83	Nozzle	Axial -
		0.8	8.91	Hoop -	14.01	Axial -	14.01	Nozzle	Axial -
		0.9	9.87	Hoop -	15.27	Axial -	15.27	Nozzle	Axial -
		1	10.75	Hoop -	15.48	Axial -	15.48	Nozzle	Axial -
	0.75	0.3	3.80	Hoop -	4.28	Hoop -	4.28	Nozzle	Hoop -
		0.4	4.63	Hoop -	5.23	Hoop -	5.23	Nozzle	Hoop -
		0.5	5.28	Hoop -	5.97	Hoop -	5.97	Nozzle	Hoop -
		0.6	6.02	Hoop -	6.91	Axial -	6.91	Nozzle	Axial -
		0.7	6.78	Hoop -	7.87	Axial -	7.87	Nozzle	Axial -

Table C1 (cont'd): SCF Results for Cylindrical Vessels with Moderate-To-Large-Diameter Nozzles

RT	tT	rR	Cylindrical Vessel		Cylindrical Nozzle		Overall SCF	Location	Type
			SCF	Type	SCF	Type			
25	0.75	0.8	7.41	Hoop -	8.64	Axial -	8.64	Nozzle	Axial -
		0.9	8.21	Hoop -	9.47	Axial -	9.47	Nozzle	Axial -
		1	8.97	Hoop -	10.19	Hoop -	10.19	Nozzle	Hoop -
	1	0.4	4.08	Hoop -	4.06	Hoop -	4.08	Vessel	Hoop -
		0.5	4.65	Hoop -	4.62	Hoop -	4.65	Vessel	Hoop -
		0.6	5.29	Hoop -	5.26	Hoop -	5.29	Vessel	Hoop -
		0.7	5.95	Hoop -	5.94	Hoop -	5.95	Vessel	Hoop -
		0.8	6.49	Hoop -	6.49	Hoop -	6.49	Vessel	Hoop -
		0.9	7.18	Hoop -	7.18	Hoop -	7.18	Nozzle	Hoop -
		1	7.82	Hoop -	7.82	Hoop -	7.82	Vessel	Hoop -
	1.25	0.5	4.17	Hoop -	3.77	Hoop -	4.17	Vessel	Hoop -
		0.6	4.74	Hoop -	4.28	Hoop -	4.74	Vessel	Hoop -
		0.7	5.33	Hoop -	4.82	Hoop -	5.33	Vessel	Hoop -
		0.8	5.81	Hoop -	5.26	Hoop -	5.81	Vessel	Hoop -
		0.9	6.41	Hoop -	5.81	Hoop -	6.41	Vessel	Hoop -
		1	6.94	Hoop -	6.30	Hoop -	6.94	Vessel	Hoop -
	1.5	0.6	4.27	Hoop -	3.60	Hoop -	4.27	Vessel	Hoop -
		0.7	4.80	Hoop -	4.04	Hoop -	4.80	Vessel	Hoop -
		0.8	5.22	Hoop -	4.41	Hoop -	5.22	Vessel	Hoop -
		0.9	5.75	Hoop -	4.85	Hoop -	5.75	Vessel	Hoop -
		1	6.19	Hoop -	5.23	Hoop -	6.19	Vessel	Hoop -
30	0.25	0.1	3.12	Hoop -	4.61	Axial -	4.61	Nozzle	Axial -
		0.2	4.60	Hoop -	7.96	Axial -	7.96	Nozzle	Axial -
		0.3	6.08	Hoop -	11.26	Axial -	11.26	Nozzle	Axial -
		0.4	7.47	Hoop -	14.23	Axial -	14.23	Nozzle	Axial -
		0.5	8.61	Hoop -	16.33	Axial -	16.33	Nozzle	Axial -
		0.6	9.89	Hoop -	18.91	Axial -	18.91	Nozzle	Axial -
		0.7	11.19	Hoop -	21.37	Axial -	21.37	Nozzle	Axial -
		0.8	12.33	Hoop -	23.38	Axial -	23.38	Nozzle	Axial -
		0.9	13.65	Hoop -	25.37	Axial -	25.37	Nozzle	Axial -
		1	14.86	Hoop -	26.16	Axial -	26.16	Nozzle	Axial -
	0.5	0.2	3.68	Hoop -	5.07	Axial -	5.07	Nozzle	Axial -
		0.3	4.81	Hoop -	7.30	Axial -	7.30	Nozzle	Axial -
		0.4	5.88	Hoop -	9.32	Axial -	9.32	Nozzle	Axial -
		0.5	6.74	Hoop -	10.80	Axial -	10.80	Nozzle	Axial -
		0.6	7.71	Hoop -	12.51	Axial -	12.51	Nozzle	Axial -

Table C1 (cont'd): SCF Results for Cylindrical Vessels with Moderate-To-Large-Diameter Nozzles

RT	tT	rR	Cylindrical Vessel		Cylindrical Nozzle		Overall SCF	Location	Type
			SCF	Type	SCF	Type			
30	0.5	0.7	8.71	Hoop -	14.19	Axial -	14.19	Nozzle	Axial -
		0.8	9.56	Hoop -	15.49	Axial -	15.49	Nozzle	Axial -
		0.9	10.63	Hoop -	16.96	Axial -	16.96	Nozzle	Axial -
		1	11.68	Hoop -	17.31	Axial -	17.31	Nozzle	Axial -
	0.75	0.3	4.05	Hoop -	4.59	Hoop -	4.59	Nozzle	Hoop -
		0.4	4.94	Hoop -	5.61	Hoop -	5.61	Nozzle	Hoop -
		0.5	5.64	Hoop -	6.55	Axial -	6.55	Nozzle	Axial -
		0.6	6.43	Hoop -	7.64	Axial -	7.64	Nozzle	Axial -
		0.7	7.24	Hoop -	8.69	Axial -	8.69	Nozzle	Axial -
		0.8	7.93	Hoop -	9.55	Axial -	9.55	Nozzle	Axial -
		0.9	8.82	Hoop -	10.50	Axial -	10.50	Nozzle	Axial -
		1	9.71	Hoop -	11.08	Hoop -	11.08	Nozzle	Hoop -
	1	0.4	4.36	Hoop -	4.35	Hoop -	4.36	Vessel	Hoop -
		0.5	4.97	Hoop -	4.95	Hoop -	4.97	Vessel	Hoop -
		0.6	5.65	Hoop -	5.65	Hoop -	5.65	Vessel	Hoop -
		0.7	6.37	Hoop -	6.37	Hoop -	6.37	Nozzle	Hoop -
		0.8	6.96	Hoop -	6.97	Hoop -	6.97	Nozzle	Hoop -
		0.9	7.73	Hoop -	7.74	Hoop -	7.74	Nozzle	Hoop -
		1	8.47	Hoop -	8.48	Hoop -	8.48	Nozzle	Hoop -
	1.25	0.5	4.47	Hoop -	4.04	Hoop -	4.47	Vessel	Hoop -
		0.6	5.08	Hoop -	4.60	Hoop -	5.08	Vessel	Hoop -
		0.7	5.72	Hoop -	5.18	Hoop -	5.72	Vessel	Hoop -
		0.8	6.25	Hoop -	5.66	Hoop -	6.25	Vessel	Hoop -
		0.9	6.92	Hoop -	6.26	Hoop -	6.92	Vessel	Hoop -
		1	7.54	Hoop -	6.84	Hoop -	7.54	Vessel	Hoop -
	1.5	0.5	4.05	Hoop -	3.41	Hoop -	4.05	Vessel	Hoop -
		0.6	4.60	Hoop -	3.88	Hoop -	4.60	Vessel	Hoop -
		0.7	5.17	Hoop -	4.36	Hoop -	5.17	Vessel	Hoop -
		0.8	5.68	Axial -	4.76	Hoop -	5.68	Vessel	Axial -
		0.9	6.23	Hoop -	5.25	Hoop -	6.23	Vessel	Hoop -
		1	6.75	Hoop -	5.70	Hoop -	6.75	Vessel	Hoop -
35	0.25	0.1	3.25	Hoop -	5.04	Axial -	5.04	Nozzle	Axial -
		0.2	4.87	Hoop -	8.73	Axial -	8.73	Nozzle	Axial -
		0.3	6.44	Hoop -	12.29	Axial -	12.29	Nozzle	Axial -
		0.4	7.92	Hoop -	15.48	Axial -	15.48	Nozzle	Axial -
		0.5	9.13	Hoop -	17.80	Axial -	17.80	Nozzle	Axial -

Table C1 (cont'd): SCF Results for Cylindrical Vessels with Moderate-To-Large-Diameter Nozzles

RT	tT	rR	Cylindrical Vessel		Cylindrical Nozzle		Overall SCF	Location	Type
			SCF	Type	SCF	Type			
35	0.25	0.6	10.51	Hoop -	20.57	Axial -	20.57	Nozzle	Axial -
		0.7	11.90	Hoop -	23.18	Axial -	23.18	Nozzle	Axial -
		0.8	13.15	Hoop -	25.51	Axial -	25.51	Nozzle	Axial -
		0.9	14.62	Hoop -	27.77	Axial -	27.77	Nozzle	Axial -
		1	16.07	Hoop -	29.03	Axial -	29.03	Nozzle	Axial -
	0.5	0.2	3.88	Hoop -	5.58	Axial -	5.58	Nozzle	Axial -
		0.3	5.08	Hoop -	7.98	Axial -	7.98	Nozzle	Axial -
		0.4	6.21	Hoop -	10.13	Axial -	10.13	Nozzle	Axial -
		0.5	7.13	Hoop -	11.74	Axial -	11.74	Nozzle	Axial -
		0.6	8.15	Hoop -	13.57	Axial -	13.57	Nozzle	Axial -
		0.7	9.22	Hoop -	15.37	Axial -	15.37	Nozzle	Axial -
		0.8	10.13	Hoop -	16.83	Axial -	16.83	Nozzle	Axial -
		0.9	11.31	Hoop -	18.48	Axial -	18.48	Nozzle	Axial -
		1	12.51	Hoop -	18.97	Axial -	18.97	Nozzle	Axial -
	0.75	0.3	4.28	Hoop -	4.86	Hoop -	4.86	Nozzle	Hoop -
		0.4	5.22	Hoop -	6.10	Axial -	6.10	Nozzle	Axial -
		0.5	5.95	Hoop -	7.11	Axial -	7.11	Nozzle	Axial -
		0.6	6.79	Hoop -	8.28	Axial -	8.28	Nozzle	Axial -
		0.7	7.66	Hoop -	9.42	Axial -	9.42	Nozzle	Axial -
		0.8	8.40	Hoop -	10.36	Axial -	10.36	Nozzle	Axial -
		0.9	9.37	Hoop -	11.43	Axial -	11.43	Nozzle	Axial -
		1	10.39	Hoop -	11.88	Hoop -	11.88	Nozzle	Hoop -
	1	0.3	3.80	Hoop -	3.80	Hoop -	3.80	Vessel	Hoop -
		0.4	4.62	Hoop -	4.61	Hoop -	4.62	Vessel	Hoop -
		0.5	5.25	Hoop -	5.25	Hoop -	5.25	Vessel	Hoop -
		0.6	5.98	Hoop -	5.99	Hoop -	5.99	Nozzle	Hoop -
		0.7	6.74	Hoop -	6.76	Hoop -	6.76	Nozzle	Hoop -
		0.8	7.39	Hoop -	7.40	Hoop -	7.40	Nozzle	Hoop -
		0.9	8.22	Hoop -	8.24	Hoop -	8.24	Nozzle	Hoop -
		1	9.07	Hoop -	9.07	Hoop -	9.07	Nozzle	Hoop -
	1.25	0.4	4.17	Hoop -	3.77	Hoop -	4.17	Vessel	Hoop -
		0.5	4.74	Hoop -	4.28	Hoop -	4.74	Vessel	Hoop -
		0.6	5.39	Hoop -	4.88	Hoop -	5.39	Vessel	Hoop -
		0.7	6.08	Hoop -	5.49	Hoop -	6.08	Vessel	Hoop -
		0.8	6.65	Hoop -	6.01	Hoop -	6.65	Vessel	Hoop -
		0.9	7.39	Hoop -	6.67	Hoop -	7.39	Vessel	Hoop -

Table C1 (cont'd): SCF Results for Cylindrical Vessels with Moderate-To-Large-Diameter Nozzles

RT	tT	rR	Cylindrical Vessel		Cylindrical Nozzle		Overall SCF	Location	Type
			SCF	Type	SCF	Type			
35	1.25	1	8.09	Hoop -	7.32	Hoop -	8.09	Vessel	Hoop -
	1.5	0.5	4.30	Hoop -	3.63	Hoop -	4.30	Vessel	Hoop -
		0.6	4.95	Axial -	4.12	Hoop -	4.95	Vessel	Axial -
		0.7	5.64	Axial -	4.64	Hoop -	5.64	Vessel	Axial -
		0.8	6.21	Axial -	5.07	Hoop -	6.21	Vessel	Axial -
		0.9	6.84	Axial -	5.61	Hoop -	6.84	Vessel	Axial -
		1	7.26	Hoop -	6.12	Hoop -	7.26	Vessel	Hoop -
40	0.25	0.1	3.37	Hoop -	5.43	Axial -	5.43	Nozzle	Axial -
		0.2	5.11	Hoop -	9.44	Axial -	9.44	Nozzle	Axial -
		0.3	6.76	Hoop -	13.23	Axial -	13.23	Nozzle	Axial -
		0.4	8.32	Hoop -	16.62	Axial -	16.62	Nozzle	Axial -
		0.5	9.62	Hoop -	19.17	Axial -	19.17	Nozzle	Axial -
		0.6	11.07	Hoop -	22.09	Axial -	22.09	Nozzle	Axial -
		0.7	12.58	Hoop -	25.03	Axial -	25.03	Nozzle	Axial -
		0.8	13.91	Hoop -	27.50	Axial -	27.50	Nozzle	Axial -
		0.9	15.50	Hoop -	30.00	Axial -	30.00	Nozzle	Axial -
		1	17.17	Hoop -	31.69	Axial -	31.69	Nozzle	Axial -
	0.5	0.2	4.07	Hoop -	6.06	Axial -	6.06	Nozzle	Axial -
		0.3	5.32	Hoop -	8.61	Axial -	8.61	Nozzle	Axial -
		0.4	6.51	Hoop -	10.87	Axial -	10.87	Nozzle	Axial -
		0.5	7.48	Hoop -	12.60	Axial -	12.60	Nozzle	Axial -
		0.6	8.57	Hoop -	14.56	Axial -	14.56	Nozzle	Axial -
		0.7	9.69	Hoop -	16.47	Axial -	16.47	Nozzle	Axial -
		0.8	10.67	Hoop -	18.06	Axial -	18.06	Nozzle	Axial -
		0.9	11.93	Hoop -	19.87	Axial -	19.87	Nozzle	Axial -
		1	13.28	Hoop -	20.57	Axial -	20.57	Nozzle	Axial -
	0.75	0.2	3.46	Hoop -	3.94	Hoop -	3.94	Nozzle	Hoop -
		0.3	4.49	Hoop -	5.13	Axial -	5.13	Nozzle	Axial -
		0.4	5.47	Hoop -	6.54	Axial -	6.54	Nozzle	Axial -
		0.5	6.25	Hoop -	7.63	Axial -	7.63	Nozzle	Axial -
		0.6	7.13	Hoop -	8.86	Axial -	8.86	Nozzle	Axial -
		0.7	8.05	Hoop -	10.09	Axial -	10.09	Nozzle	Axial -
		0.8	8.84	Hoop -	11.11	Axial -	11.11	Nozzle	Axial -
		0.9	9.88	Hoop -	12.28	Axial -	12.28	Nozzle	Axial -
		1	11.01	Hoop -	12.75	Axial -	12.75	Nozzle	Axial -
	1	0.3	3.99	Hoop -	3.99	Hoop -	3.99	Vessel	Hoop -

Table C1 (cont'd): SCF Results for Cylindrical Vessels with Moderate-To-Large-Diameter Nozzles

RT	tT	rR	Cylindrical Vessel		Cylindrical Nozzle		Overall SCF	Location	Type
			SCF	Type	SCF	Type			
40	1	0.4	4.85	Hoop -	4.85	Hoop -	4.85	Vessel	Hoop -
		0.5	5.52	Hoop -	5.52	Hoop -	5.52	Nozzle	Hoop -
		0.6	6.29	Hoop -	6.30	Hoop -	6.30	Nozzle	Hoop -
		0.7	7.10	Hoop -	7.11	Hoop -	7.11	Nozzle	Hoop -
		0.8	7.78	Hoop -	7.79	Hoop -	7.79	Nozzle	Hoop -
		0.9	8.68	Hoop -	8.69	Hoop -	8.69	Nozzle	Hoop -
		1	9.62	Hoop -	9.63	Hoop -	9.63	Nozzle	Hoop -
	1.25	0.4	4.39	Hoop -	3.97	Hoop -	4.39	Vessel	Hoop -
		0.5	4.99	Hoop -	4.51	Hoop -	4.99	Vessel	Hoop -
		0.6	5.68	Hoop -	5.13	Hoop -	5.68	Vessel	Hoop -
		0.7	6.41	Hoop -	5.79	Hoop -	6.41	Vessel	Hoop -
		0.8	7.04	Axial -	6.33	Hoop -	7.04	Vessel	Axial -
		0.9	7.81	Hoop -	7.04	Hoop -	7.81	Vessel	Hoop -
		1	8.60	Hoop -	7.77	Hoop -	8.60	Vessel	Hoop -
	1.5	0.4	3.99	Hoop -	3.37	Hoop -	3.99	Vessel	Hoop -
		0.5	4.58	Axial -	3.82	Hoop -	4.58	Vessel	Axial -
		0.6	5.32	Axial -	4.35	Hoop -	5.32	Vessel	Axial -
		0.7	6.08	Axial -	4.90	Hoop -	6.08	Vessel	Axial -
		0.8	6.71	Axial -	5.34	Hoop -	6.71	Vessel	Axial -
		0.9	7.42	Axial -	5.93	Hoop -	7.42	Vessel	Axial -
		1	7.74	Hoop -	6.50	Hoop -	7.74	Vessel	Hoop -
45	0.25	0.1	3.49	Hoop -	5.79	Axial -	5.79	Nozzle	Axial -
		0.2	5.33	Hoop -	10.11	Axial -	10.11	Nozzle	Axial -
		0.3	7.07	Hoop -	14.13	Axial -	14.13	Nozzle	Axial -
		0.4	8.69	Hoop -	17.67	Axial -	17.67	Nozzle	Axial -
		0.5	10.06	Hoop -	20.41	Axial -	20.41	Nozzle	Axial -
		0.6	11.59	Hoop -	23.51	Axial -	23.51	Nozzle	Axial -
		0.7	13.18	Hoop -	26.62	Axial -	26.62	Nozzle	Axial -
		0.8	14.62	Hoop -	29.35	Axial -	29.35	Nozzle	Axial -
		0.9	16.33	Hoop -	32.11	Axial -	32.11	Nozzle	Axial -
		1	18.17	Hoop -	34.02	Axial -	34.02	Nozzle	Axial -
	0.5	0.2	4.24	Hoop -	6.48	Axial -	6.48	Nozzle	Axial -
		0.3	5.55	Hoop -	9.18	Axial -	9.18	Nozzle	Axial -
		0.4	6.79	Hoop -	11.56	Axial -	11.56	Nozzle	Axial -
		0.5	7.80	Hoop -	13.38	Axial -	13.38	Nozzle	Axial -
		0.6	8.94	Hoop -	15.45	Axial -	15.45	Nozzle	Axial -

Table C1 (cont'd): SCF Results for Cylindrical Vessels with Moderate-To-Large-Diameter Nozzles

RT	tT	rR	Cylindrical Vessel		Cylindrical Nozzle		Overall SCF	Location	Type
			SCF	Type	SCF	Type			
45	0.5	0.7	10.13	Hoop -	17.50	Axial -	17.50	Nozzle	Axial -
		0.8	11.16	Hoop -	19.18	Axial -	19.18	Nozzle	Axial -
		0.9	12.50	Hoop -	21.15	Axial -	21.15	Nozzle	Axial -
		1	14.00	Hoop -	22.04	Axial -	22.04	Nozzle	Axial -
	0.75	0.2	3.61	Hoop -	4.11	Hoop -	4.11	Nozzle	Hoop -
		0.3	4.69	Hoop -	5.47	Axial -	5.47	Nozzle	Axial -
		0.4	5.71	Hoop -	6.95	Axial -	6.95	Nozzle	Axial -
		0.5	6.52	Hoop -	8.10	Axial -	8.10	Nozzle	Axial -
		0.6	7.44	Hoop -	9.41	Axial -	9.41	Nozzle	Axial -
		0.7	8.41	Hoop -	10.72	Axial -	10.72	Nozzle	Axial -
		0.8	9.24	Hoop -	11.80	Axial -	11.80	Nozzle	Axial -
		0.9	10.34	Hoop -	13.07	Axial -	13.07	Nozzle	Axial -
		1	11.59	Hoop -	13.62	Axial -	13.62	Nozzle	Axial -
	1	0.3	4.16	Hoop -	4.17	Hoop -	4.17	Nozzle	Hoop -
		0.4	5.06	Hoop -	5.07	Hoop -	5.07	Nozzle	Hoop -
		0.5	5.76	Hoop -	5.77	Hoop -	5.77	Nozzle	Hoop -
		0.6	6.58	Hoop -	6.59	Hoop -	6.59	Nozzle	Hoop -
		0.7	7.42	Hoop -	7.44	Hoop -	7.44	Nozzle	Hoop -
		0.8	8.14	Hoop -	8.17	Hoop -	8.17	Nozzle	Hoop -
		0.9	9.10	Hoop -	9.11	Hoop -	9.11	Nozzle	Hoop -
		1	10.14	Hoop -	10.14	Hoop -	10.14	Nozzle	Hoop -
	1.25	0.3	3.78	Hoop -	3.43	Hoop -	3.78	Vessel	Hoop -
		0.4	4.59	Hoop -	4.15	Hoop -	4.59	Vessel	Hoop -
		0.5	5.22	Hoop -	4.71	Hoop -	5.22	Vessel	Hoop -
		0.6	5.95	Axial -	5.37	Hoop -	5.95	Vessel	Axial -
		0.7	6.80	Axial -	6.06	Hoop -	6.80	Vessel	Axial -
		0.8	7.50	Axial -	6.63	Hoop -	7.50	Vessel	Axial -
		0.9	8.32	Axial -	7.38	Hoop -	8.32	Vessel	Axial -
		1	9.07	Hoop -	8.18	Hoop -	9.07	Vessel	Hoop -
	1.5	0.4	4.19	Hoop -	3.53	Hoop -	4.19	Vessel	Hoop -
		0.5	4.87	Axial -	4.00	Hoop -	4.87	Vessel	Axial -
		0.6	5.66	Axial -	4.55	Hoop -	5.66	Vessel	Axial -
		0.7	6.48	Axial -	5.13	Hoop -	6.48	Vessel	Axial -
		0.8	7.17	Axial -	5.60	Hoop -	7.17	Vessel	Axial -
		0.9	7.95	Axial -	6.22	Hoop -	7.95	Vessel	Axial -
		1	8.26	Axial -	6.86	Hoop -	8.26	Vessel	Axial -

Table C1 (cont'd): SCF Results for Cylindrical Vessels with Moderate-To-Large-Diameter Nozzles

RT	tT	rR	Cylindrical Vessel		Cylindrical Nozzle		Overall SCF	Location	Type
			SCF	Type	SCF	Type			
55	0.25	0.1	3.71	Hoop -	6.46	Axial -	6.46	Nozzle	Axial -
		0.2	5.73	Hoop -	11.33	Axial -	11.33	Nozzle	Axial -
		0.3	7.60	Hoop -	15.72	Axial -	15.72	Nozzle	Axial -
		0.4	9.36	Hoop -	19.58	Axial -	19.58	Nozzle	Axial -
		0.5	10.86	Hoop -	22.71	Axial -	22.71	Nozzle	Axial -
		0.6	12.53	Hoop -	26.04	Axial -	26.04	Nozzle	Axial -
		0.7	14.28	Hoop -	29.48	Axial -	29.48	Nozzle	Axial -
		0.8	15.87	Hoop -	32.57	Axial -	32.57	Nozzle	Axial -
		0.9	17.81	Hoop -	35.89	Axial -	35.89	Nozzle	Axial -
		1	19.99	Hoop -	38.37	Axial -	38.37	Nozzle	Axial -
	0.5	0.1	3.00	Hoop -	3.98	Axial -	3.98	Nozzle	Axial -
		0.2	4.54	Hoop -	7.28	Axial -	7.28	Nozzle	Axial -
		0.3	5.96	Hoop -	10.21	Axial -	10.21	Nozzle	Axial -
		0.4	7.29	Hoop -	12.79	Axial -	12.79	Nozzle	Axial -
		0.5	8.39	Hoop -	14.80	Axial -	14.80	Nozzle	Axial -
		0.6	9.63	Hoop -	17.08	Axial -	17.08	Nozzle	Axial -
		0.7	10.92	Hoop -	19.35	Axial -	19.35	Nozzle	Axial -
		0.8	12.06	Hoop -	21.28	Axial -	21.28	Nozzle	Axial -
		0.9	13.54	Hoop -	23.50	Axial -	23.50	Nozzle	Axial -
		1	15.30	Hoop -	24.73	Axial -	24.73	Nozzle	Axial -
	0.75	0.2	3.87	Hoop -	4.43	Hoop -	4.43	Nozzle	Hoop -
		0.3	5.03	Hoop -	6.08	Axial -	6.08	Nozzle	Axial -
		0.4	6.14	Hoop -	7.69	Axial -	7.69	Nozzle	Axial -
		0.5	7.01	Hoop -	8.95	Axial -	8.95	Nozzle	Axial -
		0.6	8.02	Hoop -	10.39	Axial -	10.39	Nozzle	Axial -
		0.7	9.08	Hoop -	11.84	Axial -	11.84	Nozzle	Axial -
		0.8	9.99	Hoop -	13.08	Axial -	13.08	Nozzle	Axial -
		0.9	11.21	Hoop -	14.53	Axial -	14.53	Nozzle	Axial -
		1	12.65	Hoop -	15.24	Axial -	15.24	Nozzle	Axial -
	1	0.2	3.46	Hoop -	3.49	Hoop -	3.49	Nozzle	Hoop -
		0.3	4.48	Hoop -	4.49	Hoop -	4.49	Nozzle	Hoop -
		0.4	5.46	Hoop -	5.47	Hoop -	5.47	Nozzle	Hoop -
		0.5	6.22	Hoop -	6.23	Hoop -	6.23	Nozzle	Hoop -
		0.6	7.10	Hoop -	7.12	Hoop -	7.12	Nozzle	Hoop -
		0.7	8.03	Hoop -	8.05	Hoop -	8.05	Nozzle	Hoop -
		0.8	8.82	Hoop -	8.84	Hoop -	8.84	Nozzle	Hoop -

Table C1 (cont'd): SCF Results for Cylindrical Vessels with Moderate-To-Large-Diameter Nozzles

RT	tT	rR	Cylindrical Vessel		Cylindrical Nozzle		Overall SCF	Location	Type
			SCF	Type	SCF	Type			
55	1	0.9	9.87	Hoop -	9.89	Hoop -	9.89	Nozzle	Hoop -
		1	11.08	Hoop -	11.08	Hoop -	11.08	Nozzle	Hoop -
	1.25	0.3	4.08	Hoop -	3.70	Hoop -	4.08	Vessel	Hoop -
		0.4	4.96	Hoop -	4.48	Hoop -	4.96	Vessel	Hoop -
		0.5	5.66	Axial -	5.09	Hoop -	5.66	Vessel	Axial -
		0.6	6.58	Axial -	5.80	Hoop -	6.58	Vessel	Axial -
		0.7	7.53	Axial -	6.54	Hoop -	7.53	Vessel	Axial -
		0.8	8.35	Axial -	7.17	Hoop -	8.35	Vessel	Axial -
		0.9	9.29	Axial -	8.00	Hoop -	9.29	Vessel	Axial -
		1	9.95	Hoop -	8.93	Hoop -	9.95	Vessel	Hoop -
	1.5	0.3	3.73	Hoop -	3.15	Hoop -	3.73	Vessel	Hoop -
		0.4	4.62	Axial -	3.82	Hoop -	4.62	Vessel	Axial -
		0.5	5.38	Axial -	4.32	Hoop -	5.38	Vessel	Axial -
		0.6	6.28	Axial -	4.92	Hoop -	6.28	Vessel	Axial -
		0.7	7.21	Axial -	5.55	Hoop -	7.21	Vessel	Axial -
		0.8	8.02	Axial -	6.07	Hoop -	8.02	Vessel	Axial -
		0.9	8.93	Axial -	6.75	Hoop -	8.93	Vessel	Axial -
		1	9.32	Axial -	7.49	Hoop -	9.32	Vessel	Axial -
60	0.25	0.1	3.82	Hoop -	6.78	Axial -	6.78	Nozzle	Axial -
		0.2	5.92	Hoop -	11.90	Axial -	11.90	Nozzle	Axial -
		0.3	7.84	Hoop -	16.41	Axial -	16.41	Nozzle	Axial -
		0.4	9.66	Hoop -	20.45	Axial -	20.45	Nozzle	Axial -
		0.5	11.23	Hoop -	23.74	Axial -	23.74	Nozzle	Axial -
		0.6	12.96	Hoop -	27.20	Axial -	27.20	Nozzle	Axial -
		0.7	14.80	Hoop -	30.87	Axial -	30.87	Nozzle	Axial -
		0.8	16.44	Hoop -	33.95	Axial -	33.95	Nozzle	Axial -
		0.9	18.45	Hoop -	37.22	Axial -	37.22	Nozzle	Axial -
		1	20.82	Hoop -	40.31	Axial -	40.31	Nozzle	Axial -
	0.5	0.1	3.09	Hoop -	4.20	Axial -	4.20	Nozzle	Axial -
		0.2	4.68	Hoop -	7.65	Axial -	7.65	Nozzle	Axial -
		0.3	6.14	Hoop -	10.67	Axial -	10.67	Nozzle	Axial -
		0.4	7.53	Hoop -	13.35	Axial -	13.35	Nozzle	Axial -
		0.5	8.66	Hoop -	15.45	Axial -	15.45	Nozzle	Axial -
		0.6	9.94	Hoop -	17.81	Axial -	17.81	Nozzle	Axial -
		0.7	11.29	Hoop -	20.19	Axial -	20.19	Nozzle	Axial -
		0.8	12.49	Hoop -	22.26	Axial -	22.26	Nozzle	Axial -

Table C1 (cont'd): SCF Results for Cylindrical Vessels with Moderate-To-Large-Diameter Nozzles

RT	tT	rR	Cylindrical Vessel		Cylindrical Nozzle		Overall SCF	Location	Type
			SCF	Type	SCF	Type			
60	0.5	0.9	14.03	Hoop -	24.60	Axial -	24.60	Nozzle	Axial -
		1	15.89	Hoop -	25.96	Axial -	25.96	Nozzle	Axial -
	0.75	0.2	3.99	Hoop -	4.57	Hoop -	4.57	Nozzle	Hoop -
		0.3	5.19	Hoop -	6.36	Axial -	6.36	Nozzle	Axial -
		0.4	6.33	Hoop -	8.02	Axial -	8.02	Nozzle	Axial -
		0.5	7.24	Hoop -	9.34	Axial -	9.34	Nozzle	Axial -
		0.6	8.28	Hoop -	10.84	Axial -	10.84	Nozzle	Axial -
		0.7	9.38	Hoop -	12.36	Axial -	12.36	Nozzle	Axial -
		0.8	10.34	Hoop -	13.68	Axial -	13.68	Nozzle	Axial -
		0.9	11.61	Hoop -	15.20	Axial -	15.20	Nozzle	Axial -
		1	13.14	Hoop -	15.98	Axial -	15.98	Nozzle	Axial -
	1	0.2	3.58	Hoop -	3.60	Hoop -	3.60	Nozzle	Hoop -
		0.3	4.63	Hoop -	4.64	Hoop -	4.64	Nozzle	Hoop -
		0.4	5.64	Hoop -	5.65	Hoop -	5.65	Nozzle	Hoop -
		0.5	6.42	Hoop -	6.44	Hoop -	6.44	Nozzle	Hoop -
		0.6	7.34	Hoop -	7.36	Hoop -	7.36	Nozzle	Hoop -
		0.7	8.30	Hoop -	8.33	Hoop -	8.33	Nozzle	Hoop -
		0.8	9.13	Hoop -	9.15	Hoop -	9.15	Nozzle	Hoop -
		0.9	10.23	Hoop -	10.24	Hoop -	10.24	Nozzle	Hoop -
		1	11.51	Hoop -	11.51	Hoop -	11.51	Vessel	Hoop -
	1.25	0.3	4.22	Hoop -	3.82	Hoop -	4.22	Vessel	Hoop -
		0.4	5.13	Hoop -	4.64	Hoop -	5.13	Vessel	Hoop -
		0.5	5.90	Axial -	5.26	Hoop -	5.90	Vessel	Axial -
		0.6	6.86	Axial -	6.00	Hoop -	6.86	Vessel	Axial -
		0.7	7.87	Axial -	6.77	Hoop -	7.87	Vessel	Axial -
		0.8	8.74	Axial -	7.42	Hoop -	8.74	Vessel	Axial -
		0.9	9.74	Axial -	8.28	Hoop -	9.74	Vessel	Axial -
		1	10.35	Hoop -	9.28	Hoop -	10.35	Vessel	Hoop -
	1.5	0.3	3.86	Hoop -	3.26	Hoop -	3.86	Vessel	Hoop -
		0.4	4.82	Axial -	3.95	Hoop -	4.82	Vessel	Axial -
		0.5	5.62	Axial -	4.47	Hoop -	5.62	Vessel	Axial -
		0.6	6.56	Axial -	5.09	Hoop -	6.56	Vessel	Axial -
		0.7	7.54	Axial -	5.74	Hoop -	7.54	Vessel	Axial -
		0.8	8.41	Axial -	6.28	Hoop -	8.41	Vessel	Axial -
		0.9	9.38	Axial -	6.99	Hoop -	9.38	Vessel	Axial -
		1	9.82	Axial -	7.79	Hoop -	9.82	Vessel	Axial -

Table C1 (cont'd): SCF Results for Cylindrical Vessels with Moderate-To-Large-Diameter Nozzles

RT	tT	rR	Cylindrical Vessel		Cylindrical Nozzle		Overall SCF	Location	Type
			SCF	Type	SCF	Type			
65	0.25	0.1	3.91	Hoop -	7.08	Axial -	7.08	Nozzle	Axial -
		0.2	6.09	Hoop -	12.43	Axial -	12.43	Nozzle	Axial -
		0.3	8.07	Hoop -	17.12	Axial -	17.12	Nozzle	Axial -
		0.4	9.95	Hoop -	21.29	Axial -	21.29	Nozzle	Axial -
		0.5	11.59	Hoop -	24.79	Axial -	24.79	Nozzle	Axial -
		0.6	13.38	Hoop -	28.36	Axial -	28.36	Nozzle	Axial -
		0.7	15.29	Hoop -	32.13	Axial -	32.13	Nozzle	Axial -
		0.8	17.00	Hoop -	35.46	Axial -	35.46	Nozzle	Axial -
		0.9	19.11	Hoop -	39.01	Axial -	39.01	Nozzle	Axial -
		1	21.61	Hoop -	42.26	Axial -	42.26	Nozzle	Axial -
	0.5	0.1	3.17	Hoop -	4.40	Axial -	4.40	Nozzle	Axial -
		0.2	4.81	Hoop -	7.99	Axial -	7.99	Nozzle	Axial -
		0.3	6.32	Hoop -	11.12	Axial -	11.12	Nozzle	Axial -
		0.4	7.74	Hoop -	13.88	Axial -	13.88	Nozzle	Axial -
		0.5	8.92	Hoop -	16.11	Axial -	16.11	Nozzle	Axial -
		0.6	10.26	Hoop -	18.57	Axial -	18.57	Nozzle	Axial -
		0.7	11.66	Hoop -	21.06	Axial -	21.06	Nozzle	Axial -
		0.8	12.89	Hoop -	23.17	Axial -	23.17	Nozzle	Axial -
		0.9	14.49	Hoop -	25.63	Axial -	25.63	Nozzle	Axial -
		1	16.46	Hoop -	27.16	Axial -	27.16	Nozzle	Axial -
	0.75	0.2	4.10	Hoop -	4.71	Hoop -	4.71	Nozzle	Hoop -
		0.3	5.35	Hoop -	6.62	Axial -	6.62	Nozzle	Axial -
		0.4	6.52	Hoop -	8.34	Axial -	8.34	Nozzle	Axial -
		0.5	7.47	Hoop -	9.73	Axial -	9.73	Nozzle	Axial -
		0.6	8.55	Hoop -	11.30	Axial -	11.30	Nozzle	Axial -
		0.7	9.69	Hoop -	12.89	Axial -	12.89	Nozzle	Axial -
		0.8	10.67	Hoop -	14.23	Axial -	14.23	Nozzle	Axial -
		0.9	11.99	Hoop -	15.83	Axial -	15.83	Nozzle	Axial -
		1	13.60	Hoop -	16.70	Axial -	16.70	Nozzle	Axial -
	1	0.2	3.68	Hoop -	3.70	Hoop -	3.70	Nozzle	Hoop -
		0.3	4.77	Hoop -	4.78	Hoop -	4.78	Nozzle	Hoop -
		0.4	5.81	Hoop -	5.82	Hoop -	5.82	Nozzle	Hoop -
		0.5	6.63	Hoop -	6.65	Hoop -	6.65	Nozzle	Hoop -
		0.6	7.58	Hoop -	7.60	Hoop -	7.60	Nozzle	Hoop -
		0.7	8.58	Hoop -	8.60	Hoop -	8.60	Nozzle	Hoop -
		0.8	9.43	Hoop -	9.45	Hoop -	9.45	Nozzle	Hoop -

Table C1 (cont'd): SCF Results for Cylindrical Vessels with Moderate-To-Large-Diameter Nozzles

RT	tT	rR	Cylindrical Vessel		Cylindrical Nozzle		Overall SCF	Location	Type
			SCF	Type	SCF	Type			
65	1	0.9	10.58	Hoop -	10.59	Hoop -	10.59	Nozzle	Hoop -
		1	11.93	Hoop -	11.93	Hoop -	11.93	Vessel	Hoop -
	1.25	0.2	3.36	Hoop -	3.08	Hoop -	3.36	Vessel	Hoop -
		0.3	4.35	Hoop -	3.94	Hoop -	4.35	Vessel	Hoop -
		0.4	5.29	Hoop -	4.78	Hoop -	5.29	Vessel	Hoop -
		0.5	6.15	Axial -	5.43	Hoop -	6.15	Vessel	Axial -
		0.6	7.17	Axial -	6.19	Hoop -	7.17	Vessel	Axial -
		0.7	8.22	Axial -	6.99	Hoop -	8.22	Vessel	Axial -
		0.8	9.11	Axial -	7.65	Hoop -	9.11	Vessel	Axial -
		0.9	10.17	Axial -	8.55	Hoop -	10.17	Vessel	Axial -
		1	10.73	Hoop -	9.61	Hoop -	10.73	Vessel	Hoop -
	1.5	0.3	3.99	Axial -	3.36	Hoop -	3.99	Vessel	Axial -
		0.4	5.01	Axial -	4.07	Hoop -	5.01	Vessel	Axial -
		0.5	5.87	Axial -	4.62	Hoop -	5.87	Vessel	Axial -
		0.6	6.86	Axial -	5.26	Hoop -	6.86	Vessel	Axial -
		0.7	7.89	Axial -	5.93	Hoop -	7.89	Vessel	Axial -
		0.8	8.78	Axial -	6.48	Hoop -	8.78	Vessel	Axial -
		0.9	9.81	Axial -	7.22	Hoop -	9.81	Vessel	Axial -
		1	10.29	Axial -	8.07	Hoop -	10.29	Vessel	Axial -
70	0.25	0.1	4.01	Hoop -	7.36	Axial -	7.36	Nozzle	Axial -
		0.2	6.25	Hoop -	12.95	Axial -	12.95	Nozzle	Axial -
		0.3	8.29	Hoop -	17.75	Axial -	17.75	Nozzle	Axial -
		0.4	10.23	Hoop -	22.07	Axial -	22.07	Nozzle	Axial -
		0.5	11.93	Hoop -	25.72	Axial -	25.72	Nozzle	Axial -
		0.6	13.79	Hoop -	29.58	Axial -	29.58	Nozzle	Axial -
		0.7	15.74	Hoop -	33.35	Axial -	33.35	Nozzle	Axial -
		0.8	17.55	Hoop -	37.00	Axial -	37.00	Nozzle	Axial -
		0.9	19.73	Hoop -	40.61	Axial -	40.61	Nozzle	Axial -
		1	22.33	Hoop -	43.92	Axial -	43.92	Nozzle	Axial -
	0.5	0.1	3.25	Hoop -	4.60	Axial -	4.60	Nozzle	Axial -
		0.2	4.94	Hoop -	8.32	Axial -	8.32	Nozzle	Axial -
		0.3	6.49	Hoop -	11.55	Axial -	11.55	Nozzle	Axial -
		0.4	7.95	Hoop -	14.40	Axial -	14.40	Nozzle	Axial -
		0.5	9.17	Hoop -	16.70	Axial -	16.70	Nozzle	Axial -
		0.6	10.55	Hoop -	19.24	Axial -	19.24	Nozzle	Axial -
		0.7	11.99	Hoop -	21.80	Axial -	21.80	Nozzle	Axial -

Table C1 (cont'd): SCF Results for Cylindrical Vessels with Moderate-To-Large-Diameter Nozzles

RT	tT	rR	Cylindrical Vessel		Cylindrical Nozzle		Overall SCF	Location	Type
			SCF	Type	SCF	Type			
70	0.5	0.8	13.27	Hoop -	24.02	Axial -	24.02	Nozzle	Axial -
		0.9	14.94	Hoop -	26.63	Axial -	26.63	Nozzle	Axial -
		1	17.02	Hoop -	28.32	Axial -	28.32	Nozzle	Axial -
	0.75	0.2	4.22	Hoop -	4.89	Axial -	4.89	Nozzle	Axial -
		0.3	5.49	Hoop -	6.88	Axial -	6.88	Nozzle	Axial -
		0.4	6.70	Hoop -	8.65	Axial -	8.65	Nozzle	Axial -
		0.5	7.67	Hoop -	10.09	Axial -	10.09	Nozzle	Axial -
		0.6	8.79	Hoop -	11.70	Axial -	11.70	Nozzle	Axial -
		0.7	9.97	Hoop -	13.36	Axial -	13.36	Nozzle	Axial -
		0.8	11.00	Hoop -	14.78	Axial -	14.78	Nozzle	Axial -
		0.9	12.36	Hoop -	16.44	Axial -	16.44	Nozzle	Axial -
		1	14.06	Hoop -	17.42	Axial -	17.42	Nozzle	Axial -
	1	0.2	3.78	Hoop -	3.80	Hoop -	3.80	Nozzle	Hoop -
		0.3	4.91	Hoop -	4.92	Hoop -	4.92	Nozzle	Hoop -
		0.4	5.97	Hoop -	5.99	Hoop -	5.99	Nozzle	Hoop -
		0.5	6.82	Hoop -	6.84	Hoop -	6.84	Nozzle	Hoop -
		0.6	7.80	Hoop -	7.82	Hoop -	7.82	Nozzle	Hoop -
		0.7	8.84	Hoop -	8.86	Hoop -	8.86	Nozzle	Hoop -
		0.8	9.72	Hoop -	9.74	Hoop -	9.74	Nozzle	Hoop -
		0.9	10.91	Hoop -	10.91	Hoop -	10.91	Nozzle	Hoop -
		1	12.33	Hoop -	12.32	Hoop -	12.33	Vessel	Hoop -
	1.25	0.2	3.46	Hoop -	3.16	Hoop -	3.46	Vessel	Hoop -
		0.3	4.47	Hoop -	4.05	Hoop -	4.47	Vessel	Hoop -
		0.4	5.45	Axial -	4.91	Hoop -	5.45	Vessel	Axial -
		0.5	6.37	Axial -	5.58	Hoop -	6.37	Vessel	Axial -
		0.6	7.42	Axial -	6.37	Hoop -	7.42	Vessel	Axial -
		0.7	8.53	Axial -	7.19	Hoop -	8.53	Vessel	Axial -
		0.8	9.47	Axial -	7.88	Hoop -	9.47	Vessel	Axial -
		0.9	10.58	Axial -	8.81	Hoop -	10.58	Vessel	Axial -
		1	11.13	Axial -	9.92	Hoop -	11.13	Vessel	Axial -
	1.5	0.3	4.14	Axial -	3.46	Hoop -	4.14	Vessel	Axial -
		0.4	5.20	Axial -	4.19	Hoop -	5.20	Vessel	Axial -
		0.5	6.08	Axial -	4.75	Hoop -	6.08	Vessel	Axial -
		0.6	7.12	Axial -	5.41	Hoop -	7.12	Vessel	Axial -
		0.7	8.20	Axial -	6.10	Hoop -	8.20	Vessel	Axial -
		0.8	9.14	Axial -	6.67	Hoop -	9.14	Vessel	Axial -

Table C1 (cont'd): SCF Results for Cylindrical Vessels with Moderate-To-Large-Diameter Nozzles

RT	tT	rR	Cylindrical Vessel		Cylindrical Nozzle		Overall SCF	Location	Type
			SCF	Type	SCF	Type			
70	1.5	0.9	10.22	Axial -	7.44	Hoop -	10.22	Vessel	Axial -
		1	10.75	Axial -	8.34	Hoop -	10.75	Vessel	Axial -
80	0.25	0.1	4.19	Hoop -	7.92	Axial -	7.92	Nozzle	Axial -
		0.2	6.56	Hoop -	13.91	Axial -	13.91	Nozzle	Axial -
		0.3	8.70	Hoop -	19.00	Axial -	19.00	Nozzle	Axial -
		0.4	10.75	Hoop -	23.59	Axial -	23.59	Nozzle	Axial -
		0.5	12.55	Hoop -	27.54	Axial -	27.54	Nozzle	Axial -
		0.6	14.54	Hoop -	31.63	Axial -	31.63	Nozzle	Axial -
		0.7	16.61	Hoop -	35.56	Axial -	35.56	Nozzle	Axial -
		0.8	18.58	Hoop -	39.77	Axial -	39.77	Nozzle	Axial -
		0.9	20.90	Hoop -	43.57	Axial -	43.57	Nozzle	Axial -
		1	23.79	Hoop -	47.54	Axial -	47.54	Nozzle	Axial -
	0.5	0.1	3.39	Hoop -	4.98	Axial -	4.98	Nozzle	Axial -
		0.2	5.18	Hoop -	8.94	Axial -	8.94	Nozzle	Axial -
		0.3	6.81	Hoop -	12.34	Axial -	12.34	Nozzle	Axial -
		0.4	8.35	Hoop -	15.36	Axial -	15.36	Nozzle	Axial -
		0.5	9.64	Hoop -	17.84	Axial -	17.84	Nozzle	Axial -
		0.6	11.10	Hoop -	20.54	Axial -	20.54	Nozzle	Axial -
		0.7	12.64	Hoop -	23.32	Axial -	23.32	Nozzle	Axial -
		0.8	14.02	Hoop -	25.76	Axial -	25.76	Nozzle	Axial -
		0.9	15.79	Hoop -	28.53	Axial -	28.53	Nozzle	Axial -
		1	18.04	Hoop -	30.53	Axial -	30.53	Nozzle	Axial -
	0.75	0.1	2.93	Hoop -	3.39	Hoop -	3.39	Nozzle	Hoop -
		0.2	4.42	Hoop -	5.26	Axial -	5.26	Nozzle	Axial -
		0.3	5.77	Hoop -	7.34	Axial -	7.34	Nozzle	Axial -
		0.4	7.04	Hoop -	9.22	Axial -	9.22	Nozzle	Axial -
		0.5	8.07	Hoop -	10.76	Axial -	10.76	Nozzle	Axial -
		0.6	9.25	Hoop -	12.49	Axial -	12.49	Nozzle	Axial -
		0.7	10.51	Hoop -	14.27	Axial -	14.27	Nozzle	Axial -
		0.8	11.61	Hoop -	15.82	Axial -	15.82	Nozzle	Axial -
		0.9	13.06	Hoop -	17.63	Axial -	17.63	Nozzle	Axial -
		1	14.91	Hoop -	18.73	Axial -	18.73	Nozzle	Axial -
	1	0.2	3.97	Hoop -	4.00	Hoop -	4.00	Nozzle	Hoop -
		0.3	5.16	Hoop -	5.17	Hoop -	5.17	Nozzle	Hoop -
		0.4	6.28	Hoop -	6.31	Hoop -	6.31	Nozzle	Hoop -
		0.5	7.18	Hoop -	7.20	Hoop -	7.20	Nozzle	Hoop -

Table C1 (cont'd): SCF Results for Cylindrical Vessels with Moderate-To-Large-Diameter Nozzles

RT	tT	rR	Cylindrical Vessel		Cylindrical Nozzle		Overall SCF	Location	Type
			SCF	Type	SCF	Type			
80	1	0.6	8.22	Hoop -	8.24	Hoop -	8.24	Nozzle	Hoop -
		0.7	9.32	Hoop -	9.34	Hoop -	9.34	Nozzle	Hoop -
		0.8	10.28	Hoop -	10.29	Hoop -	10.29	Nozzle	Hoop -
		0.9	11.54	Hoop -	11.54	Hoop -	11.54	Nozzle	Hoop -
		1	13.09	Hoop -	13.08	Hoop -	13.09	Vessel	Hoop -
	1.25	0.2	3.64	Hoop -	3.32	Hoop -	3.64	Vessel	Hoop -
		0.3	4.71	Hoop -	4.26	Hoop -	4.71	Vessel	Hoop -
		0.4	5.81	Axial -	5.17	Hoop -	5.81	Vessel	Axial -
		0.5	6.80	Axial -	5.88	Hoop -	6.80	Vessel	Axial -
		0.6	7.93	Axial -	6.71	Hoop -	7.93	Vessel	Axial -
		0.7	9.12	Axial -	7.58	Hoop -	9.12	Vessel	Axial -
		0.8	10.16	Axial -	8.32	Hoop -	10.16	Vessel	Axial -
		0.9	11.36	Axial -	9.31	Hoop -	11.36	Vessel	Axial -
		1	11.99	Axial -	10.52	Hoop -	11.99	Vessel	Axial -
	1.5	0.2	3.35	Hoop -	2.85	Hoop -	3.35	Vessel	Hoop -
		0.3	4.41	Axial -	3.65	Hoop -	4.41	Vessel	Axial -
		0.4	5.54	Axial -	4.42	Hoop -	5.54	Vessel	Axial -
		0.5	6.50	Axial -	5.01	Hoop -	6.50	Vessel	Axial -
		0.6	7.62	Axial -	5.70	Hoop -	7.62	Vessel	Axial -
		0.7	8.79	Axial -	6.43	Hoop -	8.79	Vessel	Axial -
		0.8	9.83	Axial -	7.04	Hoop -	9.83	Vessel	Axial -
		0.9	11.00	Axial -	7.86	Hoop -	11.00	Vessel	Axial -
		1	11.60	Axial -	8.84	Hoop -	11.60	Vessel	Axial -
85	0.25	0.1	4.27	Hoop -	8.18	Axial -	8.18	Nozzle	Axial -
		0.2	6.70	Hoop -	14.38	Axial -	14.38	Nozzle	Axial -
		0.3	8.91	Hoop -	19.70	Axial -	19.70	Nozzle	Axial -
		0.4	10.99	Hoop -	24.27	Axial -	24.27	Nozzle	Axial -
		0.5	12.84	Hoop -	28.31	Axial -	28.31	Nozzle	Axial -
		0.6	14.89	Hoop -	32.64	Axial -	32.64	Nozzle	Axial -
		0.7	17.04	Hoop -	36.62	Axial -	36.62	Nozzle	Axial -
		0.8	19.06	Hoop -	40.97	Axial -	40.97	Nozzle	Axial -
		0.9	21.44	Hoop -	44.86	Axial -	44.86	Nozzle	Axial -
		1	24.45	Hoop -	49.10	Axial -	49.10	Nozzle	Axial -
	0.5	0.1	3.46	Hoop -	5.15	Axial -	5.15	Nozzle	Axial -
		0.2	5.29	Hoop -	9.24	Axial -	9.24	Nozzle	Axial -
		0.3	6.95	Hoop -	12.71	Axial -	12.71	Nozzle	Axial -

Table C1 (cont'd): SCF Results for Cylindrical Vessels with Moderate-To-Large-Diameter Nozzles

RT	tT	rR	Cylindrical Vessel		Cylindrical Nozzle		Overall SCF	Location	Type
			SCF	Type	SCF	Type			
85	0.5	0.4	8.53	Hoop -	15.81	Axial -	15.81	Nozzle	Axial -
		0.5	9.87	Hoop -	18.39	Axial -	18.39	Nozzle	Axial -
		0.6	11.37	Hoop -	21.19	Axial -	21.19	Nozzle	Axial -
		0.7	12.96	Hoop -	24.05	Axial -	24.05	Nozzle	Axial -
		0.8	14.37	Hoop -	26.58	Axial -	26.58	Nozzle	Axial -
		0.9	16.19	Hoop -	29.43	Axial -	29.43	Nozzle	Axial -
		1	18.54	Hoop -	31.52	Axial -	31.52	Nozzle	Axial -
	0.75	0.1	2.99	Hoop -	3.46	Hoop -	3.46	Nozzle	Hoop -
		0.2	4.52	Hoop -	5.43	Axial -	5.43	Nozzle	Axial -
		0.3	5.89	Hoop -	7.56	Axial -	7.56	Nozzle	Axial -
		0.4	7.20	Hoop -	9.49	Axial -	9.49	Nozzle	Axial -
		0.5	8.27	Hoop -	11.10	Axial -	11.10	Nozzle	Axial -
		0.6	9.49	Hoop -	12.88	Axial -	12.88	Nozzle	Axial -
		0.7	10.78	Hoop -	14.71	Axial -	14.71	Nozzle	Axial -
		0.8	11.90	Hoop -	16.31	Axial -	16.31	Nozzle	Axial -
		0.9	13.39	Hoop -	18.18	Axial -	18.18	Nozzle	Axial -
		1	15.32	Hoop -	19.37	Axial -	19.37	Nozzle	Axial -
	1	0.2	4.06	Hoop -	4.08	Hoop -	4.08	Nozzle	Hoop -
		0.3	5.28	Hoop -	5.29	Hoop -	5.29	Nozzle	Hoop -
		0.4	6.43	Hoop -	6.45	Hoop -	6.45	Nozzle	Hoop -
		0.5	7.36	Hoop -	7.38	Hoop -	7.38	Nozzle	Hoop -
		0.6	8.43	Hoop -	8.45	Hoop -	8.45	Nozzle	Hoop -
		0.7	9.57	Hoop -	9.58	Hoop -	9.58	Nozzle	Hoop -
		0.8	10.54	Hoop -	10.55	Hoop -	10.55	Nozzle	Hoop -
		0.9	11.84	Hoop -	11.84	Hoop -	11.84	Nozzle	Hoop -
		1	13.44	Hoop -	13.43	Hoop -	13.44	Vessel	Hoop -
	1.25	0.2	3.72	Hoop -	3.39	Hoop -	3.72	Vessel	Hoop -
		0.3	4.82	Hoop -	4.36	Hoop -	4.82	Vessel	Hoop -
		0.4	5.97	Axial -	5.29	Hoop -	5.97	Vessel	Axial -
		0.5	7.01	Axial -	6.02	Hoop -	7.01	Vessel	Axial -
		0.6	8.19	Axial -	6.87	Hoop -	8.19	Vessel	Axial -
		0.7	9.42	Axial -	7.77	Hoop -	9.42	Vessel	Axial -
		0.8	10.48	Axial -	8.52	Hoop -	10.48	Vessel	Axial -
		0.9	11.73	Axial -	9.54	Hoop -	11.73	Vessel	Axial -
		1	12.40	Axial -	10.80	Hoop -	12.40	Vessel	Axial -
	1.5	0.2	3.42	Hoop -	2.91	Hoop -	3.42	Vessel	Hoop -

Table C1 (cont'd): SCF Results for Cylindrical Vessels with Moderate-To-Large-Diameter Nozzles

RT	tT	rR	Cylindrical Vessel		Cylindrical Nozzle		Overall SCF	Location	Type
			SCF	Type	SCF	Type			
85	1.5	0.3	4.54	Axial -	3.73	Hoop -	4.54	Vessel	Axial -
		0.4	5.70	Axial -	4.52	Hoop -	5.70	Vessel	Axial -
		0.5	6.72	Axial -	5.13	Hoop -	6.72	Vessel	Axial -
		0.6	7.87	Axial -	5.84	Hoop -	7.87	Vessel	Axial -
		0.7	9.09	Axial -	6.59	Hoop -	9.09	Vessel	Axial -
		0.8	10.15	Axial -	7.21	Hoop -	10.15	Vessel	Axial -
		0.9	11.38	Axial -	8.05	Hoop -	11.38	Vessel	Axial -
		1	12.00	Axial -	9.07	Hoop -	12.00	Vessel	Axial -
90	0.25	0.1	4.35	Hoop -	8.45	Axial -	8.45	Nozzle	Axial -
		0.2	6.84	Hoop -	14.81	Axial -	14.81	Nozzle	Axial -
		0.3	9.08	Hoop -	20.12	Axial -	20.12	Nozzle	Axial -
		0.4	11.22	Hoop -	24.96	Axial -	24.96	Nozzle	Axial -
		0.5	13.13	Hoop -	29.16	Axial -	29.16	Nozzle	Axial -
		0.6	15.25	Hoop -	33.58	Axial -	33.58	Nozzle	Axial -
		0.7	17.43	Hoop -	37.78	Axial -	37.78	Nozzle	Axial -
		0.8	19.51	Hoop -	42.01	Axial -	42.01	Nozzle	Axial -
		0.9	21.97	Hoop -	46.20	Axial -	46.20	Nozzle	Axial -
		1	25.14	Hoop -	50.81	Axial -	50.81	Nozzle	Axial -
	0.5	0.1	3.52	Hoop -	5.32	Axial -	5.32	Nozzle	Axial -
		0.2	5.40	Hoop -	9.52	Axial -	9.52	Nozzle	Axial -
		0.3	7.10	Hoop -	13.09	Axial -	13.09	Nozzle	Axial -
		0.4	8.72	Hoop -	16.26	Axial -	16.26	Nozzle	Axial -
		0.5	10.07	Hoop -	18.88	Axial -	18.88	Nozzle	Axial -
		0.6	11.61	Hoop -	21.75	Axial -	21.75	Nozzle	Axial -
		0.7	13.24	Hoop -	24.71	Axial -	24.71	Nozzle	Axial -
		0.8	14.71	Hoop -	27.36	Axial -	27.36	Nozzle	Axial -
		0.9	16.58	Hoop -	30.34	Axial -	30.34	Nozzle	Axial -
		1	19.00	Hoop -	32.50	Axial -	32.50	Nozzle	Axial -
	0.75	0.1	3.05	Hoop -	3.53	Hoop -	3.53	Nozzle	Hoop -
		0.2	4.61	Hoop -	5.60	Axial -	5.60	Nozzle	Axial -
		0.3	6.02	Hoop -	7.78	Axial -	7.78	Nozzle	Axial -
		0.4	7.36	Hoop -	9.75	Axial -	9.75	Nozzle	Axial -
		0.5	8.44	Hoop -	11.38	Axial -	11.38	Nozzle	Axial -
		0.6	9.69	Hoop -	13.22	Axial -	13.22	Nozzle	Axial -
		0.7	11.01	Hoop -	15.11	Axial -	15.11	Nozzle	Axial -
		0.8	12.18	Hoop -	16.79	Axial -	16.79	Nozzle	Axial -

Table C1 (cont'd): SCF Results for Cylindrical Vessels with Moderate-To-Large-Diameter Nozzles

RT	tT	rR	Cylindrical Vessel		Cylindrical Nozzle		Overall SCF	Location	Type
			SCF	Type	SCF	Type			
90	0.75	0.9	13.70	Hoop -	18.71	Axial -	18.71	Nozzle	Axial -
		1	15.71	Hoop -	19.98	Axial -	19.98	Nozzle	Axial -
	1	0.2	4.15	Hoop -	4.17	Hoop -	4.17	Nozzle	Hoop -
		0.3	5.40	Hoop -	5.41	Hoop -	5.41	Nozzle	Hoop -
		0.4	6.58	Hoop -	6.60	Hoop -	6.60	Nozzle	Hoop -
		0.5	7.52	Hoop -	7.54	Hoop -	7.54	Nozzle	Hoop -
		0.6	8.62	Hoop -	8.64	Hoop -	8.64	Nozzle	Hoop -
		0.7	9.78	Hoop -	9.80	Hoop -	9.80	Nozzle	Hoop -
		0.8	10.79	Hoop -	10.80	Hoop -	10.80	Nozzle	Hoop -
		0.9	12.12	Hoop -	12.12	Hoop -	12.12	Nozzle	Hoop -
		1	13.80	Hoop -	13.79	Hoop -	13.80	Vessel	Hoop -
	1.25	0.2	3.80	Hoop -	3.46	Hoop -	3.80	Vessel	Hoop -
		0.3	4.94	Hoop -	4.46	Hoop -	4.94	Vessel	Hoop -
		0.4	6.14	Axial -	5.41	Hoop -	6.14	Vessel	Axial -
		0.5	7.19	Axial -	6.15	Hoop -	7.19	Vessel	Axial -
		0.6	8.41	Axial -	7.02	Hoop -	8.41	Vessel	Axial -
		0.7	9.67	Axial -	7.94	Hoop -	9.67	Vessel	Axial -
		0.8	10.79	Axial -	8.72	Hoop -	10.79	Vessel	Axial -
		0.9	12.08	Axial -	9.77	Hoop -	12.08	Vessel	Axial -
		1	12.80	Axial -	11.08	Hoop -	12.80	Vessel	Axial -
	1.5	0.2	3.50	Hoop -	2.98	Hoop -	3.50	Vessel	Hoop -
		0.3	4.67	Axial -	3.82	Hoop -	4.67	Vessel	Axial -
		0.4	5.86	Axial -	4.63	Hoop -	5.86	Vessel	Axial -
		0.5	6.89	Axial -	5.24	Hoop -	6.89	Vessel	Axial -
		0.6	8.09	Axial -	5.97	Hoop -	8.09	Vessel	Axial -
		0.7	9.34	Axial -	6.73	Hoop -	9.34	Vessel	Axial -
		0.8	10.45	Axial -	7.38	Hoop -	10.45	Vessel	Axial -
		0.9	11.73	Axial -	8.24	Hoop -	11.73	Vessel	Axial -
		1	12.40	Axial -	9.30	Hoop -	12.40	Vessel	Axial -
95	0.25	0.1	4.43	Hoop -	8.69	Axial -	8.69	Nozzle	Axial -
		0.2	6.97	Hoop -	15.24	Axial -	15.24	Nozzle	Axial -
		0.3	9.26	Hoop -	20.67	Axial -	20.67	Nozzle	Axial -
		0.4	11.46	Hoop -	25.64	Axial -	25.64	Nozzle	Axial -
		0.5	13.42	Hoop -	30.00	Axial -	30.00	Nozzle	Axial -
		0.6	15.58	Hoop -	34.43	Axial -	34.43	Nozzle	Axial -
		0.7	17.81	Hoop -	38.66	Axial -	38.66	Nozzle	Axial -

Table C1 (cont'd): SCF Results for Cylindrical Vessels with Moderate-To-Large-Diameter Nozzles

RT	tT	rR	Cylindrical Vessel		Cylindrical Nozzle		Overall SCF	Location	Type
			SCF	Type	SCF	Type			
95	0.25	0.8	19.99	Hoop -	43.58	Axial -	43.58	Nozzle	Axial -
		0.9	22.52	Hoop -	47.77	Axial -	47.77	Nozzle	Axial -
		1	25.76	Hoop -	52.30	Axial -	52.30	Nozzle	Axial -
	0.5	0.1	3.58	Hoop -	5.49	Axial -	5.49	Nozzle	Axial -
		0.2	5.50	Hoop -	9.79	Axial -	9.79	Nozzle	Axial -
		0.3	7.24	Hoop -	13.43	Axial -	13.43	Nozzle	Axial -
		0.4	8.89	Hoop -	16.68	Axial -	16.68	Nozzle	Axial -
		0.5	10.28	Hoop -	19.39	Axial -	19.39	Nozzle	Axial -
		0.6	11.86	Hoop -	22.34	Axial -	22.34	Nozzle	Axial -
		0.7	13.54	Hoop -	25.37	Axial -	25.37	Nozzle	Axial -
		0.8	15.04	Hoop -	28.11	Axial -	28.11	Nozzle	Axial -
		0.9	16.96	Hoop -	31.14	Axial -	31.14	Nozzle	Axial -
		1	19.48	Hoop -	33.55	Axial -	33.55	Nozzle	Axial -
	0.75	0.1	3.11	Hoop -	3.59	Hoop -	3.59	Nozzle	Hoop -
		0.2	4.71	Hoop -	5.75	Axial -	5.75	Nozzle	Axial -
		0.3	6.14	Hoop -	7.98	Axial -	7.98	Nozzle	Axial -
		0.4	7.51	Hoop -	10.00	Axial -	10.00	Nozzle	Axial -
		0.5	8.62	Hoop -	11.69	Axial -	11.69	Nozzle	Axial -
		0.6	9.90	Hoop -	13.58	Axial -	13.58	Nozzle	Axial -
		0.7	11.26	Hoop -	15.53	Axial -	15.53	Nozzle	Axial -
		0.8	12.45	Hoop -	17.24	Axial -	17.24	Nozzle	Axial -
		0.9	14.03	Hoop -	19.24	Axial -	19.24	Nozzle	Axial -
		1	16.08	Hoop -	20.56	Axial -	20.56	Nozzle	Axial -
	1	0.2	4.24	Hoop -	4.26	Hoop -	4.26	Nozzle	Hoop -
		0.3	5.51	Hoop -	5.52	Hoop -	5.52	Nozzle	Hoop -
		0.4	6.71	Hoop -	6.74	Hoop -	6.74	Nozzle	Hoop -
		0.5	7.68	Hoop -	7.70	Hoop -	7.70	Nozzle	Hoop -
		0.6	8.81	Hoop -	8.83	Hoop -	8.83	Nozzle	Hoop -
		0.7	10.00	Hoop -	10.02	Hoop -	10.02	Nozzle	Hoop -
		0.8	11.04	Hoop -	11.05	Hoop -	11.05	Nozzle	Hoop -
		0.9	12.41	Hoop -	12.41	Hoop -	12.41	Vessel	Hoop -
		1	14.14	Hoop -	14.13	Hoop -	14.14	Vessel	Hoop -
	1.25	0.2	3.88	Hoop -	3.53	Hoop -	3.88	Vessel	Hoop -
		0.3	5.04	Hoop -	4.55	Hoop -	5.04	Vessel	Hoop -
		0.4	6.29	Axial -	5.52	Hoop -	6.29	Vessel	Axial -
		0.5	7.39	Axial -	6.28	Hoop -	7.39	Vessel	Axial -

Table C1 (cont'd): SCF Results for Cylindrical Vessels with Moderate-To-Large-Diameter Nozzles

RT	tT	rR	Cylindrical Vessel		Cylindrical Nozzle		Overall SCF	Location	Type
			SCF	Type	SCF	Type			
95	1.25	0.6	8.64	Axial -	7.18	Hoop -	8.64	Vessel	Axial -
		0.7	9.95	Axial -	8.11	Hoop -	9.95	Vessel	Axial -
		0.8	11.10	Axial -	8.91	Hoop -	11.10	Vessel	Axial -
		0.9	12.44	Axial -	9.99	Hoop -	12.44	Vessel	Axial -
		1	13.18	Axial -	11.34	Hoop -	13.18	Vessel	Axial -
	1.5	0.2	3.58	Hoop -	3.04	Hoop -	3.58	Vessel	Hoop -
		0.3	4.79	Axial -	3.90	Hoop -	4.79	Vessel	Axial -
		0.4	6.01	Axial -	4.72	Hoop -	6.01	Vessel	Axial -
		0.5	7.08	Axial -	5.35	Hoop -	7.08	Vessel	Axial -
		0.6	8.32	Axial -	6.10	Hoop -	8.32	Vessel	Axial -
		0.7	9.61	Axial -	6.88	Hoop -	9.61	Vessel	Axial -
		0.8	10.76	Axial -	7.54	Hoop -	10.76	Vessel	Axial -
		0.9	12.08	Axial -	8.43	Hoop -	12.08	Vessel	Axial -
		1	12.78	Axial -	9.52	Hoop -	12.78	Vessel	Axial -
105	0.25	0.1	4.58	Hoop -	9.18	Axial -	9.18	Nozzle	Axial -
		0.2	7.23	Hoop -	16.06	Axial -	16.06	Nozzle	Axial -
		0.3	9.62	Hoop -	21.90	Axial -	21.90	Nozzle	Axial -
		0.4	11.89	Hoop -	26.91	Axial -	26.91	Nozzle	Axial -
		0.5	13.92	Hoop -	31.33	Axial -	31.33	Nozzle	Axial -
		0.6	16.20	Hoop -	36.21	Axial -	36.21	Nozzle	Axial -
		0.7	18.57	Hoop -	40.78	Axial -	40.78	Nozzle	Axial -
		0.8	20.88	Hoop -	45.98	Axial -	45.98	Nozzle	Axial -
		0.9	23.52	Hoop -	50.24	Axial -	50.24	Nozzle	Axial -
		1	26.98	Hoop -	55.43	Axial -	55.43	Nozzle	Axial -
	0.5	0.1	3.70	Hoop -	5.80	Axial -	5.80	Nozzle	Axial -
		0.2	5.70	Hoop -	10.30	Axial -	10.30	Nozzle	Axial -
		0.3	7.51	Hoop -	14.09	Axial -	14.09	Nozzle	Axial -
		0.4	9.23	Hoop -	17.48	Axial -	17.48	Nozzle	Axial -
		0.5	10.68	Hoop -	20.35	Axial -	20.35	Nozzle	Axial -
		0.6	12.34	Hoop -	23.45	Axial -	23.45	Nozzle	Axial -
		0.7	14.10	Hoop -	26.65	Axial -	26.65	Nozzle	Axial -
		0.8	15.67	Hoop -	29.43	Axial -	29.43	Nozzle	Axial -
		0.9	17.68	Hoop -	32.69	Axial -	32.69	Nozzle	Axial -
		1	20.36	Hoop -	35.38	Axial -	35.38	Nozzle	Axial -
	0.75	0.1	3.22	Hoop -	3.71	Hoop -	3.71	Nozzle	Hoop -
		0.2	4.88	Hoop -	6.05	Axial -	6.05	Nozzle	Axial -

Table C1 (cont'd): SCF Results for Cylindrical Vessels with Moderate-To-Large-Diameter Nozzles

RT	tT	rR	Cylindrical Vessel		Cylindrical Nozzle		Overall SCF	Location	Type
			SCF	Type	SCF	Type			
105	0.75	0.3	6.37	Hoop -	8.37	Axial -	8.37	Nozzle	Axial -
		0.4	7.79	Hoop -	10.48	Axial -	10.48	Nozzle	Axial -
		0.5	8.96	Hoop -	12.27	Axial -	12.27	Nozzle	Axial -
		0.6	10.30	Hoop -	14.25	Axial -	14.25	Nozzle	Axial -
		0.7	11.73	Hoop -	16.29	Axial -	16.29	Nozzle	Axial -
		0.8	12.99	Hoop -	18.14	Axial -	18.14	Nozzle	Axial -
		0.9	14.62	Hoop -	20.23	Axial -	20.23	Nozzle	Axial -
		1	16.82	Hoop -	21.73	Axial -	21.73	Nozzle	Axial -
	1	0.1	2.92	Hoop -	2.98	Hoop -	2.98	Nozzle	Hoop -
		0.2	4.39	Hoop -	4.41	Hoop -	4.41	Nozzle	Hoop -
		0.3	5.72	Hoop -	5.74	Hoop -	5.74	Nozzle	Hoop -
		0.4	6.98	Hoop -	7.00	Hoop -	7.00	Nozzle	Hoop -
		0.5	7.99	Hoop -	8.01	Hoop -	8.01	Nozzle	Hoop -
		0.6	9.18	Hoop -	9.19	Hoop -	9.19	Nozzle	Hoop -
		0.7	10.43	Hoop -	10.43	Hoop -	10.43	Nozzle	Hoop -
		0.8	11.52	Hoop -	11.52	Hoop -	11.52	Nozzle	Hoop -
		0.9	12.95	Hoop -	12.95	Hoop -	12.95	Vessel	Hoop -
		1	14.78	Hoop -	14.77	Hoop -	14.78	Vessel	Hoop -
	1.25	0.2	4.03	Hoop -	3.66	Hoop -	4.03	Vessel	Hoop -
		0.3	5.26	Axial -	4.73	Hoop -	5.26	Vessel	Axial -
		0.4	6.59	Axial -	5.74	Hoop -	6.59	Vessel	Axial -
		0.5	7.75	Axial -	6.53	Hoop -	7.75	Vessel	Axial -
		0.6	9.07	Axial -	7.47	Hoop -	9.07	Vessel	Axial -
		0.7	10.46	Axial -	8.45	Hoop -	10.46	Vessel	Axial -
		0.8	11.69	Axial -	9.29	Hoop -	11.69	Vessel	Axial -
		0.9	13.10	Axial -	10.41	Hoop -	13.10	Vessel	Axial -
		1	13.92	Axial -	11.85	Hoop -	13.92	Vessel	Axial -
	1.5	0.2	3.72	Hoop -	3.15	Hoop -	3.72	Vessel	Hoop -
		0.3	5.01	Axial -	4.05	Hoop -	5.01	Vessel	Axial -
		0.4	6.30	Axial -	4.91	Hoop -	6.30	Vessel	Axial -
		0.5	7.44	Axial -	5.57	Hoop -	7.44	Vessel	Axial -
		0.6	8.74	Axial -	6.34	Hoop -	8.74	Vessel	Axial -
		0.7	10.12	Axial -	7.16	Hoop -	10.12	Vessel	Axial -
		0.8	11.35	Axial -	7.85	Hoop -	11.35	Vessel	Axial -
		0.9	12.74	Axial -	8.78	Hoop -	12.74	Vessel	Axial -
		1	13.50	Axial -	9.94	Hoop -	13.50	Vessel	Axial -

Table C1 (cont'd): SCF Results for Cylindrical Vessels with Moderate-To-Large-Diameter Nozzles

RT	tT	rR	Cylindrical Vessel		Cylindrical Nozzle		Overall SCF	Location	Type
			SCF	Type	SCF	Type			
110	0.25	0.1	4.65	Hoop -	9.41	Axial -	9.41	Nozzle	Axial -
		0.2	7.35	Hoop -	16.45	Axial -	16.45	Nozzle	Axial -
		0.3	9.76	Hoop -	22.17	Axial -	22.17	Nozzle	Axial -
		0.4	12.11	Hoop -	27.56	Axial -	27.56	Nozzle	Axial -
		0.5	14.20	Hoop -	32.12	Axial -	32.12	Nozzle	Axial -
		0.6	16.53	Hoop -	37.11	Axial -	37.11	Nozzle	Axial -
		0.7	18.92	Hoop -	41.58	Axial -	41.58	Nozzle	Axial -
		0.8	21.29	Hoop -	47.04	Axial -	47.04	Nozzle	Axial -
		0.9	23.96	Hoop -	51.06	Axial -	51.06	Nozzle	Axial -
		1	27.58	Hoop -	56.89	Axial -	56.89	Nozzle	Axial -
	0.5	0.1	3.76	Hoop -	5.95	Axial -	5.95	Nozzle	Axial -
		0.2	5.80	Hoop -	10.56	Axial -	10.56	Nozzle	Axial -
		0.3	7.64	Hoop -	14.44	Axial -	14.44	Nozzle	Axial -
		0.4	9.39	Hoop -	17.88	Axial -	17.88	Nozzle	Axial -
		0.5	10.90	Hoop -	20.86	Axial -	20.86	Nozzle	Axial -
		0.6	12.59	Hoop -	24.03	Axial -	24.03	Nozzle	Axial -
		0.7	14.39	Hoop -	27.31	Axial -	27.31	Nozzle	Axial -
		0.8	15.98	Hoop -	30.16	Axial -	30.16	Nozzle	Axial -
		0.9	18.04	Hoop -	33.54	Axial -	33.54	Nozzle	Axial -
		1	20.79	Hoop -	36.28	Axial -	36.28	Nozzle	Axial -
	0.75	0.1	3.27	Hoop -	3.77	Hoop -	3.77	Nozzle	Hoop -
		0.2	4.96	Hoop -	6.20	Axial -	6.20	Nozzle	Axial -
		0.3	6.49	Hoop -	8.56	Axial -	8.56	Nozzle	Axial -
		0.4	7.93	Hoop -	10.72	Axial -	10.72	Nozzle	Axial -
		0.5	9.14	Hoop -	12.57	Axial -	12.57	Nozzle	Axial -
		0.6	10.52	Hoop -	14.61	Axial -	14.61	Nozzle	Axial -
		0.7	11.98	Hoop -	16.72	Axial -	16.72	Nozzle	Axial -
		0.8	13.24	Hoop -	18.50	Axial -	18.50	Nozzle	Axial -
		0.9	14.92	Hoop -	20.73	Axial -	20.73	Nozzle	Axial -
		1	17.17	Hoop -	22.28	Axial -	22.28	Nozzle	Axial -
	1	0.1	2.97	Hoop -	3.03	Hoop -	3.03	Nozzle	Hoop -
		0.2	4.47	Hoop -	4.49	Hoop -	4.49	Nozzle	Hoop -
		0.3	5.83	Hoop -	5.84	Hoop -	5.84	Nozzle	Hoop -
		0.4	7.11	Hoop -	7.13	Hoop -	7.13	Nozzle	Hoop -
		0.5	8.16	Hoop -	8.17	Hoop -	8.17	Nozzle	Hoop -
		0.6	9.37	Hoop -	9.39	Hoop -	9.39	Nozzle	Hoop -

Table C1 (cont'd): SCF Results for Cylindrical Vessels with Moderate-To-Large-Diameter Nozzles

RT	tT	rR	Cylindrical Vessel		Cylindrical Nozzle		Overall SCF	Location	Type
			SCF	Type	SCF	Type			
110	1	0.7	10.65	Hoop -	10.66	Hoop -	10.66	Nozzle	Hoop -
		0.8	11.76	Axial -	11.75	Hoop -	11.76	Vessel	Axial -
		0.9	13.21	Hoop -	13.20	Hoop -	13.21	Vessel	Hoop -
		1	15.10	Hoop -	15.09	Hoop -	15.10	Vessel	Hoop -
	1.25	0.2	4.11	Hoop -	3.73	Hoop -	4.11	Vessel	Hoop -
		0.3	5.38	Axial -	4.81	Hoop -	5.38	Vessel	Axial -
		0.4	6.74	Axial -	5.85	Hoop -	6.74	Vessel	Axial -
		0.5	7.95	Axial -	6.67	Hoop -	7.95	Vessel	Axial -
		0.6	9.30	Axial -	7.62	Hoop -	9.30	Vessel	Axial -
		0.7	10.73	Axial -	8.62	Hoop -	10.73	Vessel	Axial -
		0.8	11.97	Axial -	9.47	Hoop -	11.97	Vessel	Axial -
		0.9	13.41	Axial -	10.61	Hoop -	13.41	Vessel	Axial -
		1	14.29	Axial -	12.10	Hoop -	14.29	Vessel	Axial -
	1.5	0.2	3.79	Hoop -	3.21	Hoop -	3.79	Vessel	Hoop -
		0.3	5.13	Axial -	4.13	Hoop -	5.13	Vessel	Axial -
		0.4	6.45	Axial -	5.00	Hoop -	6.45	Vessel	Axial -
		0.5	7.63	Axial -	5.68	Hoop -	7.63	Vessel	Axial -
		0.6	8.97	Axial -	6.47	Hoop -	8.97	Vessel	Axial -
		0.7	10.38	Axial -	7.30	Hoop -	10.38	Vessel	Axial -
		0.8	11.62	Axial -	8.00	Hoop -	11.62	Vessel	Axial -
		0.9	13.05	Axial -	8.95	Hoop -	13.05	Vessel	Axial -
		1	13.86	Axial -	10.16	Hoop -	13.86	Vessel	Axial -
115	0.25	0.1	4.72	Hoop -	9.64	Axial -	9.64	Nozzle	Axial -
		0.2	7.46	Hoop -	16.83	Axial -	16.83	Nozzle	Axial -
		0.3	9.92	Hoop -	22.67	Axial -	22.67	Nozzle	Axial -
		0.4	12.31	Hoop -	28.16	Axial -	28.16	Nozzle	Axial -
		0.5	14.43	Hoop -	32.80	Axial -	32.80	Nozzle	Axial -
		0.6	16.81	Hoop -	37.89	Axial -	37.89	Nozzle	Axial -
		0.7	19.24	Hoop -	42.33	Axial -	42.33	Nozzle	Axial -
		0.8	21.63	Hoop -	47.61	Axial -	47.61	Nozzle	Axial -
		0.9	24.41	Hoop -	52.25	Axial -	52.25	Nozzle	Axial -
		1	28.15	Hoop -	58.11	Axial -	58.11	Nozzle	Axial -
	0.5	0.1	3.81	Hoop -	6.10	Axial -	6.10	Nozzle	Axial -
		0.2	5.89	Hoop -	10.80	Axial -	10.80	Nozzle	Axial -
		0.3	7.76	Hoop -	14.73	Axial -	14.73	Nozzle	Axial -
		0.4	9.55	Hoop -	18.27	Axial -	18.27	Nozzle	Axial -

Table C1 (cont'd): SCF Results for Cylindrical Vessels with Moderate-To-Large-Diameter Nozzles

RT	tT	rR	Cylindrical Vessel		Cylindrical Nozzle		Overall SCF	Location	Type
			SCF	Type	SCF	Type			
115	0.5	0.5	11.07	Hoop -	21.27	Axial -	21.27	Nozzle	Axial -
		0.6	12.80	Hoop -	24.51	Axial -	24.51	Nozzle	Axial -
		0.7	14.60	Hoop -	27.77	Axial -	27.77	Nozzle	Axial -
		0.8	16.27	Hoop -	30.81	Axial -	30.81	Nozzle	Axial -
		0.9	18.36	Hoop -	34.15	Axial -	34.15	Nozzle	Axial -
		1	21.18	Hoop -	37.21	Axial -	37.21	Nozzle	Axial -
	0.75	0.1	3.32	Hoop -	3.83	Hoop -	3.83	Nozzle	Hoop -
		0.2	5.04	Hoop -	6.34	Axial -	6.34	Nozzle	Axial -
		0.3	6.59	Hoop -	8.74	Axial -	8.74	Nozzle	Axial -
		0.4	8.07	Hoop -	10.95	Axial -	10.95	Nozzle	Axial -
		0.5	9.29	Hoop -	12.82	Axial -	12.82	Nozzle	Axial -
		0.6	10.69	Hoop -	14.89	Axial -	14.89	Nozzle	Axial -
		0.7	12.18	Hoop -	17.05	Axial -	17.05	Nozzle	Axial -
		0.8	13.49	Hoop -	18.93	Axial -	18.93	Nozzle	Axial -
		0.9	15.19	Hoop -	21.17	Axial -	21.17	Nozzle	Axial -
		1	17.51	Hoop -	22.82	Axial -	22.82	Nozzle	Axial -
	1	0.1	3.01	Hoop -	3.08	Hoop -	3.08	Nozzle	Hoop -
		0.2	4.55	Hoop -	4.57	Hoop -	4.57	Nozzle	Hoop -
		0.3	5.93	Hoop -	5.94	Hoop -	5.94	Nozzle	Hoop -
		0.4	7.23	Hoop -	7.26	Hoop -	7.26	Nozzle	Hoop -
		0.5	8.30	Hoop -	8.31	Hoop -	8.31	Nozzle	Hoop -
		0.6	9.53	Hoop -	9.54	Hoop -	9.54	Nozzle	Hoop -
		0.7	10.83	Hoop -	10.85	Hoop -	10.85	Nozzle	Hoop -
		0.8	12.02	Axial -	11.97	Hoop -	12.02	Vessel	Axial -
		0.9	13.46	Hoop -	13.45	Hoop -	13.46	Vessel	Hoop -
		1	15.41	Hoop -	15.40	Hoop -	15.41	Vessel	Hoop -
	1.25	0.2	4.18	Hoop -	3.79	Hoop -	4.18	Vessel	Hoop -
		0.3	5.48	Axial -	4.90	Hoop -	5.48	Vessel	Axial -
		0.4	6.89	Axial -	5.95	Hoop -	6.89	Vessel	Axial -
		0.5	8.10	Axial -	6.78	Hoop -	8.10	Vessel	Axial -
		0.6	9.49	Axial -	7.74	Hoop -	9.49	Vessel	Axial -
		0.7	10.95	Axial -	8.77	Hoop -	10.95	Vessel	Axial -
		0.8	12.23	Axial -	9.64	Hoop -	12.23	Vessel	Axial -
		0.9	13.71	Axial -	10.81	Hoop -	13.71	Vessel	Axial -
		1	14.63	Axial -	12.34	Hoop -	14.63	Vessel	Axial -
	1.5	0.2	3.86	Hoop -	3.27	Hoop -	3.86	Vessel	Hoop -

Table C1 (cont'd): SCF Results for Cylindrical Vessels with Moderate-To-Large-Diameter Nozzles

RT	tT	rR	Cylindrical Vessel		Cylindrical Nozzle		Overall SCF	Location	Type
			SCF	Type	SCF	Type			
115	1.5	0.3	5.24	Axial -	4.20	Hoop -	5.24	Vessel	Axial -
		0.4	6.59	Axial -	5.09	Hoop -	6.59	Vessel	Axial -
		0.5	7.78	Axial -	5.77	Hoop -	7.78	Vessel	Axial -
		0.6	9.15	Axial -	6.58	Hoop -	9.15	Vessel	Axial -
		0.7	10.60	Axial -	7.43	Hoop -	10.60	Vessel	Axial -
		0.8	11.88	Axial -	8.15	Hoop -	11.88	Vessel	Axial -
		0.9	13.34	Axial -	9.11	Hoop -	13.34	Vessel	Axial -
		1	14.20	Axial -	10.35	Hoop -	14.20	Vessel	Axial -
120	0.25	0.1	4.79	Hoop -	9.87	Axial -	9.87	Nozzle	Axial -
		0.2	7.58	Hoop -	17.20	Axial -	17.20	Nozzle	Axial -
		0.3	10.07	Hoop -	23.13	Axial -	23.13	Nozzle	Axial -
		0.4	12.50	Hoop -	28.71	Axial -	28.71	Nozzle	Axial -
		0.5	14.66	Hoop -	33.38	Axial -	33.38	Nozzle	Axial -
		0.6	17.08	Hoop -	38.66	Axial -	38.66	Nozzle	Axial -
		0.7	19.62	Hoop -	43.43	Axial -	43.43	Nozzle	Axial -
		0.8	22.09	Hoop -	48.90	Axial -	48.90	Nozzle	Axial -
		0.9	24.95	Hoop -	53.99	Axial -	53.99	Nozzle	Axial -
		1	28.75	Hoop -	59.78	Axial -	59.78	Nozzle	Axial -
	0.5	0.1	3.87	Hoop -	6.24	Axial -	6.24	Nozzle	Axial -
		0.2	5.97	Hoop -	11.02	Axial -	11.02	Nozzle	Axial -
		0.3	7.88	Hoop -	15.01	Axial -	15.01	Nozzle	Axial -
		0.4	9.69	Hoop -	18.61	Axial -	18.61	Nozzle	Axial -
		0.5	11.25	Hoop -	21.71	Axial -	21.71	Nozzle	Axial -
		0.6	13.01	Hoop -	25.01	Axial -	25.01	Nozzle	Axial -
		0.7	14.86	Hoop -	28.37	Axial -	28.37	Nozzle	Axial -
		0.8	16.58	Hoop -	31.51	Axial -	31.51	Nozzle	Axial -
		0.9	18.69	Hoop -	34.99	Axial -	34.99	Nozzle	Axial -
		1	21.62	Hoop -	38.02	Axial -	38.02	Nozzle	Axial -
	0.75	0.1	3.36	Hoop -	3.89	Hoop -	3.89	Nozzle	Hoop -
		0.2	5.12	Hoop -	6.46	Axial -	6.46	Nozzle	Axial -
		0.3	6.69	Hoop -	8.91	Axial -	8.91	Nozzle	Axial -
		0.4	8.20	Hoop -	11.16	Axial -	11.16	Nozzle	Axial -
		0.5	9.44	Hoop -	13.08	Axial -	13.08	Nozzle	Axial -
		0.6	10.87	Hoop -	15.21	Axial -	15.21	Nozzle	Axial -
		0.7	12.39	Hoop -	17.41	Axial -	17.41	Nozzle	Axial -
		0.8	13.74	Hoop -	19.39	Axial -	19.39	Nozzle	Axial -

Table C1 (cont'd): SCF Results for Cylindrical Vessels with Moderate-To-Large-Diameter Nozzles

RT	tT	rR	Cylindrical Vessel		Cylindrical Nozzle		Overall SCF	Location	Type
			SCF	Type	SCF	Type			
120	0.75	0.9	15.48	Hoop -	21.64	Axial -	21.64	Nozzle	Axial -
		1	17.85	Hoop -	23.35	Axial -	23.35	Nozzle	Axial -
	1	0.1	3.06	Hoop -	3.12	Hoop -	3.12	Nozzle	Hoop -
		0.2	4.62	Hoop -	4.64	Hoop -	4.64	Nozzle	Hoop -
		0.3	6.02	Hoop -	6.04	Hoop -	6.04	Nozzle	Hoop -
		0.4	7.35	Hoop -	7.37	Hoop -	7.37	Nozzle	Hoop -
		0.5	8.44	Hoop -	8.45	Hoop -	8.45	Nozzle	Hoop -
		0.6	9.69	Hoop -	9.71	Hoop -	9.71	Nozzle	Hoop -
		0.7	11.03	Hoop -	11.04	Hoop -	11.04	Nozzle	Hoop -
		0.8	12.27	Axial -	12.20	Hoop -	12.27	Vessel	Axial -
		0.9	13.74	Axial -	13.71	Hoop -	13.74	Vessel	Axial -
		1	15.71	Hoop -	15.70	Hoop -	15.71	Vessel	Hoop -
	1.25	0.2	4.24	Hoop -	3.85	Hoop -	4.24	Vessel	Hoop -
		0.3	5.58	Axial -	4.97	Hoop -	5.58	Vessel	Axial -
		0.4	7.01	Axial -	6.04	Hoop -	7.01	Vessel	Axial -
		0.5	8.27	Axial -	6.89	Hoop -	8.27	Vessel	Axial -
		0.6	9.69	Axial -	7.88	Hoop -	9.69	Vessel	Axial -
		0.7	11.18	Axial -	8.92	Hoop -	11.18	Vessel	Axial -
		0.8	12.51	Axial -	9.82	Hoop -	12.51	Vessel	Axial -
		0.9	14.03	Axial -	11.01	Hoop -	14.03	Vessel	Axial -
		1	14.97	Axial -	12.58	Hoop -	14.97	Vessel	Axial -
	1.5	0.2	3.92	Hoop -	3.32	Hoop -	3.92	Vessel	Hoop -
		0.3	5.33	Axial -	4.27	Hoop -	5.33	Vessel	Axial -
		0.4	6.72	Axial -	5.17	Hoop -	6.72	Vessel	Axial -
		0.5	7.95	Axial -	5.87	Hoop -	7.95	Vessel	Axial -
		0.6	9.35	Axial -	6.69	Hoop -	9.35	Vessel	Axial -
		0.7	10.83	Axial -	7.55	Hoop -	10.83	Vessel	Axial -
		0.8	12.16	Axial -	8.29	Hoop -	12.16	Vessel	Axial -
		0.9	13.65	Axial -	9.27	Hoop -	13.65	Vessel	Axial -
		1	14.53	Axial -	10.55	Hoop -	14.53	Vessel	Axial -
130	0.25	0.1	4.92	Hoop -	10.31	Axial -	10.31	Nozzle	Axial -
		0.2	7.80	Hoop -	17.92	Axial -	17.92	Nozzle	Axial -
		0.3	10.41	Hoop -	24.33	Axial -	24.33	Nozzle	Axial -
		0.4	12.89	Hoop -	29.81	Axial -	29.81	Nozzle	Axial -
		0.5	15.14	Hoop -	34.75	Axial -	34.75	Nozzle	Axial -
		0.6	17.65	Hoop -	40.14	Axial -	40.14	Nozzle	Axial -

Table C1 (cont'd): SCF Results for Cylindrical Vessels with Moderate-To-Large-Diameter Nozzles

RT	tT	rR	Cylindrical Vessel		Cylindrical Nozzle		Overall SCF	Location	Type
			SCF	Type	SCF	Type			
130	0.25	0.7	20.26	Hoop -	45.08	Axial -	45.08	Nozzle	Axial -
		0.8	22.84	Hoop -	50.79	Axial -	50.79	Nozzle	Axial -
		0.9	25.85	Hoop -	56.29	Axial -	56.29	Nozzle	Axial -
		1	29.86	Hoop -	63.30	Axial -	63.30	Nozzle	Axial -
	0.5	0.1	3.97	Hoop -	6.51	Axial -	6.51	Nozzle	Axial -
		0.2	6.15	Hoop -	11.47	Axial -	11.47	Nozzle	Axial -
		0.3	8.11	Hoop -	15.60	Axial -	15.60	Nozzle	Axial -
		0.4	9.99	Hoop -	19.34	Axial -	19.34	Nozzle	Axial -
		0.5	11.62	Hoop -	22.58	Axial -	22.58	Nozzle	Axial -
		0.6	13.44	Hoop -	26.00	Axial -	26.00	Nozzle	Axial -
		0.7	15.39	Hoop -	29.59	Axial -	29.59	Nozzle	Axial -
		0.8	17.14	Hoop -	32.76	Axial -	32.76	Nozzle	Axial -
		0.9	19.35	Hoop -	36.39	Axial -	36.39	Nozzle	Axial -
		1	22.37	Hoop -	39.63	Axial -	39.63	Nozzle	Axial -
	0.75	0.1	3.46	Hoop -	3.99	Hoop -	3.99	Nozzle	Hoop -
		0.2	5.27	Hoop -	6.72	Axial -	6.72	Nozzle	Axial -
		0.3	6.90	Hoop -	9.25	Axial -	9.25	Nozzle	Axial -
		0.4	8.45	Hoop -	11.58	Axial -	11.58	Nozzle	Axial -
		0.5	9.75	Hoop -	13.60	Axial -	13.60	Nozzle	Axial -
		0.6	11.23	Hoop -	15.81	Axial -	15.81	Nozzle	Axial -
		0.7	12.81	Hoop -	18.09	Axial -	18.09	Nozzle	Axial -
		0.8	14.21	Hoop -	20.15	Axial -	20.15	Nozzle	Axial -
		0.9	16.02	Hoop -	22.55	Axial -	22.55	Nozzle	Axial -
		1	18.50	Hoop -	24.37	Axial -	24.37	Nozzle	Axial -
	1	0.1	3.14	Hoop -	3.20	Hoop -	3.20	Nozzle	Hoop -
		0.2	4.76	Hoop -	4.78	Hoop -	4.78	Nozzle	Hoop -
		0.3	6.21	Hoop -	6.23	Hoop -	6.23	Nozzle	Hoop -
		0.4	7.58	Hoop -	7.61	Hoop -	7.61	Nozzle	Hoop -
		0.5	8.72	Hoop -	8.73	Hoop -	8.73	Nozzle	Hoop -
		0.6	10.02	Hoop -	10.04	Hoop -	10.04	Nozzle	Hoop -
		0.7	11.46	Axial -	11.41	Hoop -	11.46	Vessel	Axial -
		0.8	12.81	Axial -	12.75	Axial -	12.81	Vessel	Axial -
		0.9	14.32	Axial -	14.28	Axial -	14.32	Vessel	Axial -
		1	16.27	Hoop -	16.26	Hoop -	16.27	Vessel	Hoop -
	1.25	0.1	2.90	Hoop -	2.70	Hoop -	2.90	Vessel	Hoop -
		0.2	4.38	Hoop -	3.97	Hoop -	4.38	Vessel	Hoop -

Table C1 (cont'd): SCF Results for Cylindrical Vessels with Moderate-To-Large-Diameter Nozzles

RT	tT	rR	Cylindrical Vessel		Cylindrical Nozzle		Overall SCF	Location	Type
			SCF	Type	SCF	Type			
130	1.25	0.3	5.79	Axial -	5.13	Hoop -	5.79	Vessel	Axial -
		0.4	7.28	Axial -	6.23	Hoop -	7.28	Vessel	Axial -
		0.5	8.59	Axial -	7.11	Hoop -	8.59	Vessel	Axial -
		0.6	10.08	Axial -	8.13	Hoop -	10.08	Vessel	Axial -
		0.7	11.63	Axial -	9.22	Hoop -	11.63	Vessel	Axial -
		0.8	13.06	Axial -	10.16	Hoop -	13.06	Vessel	Axial -
		0.9	14.64	Axial -	11.39	Hoop -	14.64	Vessel	Axial -
		1	15.62	Axial -	13.02	Hoop -	15.62	Vessel	Axial -
	1.5	0.2	4.05	Hoop -	3.42	Hoop -	4.05	Vessel	Hoop -
		0.3	5.54	Axial -	4.40	Hoop -	5.54	Vessel	Axial -
		0.4	6.98	Axial -	5.33	Hoop -	6.98	Vessel	Axial -
		0.5	8.27	Axial -	6.06	Hoop -	8.27	Vessel	Axial -
		0.6	9.74	Axial -	6.91	Hoop -	9.74	Vessel	Axial -
		0.7	11.28	Axial -	7.80	Hoop -	11.28	Vessel	Axial -
		0.8	12.71	Axial -	8.58	Hoop -	12.71	Vessel	Axial -
		0.9	14.26	Axial -	9.59	Hoop -	14.26	Vessel	Axial -
		1	15.16	Axial -	10.92	Hoop -	15.16	Vessel	Axial -
135	0.25	0.1	4.98	Hoop -	10.52	Axial -	10.52	Nozzle	Axial -
		0.2	7.90	Hoop -	18.25	Axial -	18.25	Nozzle	Axial -
		0.3	10.51	Hoop -	24.44	Axial -	24.44	Nozzle	Axial -
		0.4	13.08	Hoop -	30.38	Axial -	30.38	Nozzle	Axial -
		0.5	15.41	Hoop -	35.51	Axial -	35.51	Nozzle	Axial -
		0.6	18.00	Hoop -	41.26	Axial -	41.26	Nozzle	Axial -
		0.7	20.65	Hoop -	46.34	Axial -	46.34	Nozzle	Axial -
		0.8	23.22	Hoop -	51.84	Axial -	51.84	Nozzle	Axial -
		0.9	26.23	Hoop -	57.34	Axial -	57.34	Nozzle	Axial -
		1	30.34	Hoop -	63.83	Axial -	63.83	Nozzle	Axial -
	0.5	0.1	4.02	Hoop -	6.65	Axial -	6.65	Nozzle	Axial -
		0.2	6.23	Hoop -	11.69	Axial -	11.69	Nozzle	Axial -
		0.3	8.23	Hoop -	15.90	Axial -	15.90	Nozzle	Axial -
		0.4	10.13	Hoop -	19.67	Axial -	19.67	Nozzle	Axial -
		0.5	11.81	Hoop -	23.06	Axial -	23.06	Nozzle	Axial -
		0.6	13.68	Hoop -	26.57	Axial -	26.57	Nozzle	Axial -
		0.7	15.66	Hoop -	30.22	Axial -	30.22	Nozzle	Axial -
		0.8	17.42	Hoop -	33.42	Axial -	33.42	Nozzle	Axial -
		0.9	19.67	Hoop -	37.11	Axial -	37.11	Nozzle	Axial -

Table C1 (cont'd): SCF Results for Cylindrical Vessels with Moderate-To-Large-Diameter Nozzles

RT	tT	rR	Cylindrical Vessel		Cylindrical Nozzle		Overall SCF	Location	Type
			SCF	Type	SCF	Type			
135	0.5	1	22.77	Hoop -	40.54	Axial -	40.54	Nozzle	Axial -
	0.75	0.1	3.50	Hoop -	4.04	Hoop -	4.04	Nozzle	Hoop -
		0.2	5.34	Hoop -	6.85	Axial -	6.85	Nozzle	Axial -
		0.3	7.00	Hoop -	9.42	Axial -	9.42	Nozzle	Axial -
		0.4	8.58	Hoop -	11.79	Axial -	11.79	Nozzle	Axial -
		0.5	9.92	Hoop -	13.89	Axial -	13.89	Nozzle	Axial -
		0.6	11.44	Hoop -	16.16	Axial -	16.16	Nozzle	Axial -
		0.7	13.05	Hoop -	18.51	Axial -	18.51	Nozzle	Axial -
		0.8	14.43	Hoop -	20.48	Axial -	20.48	Nozzle	Axial -
		0.9	16.29	Hoop -	22.98	Axial -	22.98	Nozzle	Axial -
		1	18.82	Hoop -	24.87	Axial -	24.87	Nozzle	Axial -
	1	0.1	3.19	Hoop -	3.24	Hoop -	3.24	Nozzle	Hoop -
		0.2	4.83	Hoop -	4.85	Hoop -	4.85	Nozzle	Hoop -
		0.3	6.30	Hoop -	6.32	Hoop -	6.32	Nozzle	Hoop -
		0.4	7.70	Hoop -	7.72	Hoop -	7.72	Nozzle	Hoop -
		0.5	8.87	Hoop -	8.88	Hoop -	8.88	Nozzle	Hoop -
		0.6	10.21	Hoop -	10.22	Hoop -	10.22	Nozzle	Hoop -
		0.7	11.68	Axial -	11.60	Hoop -	11.68	Vessel	Axial -
		0.8	13.00	Axial -	12.92	Axial -	13.00	Vessel	Axial -
		0.9	14.58	Axial -	14.54	Axial -	14.58	Vessel	Axial -
		1	16.57	Hoop -	16.56	Hoop -	16.57	Vessel	Hoop -
	1.25	0.1	2.94	Hoop -	2.73	Hoop -	2.94	Vessel	Hoop -
		0.2	4.44	Hoop -	4.03	Hoop -	4.44	Vessel	Hoop -
		0.3	5.90	Axial -	5.21	Hoop -	5.90	Vessel	Axial -
		0.4	7.41	Axial -	6.33	Hoop -	7.41	Vessel	Axial -
		0.5	8.79	Axial -	7.24	Hoop -	8.79	Vessel	Axial -
		0.6	10.31	Axial -	8.28	Hoop -	10.31	Vessel	Axial -
		0.7	11.89	Axial -	9.38	Hoop -	11.89	Vessel	Axial -
		0.8	13.29	Axial -	10.32	Hoop -	13.29	Vessel	Axial -
		0.9	14.90	Axial -	11.57	Hoop -	14.90	Vessel	Axial -
		1	15.96	Axial -	13.25	Hoop -	15.96	Vessel	Axial -
	1.5	0.2	4.11	Axial -	3.47	Hoop -	4.11	Vessel	Axial -
		0.3	5.64	Axial -	4.47	Hoop -	5.64	Vessel	Axial -
		0.4	7.11	Axial -	5.41	Hoop -	7.11	Vessel	Axial -
		0.5	8.46	Axial -	6.16	Hoop -	8.46	Vessel	Axial -
		0.6	9.96	Axial -	7.03	Hoop -	9.96	Vessel	Axial -

Table C1 (cont'd): SCF Results for Cylindrical Vessels with Moderate-To-Large-Diameter Nozzles

RT	tT	rR	Cylindrical Vessel		Cylindrical Nozzle		Overall SCF	Location	Type
			SCF	Type	SCF	Type			
135	1.5	0.7	11.54	Axial -	7.94	Hoop -	11.54	Vessel	Axial -
		0.8	12.93	Axial -	8.71	Hoop -	12.93	Vessel	Axial -
		0.9	14.52	Axial -	9.74	Hoop -	14.52	Vessel	Axial -
		1	15.50	Axial -	11.11	Hoop -	15.50	Vessel	Axial -
140	0.25	0.1	5.04	Hoop -	10.73	Axial -	10.73	Nozzle	Axial -
		0.2	8.00	Hoop -	18.58	Axial -	18.58	Nozzle	Axial -
		0.3	10.65	Hoop -	24.87	Axial -	24.87	Nozzle	Axial -
		0.4	13.26	Hoop -	30.92	Axial -	30.92	Nozzle	Axial -
		0.5	15.62	Hoop -	36.10	Axial -	36.10	Nozzle	Axial -
		0.6	18.26	Hoop -	41.98	Axial -	41.98	Nozzle	Axial -
		0.7	20.93	Hoop -	46.98	Axial -	46.98	Nozzle	Axial -
		0.8	23.60	Hoop -	52.85	Axial -	52.85	Nozzle	Axial -
		0.9	26.68	Hoop -	58.72	Axial -	58.72	Nozzle	Axial -
		1	30.85	Hoop -	64.92	Axial -	64.92	Nozzle	Axial -
	0.5	0.1	4.07	Hoop -	6.78	Axial -	6.78	Nozzle	Axial -
		0.2	6.31	Hoop -	11.90	Axial -	11.90	Nozzle	Axial -
		0.3	8.33	Hoop -	16.14	Axial -	16.14	Nozzle	Axial -
		0.4	10.27	Hoop -	20.01	Axial -	20.01	Nozzle	Axial -
		0.5	11.98	Hoop -	23.44	Axial -	23.44	Nozzle	Axial -
		0.6	13.87	Hoop -	27.01	Axial -	27.01	Nozzle	Axial -
		0.7	15.85	Hoop -	30.65	Axial -	30.65	Nozzle	Axial -
		0.8	17.69	Hoop -	34.04	Axial -	34.04	Nozzle	Axial -
		0.9	19.97	Hoop -	37.76	Axial -	37.76	Nozzle	Axial -
		1	23.12	Hoop -	41.22	Axial -	41.22	Nozzle	Axial -
	0.75	0.1	3.54	Hoop -	4.10	Hoop -	4.10	Nozzle	Hoop -
		0.2	5.41	Hoop -	6.97	Axial -	6.97	Nozzle	Axial -
		0.3	7.09	Hoop -	9.58	Axial -	9.58	Nozzle	Axial -
		0.4	8.69	Hoop -	11.99	Axial -	11.99	Nozzle	Axial -
		0.5	10.06	Hoop -	14.12	Axial -	14.12	Nozzle	Axial -
		0.6	11.60	Hoop -	16.43	Axial -	16.43	Nozzle	Axial -
		0.7	13.21	Hoop -	18.76	Axial -	18.76	Nozzle	Axial -
		0.8	14.68	Hoop -	20.97	Axial -	20.97	Nozzle	Axial -
		0.9	16.53	Hoop -	23.31	Axial -	23.31	Nozzle	Axial -
		1	19.12	Hoop -	25.35	Axial -	25.35	Nozzle	Axial -
	1	0.1	3.23	Hoop -	3.28	Hoop -	3.28	Nozzle	Hoop -
		0.2	4.89	Hoop -	4.91	Hoop -	4.91	Nozzle	Hoop -

Table C1 (cont'd): SCF Results for Cylindrical Vessels with Moderate-To-Large-Diameter Nozzles

RT	tT	rR	Cylindrical Vessel		Cylindrical Nozzle		Overall SCF	Location	Type
			SCF	Type	SCF	Type			
140	1	0.3	6.39	Hoop -	6.41	Hoop -	6.41	Nozzle	Hoop -
		0.4	7.81	Hoop -	7.83	Hoop -	7.83	Nozzle	Hoop -
		0.5	9.00	Hoop -	9.02	Hoop -	9.02	Nozzle	Hoop -
		0.6	10.37	Axial -	10.37	Hoop -	10.37	Vessel	Axial -
		0.7	11.91	Axial -	11.81	Axial -	11.91	Vessel	Axial -
		0.8	13.28	Axial -	13.22	Axial -	13.28	Vessel	Axial -
		0.9	14.85	Axial -	14.81	Axial -	14.85	Vessel	Axial -
		1	16.84	Hoop -	16.83	Hoop -	16.84	Vessel	Hoop -
	1.25	0.1	2.98	Hoop -	2.77	Hoop -	2.98	Vessel	Hoop -
		0.2	4.50	Hoop -	4.08	Hoop -	4.50	Vessel	Hoop -
		0.3	5.99	Axial -	5.28	Hoop -	5.99	Vessel	Axial -
		0.4	7.54	Axial -	6.42	Hoop -	7.54	Vessel	Axial -
		0.5	8.93	Axial -	7.34	Hoop -	8.93	Vessel	Axial -
		0.6	10.49	Axial -	8.40	Hoop -	10.49	Vessel	Axial -
		0.7	12.10	Axial -	9.52	Hoop -	12.10	Vessel	Axial -
		0.8	13.53	Axial -	10.48	Hoop -	13.53	Vessel	Axial -
		0.9	15.17	Axial -	11.75	Hoop -	15.17	Vessel	Axial -
		1	16.27	Axial -	13.47	Hoop -	16.27	Vessel	Axial -
	1.5	0.2	4.18	Axial -	3.52	Hoop -	4.18	Vessel	Axial -
		0.3	5.73	Axial -	4.53	Hoop -	5.73	Vessel	Axial -
		0.4	7.23	Axial -	5.49	Hoop -	7.23	Vessel	Axial -
		0.5	8.60	Axial -	6.25	Hoop -	8.60	Vessel	Axial -
		0.6	10.14	Axial -	7.13	Hoop -	10.14	Vessel	Axial -
		0.7	11.75	Axial -	8.05	Hoop -	11.75	Vessel	Axial -
		0.8	13.18	Axial -	8.84	Hoop -	13.18	Vessel	Axial -
		0.9	14.80	Axial -	9.89	Hoop -	14.80	Vessel	Axial -
		1	15.79	Axial -	11.29	Hoop -	15.79	Vessel	Axial -
145	0.25	0.1	5.10	Hoop -	10.93	Axial -	10.93	Nozzle	Axial -
		0.2	8.11	Hoop -	18.93	Axial -	18.93	Nozzle	Axial -
		0.3	10.79	Hoop -	25.31	Axial -	25.31	Nozzle	Axial -
		0.4	13.44	Hoop -	31.45	Axial -	31.45	Nozzle	Axial -
		0.5	15.77	Hoop -	36.45	Axial -	36.45	Nozzle	Axial -
		0.6	18.44	Hoop -	42.64	Axial -	42.64	Nozzle	Axial -
		0.7	21.21	Hoop -	47.67	Axial -	47.67	Nozzle	Axial -
		0.8	23.98	Hoop -	53.72	Axial -	53.72	Nozzle	Axial -
		0.9	27.14	Hoop -	60.03	Axial -	60.03	Nozzle	Axial -

Table C1 (cont'd): SCF Results for Cylindrical Vessels with Moderate-To-Large-Diameter Nozzles

RT	tT	rR	Cylindrical Vessel		Cylindrical Nozzle		Overall SCF	Location	Type
			SCF	Type	SCF	Type			
145	0.25	1	31.36	Hoop -	66.03	Axial -	66.03	Nozzle	Axial -
	0.5	0.1	4.12	Hoop -	6.91	Axial -	6.91	Nozzle	Axial -
		0.2	6.40	Hoop -	12.12	Axial -	12.12	Nozzle	Axial -
		0.3	8.44	Hoop -	16.42	Axial -	16.42	Nozzle	Axial -
		0.4	10.41	Hoop -	20.36	Axial -	20.36	Nozzle	Axial -
		0.5	12.11	Hoop -	23.77	Axial -	23.77	Nozzle	Axial -
		0.6	14.04	Hoop -	27.41	Axial -	27.41	Nozzle	Axial -
		0.7	16.05	Hoop -	31.11	Axial -	31.11	Nozzle	Axial -
		0.8	17.95	Hoop -	34.65	Axial -	34.65	Nozzle	Axial -
		0.9	20.27	Hoop -	38.41	Axial -	38.41	Nozzle	Axial -
		1	23.50	Hoop -	42.33	Axial -	42.33	Nozzle	Axial -
	0.75	0.1	3.59	Hoop -	4.15	Hoop -	4.15	Nozzle	Hoop -
		0.2	5.49	Hoop -	7.10	Axial -	7.10	Nozzle	Axial -
		0.3	7.19	Hoop -	9.73	Axial -	9.73	Nozzle	Axial -
		0.4	8.82	Hoop -	12.19	Axial -	12.19	Nozzle	Axial -
		0.5	10.17	Hoop -	14.32	Axial -	14.32	Nozzle	Axial -
		0.6	11.74	Hoop -	16.66	Axial -	16.66	Nozzle	Axial -
		0.7	13.38	Hoop -	19.03	Axial -	19.03	Nozzle	Axial -
		0.8	14.90	Hoop -	21.34	Axial -	21.34	Nozzle	Axial -
		0.9	16.77	Hoop -	23.71	Axial -	23.71	Nozzle	Axial -
		1	19.43	Hoop -	25.86	Axial -	25.86	Nozzle	Axial -
	1	0.1	3.27	Hoop -	3.32	Hoop -	3.32	Nozzle	Hoop -
		0.2	4.96	Hoop -	4.98	Hoop -	4.98	Nozzle	Hoop -
		0.3	6.48	Hoop -	6.50	Hoop -	6.50	Nozzle	Hoop -
		0.4	7.92	Hoop -	7.94	Hoop -	7.94	Nozzle	Hoop -
		0.5	9.11	Hoop -	9.12	Hoop -	9.12	Nozzle	Hoop -
		0.6	10.52	Axial -	10.50	Hoop -	10.52	Vessel	Axial -
		0.7	12.09	Axial -	12.00	Axial -	12.09	Vessel	Axial -
		0.8	13.52	Axial -	13.45	Axial -	13.52	Vessel	Axial -
		0.9	15.11	Axial -	15.08	Axial -	15.11	Vessel	Axial -
		1	17.11	Hoop -	17.10	Hoop -	17.11	Vessel	Hoop -
	1.25	0.1	3.02	Hoop -	2.80	Hoop -	3.02	Vessel	Hoop -
		0.2	4.57	Hoop -	4.14	Hoop -	4.57	Vessel	Hoop -
		0.3	6.09	Axial -	5.35	Hoop -	6.09	Vessel	Axial -
		0.4	7.67	Axial -	6.50	Hoop -	7.67	Vessel	Axial -
		0.5	9.05	Axial -	7.42	Hoop -	9.05	Vessel	Axial -

Table C1 (cont'd): SCF Results for Cylindrical Vessels with Moderate-To-Large-Diameter Nozzles

RT	tT	rR	Cylindrical Vessel		Cylindrical Nozzle		Overall SCF	Location	Type
			SCF	Type	SCF	Type			
145	1.25	0.6	10.64	Axial -	8.50	Hoop -	10.64	Vessel	Axial -
		0.7	12.28	Axial -	9.64	Hoop -	12.28	Vessel	Axial -
		0.8	13.78	Axial -	10.64	Hoop -	13.78	Vessel	Axial -
		0.9	15.45	Axial -	11.93	Hoop -	15.45	Vessel	Axial -
		1	16.58	Axial -	13.68	Hoop -	16.58	Vessel	Axial -
	1.5	0.2	4.25	Axial -	3.57	Hoop -	4.25	Vessel	Axial -
		0.3	5.82	Axial -	4.60	Hoop -	5.82	Vessel	Axial -
		0.4	7.35	Axial -	5.57	Hoop -	7.35	Vessel	Axial -
		0.5	8.72	Axial -	6.32	Hoop -	8.72	Vessel	Axial -
		0.6	10.29	Axial -	7.22	Hoop -	10.29	Vessel	Axial -
		0.7	11.92	Axial -	8.15	Hoop -	11.92	Vessel	Axial -
		0.8	13.42	Axial -	8.97	Hoop -	13.42	Vessel	Axial -
		0.9	15.06	Axial -	10.04	Hoop -	15.06	Vessel	Axial -
		1	16.10	Axial -	11.47	Hoop -	16.10	Vessel	Axial -

Table C2: SCF Results for Spherical and Cylindrical Vessels with Small-Diameter Nozzles

RT	tT	rR	Spherical Vessel				Cylindrical Vessel			
			Vessel		Nozzle		Vessel		Nozzle	
			SCF	Type	SCF	Type	SCF	Type	SCF	Type
10	0.25	0.025	1.88	Axial +	1.21	Hoop -	1.09	Hoop -	1.52	Hoop -
		0.05	2.03	Axial +	1.54	Axial +	1.37	Hoop -	1.75	Hoop -
	0.5	0.05	2.22	Axial +	1.21	Hoop -	1.16	Hoop -	1.50	Hoop -
	0.75	0.05	2.27	Axial +	1.19	Hoop -	1.10	Hoop -	1.29	Hoop -
		0.075	2.39	Axial +	1.22	Hoop -	1.22	Hoop -	1.46	Hoop -
15	0.25	0.017	1.78	Axial +	1.18	Hoop -	1.09	Hoop -	1.41	Hoop -
		0.05	1.98	Axial +	1.78	Axial +	1.61	Hoop -	1.80	Hoop -
	0.5	0.033	2.06	Axial +	1.17	Hoop -	1.16	Hoop -	1.39	Hoop -
		0.05	2.15	Axial +	1.24	Hoop -	1.33	Hoop -	1.62	Hoop -
	0.75	0.05	2.19	Axial +	1.17	Hoop -	1.21	Hoop -	1.46	Hoop -
	1	0.05	2.21	Axial +	1.15	Hoop -	1.15	Hoop -	1.39	Hoop -
		0.067	2.28	Axial +	1.19	Hoop -	1.24	Hoop -	1.47	Hoop -
	1.25	0.05	2.23	Axial +	1.19	Hoop -	1.13	Hoop -	1.29	Hoop -
		0.083	2.36	Axial +	1.23	Hoop -	1.24	Hoop -	1.47	Hoop -
20	0.25	0.013	1.70	Axial +	1.16	Hoop -	1.08	Hoop -	1.53	Hoop -
		0.05	1.95	Hoop +	1.97	Axial +	1.82	Hoop -	1.81	Hoop -
	0.5	0.025	1.94	Axial +	1.14	Hoop -	1.16	Hoop -	1.40	Hoop -
		0.05	2.08	Axial +	1.27	Hoop -	1.49	Hoop -	1.65	Hoop -
	0.75	0.038	2.05	Axial +	1.14	Hoop -	1.21	Hoop -	1.46	Hoop -
		0.05	2.10	Axial +	1.19	Hoop -	1.33	Hoop -	1.56	Hoop -
	1	0.05	2.13	Axial +	1.16	Hoop -	1.24	Hoop -	1.49	Hoop -
	1.25	0.05	2.16	Axial +	1.15	Hoop -	1.18	Hoop -	1.39	Hoop -
		0.063	2.19	Axial +	1.20	Hoop -	1.24	Hoop -	1.46	Hoop -
25	0.25	0.05	2.01	Axial +	1.35	Hoop +	1.63	Hoop -	1.70	Hoop -
		0.03	1.95	Axial +	1.12	Hoop -	1.21	Hoop -	1.50	Hoop -
	0.5	0.02	1.85	Axial +	1.13	Hoop -	1.16	Hoop -	1.47	Hoop -
		0.05	2.01	Axial +	1.35	Hoop +	1.63	Hoop -	1.70	Hoop -
	0.75	0.03	1.95	Axial +	1.12	Hoop -	1.21	Hoop -	1.50	Hoop -
		0.05	2.03	Axial +	1.22	Hoop -	1.43	Hoop -	1.60	Hoop -
	1	0.04	2.02	Axial +	1.15	Hoop -	1.24	Hoop -	1.44	Hoop -
		0.05	2.05	Axial +	1.19	Hoop -	1.31	Hoop -	1.52	Hoop -
	1.25	0.05	2.07	Axial +	1.18	Hoop -	1.24	Hoop -	1.46	Hoop -
	1.5	0.05	2.07	Axial +	1.18	Hoop -	1.18	Hoop -	1.40	Hoop -

Table C2 (Cont'd): SCF Results for Spherical and Cylindrical Vessels with Small-Diameter Nozzles

RT	tT	rR	Spherical Vessel				Cylindrical Vessel			
			Vessel		Nozzle		Vessel		Nozzle	
			SCF	Type	SCF	Type	SCF	Type	SCF	Type
25	1.5	0.06	2.11	Axial +	1.22	Hoop -	1.22	Hoop -	1.47	Hoop -
30	0.25	0.008	1.59	Axial +	1.15	Hoop -	1.08	Hoop -	1.37	Hoop -
		0.05	2.15	Hoop +	2.31	Hoop +	2.07	Hoop -	1.81	Hoop -
	0.5	0.017	1.78	Axial +	1.12	Hoop -	1.16	Hoop -	1.47	Hoop -
		0.05	1.96	Axial +	1.45	Hoop +	1.75	Hoop -	1.73	Hoop -
	0.75	0.025	1.87	Axial +	1.11	Hoop -	1.21	Hoop -	1.38	Hoop -
		0.05	1.98	Axial +	1.24	Hoop -	1.52	Hoop -	1.65	Hoop -
	1	0.033	1.93	Axial +	1.13	Hoop -	1.24	Hoop -	1.43	Hoop -
		0.05	2.00	Axial +	1.22	Hoop -	1.38	Hoop -	1.60	Hoop -
	1.25	0.042	1.98	Axial +	1.16	Hoop -	1.24	Hoop -	1.46	Hoop -
		0.05	2.01	Axial +	1.21	Hoop -	1.29	Hoop -	1.51	Hoop -
	1.5	0.05	2.02	Axial +	1.20	Hoop -	1.22	Hoop -	1.46	Hoop -
35	0.25	0.007	1.55	Axial +	1.14	Hoop -	1.08	Hoop -	1.57	Hoop -
		0.05	2.22	Hoop +	2.45	Hoop +	2.13	Hoop -	1.84	Hoop +
	0.5	0.014	1.72	Axial +	1.11	Hoop -	1.16	Hoop -	1.39	Hoop -
		0.05	1.92	Axial +	1.55	Hoop +	1.82	Hoop -	1.74	Hoop -
	0.75	0.021	1.81	Axial +	1.10	Hoop -	1.21	Hoop -	1.43	Hoop -
		0.05	1.93	Axial +	1.27	Hoop -	1.59	Hoop -	1.68	Hoop -
	1	0.029	1.86	Axial +	1.12	Hoop -	1.24	Hoop -	1.43	Hoop -
		0.05	1.95	Axial +	1.24	Hoop -	1.44	Hoop -	1.60	Hoop -
	1.25	0.036	1.91	Axial +	1.16	Hoop -	1.24	Hoop -	1.47	Hoop -
		0.05	1.96	Axial +	1.23	Hoop -	1.33	Hoop -	1.55	Hoop -
	1.5	0.043	1.94	Axial +	1.19	Hoop -	1.22	Hoop -	1.42	Hoop -
		0.05	1.97	Axial +	1.22	Hoop -	1.26	Hoop -	1.51	Hoop -
40	0.25	0.006	1.51	Axial +	1.14	Hoop -	1.08	Hoop -	1.40	Hoop -
		0.05	2.28	Hoop +	2.59	Hoop +	2.20	Hoop -	2.02	Hoop +
	0.5	0.013	1.67	Axial +	1.11	Hoop -	1.16	Hoop -	1.39	Hoop -
		0.05	1.88	Axial +	1.63	Hoop +	1.89	Hoop -	1.75	Hoop -
	0.75	0.019	1.75	Axial +	1.10	Hoop -	1.21	Hoop -	1.42	Hoop -
		0.05	1.90	Axial +	1.29	Hoop -	1.65	Hoop -	1.71	Hoop -
	1	0.025	1.81	Axial +	1.12	Hoop -	1.24	Hoop -	1.44	Hoop -
		0.05	1.91	Axial +	1.27	Hoop -	1.49	Hoop -	1.66	Hoop -
	1.25	0.031	1.84	Axial +	1.15	Hoop -	1.24	Hoop -	1.45	Hoop -
		0.05	1.92	Axial +	1.25	Hoop -	1.37	Hoop -	1.61	Hoop -
	1.5	0.038	1.88	Axial +	1.19	Hoop -	1.22	Hoop -	1.42	Hoop -

Table C2 (Cont'd): SCF Results for Spherical and Cylindrical Vessels with Small-Diameter Nozzles

RT	tT	rR	Spherical Vessel				Cylindrical Vessel			
			Vessel		Nozzle		Vessel		Nozzle	
			SCF	Type	SCF	Type	SCF	Type	SCF	Type
40	1.5	0.05	1.92	Axial +	1.24	Hoop -	1.29	Hoop -	1.57	Hoop -
45	0.25	0.006	1.48	Axial +	1.14	Hoop -	1.08	Hoop -	1.41	Hoop -
		0.05	2.34	Hoop +	2.70	Hoop +	2.25	Hoop -	2.21	Hoop +
	0.5	0.011	1.64	Axial +	1.10	Hoop -	1.16	Hoop -	1.36	Hoop -
		0.05	1.87	Axial +	1.70	Hoop +	1.94	Hoop -	1.76	Hoop -
	0.75	0.017	1.71	Axial +	1.09	Hoop -	1.21	Hoop -	1.40	Hoop -
		0.05	1.87	Axial +	1.31	Hoop -	1.70	Hoop -	1.73	Hoop -
	1	0.022	1.76	Axial +	1.11	Hoop -	1.24	Hoop -	1.44	Hoop -
		0.05	1.88	Axial +	1.29	Hoop -	1.53	Hoop -	1.68	Hoop -
	1.25	0.028	1.79	Axial +	1.15	Hoop -	1.23	Hoop -	1.36	Hoop -
		0.05	1.89	Axial +	1.27	Hoop -	1.41	Hoop -	1.64	Hoop -
	1.5	0.033	1.82	Axial +	1.18	Hoop -	1.22	Hoop -	1.46	Hoop -
		0.05	1.89	Axial +	1.26	Hoop -	1.31	Hoop -	1.57	Hoop -
55	0.25	0.005	1.44	Axial +	1.13	Hoop -	1.08	Hoop -	1.50	Hoop -
		0.05	2.44	Hoop +	2.91	Hoop +	2.34	Hoop +	2.40	Hoop +
	0.5	0.009	1.57	Axial +	1.10	Hoop -	1.16	Hoop -	1.36	Hoop -
		0.05	1.93	Hoop +	1.84	Hoop +	2.03	Hoop -	1.78	Hoop -
	0.75	0.014	1.64	Axial +	1.08	Hoop -	1.21	Hoop -	1.45	Hoop -
		0.05	1.83	Axial +	1.34	Hoop -	1.78	Hoop -	1.75	Hoop -
	1	0.018	1.68	Axial +	1.11	Hoop -	1.23	Hoop -	1.36	Hoop -
		0.05	1.84	Axial +	1.32	Hoop -	1.60	Hoop -	1.72	Hoop -
	1.25	0.023	1.71	Axial +	1.14	Hoop -	1.24	Hoop -	1.36	Hoop -
		0.05	1.84	Axial +	1.31	Hoop -	1.46	Hoop -	1.68	Hoop -
	1.5	0.027	1.74	Axial +	1.17	Hoop -	1.22	Hoop -	1.47	Hoop -
		0.05	1.84	Axial +	1.29	Hoop -	1.35	Hoop -	1.63	Hoop -
60	0.25	0.004	1.42	Axial +	1.13	Hoop -	1.08	Hoop -	1.38	Hoop -
		0.05	2.48	Hoop +	3.00	Hoop +	2.43	Hoop +	2.51	Hoop +
	0.5	0.008	1.54	Axial +	1.09	Hoop -	1.16	Hoop -	1.47	Hoop -
		0.05	1.97	Hoop +	1.90	Hoop +	2.05	Hoop -	1.78	Hoop -
	0.75	0.013	1.61	Axial +	1.08	Hoop -	1.21	Hoop -	1.35	Hoop -
		0.05	1.81	Axial +	1.35	Hoop -	1.80	Hoop -	1.77	Hoop -
	1	0.017	1.65	Axial +	1.10	Hoop -	1.24	Hoop -	1.40	Hoop -
		0.05	1.83	Axial +	1.34	Hoop -	1.63	Hoop -	1.74	Hoop -
	1.25	0.021	1.68	Axial +	1.14	Hoop -	1.24	Hoop -	1.37	Hoop -
		0.05	1.83	Axial +	1.32	Hoop -	1.48	Hoop -	1.71	Hoop -

Table C2 (Cont'd): SCF Results for Spherical and Cylindrical Vessels with Small-Diameter Nozzles

RT	tT	rR	Spherical Vessel				Cylindrical Vessel			
			Vessel		Nozzle		Vessel		Nozzle	
			SCF	Type	SCF	Type	SCF	Type	SCF	Type
60	1.5	0.025	1.71	Axial +	1.17	Hoop -	1.22	Hoop -	1.47	Hoop -
		0.05	1.82	Axial +	1.30	Hoop -	1.37	Hoop -	1.65	Hoop -
65	0.25	0.004	1.40	Axial +	1.13	Hoop -	1.08	Hoop -	1.41	Hoop -
		0.05	2.52	Hoop +	3.09	Hoop +	2.45	Hoop +	2.68	Hoop +
	0.5	0.008	1.52	Axial +	1.09	Hoop -	1.16	Hoop -	1.43	Hoop -
		0.05	2.01	Hoop +	1.95	Hoop +	2.09	Hoop -	1.80	Hoop -
	0.75	0.012	1.58	Axial +	1.08	Hoop -	1.21	Hoop -	1.35	Hoop -
		0.05	1.81	Axial +	1.38	Hoop +	1.83	Hoop -	1.79	Hoop -
	1	0.015	1.62	Axial +	1.10	Hoop -	1.24	Hoop -	1.39	Hoop -
		0.05	1.82	Axial +	1.35	Hoop -	1.64	Hoop -	1.75	Hoop -
	1.25	0.019	1.65	Axial +	1.14	Hoop -	1.24	Hoop -	1.46	Hoop -
		0.05	1.82	Axial +	1.34	Hoop -	1.50	Hoop -	1.72	Hoop -
	1.5	0.023	1.68	Axial +	1.17	Hoop -	1.22	Hoop -	1.47	Hoop -
		0.05	1.81	Axial +	1.32	Hoop -	1.39	Hoop -	1.68	Hoop -
70	0.25	0.004	1.39	Axial +	1.13	Hoop -	1.08	Hoop -	1.39	Hoop -
		0.05	2.55	Hoop +	3.17	Hoop +	2.61	Hoop +	2.80	Hoop +
	0.5	0.007	1.50	Axial +	1.09	Hoop -	1.16	Hoop -	1.51	Hoop -
		0.05	2.04	Hoop +	2.01	Hoop +	2.11	Hoop -	1.80	Hoop -
	0.75	0.011	1.56	Axial +	1.08	Hoop -	1.21	Hoop -	1.45	Hoop -
		0.05	1.80	Axial +	1.42	Hoop +	1.85	Hoop -	1.80	Hoop -
	1	0.014	1.60	Axial +	1.10	Hoop -	1.24	Hoop -	1.36	Hoop -
		0.05	1.81	Axial +	1.37	Hoop -	1.66	Hoop -	1.77	Hoop -
	1.25	0.018	1.63	Axial +	1.14	Hoop -	1.24	Hoop -	1.33	Hoop -
		0.05	1.81	Axial +	1.35	Hoop -	1.52	Hoop -	1.74	Hoop -
	1.5	0.021	1.65	Axial +	1.17	Hoop -	1.22	Hoop -	1.33	Hoop -
		0.05	1.79	Axial +	1.33	Hoop -	1.41	Hoop -	1.69	Hoop -
80	0.25	0.003	1.37	Axial +	1.13	Hoop -	1.06	Hoop -	1.38	Hoop -
		0.05	2.62	Hoop +	3.32	Hoop +	2.72	Hoop +	2.93	Hoop +
	0.5	0.006	1.46	Axial +	1.09	Hoop -	1.16	Hoop -	1.48	Hoop -
		0.05	2.10	Hoop +	2.10	Hoop +	2.14	Hoop -	1.84	Hoop +
	0.75	0.009	1.51	Axial +	1.07	Hoop -	1.21	Hoop -	1.44	Hoop -
		0.05	1.83	Hoop +	1.49	Hoop +	1.89	Hoop -	1.80	Hoop -
	1	0.013	1.55	Axial +	1.10	Hoop -	1.24	Hoop -	1.37	Hoop -
		0.05	1.79	Axial +	1.39	Hoop -	1.70	Hoop -	1.79	Hoop -
	1.25	0.016	1.58	Axial +	1.13	Hoop -	1.24	Hoop -	1.36	Hoop -

Table C2 (Cont'd): SCF Results for Spherical and Cylindrical Vessels with Small-Diameter Nozzles

RT	tT	rR	Spherical Vessel				Cylindrical Vessel			
			Vessel		Nozzle		Vessel		Nozzle	
			SCF	Type	SCF	Type	SCF	Type	SCF	Type
80	1.25	0.05	1.79	Axial +	1.38	Hoop -	1.55	Hoop -	1.76	Hoop -
	1.5	0.019	1.60	Axial +	1.17	Hoop -	1.22	Hoop -	1.41	Hoop -
		0.05	1.77	Axial +	1.36	Hoop -	1.43	Hoop -	1.71	Hoop -
85	0.25	0.003	1.35	Axial +	1.13	Hoop -	1.06	Hoop -	1.42	Hoop -
		0.05	2.65	Hoop +	3.40	Axial +	2.66	Hoop +	2.97	Hoop +
	0.5	0.006	1.45	Axial +	1.08	Hoop -	1.16	Hoop -	1.40	Hoop -
		0.05	2.12	Hoop +	2.15	Hoop +	2.18	Hoop +	1.94	Hoop +
	0.75	0.009	1.50	Axial +	1.07	Hoop -	1.21	Hoop -	1.43	Hoop -
		0.05	1.86	Hoop +	1.53	Hoop +	1.91	Hoop -	1.82	Hoop -
	1	0.012	1.53	Axial +	1.10	Hoop -	1.24	Hoop -	1.38	Hoop -
		0.05	1.79	Axial +	1.40	Hoop -	1.71	Hoop -	1.80	Hoop -
	1.25	0.015	1.56	Axial +	1.13	Hoop -	1.24	Hoop -	1.37	Hoop -
		0.05	1.78	Axial +	1.39	Hoop -	1.56	Hoop -	1.76	Hoop -
	1.5	0.018	1.58	Axial +	1.17	Hoop -	1.22	Hoop -	1.42	Hoop -
		0.05	1.77	Axial +	1.37	Hoop -	1.44	Hoop -	1.72	Hoop -
90	0.25	0.003	1.35	Axial +	1.13	Hoop -	1.06	Hoop -	1.44	Hoop -
		0.05	2.67	Hoop +	3.47	Axial +	2.76	Hoop +	3.12	Hoop +
	0.5	0.006	1.43	Axial +	1.08	Hoop -	1.16	Hoop -	1.41	Hoop -
		0.05	2.15	Hoop +	2.20	Hoop +	2.18	Hoop +	2.05	Hoop +
	0.75	0.008	1.48	Axial +	1.07	Hoop -	1.22	Hoop -	1.35	Hoop -
		0.05	1.89	Hoop +	1.56	Hoop +	1.91	Hoop -	1.81	Hoop -
	1	0.011	1.52	Axial +	1.09	Hoop -	1.24	Hoop -	1.31	Hoop -
		0.05	1.79	Axial +	1.41	Hoop -	1.73	Hoop -	1.80	Hoop -
	1.25	0.014	1.54	Axial +	1.13	Hoop -	1.24	Hoop -	1.43	Hoop -
		0.05	1.78	Axial +	1.40	Hoop -	1.57	Hoop -	1.77	Hoop -
	1.5	0.017	1.56	Axial +	1.16	Hoop -	1.22	Hoop -	1.44	Hoop -
		0.05	1.76	Axial +	1.38	Hoop -	1.46	Hoop -	1.73	Hoop -
95	0.25	0.003	1.34	Axial +	1.14	Hoop -	1.06	Hoop -	1.47	Hoop -
		0.05	2.70	Hoop +	3.55	Axial +	2.78	Hoop +	3.16	Hoop +
	0.5	0.005	1.42	Axial +	1.08	Hoop -	1.16	Hoop -	1.39	Hoop -
		0.05	2.17	Hoop +	2.23	Hoop +	2.26	Hoop +	2.04	Hoop +
	0.75	0.008	1.47	Axial +	1.07	Hoop -	1.21	Hoop -	1.44	Hoop -
		0.05	1.91	Hoop +	1.59	Hoop +	1.93	Hoop -	1.83	Hoop -
	1	0.011	1.50	Axial +	1.09	Hoop -	1.24	Hoop -	1.44	Hoop -
		0.05	1.79	Axial +	1.43	Hoop -	1.74	Hoop -	1.81	Hoop -

Table C2 (Cont'd): SCF Results for Spherical and Cylindrical Vessels with Small-Diameter Nozzles

RT	tT	rR	Spherical Vessel				Cylindrical Vessel			
			Vessel		Nozzle		Vessel		Nozzle	
			SCF	Type	SCF	Type	SCF	Type	SCF	Type
95	1.25	0.013	1.53	Axial +	1.13	Hoop -	1.24	Hoop -	1.37	Hoop -
		0.05	1.78	Axial +	1.41	Hoop -	1.59	Hoop -	1.78	Hoop -
	1.5	0.016	1.55	Axial +	1.16	Hoop -	1.23	Hoop -	1.36	Hoop -
		0.05	1.76	Axial +	1.39	Hoop -	1.47	Hoop -	1.73	Hoop -
105	0.25	0.002	1.32	Axial +	1.14	Hoop -	1.08	Hoop -	1.36	Hoop -
		0.05	2.75	Hoop +	3.70	Axial +	2.94	Hoop +	3.46	Hoop +
	0.5	0.005	1.39	Axial +	1.08	Hoop -	1.16	Hoop -	1.34	Hoop -
		0.05	2.22	Hoop +	2.32	Hoop +	2.33	Hoop +	2.15	Hoop +
	0.75	0.007	1.44	Axial +	1.07	Hoop -	1.21	Hoop -	1.43	Hoop -
		0.05	1.96	Hoop +	1.64	Hoop +	1.95	Hoop -	1.83	Hoop -
	1	0.010	1.47	Axial +	1.09	Hoop -	1.24	Hoop -	1.37	Hoop -
		0.05	1.81	Hoop +	1.45	Hoop -	1.78	Hoop +	1.83	Hoop -
	1.25	0.012	1.50	Axial +	1.13	Hoop -	1.24	Hoop -	1.40	Hoop -
		0.05	1.78	Axial +	1.44	Hoop -	1.61	Hoop -	1.80	Hoop -
	1.5	0.014	1.51	Axial +	1.16	Hoop -	1.23	Hoop -	1.43	Hoop -
		0.05	1.75	Axial +	1.41	Hoop -	1.48	Hoop -	1.75	Hoop -
110	0.25	0.002	1.31	Axial +	1.14	Hoop -	1.09	Hoop -	1.44	Hoop -
		0.05	2.77	Hoop +	3.78	Axial +	2.99	Hoop +	3.43	Hoop +
	0.5	0.005	1.39	Axial +	1.08	Hoop -	1.16	Hoop -	1.37	Hoop -
		0.05	2.24	Hoop +	2.35	Hoop +	2.31	Hoop +	2.17	Hoop +
	0.75	0.007	1.43	Axial +	1.07	Hoop -	1.21	Hoop -	1.44	Hoop -
		0.05	1.98	Hoop +	1.67	Hoop +	2.01	Hoop +	1.84	Hoop -
	1	0.009	1.46	Axial +	1.10	Hoop -	1.24	Hoop -	1.37	Hoop -
		0.05	1.83	Hoop +	1.46	Hoop -	1.77	Hoop -	1.84	Hoop -
	1.25	0.011	1.48	Axial +	1.13	Hoop -	1.24	Hoop -	1.44	Hoop -
		0.05	1.77	Axial +	1.45	Hoop -	1.62	Hoop -	1.81	Hoop -
	1.5	0.014	1.50	Axial +	1.16	Hoop -	1.22	Hoop -	1.41	Hoop -
		0.05	1.75	Axial +	1.42	Hoop -	1.49	Hoop -	1.75	Hoop -
115	0.25	0.002	1.31	Axial +	1.14	Hoop -	1.06	Hoop -	1.43	Hoop -
		0.05	2.79	Hoop +	3.85	Axial +	3.03	Hoop +	3.50	Hoop +
	0.5	0.004	1.38	Axial +	1.08	Hoop -	1.16	Hoop -	1.46	Hoop -
		0.05	2.26	Hoop +	2.39	Hoop +	2.43	Hoop +	2.26	Hoop +
	0.75	0.007	1.42	Axial +	1.07	Hoop -	1.22	Hoop -	1.35	Hoop -
		0.05	2.00	Hoop +	1.70	Hoop +	2.02	Hoop +	1.84	Hoop -
	1	0.009	1.45	Axial +	1.09	Hoop -	1.23	Hoop -	1.37	Hoop -

Table C2 (Cont'd): SCF Results for Spherical and Cylindrical Vessels with Small-Diameter Nozzles

RT	tT	rR	Spherical Vessel				Cylindrical Vessel			
			Vessel		Nozzle		Vessel		Nozzle	
			SCF	Type	SCF	Type	SCF	Type	SCF	Type
115	1	0.05	1.85	Hoop +	1.46	Hoop -	1.79	Hoop +	1.84	Hoop -
	1.25	0.011	1.47	Axial +	1.13	Hoop -	1.24	Hoop -	1.44	Hoop -
		0.05	1.78	Axial +	1.45	Hoop -	1.64	Hoop +	1.81	Hoop -
	1.5	0.013	1.49	Axial +	1.16	Hoop -	1.23	Hoop -	1.43	Hoop -
		0.05	1.75	Axial +	1.43	Hoop -	1.50	Hoop -	1.76	Hoop -
120	0.25	0.002	1.30	Axial +	1.13	Hoop -	1.08	Hoop -	1.44	Hoop -
		0.05	2.81	Hoop +	3.93	Axial +	3.03	Hoop +	3.57	Hoop +
	0.5	0.004	1.37	Axial +	1.08	Hoop -	1.16	Hoop -	1.37	Hoop -
		0.05	2.28	Hoop +	2.42	Hoop +	2.44	Hoop +	2.37	Hoop +
	0.75	0.006	1.41	Axial +	1.07	Hoop -	1.21	Hoop -	1.34	Hoop -
		0.05	2.02	Hoop +	1.72	Hoop +	2.05	Hoop +	1.84	Hoop -
	1	0.008	1.44	Axial +	1.09	Hoop -	1.24	Hoop -	1.38	Hoop -
		0.05	1.87	Hoop +	1.47	Hoop -	1.82	Hoop +	1.84	Hoop -
	1.25	0.010	1.46	Axial +	1.13	Hoop -	1.24	Hoop -	1.36	Hoop -
		0.05	1.78	Axial +	1.46	Hoop -	1.67	Hoop +	1.81	Hoop -
	1.5	0.013	1.47	Axial +	1.16	Hoop -	1.23	Hoop -	1.42	Hoop -
		0.05	1.75	Axial +	1.44	Hoop -	1.51	Hoop -	1.76	Hoop -
	125	0.25	0.002	1.29	Axial +	1.13	Hoop -	1.08	Hoop -	1.45
0.05			2.84	Hoop +	3.99	Axial +	3.10	Hoop +	3.63	Hoop +
0.5		0.004	1.36	Axial +	1.08	Hoop -	1.16	Hoop -	1.38	Hoop -
		0.05	2.30	Hoop +	2.46	Hoop +	2.44	Hoop +	2.41	Hoop +
0.75		0.006	1.40	Axial +	1.07	Hoop -	1.21	Hoop -	1.38	Hoop -
		0.05	2.04	Hoop +	1.74	Hoop +	2.10	Hoop +	1.85	Hoop -
1		0.008	1.43	Axial +	1.09	Hoop -	1.24	Hoop -	1.35	Hoop -
		0.05	1.89	Hoop +	1.48	Hoop -	1.85	Hoop +	1.85	Hoop -
1.25		0.01	1.45	Axial +	1.13	Hoop -	1.24	Hoop -	1.44	Hoop -
		0.05	1.78	Axial +	1.47	Hoop -	1.70	Hoop +	1.82	Hoop -
1.5		0.012	1.47	Axial +	1.15	Hoop -	1.22	Hoop -	1.42	Hoop -
		0.05	1.75	Axial +	1.45	Hoop -	1.52	Hoop -	1.78	Hoop -
130		0.25	0.002	1.29	Axial +	1.13	Hoop -	1.07	Hoop -	1.46
	0.05		2.86	Hoop +	4.06	Axial +	3.12	Hoop +	3.71	Hoop +
	0.5	0.004	1.35	Axial +	1.08	Hoop -	1.16	Hoop -	1.47	Hoop -
		0.05	2.32	Hoop +	2.49	Hoop +	2.51	Hoop +	2.42	Hoop +
	0.75	0.006	1.39	Axial +	1.07	Hoop -	1.21	Hoop -	1.37	Hoop -
		0.05	2.06	Hoop +	1.77	Hoop +	2.15	Hoop +	1.85	Hoop -

Table C2 (Cont'd): SCF Results for Spherical and Cylindrical Vessels with Small-Diameter Nozzles

RT	tT	rR	Spherical Vessel				Cylindrical Vessel			
			Vessel		Nozzle		Vessel		Nozzle	
			SCF	Type	SCF	Type	SCF	Type	SCF	Type
130	1	0.008	1.42	Axial +	1.09	Hoop -	1.24	Hoop -	1.39	Hoop -
		0.05	1.91	Hoop +	1.49	Hoop -	1.92	Hoop +	1.86	Hoop -
	1.25	0.010	1.44	Axial +	1.13	Hoop -	1.24	Hoop -	1.32	Hoop -
		0.05	1.79	Hoop +	1.48	Hoop -	1.75	Hoop +	1.82	Hoop -
	1.5	0.012	1.45	Axial +	1.16	Hoop -	1.23	Hoop -	1.42	Hoop -
		0.05	1.76	Axial +	1.46	Hoop -	1.55	Hoop +	1.78	Hoop -
135	0.25	0.002	1.28	Axial +	1.14	Hoop -	1.05	Hoop -	1.44	Hoop -
		0.05	2.88	Hoop +	4.13	Axial +	3.15	Hoop +	3.81	Hoop +
	0.5	0.004	1.34	Axial +	1.08	Hoop -	1.16	Hoop -	1.36	Hoop -
		0.05	2.34	Hoop +	2.52	Hoop +	2.53	Hoop +	2.49	Hoop +
	0.75	0.006	1.38	Axial +	1.07	Hoop -	1.21	Hoop -	1.44	Hoop -
		0.05	2.08	Hoop +	1.79	Hoop +	2.17	Hoop +	1.85	Hoop -
	1	0.007	1.41	Axial +	1.09	Hoop -	1.24	Hoop -	1.36	Hoop -
		0.05	1.93	Hoop +	1.50	Hoop -	1.95	Hoop +	1.86	Hoop -
	1.25	0.009	1.43	Axial +	1.13	Hoop -	1.24	Hoop -	1.43	Hoop -
		0.05	1.81	Hoop +	1.49	Hoop -	1.75	Hoop +	1.83	Hoop -
	1.5	0.011	1.44	Axial +	1.16	Hoop -	1.23	Hoop -	1.42	Hoop -
		0.05	1.76	Axial +	1.46	Hoop -	1.57	Hoop +	1.79	Hoop -
140	0.25	0.002	1.28	Axial +	1.14	Hoop -	1.05	Hoop -	1.39	Hoop -
		0.05	2.90	Hoop +	4.19	Axial +	3.19	Hoop +	3.87	Hoop +
	0.5	0.004	1.34	Axial +	1.08	Hoop -	1.16	Hoop -	1.37	Hoop -
		0.05	2.36	Hoop +	2.55	Hoop +	2.55	Hoop +	2.52	Hoop +
	0.75	0.005	1.37	Axial +	1.07	Hoop -	1.21	Hoop -	1.35	Hoop -
		0.05	2.10	Hoop +	1.81	Hoop +	2.24	Hoop +	1.86	Hoop -
	1	0.007	1.40	Axial +	1.09	Hoop -	1.24	Hoop -	1.37	Hoop -
		0.05	1.95	Hoop +	1.51	Hoop -	1.97	Hoop +	1.86	Hoop -
	1.25	0.009	1.42	Axial +	1.13	Hoop -	1.24	Hoop -	1.37	Hoop -
		0.05	1.83	Hoop +	1.50	Hoop -	1.78	Hoop +	1.84	Hoop -
	1.5	0.011	1.43	Axial +	1.16	Hoop -	1.23	Hoop -	1.42	Hoop -
		0.05	1.76	Axial +	1.47	Hoop -	1.64	Hoop +	1.79	Hoop -
145	0.25	0.002	1.27	Axial +	1.15	Hoop -	1.05	Hoop -	1.32	Hoop -
		0.05	2.91	Hoop +	4.24	Axial +	3.21	Hoop +	3.96	Hoop +
	0.5	0.003	1.33	Axial +	1.08	Hoop -	1.16	Hoop -	1.32	Hoop -
		0.05	2.38	Hoop +	2.58	Hoop +	2.60	Hoop +	2.59	Hoop +
	0.75	0.005	1.37	Axial +	1.07	Hoop -	1.21	Hoop -	1.44	Hoop -

Table C2 (Cont'd): SCF Results for Spherical and Cylindrical Vessels with Small-Diameter Nozzles

RT	tT	rR	Spherical Vessel				Cylindrical Vessel			
			Vessel		Nozzle		Vessel		Nozzle	
			SCF	Type	SCF	Type	SCF	Type	SCF	Type
145	0.75	0.05	2.12	Hoop +	1.83	Hoop +	2.24	Hoop +	1.86	Hoop -
	1	0.007	1.39	Axial +	1.09	Hoop -	1.24	Hoop -	1.38	Hoop -
		0.05	1.97	Hoop +	1.51	Hoop -	2.01	Hoop +	1.86	Hoop -
	1.25	0.009	1.41	Axial +	1.13	Hoop -	1.24	Hoop -	1.40	Hoop -
		0.05	1.85	Hoop +	1.51	Hoop -	1.82	Hoop +	1.84	Hoop -
	1.5	0.010	1.43	Axial +	1.16	Hoop -	1.23	Hoop -	1.39	Hoop -
		0.05	1.77	Axial +	1.48	Hoop -	1.66	Hoop +	1.79	Hoop -

VITA

NAME : **Faisal Muhammad Mukhtar**
PLACE OF BIRTH : Daura, Katsina State, Nigeria.
E-MAIL : faisalmmukhtar@gmail.com

EDUCATIONAL QUALIFICATIONS

- **Ph.D. Civil Engineering - Structures** (May, 2015)
King Fahd University of Petroleum & Minerals, Dhahran, Saudi Arabia.
- **M.Sc Civil Engineering - Structures** (January, 2012)
King Fahd University of Petroleum & Minerals, Dhahran, Saudi Arabia.
- **B.Eng Civil Engineering** (February, 2008)
Bayero University Kano, Nigeria.

MAJOR ACHIEVEMENTS AND AWARDS

- Obtained First Class Honors at the completion of the B.Eng program.
- Award for the best final year research project in the B.Eng program.
- KFUPM M.Sc Scholarship, 2009.
- Obtained First Class Honors at the completion of the M.Sc Course-Work.
- KFUPM Ph.D. Scholarship, 2012.
- Obtained First Class Honors at the completion of the Ph.D. Course-Work.

WORK EXPERIENCE

- Lecturer-B, King Fahd University of Petroleum & Minerals, 2012 - 2015
- Research Assistant, King Fahd University of Petroleum & Minerals, 2009 - 2012
- Assistant Lecturer during the National Youth Service Corps (NYSC) Scheme, Federal Polytechnic Idah, Nigeria, 2008 – 2009

- Intern under Students' Industrial Work Experience Scheme at Standard Construction Ltd., Nigeria, 2006
- Intern under Students' Industrial Work Experience Scheme at Wuro Associates Consultancy Firm, Nigeria, 2005

SYMPOSIUM, SEMINARS, WORKSHOPS, AND SHORT COURSE(S)

(a) Educational

- Workshop on 'Introduction to Maplesoft' organized by Dassault Systèmes Simulia Corp., March 2015
- Seminar titled 'Enhancing Research Skills' organized by Teaching & Learning Center, Deanship of Academic Development KFUPM, March 2015
- Short course titled 'Process Oriented Guided Inquiry Learning (POGIL)' organized by Teaching & Learning Center, Deanship of Academic Development KFUPM, Feb. 2015
- Short course titled 'Experience Sharing Forum on Students Centered Learning Techniques' organized by Teaching & Learning Center, Deanship of Academic Development KFUPM, Feb. 2015
- Workshop on 'Instructional Objectives' organized by Teaching & Learning Center, Deanship of Academic Development KFUPM, Nov. 2014
- Short course in 'Geotechnical Earthquake Engineering – Contemporary Topics' offered by the Civil & Environmental Engineering Department KFUPM, Mar. 2014
- Workshop on 'Participatory Classrooms' organized by Teaching & Learning Center, Deanship of Academic Development KFUPM, Feb. 2014
- 3rd KFUPM Research Day, organized by Deanship of Research, KFUPM, May 2013
- 'Finite Element Analysis Using ABAQUS', Dassault Systèmes Simulia Corp., 2012
- 'Introduction to Advanced Element Analysis' organized by Center for Engineering Research, Research Institute, KFUPM, 2010
- 'Finite Element Analysis Using COMSOL' organized by Center for Engineering Research, Research Institute, KFUPM, 2010
- Training on 'New Curriculum for Teachers' organized by Federal Polytechnic, Idah, Nigeria, Dec. 2008

(b) Technical

- 6th Workshop on Concrete Deterioration and its Prevention, KFUPM, 2013
- ‘Prescription to Performance-Based Specifications’ Technical Seminar, Al-Khobar, Feb. 2012
- ACI Technical Seminar ‘Concrete Products Containing Microsilica and Fly Ash’, Dec. 2010
- ACI Technical Seminar ‘Engineering An Idea – The Burj Khalifa Tower’, Oct. 2010

PRESENTATIONS

- ‘Modeling and Simulation Using COMSOL Multiphysics’, presented to CEE Graduate Students (CE-510 Term 132), KFUPM, May 2014.
- ‘Numerical Simulation of Slump Flow and L-box Tests for Self-Compacting Concrete (SCC)’, presented at the 9CONCRETE-2013, Hilton Hotel, Manama, Bahrain, Feb 2013.
- ‘Computational Fluid Dynamics Simulation of SCC Using NSYS/FLUENT’, presented at the ACI Eastern Province’s board meeting, Oct. 2011.

PUBLICATIONS

(a) Journals

- Husain J. Al-Gahtani and **Faisal M. Mukhtar**, (2014), ‘RBF-based meshless method for the free vibration of beams on elastic foundations’, *Applied Mathematics and Computation*, 249:198-208. doi: 10.1016/j.amc.2014.09.097
- **Faisal M. Mukhtar** and Ali H. Al-Gadhib, (2014), ‘Collocation Method for Elastoplastic Analysis of a Pressurized Functionally Graded Tube’, *Arabian Journal for Science & Engineering*, 39(11): 7701-7716. doi: 10.1007/s13369-014-1383-1
- **Faisal M. Mukhtar** and Husain J. Al-Gahtani, (2014), ‘Application of radial basis functions to the problem of elasto-plastic torsion of prismatic bars’, submitted to *Applied Mathematical Modeling*, (reviewers’ comments received; minor corrections in progress, manuscript APM-D-14-00113)
- **Mukhtar, F. M.** and Al-Gahtani, H. J., (2014), ‘Comprehensive evaluation of SCF for spherical pressure vessels intersected by radial cylindrical nozzles’, submitted to *International Journal of Pressure Vessels & Piping* (manuscript IPVP-D-14-00229)

- Al-Gahtani, H. J. and **Mukhtar, F. M.**, (2015), ‘Simplified formulation of stress concentration factors for spherical pressure vessel-cylindrical nozzle juncture’, submitted to ASME Pressure Vessel Technology (manuscript PVT-15-1013)
- **F. M. Mukhtar** and H. J. Al-Gahtani, ‘Analysis of discontinuity stresses in cylindrical vessel-cylindrical nozzle intersections’, in progress
- **F. M. Mukhtar** and H. J. Al-Gahtani, ‘Finite element analysis and development of design charts for spherical vessels with small-diameter nozzles under internal pressure’, in progress
- Al-Gahtani, H. J. and **Mukhtar, F. M.**, ‘Analysis and development of design charts for cylindrical pressure vessels intersected by small-diameter nozzles’, in progress

(b) Conferences

- M. H. Baluch, M. K. Rahman and **F. M. Mukhtar**, ‘Simulation of Flow and Formwork Pressure in Self Consolidating Concrete (SCC)’, *The Fifth North American Conference on the Design and Use of Self-Consolidating Concrete*, Chicago, USA, May 2013.
- **F. M. Mukhtar**, M. H. Baluch and M. K. Rahman, ‘Numerical Simulation of Slump Flow and L-box Tests for Self-Compacting Concrete (SCC)’, *9th International Concrete Conference (9CONCRETE-2013)*, Manama, Bahrain, Feb 2013.
- M. H. Baluch, M. K. Rahman, **F. M. Mukhtar** and N. Saleem, ‘Finite Element Modeling for Predicting the Evolution of Formwork Pressure by Self Compacting Concrete’, *International Conference on Advanced Concrete Technology & Its Applications (ACTA-2012)*, NUST, Islamabad, Pakistan, Nov 2012.
- H. Al-Gadhib, J. Wang and **F. Mukhtar**, ‘Assessment and Modeling of Qualitative Damage-Induced Chloride Diffusivity on Concrete Durability’, *International Congress on Durability of Concrete*, Trondheim, Norway, Jun 2012.
- M. H. Baluch, M. K. Rahman, M. Q. Saeed, **F. Mukhtar**, ‘Computational Modeling of Concrete in Fresh and in Hardened States’, *Workshop on the*

Sustainability of Concrete Industry in Saudi Arabia, University of Dammam, Saudi Arabia, April 2012.

- **F. Mukhtar** and A. H. Al-Gadhib, 'Numerical Simulation of Chloride Front Movement into Stressed Reinforced Concrete', *Thirteenth International Conference on Civil, Structural and Environmental Engineering Computing*, Chania, Greece, Sep 2011.
- M. H. Baluch, M. K. Rahman, **F. Mukhtar** and M. A. Malik, 'A 2-D computational fluid dynamics simulation of slump flow and L-box test on SCC using ANSYS/FLUENT', *Annual Conference - Canadian Society for Civil Engineering*, Ottawa, Canada, Jun 2011.
- **F. Mukhtar**, 'Properties of Recycled Concrete Aggregate (RCA)', *The 2nd Scientific Conference for Higher Education Students*, Jeddah, Saudi Arabia, Mar 2011.

REPORTS

- **F. M. Mukhtar** (2015), 'Analytical and Numerical Analysis of Cylindrical and Spherical Pressure Vessels with Small Diameter Nozzles', Ph.D. Dissertation, KFUPM, Saudi Arabia.
- **Faisal M. Mukhtar**, Amana J. Kedir and Khaja Najmuddeen (2015), 'Benchmarking International Undergraduate Experience: Opportunities for Improvements and Provision of New Developments to KFUPM Experience', KFUPM, Saudi Arabia.
- Husain J. Al-Gahtani and **Faisal M. Mukhtar**, (2014), '2nd Progress Report: Mesh-free Modeling of Elasto-plastic Problems', submitted to Deanship of Research, KFUPM, Saudi Arabia.
- Husain J. Al-Gahtani and **Faisal M. Mukhtar**, (2013), '1st Progress Report: Mesh-free Modeling of Elasto-plastic Problems', submitted to Deanship of Research, KFUPM, Saudi Arabia.
- **F. M. Mukhtar**, S. Lukman, G. Mahyoub, H. Ali and I. Reza (2013), 'CEE Graduate Program Review (Vol. I and II)', Report submitted to the department of Civil & Environmental Engineering, KFUPM, Saudi Arabia.
- Baluch M. H., Rahman M. K., Gadhib, A. H. and **Mukhtar, F. M.**, (2012), '2nd Progress Report: Computer-Aided Modeling and Simulation of Flow of Self Compacting Concrete', submitted to Deanship of Research, KFUPM, Saudi Arabia.

- Baluch M. H., Rahman M. K., Gadhib, A. H. and **Mukhtar, F. M.**, (2011), ‘1st Progress Report: Computer-Aided Modeling and Simulation of Flow of Self Compacting Concrete’, submitted to Deanship of Research, KFUPM, Saudi Arabia.
- **F. Mukhtar** (2011), ‘Computer-Aided Modeling and Simulation of Flow of Self Compacting Concrete’, M.S. Thesis, KFUPM, Saudi Arabia.
- **F. Mukhtar** (2007), ‘Effect of Recycled Concrete Aggregate (RCA) on Compressive Strength of Concrete (Case Study of Grade 30 Concrete)’, B. Eng. Thesis, BUK, Nigeria.

COMMUNITY SERVICES

- Worked in a committee tasked with carrying out a survey and producing a report titled ‘Benchmarking International Undergraduate Experience: Opportunities for Improvements and Provision of New Developments to KFUPM Experience’, KFUPM, 2015.
- Member in Course Offering Committee, Dep’t of Civil & Environmental Engineering (CEE), KFUPM, 2015.
- Chairman of Committee on Graduate Curriculum Review, CEE Department, KFUPM, Summer 123, 2013.
- Coordinator CEE Lecturer-Bs, Research and Graduate Assistants workforce & supervision, KFUPM, 2013-2014.
- Coordinator CEE Full-Time Graduate/Undergraduate Students Hiring, KFUPM, 2013-2014.
- CEE Dep’t webmaster and member CEE Department Website Management Committee, KFUPM, 2013-2014.
- Secretary of Charity & Sanitation Community Development NYSC Group, Idah Local Government, Kogi State, Nigeria, 2008/2009.
- Chairman of Tutorials Committee, Muslim Engineering Students’ Association, Bayero University Kano, Nigeria, 2006/2007.